Non-linear hydroelastic response analysis in irregular head waves, for a large bulk carrier structure, and fatigue based preliminary ship service life prediction

Bianca Cristea

Master Thesis

presented in partial fulfilment
of the requirements for the double degree:
“Advanced Master in Naval Architecture” conferred by University of Liege
"Master of Sciences in Applied Mechanics, specialization in Hydrodynamics, Energetics and Propulsion” conferred by EcoleCentrale de Nantes

developed at "Dunarea de Jos" University of Galati
in the framework of the

“EMSHIP”
Erasmus Mundus Master Course
in “Integrated Advanced Ship Design”

Ref. 159652-1-2009-1-BE-ERA MUNDUS-EMMC

Supervisor: Prof. Leonard Domnisoru, "Dunarea de Jos" University of Galati

Reviewer: Prof. Dario Boote, University of Genoa

Galati, February 2013

ABSTRACT

Non-linear hydroelastic response analysis in irregular head waves, for a large bulk carrier structure, and fatigue based preliminary ship service life prediction

By Bianca Cristea

The objective of this master thesis is to provide the specific knowledge to determine the steady state and transitory ship hull hydroelastic dynamic response (oscillations and vibrations) induced by irregular head waves and coupled with cumulative damage factor fatigue analysis to predict the preliminary design ship life.

The studied ship model is a large double hull bulk carrier, with length between perpendiculars 279.00 m. The significant loading cases considered in this work are: full cargo and ballast. The numerical analyses are divided in three-interlinked parts:

- *Part 1 - Global-local Strength Analysis in Equivalent Quasi-static Head Waves* - there are considered two types of analysis models, the equivalent ship 1D-girder and 3D-FEM hull model extended over the whole ship length. In order to obtain the floating and trim equilibrium condition in vertical plane, the iterative numerical procedures, analogues to the method developed in the MARSTRUCT EU-FP6-Project, Work package Methods and Tools for Strength Assessment by Domnisoru & Stoicescu 2005, 2007, are applied. The 3D-FEM hull model has been developed by NASTRAN NX for FEMAP ver. 10.2 program (Femap 2010). Taking into account the thesis objective, form this analysis the 3D/1D stress correlation factors are obtained for selected structural details.

- *Part 2 - Non-linear Hydroelastic Response Analysis in Head Irregular Waves* - there are analysed the wave induced dynamic response, including: the linear and non-linear oscillation components, taking into account the bottom and side slamming phenomena, and also the vibration components, on the first and higher order elastic modes, the springing phenomenon, linear and non-linear steady state dynamic response, due to the ship structure-wave resonance, and the whipping phenomenon, slamming induced transitory dynamic response. The analyses have been carried on with DYN program codes package developed at Galati Naval Architecture Faculty (Domnisoru et al., 2009, 2011), for head waves first order ITTC power density spectrum, with the significant wave height $h_{1/3}$ = 0-12 m and second order wave interference components (wave model Longuet-Higgins).

- *Part 3 - Fatigue Analysis and the Preliminary Ship Service* Life Prediction - the analysis is based on the fatigue strengths assessment of the ship hull structure, using the wave induced short term significant stresses. In order to evaluate the ship fatigue strength criterion, according to Germanischer Lloyd Register 2011, was applied the cumulative damage ratio D method, based on Palmgren-Miner method and steel standard design stress-cycles S-N curves. The stress values are selected from the hydroelastic analysis (part 2 analysis) multiplied by the 3D/1D correlations factors (part 1 analysis). The fatigue analysis was carried out considering the dynamic response with or without higher frequency dynamic response (vibrations), besides the low frequency dynamic response (oscillations), involving two different long-term wave significant height histograms North Atlantic and World Wide Trade. For the two loading cases, full cargo and ballast, it is considered a simplified travel scenario with the same occurrence probability ($D = 0.5D_{full} + 0.5D_{ballast}$), for a reference time of R = 20 years.

The numerical results obtained from the first part (ship global-local strength analyses), based on 3D-FEM and 1D girder models, are the stress 3D/1D correlation factors for the deck structural details with maximum stress values. The numerical results from the second part outlined the extreme wave loads, from slamming-whipping and springing hydroelastic dynamic responses. The third part is focused on the influences of the hydroelastic responses on the fatigue strength assessment and how the ship preliminary service life prediction can be obtained more realistic for large elastic ships.

CONTENTS

Declaration of Authorship

I declare that this thesis and the work presented in it are my own and has been generated by me as the result of my own original research.

Where I have consulted the published work of others, this is always clearly attributed.

Where I have quoted from the work of others, the source is always given. With the exception of such quotations, this thesis is entirely my own work.

I have acknowledged all main sources of help.

Where the thesis is based on work done by myself jointly with others, I have made clear exactly what was done by others and what I have contributed myself.

This thesis contains no material that has been submitted previously, in whole or in part, for the award of any other academic degree or diploma.

I cede copyright of the thesis in favour of the "Dunarea de Jos" University of Galati.

Date: Signature
21.01.2013

1. INTRODUCTION

1.1. Subject and Objectives of the Master Thesis

The subject of the master thesis presented in this report is: "Non-linear Hydroelastic response analysis in irregular head waves, for a large bulk carrier structure, and fatigue based preliminary ship service live prediction".

In this study the numerical analysis are carried out on a large double hull bulk carrier, with length between perpendiculars 279.00 m. For the large bulk carrier are considered the full cargo and ballast load cases, under head waves conditions. The significant load cases considered in this work are: full cargo and ballast. The ship structure initial design has been developed during the internship program at ICEPRONAV S.A Galati.

In the standard analyses of the wave induced ship dynamic response are included only the ship rigid hull oscillations, as it is presented in Bhattacharyya 1978 and Bertram 2000. Nowadays for the design of a large and elastic ship the naval architect must determine with accuracy the ship dynamic loads. For this, in order to analyse the wave induced ship dynamic response is used the theory of hydroelasticity, based on non-linear formulation and statistical models for irregular waves, including the low frequency (oscillations) and high frequency components (vibrations), (Hirdaris & Chunhua 2005).

Taking into account the new requirements presented in the upper paragraph, the objective of the study presented in this report is to provide the specific knowledge to determine the steady state and transitory ship hull hydroelastic dynamic response (low and high frequency) induced by irregular head waves and coupled with cumulative damage factor fatigue analysis to obtain the prediction of the preliminary design ship life.

Based on the ship hull stress values induced by the wave loads, the fatigue strength will be carried out using the cumulative damage ratio D method, based on Palmgren-Miner method and steel standard design fatigue stress-cycles S-N curves (GL 2011), involving two different long-term wave significant height histograms North Atlantic and World Wide Trade.

1.2. Structure of the Study

In this study are presented the numerical analyses for dynamic response of a full scale large bulk carrier ship hull, based on the linear and non-linear hydroelasticity theory, induced by irregular head waves model Longuet-Higgins, and fatigue based preliminary ship service live prediction, using the cumulative damage ratio D method (Palmgren-Miner method and steel standard design stress-cycles S-N curves). Considering the complexity of the subject the numerical analysis are divided in three interlinked analyses.

To have a clear image on the configuration of this study I have developed the scheme of the study presented in Figure 1. The study structure is composed by five parts, as follows:

- Part 1 - Structural Characteristics of the Bulk Carrier Ship for Numerical Analysis: in this part will be presented all the information needed to complete the numerical analyses of the wave induced dynamic responses of a large bulk carrier ship hull. As it is described in Figure 1, here will be presented the general characteristics (main dimensions, cargo arrangement, general arrangement, offset line of the ship) about the large bulk carrier that has been used in this study, and the scantling results that will be used to develop the 3D CAD/FEM model of the bulk carrier. The hull structural scantling of the bulk carrier is done in according to CSR-BC Rules and Germanischer Lloyd Register 2011 using GL - Poseidon ND.11 program.

- Part 2 - Global-local Strength Analysis in Equivalent Quasi-static Head Waves - in this part are considered two types of analysis models, the equivalent ship 1D-girder and 3D-FEM hull model extended over the whole ship length. In order to obtain the floating and trim equilibrium condition in vertical plane, the iterative numerical procedures, analogues to the method developed in the MARSTRUCT EU-FP6-Project, Work package Methods and Tools for Strength Assessment by Domnisoru & Stoicescu 2005, 2007, are applied. The 3D-FEM hull model has been developed by NASTRAN NX for FEMAP ver. 10.2 finite element modelling and post processing program (Femap 2010). The numerical results obtained in this part of the study are the maximum deck, bottom and side shell stresses, based on 3D-FEM and 1D girder models. These results are used in order to obtain the stress 3D/1D correlation factors, as input data for the fourth part of the work.

- Part 3 - Non-linear Hydroelastic Response Analysis in Head Waves - here are analysed the wave induced dynamic responses, including: the linear and non-linear oscillation components, taking into account the bottom and side slamming phenomena, and also the vibration components, on the first and higher order elastic modes, the springing phenomenon, linear and non-linear steady state dynamic response, due to the ship structure-wave resonance, and the whipping phenomenon, slamming induced transitory dynamic response. The analyses have been carried out with DYN program codes package developed at Galati Naval Architecture Faculty (Domnisoru et al., 2009, 2011), for head waves first order ITTC power density spectrum, with the significant wave height $h_{1/3}$ = 0 - 12 m and second order wave model Longuet-Higgins, with wave interference components. The numerical results obtained in this part outlined the extreme wave loads, from slamming-whipping and springing hydroelastic dynamic responses.

- Part 4 - Fatigue Analysis and the Preliminary Ship Service Life Evaluation - the analysis is based on the fatigue strengths assessment of the ship hull structure, using the short term significant stresses for irregular waves loads. In order to evaluate the ship fatigue strength criterion, according to Germanischer Lloyd Register 2011, was applied the cumulative damage ratio D method, based on Palmgren-Miner method and steel standard design stress-cycles S-N curves. The stress values are taken from the hydroelastic analysis (part 3) multiplied by stress 3D/1D correlations factors (based on part 2 structure analysis). The fatigue analysis was carried out considering the dynamic response with or without higher frequency dynamic response (vibrations), involving two different long-term wave significant height histograms North Atlantic and World Wide Trade. For the two loading cases, full cargo and ballast, is considered a simplified travel scenario with the same occurrence probability ($D = 0.5D_{full} + 0.5D_{ballast}$), for a reference time of R = 20 years. The numerical results from this part will outlined the influences of the hydroelastic responses on the fatigue strength and the ship preliminary service life prediction.

- Part 5 - Remarks and Conclusion: in the last part of the work are presented the final remarks and the conclusions of this master thesis.

For a clearer presentation of the study, the structure of the report follows the same scheme of the study presented in Figure 1.

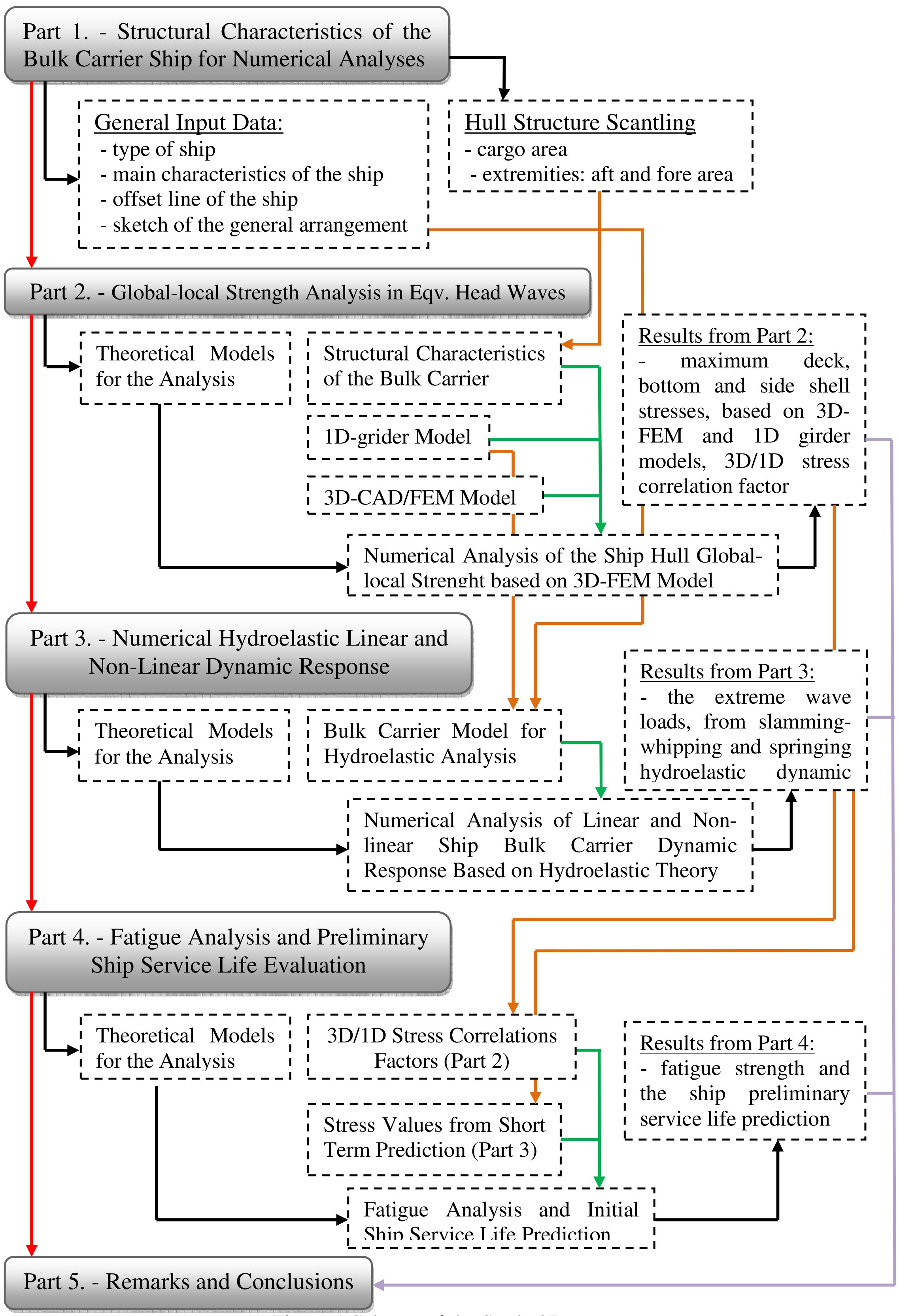

Figure 1.Scheme of the Study / Report

2. STRUCTURAL CHARACTERISTICS OF THE BULK CARRIER SHIP FOR NUMERICAL ANALYSES

2.1. General Input Data

As prototype ship was selected from "Shipbuilding and Marine Engineering" Magazine (JSEA Magazine, 2004) Azul Frontier 170 000 tdw bulk carrier (see Figure 2). The Azul Frontier bulk was built by Namura Shipbuilding Co, Ltd and delivered to the owner on 31 July 2003. The ship is a capsize bulk carrier featuring a large cargo hold capacity, with nine cargo holds with side rolling, with individual hatch covers and duct keel in the double bottom space for use as a pipe passage.

Figure 2. Bulk Carrier Azul Frontier (JSEA Magazine 2004)

Based on catalogue information for the Azul Frontier bulk carrier, the main dimensions and characteristics of the test ship that was analysed in this study are presented in Table 1. In the "Shipbuilding and Marine Engineering" Magazine (JSEA Magazine 2004) are only a few technical data and the main dimensions of the selected bulk carrier. The other information required for the study as: preliminary of the general arrangement, the offset lines, structural characteristics of the hull, material characteristics and mass distributions, I have designed them using drawings and information, during the internship program, from similar ships that were designed in ICEPRONAV S.A Galati in the last years.

Table 1. Main Dimensions and Characteristics of the studied bulk carrier

Main Dimensions	
Dimension	**Value**
Length overall (Loa)	289.87 m
Length between perpendiculars (Lpp)	279.00 m
Rule Length (L)	279.00 m
Breadth (B)	45.00 m
Depth (D)	24.00 m
Design Draft (T)	15.20 m
Minimum ballast draught aft abt.(Tbf)	12.50 m
Minimum ballast draught forward abt. (Tba)	10.50 m
Service Speed (v_0)	16.00 Knots
Maximum Speed (v_{max})	17.50 Knots
Block coefficient (C_B)	0.805
Deadweight (DWT)	162 000 tdw
Number of Cargo Holds	9
Main Characteristics	
Description	**Observations**
Classification Society Germanischer Lloyd Grope 2011	In the same time were respected the CSR BC Rules.
Materials used: - the hull structure is build with normal steel and in the solicited parts of the hull (as deck and bottom) is used with high steel.	The material characteristics were selected according to GL 2011 - I Part 1, Chapter 1, Section 2. More information about the material characteristics are presented in Section 2.1.1.
Offset Line: - was made using the program MaxSurf ver.13 (MaxSurf 2012).	In Figure 3 is presented the offset lines, and in Figure 4 is exposed for a clear examination the transversal view of the offset line.
General Arrangement: - using a few models of general arrangements for similar ship, provided by ICEPRONAV S.A, was completed a preliminary of the general arrangement of the studied ship.	In Figure 5 is presented the preliminary general arrangement of the studied bulk carrier.
Structural Characteristics of the Hull - the hull structural scantling of the hull was done according to CSR-BC Rules and Germanischer Lloyd Register 2011 using GL - Poseidon ND.11 program.	The hull structural scantling of the tested bulk carrier is presented in sub-section 2.2 of the present report.

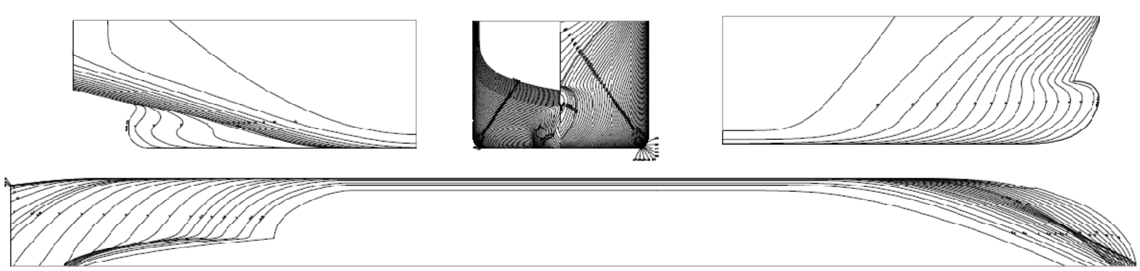

Figure 3. - Offset line of the studied bulk carrier

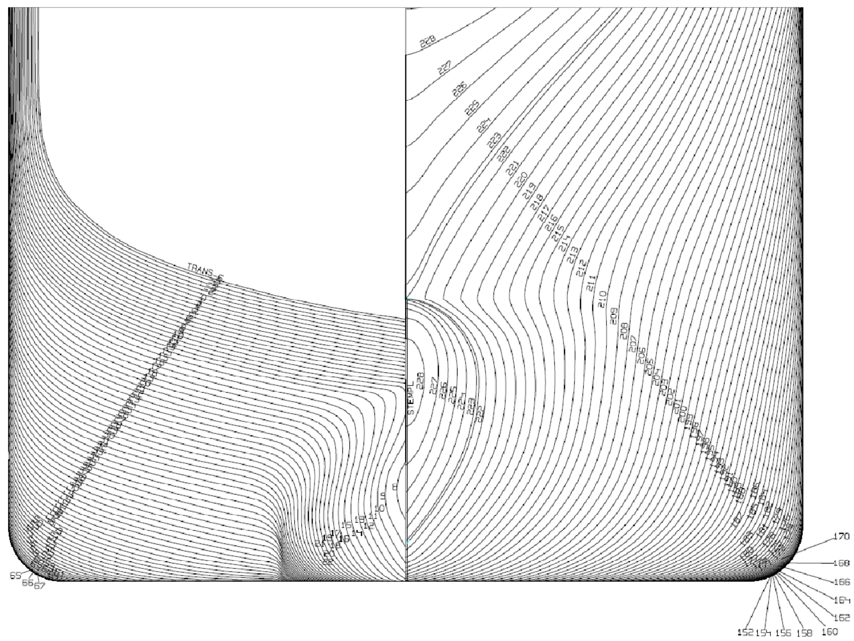

Figure 4. Transversal view of the offset line

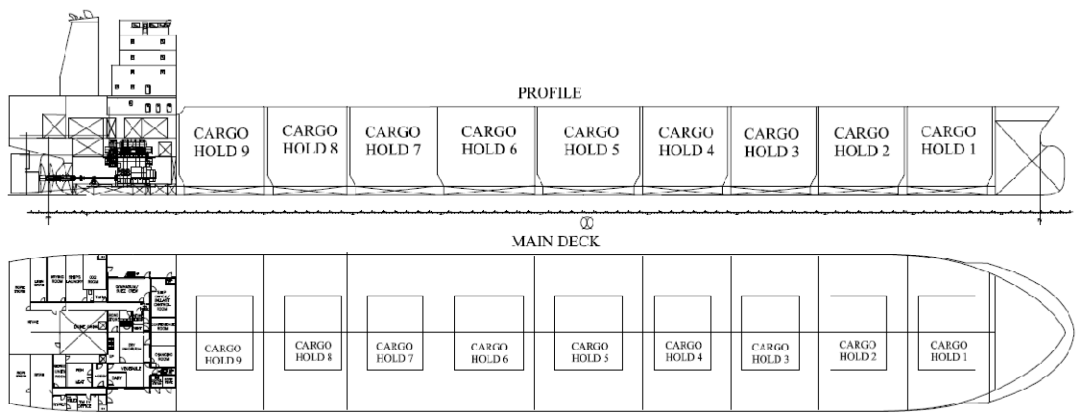

Figure 5. Preliminary General Arrangement of the studied bulk carrier

2.1.1. Material Characteristics

The material selection of the hull structure is one of the most important structural considerations, and the choice of the material should be defined and taken into consideration during the earliest stage of the structural design. The material of the hull structure is playing an important role in the preliminary design estimation of the ship.

It is already known that for some areas of the structure in case of the bulk carriers, such as deck, side shell and bottom structures have to resist against higher stresses, so that for those regions is used a better quality of the material. To develop the de initial design of the studied bulk carrier, steel has been selected for the entire hull structure, where have been used three categories of steel grades in different structural regions of the bulk carrier.

In Table 2 are presented the steel grades adopted for this study, the yield limit - R_{eH}, the tensile strength - R_m, the material factor - k and the structural members where have been used. The steel characteristics in conformity with GL2011 are:

- E = 206000 N/mm² - Young's modulus;
- G = 79200 N/mm² - Shear modulus;
- ν = 0.3 - Poisson's coefficient.

Table 2 - Steel Grades

Steel grade	R_{eH} [N/mm^2]	R_m [N/mm^2]	k	Structural regions
A	235	400	1.00	- aft and fore area - deckhouse and funnel - central and secondary girders in inner bottom - platforms in inner side - web frames in inner bottom, inner side, hopper and wing tanks - transversal bulkheads
AH32	315	440	0.78	- keel, bottom and side shell - inner bottom and inner side - wing and hopper tanks
AH36	355	490	0.72	- main deck - hatch coming

According to GL - IACS - CSR Bulk Carrier - Chapter 5 - Section 1 - 3.1, the allowable normal stress - $\sigma_{1,ALL}$ (1) and the allowable shear stress - $\tau_{1.ALL}$(2) for the global-local strength analysis are:

$$\sigma_{1,ALL} = \begin{cases} \frac{130}{k}; & \text{for } \frac{x}{L} \le 0.1 \\ \frac{190}{k} - \frac{1500}{k}\left(\frac{x}{L} - 0.3\right)^2; & \text{for } 0.1 < \frac{x}{L} < 0.3 \\ \frac{190}{k}; & \text{for } 0.3 \le \frac{x}{L} \le 0.7 \\ \frac{190}{k} - \frac{1500}{k}\left(\frac{x}{L} - 0.7\right)^2; & \text{for } 0.7 < \frac{x}{L} < 0.9 \\ \frac{130}{k}; & \text{for } \frac{x}{L} \le 0.9 \end{cases} \quad (1)$$

$$\tau_{1,ALL} = \frac{120}{k} \quad (2)$$

2.2. Hull Structural Scantling

The hull structural scantling was performed according to CSR-BC Rules and Germanischer Lloyd Register 2011 using GL - Poseidon ND.11 program. The scantling of the hull is divided in two areas: scantling of the cargo area and the scantling of the ship extremities. The input data used for the scantling of the both areas are presented in Table 3.

Table 3. General Input Data used for the Two Scantling Areas

<table>
<tr><th colspan="3">Ship Type</th><td colspan="6">Bulk Carrier - double side</td></tr>
<tr><th colspan="9">Principal Dimensions</th></tr>
<tr><td colspan="9">The main dimensions presented in Table 1 (subsection 2.1)</td></tr>
<tr><th colspan="9">Linear Isotropic Material</th></tr>
<tr><td colspan="2">Mat. No</td><td colspan="2">E - Modulus [kN/m^2]</td><td colspan="2">G - Modulus [kN/m^2]</td><td>Density [kg/m^3]</td><td colspan="2">Yield Stress [N/mm^2]</td></tr>
<tr><td colspan="2">1 - A</td><td colspan="2">206000000</td><td colspan="2">79230769</td><td>8000</td><td colspan="2">235</td></tr>
<tr><td colspan="2">2 - AH32</td><td colspan="2">206000000</td><td colspan="2">79230769</td><td>8000</td><td colspan="2">315</td></tr>
<tr><td colspan="2">3 - AH35</td><td colspan="2">206000000</td><td colspan="2">79230769</td><td>8000</td><td colspan="2">355</td></tr>
<tr><th colspan="9">Frame spacing</th></tr>
<tr><td colspan="3">Zone 1</td><td colspan="6">Fr.-10 to Fr.18 - a = 0.6 m</td></tr>
<tr><td colspan="3">Zone 2</td><td colspan="6">Fr.18 to Fr.54 - a = 0.7 m</td></tr>
<tr><td colspan="3">Zone 3</td><td colspan="6">Fr.54 to Fr.342 - a = 0.8 m</td></tr>
<tr><td colspan="3">Zone 4</td><td colspan="6">Fr.342 to Fr.369 - a = 0.7 m.</td></tr>
<tr><th colspan="9">Hold Arrangement</th></tr>
<tr><td rowspan="2">Hold No.</td><td colspan="2">Start of the Hold</td><td colspan="3">End of the Hold</td><td colspan="3" rowspan="2">Length of the Hold [m]</td></tr>
<tr><td>Fr.</td><td>x from AP [m]</td><td>Fr.</td><td colspan="2">x from AP [m]</td></tr>
<tr><td>9</td><td>54</td><td>36.00</td><td>85</td><td colspan="2">60.80</td><td colspan="3">24.80</td></tr>
<tr><td>8</td><td>85</td><td>60.80</td><td>114</td><td colspan="2">84.00</td><td colspan="3">23.20</td></tr>
<tr><td>7</td><td>114</td><td>84.00</td><td>145</td><td colspan="2">108.80</td><td colspan="3">24.80</td></tr>
<tr><td>6</td><td>145</td><td>108.80</td><td>180</td><td colspan="2">136.80</td><td colspan="3">28.00</td></tr>
<tr><td>5</td><td>180</td><td>136.80</td><td>218</td><td colspan="2">167.20</td><td colspan="3">30.40</td></tr>
<tr><td>4</td><td>218</td><td>167.20</td><td>249</td><td colspan="2">192.00</td><td colspan="3">24.80</td></tr>
<tr><td>3</td><td>249</td><td>192.00</td><td>280</td><td colspan="2">216.80</td><td colspan="3">24.80</td></tr>
<tr><td>2</td><td>280</td><td>216.80</td><td>311</td><td colspan="2">241.60</td><td colspan="3">24.80</td></tr>
<tr><td>1</td><td>311</td><td>241.60</td><td>342</td><td colspan="2">266.40</td><td colspan="3">24.80</td></tr>
</table>

The bending moments, share forces and torsional moment used in scantling calculation are:

- for still water were determined according to GL 2011 - I-Part 1. Ch.1 Sec.5 B2, and are presented in Table 4 and Figure 6;

- for equivalent quasi-static wave load were determined according to GL 2011 - I- Part 1. Ch.1 Sec.5 B3, and are presented in Table 5 and Figure 7.

Table 4. Still Water Bending Moments, Shear Forces and Torsional Moment

Frame No.	Bending Moments BM		Shear Forces SF		Tors. Moment
	Max [kNm]	Min [kNm]	Max [kN]	Min [kN]	+/- [kNm]
0L	0.00	0.00	0.00	0.00	0.00
0.3L	4120894	-3652681	76999	-73552	378807
0.7L	4120894	-3652681	76999	-73552	345554
1.0L	0.00	0.00	0.00	0.00	0.00

Table 5. Wave Bending Moments, Shear Forces and Torsional Moment for statistic wave $h_w = 10.65$m

Position		Vertical Bending		Horizontal Bending		Torsion rel to B
Frame No.		BM [kNm]	SF [kN]	BM [kNm]	SF [kN]	Mtor [kNm]
0L	Min	0.00	0.00	0.00	-21837	0.00
	Max	0.00	0.00	0.00	-21837	0.00
0.3L	Min	-4633557	-55560	-3655521	-54593	-1355199
	Max	4280897	51332	3655521	54593	-1355199
0.7L	Min	-5295494	-55795	-4177738	-54593	-1205179
	Max	4892454	60392	4177738	54593	1205179
1.0L	Min	0.00	0.00	0.00	-8189	0.00
	Max	0.00	0.00	0.00	8189	0.00

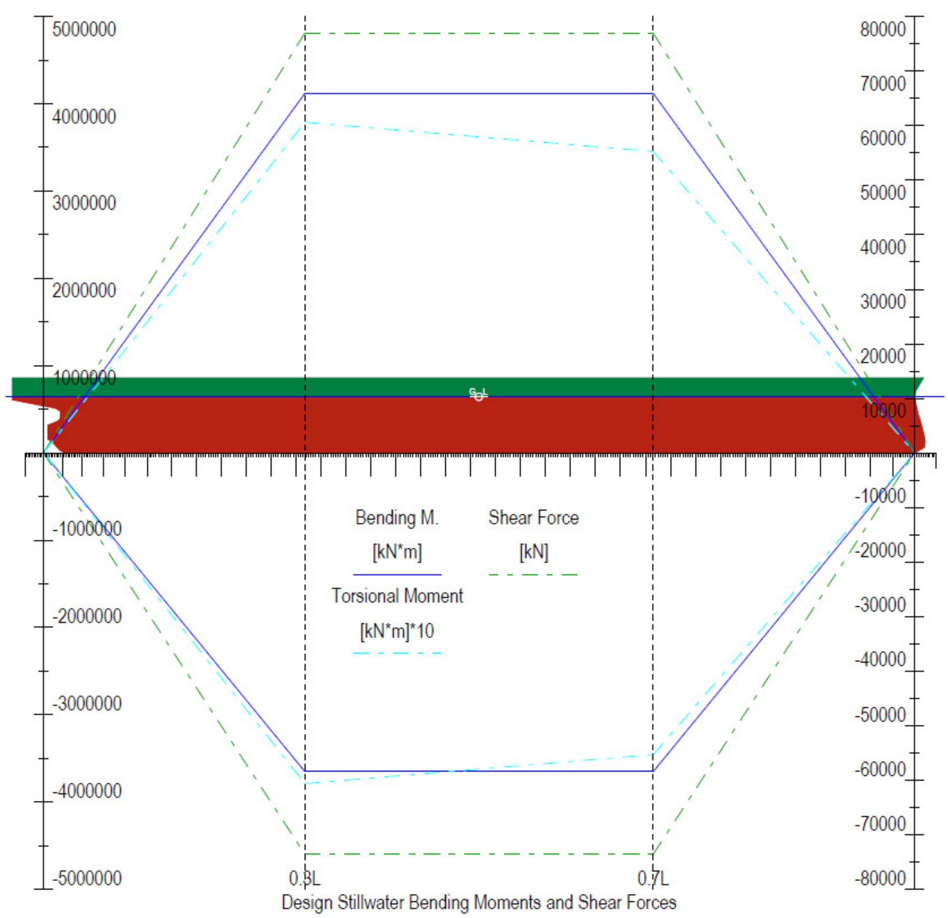

Figure 6. Design Still water Bending Moments, Shear Forces and Torsional Moment

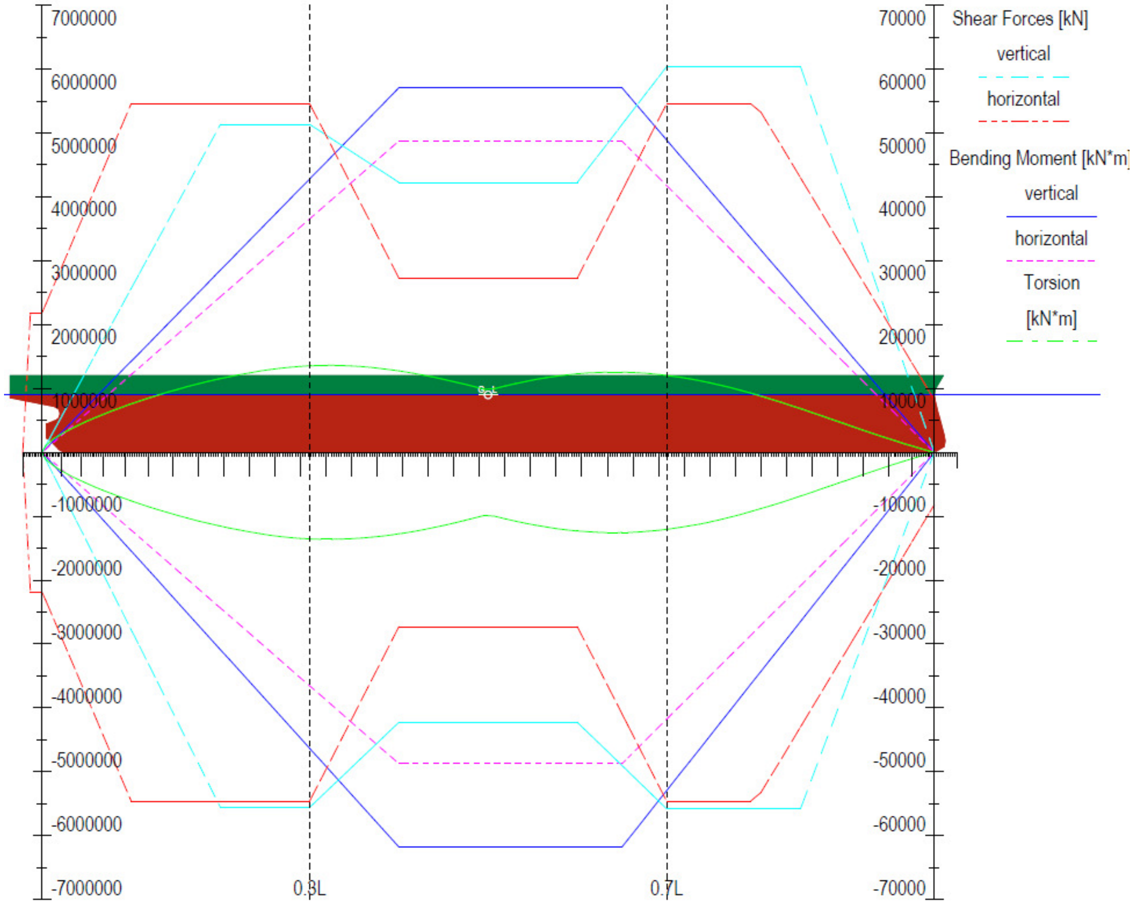

Figure 7. Design Wave Bending Moments, Shear Forces and Torsional Moment for rule based statistical wave height h_w= 10.65m

The scantling of the longitudinal structural members was completed with Poseidon ND.11 (GL 2011) and is based on the design loads presented in Table 4 and Table 5, being analysed three cases:

- LC1 - for this load conditions were used only bending moments and shear forces (maximum value form the Table 4-Table 5);

- LC2 - in this case all cargo tanks were full with cargo density 1.1 t/m^2 at maximum draught, all ballast tanks were empty and bending moments and shear forces were considered as in LC1;

- LC3- in this case all ballast tanks were full with saltwater (density 1.025 t/m^2), all cargo tanks were empty and bending moments and shear forces were considered as in LC1;

The hull structural scantling was completed on eleven areas presented in Table 6.

Table 6. Scantling areas over the ship length

Scantling Area		Specific Frame	x [m] from AP
Aft Area	Zone 1 - Fr.-8 to Fr.22	Fr. 10	6.00
	Zone 2 - Fr.22 to Fr.34	Fr.24	18.50
Cargo Area	Zone 3 - Fr.34 to Fr.54	Fr. 43	28.30
	Zone 4 - Fr.54 to Fr.73	Fr.64	44.00
	Zone 5 - Fr. 73 to Fr. 92	Fr. 82	58.40
	Zone 6 - Fr. 92 to Fr.112	Fr.101	73.60
	Zone 7 - Fr. 112 to Fr. 253 - Amidships Area	Fr. 184 and Fr.195	141.60 150.40
	Zone 8 - Fr. 253 to Fr.273	Fr. 264	205.60
	Zone 9 - Fr.273 to Fr.292	Fr.282	220.00
	Zone 10 - Fr.292 to Fr.325	Fr.307	240.00
	Zone 11 - Fr.325 to Fr.342	Fr.327	256.00
Fore Area	Zone 12 - Fr.342 to Fr.368	Fr.350	273.60

In Figure 8 are presented the scantling results of zone 2 - aft area of the studied ship, in this case the specific frame being Fr.24 (at 18.50m from AP). The scantling results of the cargo area presented in Figure 9 and Figure 10 (the results are for zone 7 and specific frame 180 and 181). For the fore area of the bulk carrier the scantling results are presented in Figure 11. All the transversal bulkheads (TBH) of the studied ship are the same, and the characteristic bulkhead form cargo area is presented in Figure 12.

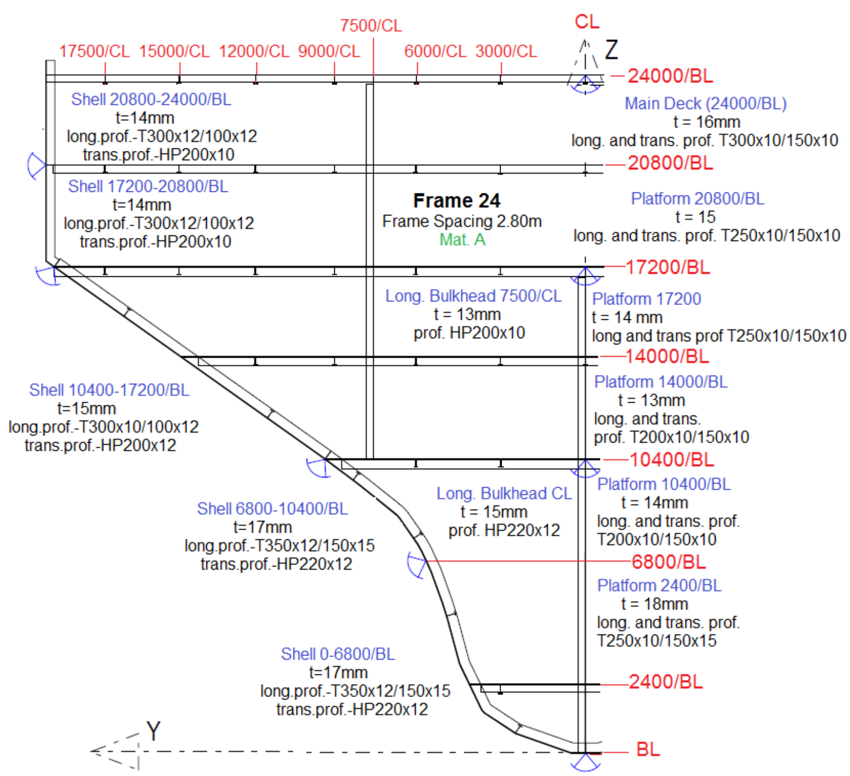

Figure 8.Scantling results for aft area (zone 2 – Fr. 24)

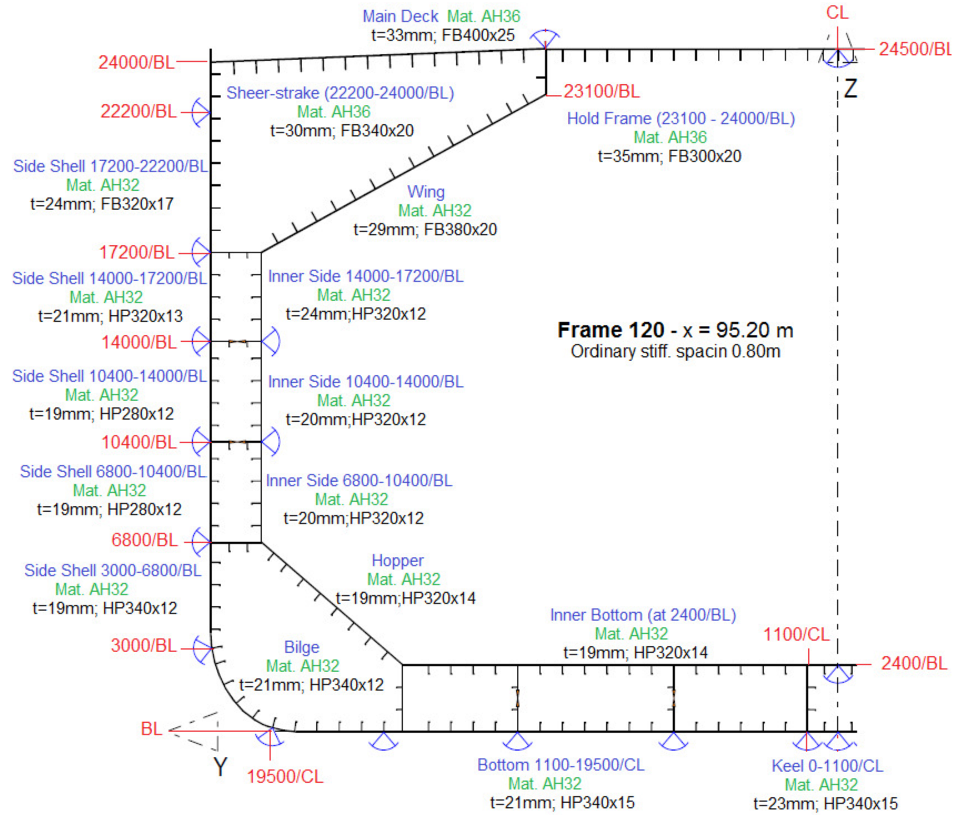

Figure 9. Scantling results for cargo area - between frames (zone 7 - FR.120)

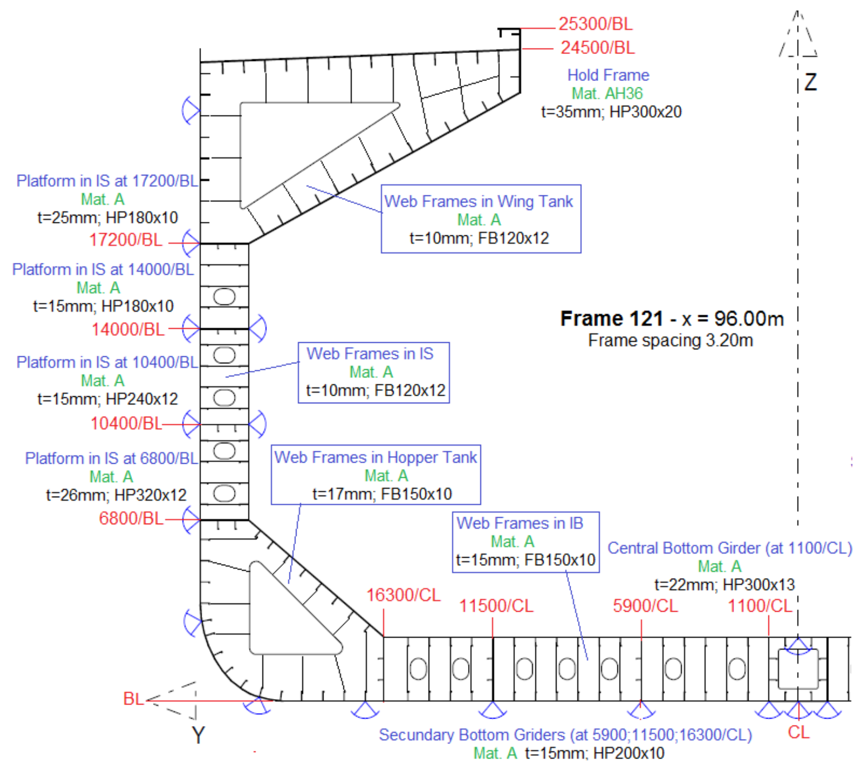

Figure 10. Scantling results for cargo area - web frame (zone 7 - Fr.121)

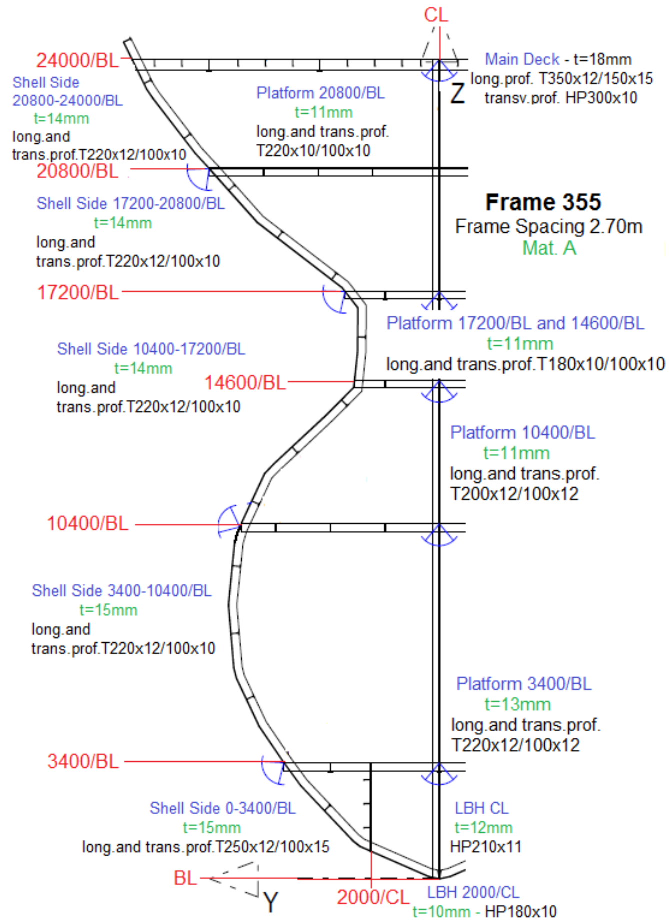

Figure 11.Scantling results for fore area (zone 12 - Fr.355)

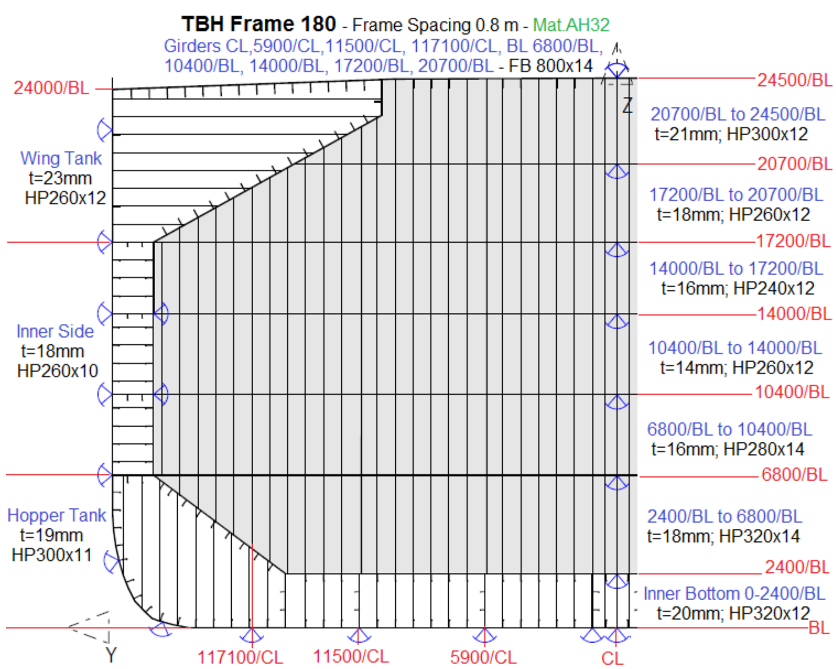

Figure 12.Transversal bulkhead (TBH) Fr.180 from cargo area

3. GLOBAL-LOCAL STRENGTH ANALYSIS IN HEAD EQUIVALENT QUASI-STATIC WAVES

The main topic of this section is the global strengths analysis for the ship hull, in the vertical plane, under the own mass, cargo or ballast load, still water and equivalent quasi-static head wave loads. There were considered two types of analysis models: the 1D-equivalent ship girder and the 3D-FEM model full extended over the ship length. Based on these analyses it results the stress 3D/1D model correlation factors.

3.1. The Theoretical Models for the Analysis of the Ship Structure Global Strength

3.1.1. The Theoretical Aspects of the Global Ship Strengths Analysis based on 1D-girder Method

In this section is presented a short description of the method for 1D-girder global strength analysis (Domnisoru 2006).

<u>The Ship 1D-girder Loads from Head Equivalent Quasi-static Waves</u>

In this part are consider the loads from quasi-static head waves where wave length it equal with ship length ($\lambda = L$) and the amplitude of the wave is $a_w = h_w/2$. The calculation of the specific wave height (h_w) corresponding to the analysed ship is based on GL2011 I-Part 1, Ch.1Sec.4 A.2.2, it results from the following expression:

$$\mathrm{h_w} = \left[10.75 - \left(\frac{300 - \mathrm{L}}{100}\right)^{3/2}\right] \cdot \mathrm{c_{RW}}[\mathrm{m}]; \quad 90\mathrm{m} \leq \mathrm{L} \geq 300\mathrm{m} \tag{3}$$

where L is the ship length, $c_{RW} \in \{1.00 \quad 0.90 \quad 0.75 \quad 0.66 \quad 0.60\}$ is the zone navigation coefficient, in our case was used unrestricted navigation zone ($c_{RW} = 1.00$).

In order to take into account the real ship offset lines, it is used a non-linear iterative procedure with two steps. In this case the medium draft (d_m), aft draft (d_{pp}), forward draft (d_{pv}) and trim become the parameters that can define the position of the median plane of the equivalent quasi-static head wave, taking as reference the base line plane (BL) of the hull. For the considered loading case there are known: Δ, V, x_G, L, the offset lines, the ship hydrostatics, Bonjean diagrams.

Step I - the free floating condition (4)

iter. = 0 $d_m^{(0)} = 0 \rightarrow d_i^{(0)} = d_m^{(0)} \pm \frac{h_w}{2}\cos\left(\frac{2\pi x_i}{L}\right) \rightarrow A_{Ti}^{(0)} \quad i = 1, n$ from Bonjean

$$V^{(0)} = \int_0^L A_T^{(0)}(x)dx = \delta x \sum_{i=1}^{n} A_{Ti}^{(0)} \; M_y^{(0)} = \int_0^L x \cdot A_T^{(0)}(x)dx = \delta x \sum_{i=1}^{n} x_i A_{Ti}^{(0)} \; x_B^{(0)} = \frac{M_y^{(0)}}{V^{(0)}}$$

iter. = k $d_m^{(k)} = d_m^{(k-1)} + 0.001 \rightarrow d_i^{(k)} = d_m^{(k)} \pm \frac{h_w}{2}\cos\left(\frac{2\pi x_i}{L}\right) \rightarrow A_{Ti}^{(k)} \; i = 1, n$ from Bonjean

$V^{(k)} = \int_0^L A_T^{(k)}(x)dx = \delta x \sum_{i=1}^{n} A_{Ti}^{(k)} \; M_y^{(k)} = \int_0^L x \cdot A_T^{(k)}(x)dx = \delta x \sum_{i=1}^{n} x_i A_{Ti}^{(k)} \; x_B^{(k)} = \frac{M_y^{(0)}}{V^{(0)}}$

and the iteration will stop when $V^{(k)} \geq V$.

The solution is refined, using the half domain method, so that at the last iteration "m" it is achieved the convergence criteria $\left|V - V^{(m)}\right| < 0.001V$. At the end of the first step are resulting the next parameters:

$$x_B^I = x_B^{(m)} d_m^I = d_m^{(m)} \rightarrow x_F^I \text{ and } A_{wL}^I \tag{5}$$

Step II - the fre trim condition (in ship longitudinal plane)

$$x_G > x_B^I \rightarrow \delta trim = 0.00001 \quad \text{or } x_G < x_B^I \rightarrow \delta trim = -0.00001 \tag{6}$$

iter.=0 $d_m^{(0)} = d_m^I;\ x_F^{(0)} = x_F^I;\ A_{wL}^{(0)} = A_{wL}^I;\ trim^{(0)} = \delta trim$

$$d_{pp}^{(0)} = d_m^{(0)} - x_F^{(0)} \cdot trim^{(0)};\ d_{pv}^{(0)} = d_m^{(0)} + \left(L - x_F^{(0)}\right) \cdot trim^{(0)}$$

$$d_i^{(0)} = d_{pp}^{(0)} + \left(d_{pv}^{(0)} - d_{pp}^{(0)}\right)\frac{x_i}{L} \pm \frac{h_w}{2}\cos\left(\frac{2\pi x_i}{L}\right) \rightarrow A_{Ti}^{(0)} \quad i = 1, n \text{ from Bonjean}$$

$$V^{(0)} = \int_0^L A_T^{(0)}(x)dx = \delta x \sum_{i=1}^{n} A_{Ti}^{(0)} \; M_y^{(0)} = \int_0^L x A_T^{(0)}(x)dx = \delta x \sum_{i=1}^{n} x_i A_{Ti}^{(0)} \; x_B^{(0)} = \frac{M_y^{(0)}}{V^{(0)}}$$

$$x_G > x_B^{(0)} \rightarrow \delta trim = 0.00001 \quad \text{or } \; x_G < x_B^{(0)} \rightarrow \delta trim = -0.00001$$

iter=k $d_n^{(k)} = d_m^{(k-1)} + \frac{V - V^{(k-1)}}{A_{wL}^{(k-1)}} \rightarrow x_F^{(k)};\quad A_{wL}^{(k)} trim^{(k)} = trim^{(k-1)} + \delta trim$

$$d_{pp}^{(k)} = d_{pp}^{(k)} - x_F^{(k)} \cdot trim^{(k)};\ d_{pp}^{(k)} = d_m^{(k)} + \left(L - x_F^{(k)}\right) \cdot trim^{(k)}$$

$$d_i^{(k)} = d_{pp}^{(k)} + \left(d_{pv}^{(k)} + d_{pp}^{(k)}\right)\frac{x_i}{L} \pm \frac{h_w}{2}\cos\left(\frac{2\pi x_i}{L}\right) \rightarrow A_{Ti}^{(x)} \quad i = 1, n \text{ from Bonjean}$$

$$V^{(k)} = \int_0^L A_T^{(k)}(x)dx = \delta x \sum_{i=1}^{n} A_{Ti}^{(k)} \; M_y^{(k)} = \int_0^L x A_T^{(k)}(x)dx = \delta x \sum_{i=1}^{n} x_i A_{Ti}^{(k)} \; x_B^{(k)} = \frac{M_y^{(k)}}{V^{(k)}}$$

$$x_G > x_B^{(k)} \rightarrow \delta trim = 0.00001 \quad \text{or } \; x_G < x_B^{(k)} \rightarrow \delta trim = -0.00001$$

and it is iterated until δtrim is changing the sign.

The solution is refined with the half domain method, so that at the last iteration "m" there are satisfied the convergence criteria: $|V - V^m| < 0.001V$and $\left|x_G - x_B^{(m)}\right| < 0.001 < L$. At the end of the second step there result the following data:

$$d_m = d_m^{(m)}, \ d_{pp} = d_{pp}^{(m)}, \quad d_{pv} = d_{pv}^{(m)}, \quad trim = trim^{(m)}, \quad A_{Ti} = A_{Ti}^{(m)} i = 1, n \tag{7}$$

The total vertical load from equivalent quasi-static head wave can be obtained with the following expression:

$$p_{xi} = g_{xi} - \rho g A_{Ti} \quad i = 1, n \quad \rightarrow p_x(x) \quad x \in [0, Loa] \tag{8}$$

The total vertical in plane shear forces and bending moments from equivalent quasi-static head wave can be calculated with the next formulas:

$$T(x) = \int_0^x P_{cx}(x)\,dx; \qquad M(x) = \int_0^x T(x)dx \quad x \in [0, Loa] \tag{9}$$

3.1.2. The Theoretical Aspects of the Global - local Ship Strengths Analysis based on 3D-FEM Models

Compared with the global ship strengths analysis based on 1D-girder method, the approach based on 3D-FEM model on full length has the following main advantages (Domnisoru 2006):

- the ship structure with details is taken into account, with the corresponding geometry and material properties;
- there are used a reduced number of boundary conditions;
- the accuracy for the 3D stress and deformations distributions in the ship structure is better that can be used for the detection of the hot spots domains;
- with no restriction to the ship hull offset lines form free floating and trim equilibrium position are obtained the still water and equivalent quasi-static head waves conditions.

The main steps for the global-local strength analysis, based on 3D-FEM model developed over the full length of the ship are:

- <u>Step 1 - The 3D-CAD Model of the Ship Hull Structure</u> - in this step is developed the ship shell surface based on the offset lines of the studied large bulk carrier, in our case the shell surface was prepared in MaxSurf Version13 (MaxSurf 2012). The ship hull main geometry (main deck, inner side, double bottom, transversal bulkheads etc.) was developed directly in Geometry module from NASTRAN NX for FEMAP ver. 10.2 (Femap 2010).

- Step 2 - The 3D-FEM Mesh of the Ship Hull Structure - in this step is complete the mesh of the 3D-CAD model, the mesh on the ship structure have been done manually using the Mesh module from NASTRAN NX for FEMAP ver. 10.2 (Femap 2010).

- Step 3 - The Boundary Conditions on the 3D-FEM Model of the Ship Hull Structure - in this step are modelled the boundary conditions for the 3D-FEM hull model full extended over the ship length. In the case of the 3D-FEM models developed only on one side of the hull: the symmetry conditions are applied on the nodes disposed in the centre line plane (CL) of the ship and vertical support conditions are applied on two nodes disposed at the ship hull structure extremities (in CL). At the vertical equilibrium conditions, at still water or equivalent quasi-static head waves, the reactions forces in the two vertical supports have to become zero.

- Step 4 - The Loading Conditions and the Numerical Analyses based on 3D-FEM Model - the fourth analysis step consist in the modelling of the loads conditions (full and ballast load conditions) and the effective numerical analysis of the 3D-FEM model developed over the full ship length, in order to obtain the deformations and stress distributions at the global-local strengths analysis. The following loads were taken in account over the ship hull (considering FEMPA ver. 10.2 implementation):

- the gravity loads from the structure weight and other mass components of the displacement, except the cargo or ballast masses;

- the cargo or ballast loads, considered as local hydrostatic pressures over the cargo hold structure or ballast tanks structure;

- the equivalent quasi-static head wave pressure loads for the following cases: $h_w = 0$ (still water case), $h_w = 1.0$ to 12.0m in sagging and hogging conditions and $h_w = 10.65$m (the specific wave height corresponding to the analysed ship according to GL2011 I-Part 1, Ch.1. Sec.4 A.2.2), using an the free floating and trim conditions equilibrium initiate out from the 1D analysis.

- Step 5 - The Numerical Results Evaluation **-** In this step of the global-local strengths analysis, based on 3D-FEM models, are obtained the following numerical results:

- the global and local deformations of the ship hull structure;

- the global and local equivalent von Misses stress distributions over the full girder length of the bulk carrier;

- the hot spots domains from the ship hull structure.

3.2. The Bulk Carrier Ship Equivalent 1D-girder Model

To complete the numerical analyses presented in this report are required the next input data:

- the main dimensions of the studied bulk carrier are presented in Table 1;
- the ship hull offset line and preliminary general arrangement of the bulk carrier (see Figure 3 and Figure 5);
- transversal sections in cargo area are presented in Figure 17;
- the transversal sections characteristics for the studied bulk carrier are presented in Table 7. Based on those data, we have idealized with trapezoidal distributions over the ship length, the diagrams of the transversal sections characteristics;
- the mass diagrams of the two loading cases analysed in this study are presented in Figure 19 and Figure 20;
- based on the rigidity and inertial characteristics of the studies bulk carrier, there are obtained the natural ship hull oscillation/vibration modes from Table 8, in Figure 21 and Figure 22 are presented the additional masses C33 and the damping coefficients λ_{33} .

Table 7 - Transversal sections characteristics

Zones	Zone 2 - Fr.22 to 34	Zone 7 - Fr.112 to 253	Zone 12 - Fr.342 to 368	Figures
Specific Fr.	Fr.24 (see Figure 8)	Fr.120 (see Figure 9)	Fr.355 (see Figure 11)	
x from AP [m]	7.25	150.40	273.60	-
I_{yy} [m^4]	98.53	674.73	53.28	Figure 13
A[m^2]	1.91	2.78	1.92	Figure 14
A_{fz} [m^2]	1.146	1.66	1.152	
$k_{\tau nn}$ [1/m^2]	0.87	0.60	0.87	Figure 15
J_{yy} [tm^2/m]	788.24	5397.88	426.24	Figure 16
W_D [m^3]	8.35	51.53	4.59	Figure 18
W_B [m^3]	8.08	59.03	4.29	

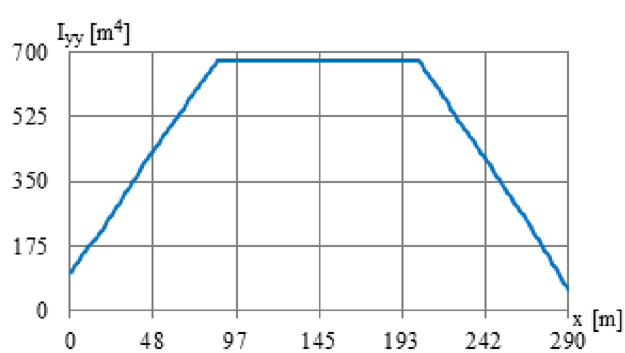

Figure 13.The diagram of the inertial moment (I_{yy} [m^4]) of the transversal sections

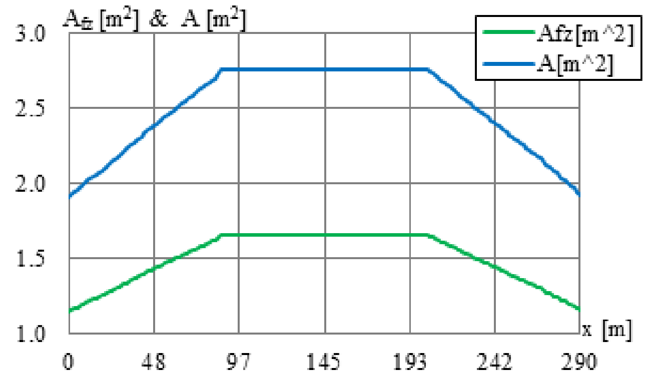

Figure 14.The diagram of the total area and shear area (A and A_{fz} [m^2])of the transversal sections

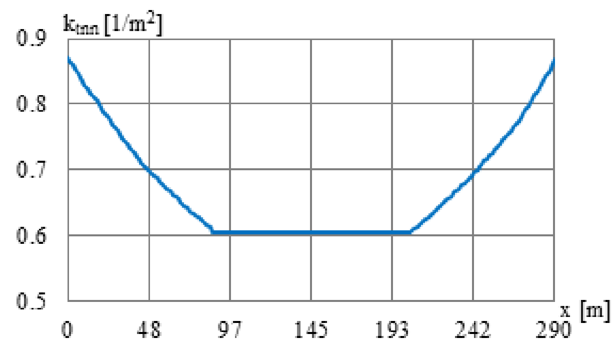

Figure 15.The diagram of mass moment of inertia per unit length (k_{tnn} [$1/m^2$]) of the transversal sections

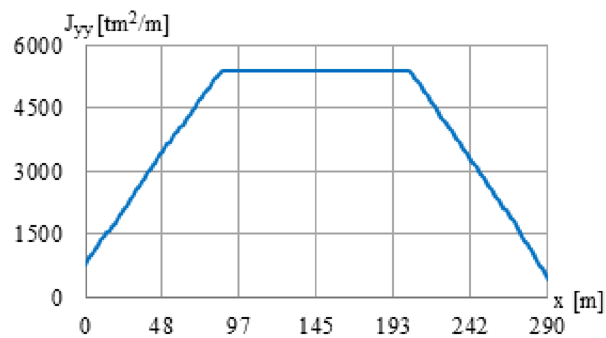

Figure 16.The diagram of the tangential shear stresses coefficient in the neutral axis (J_{yy} [tm^2/m]) of the transversal sections

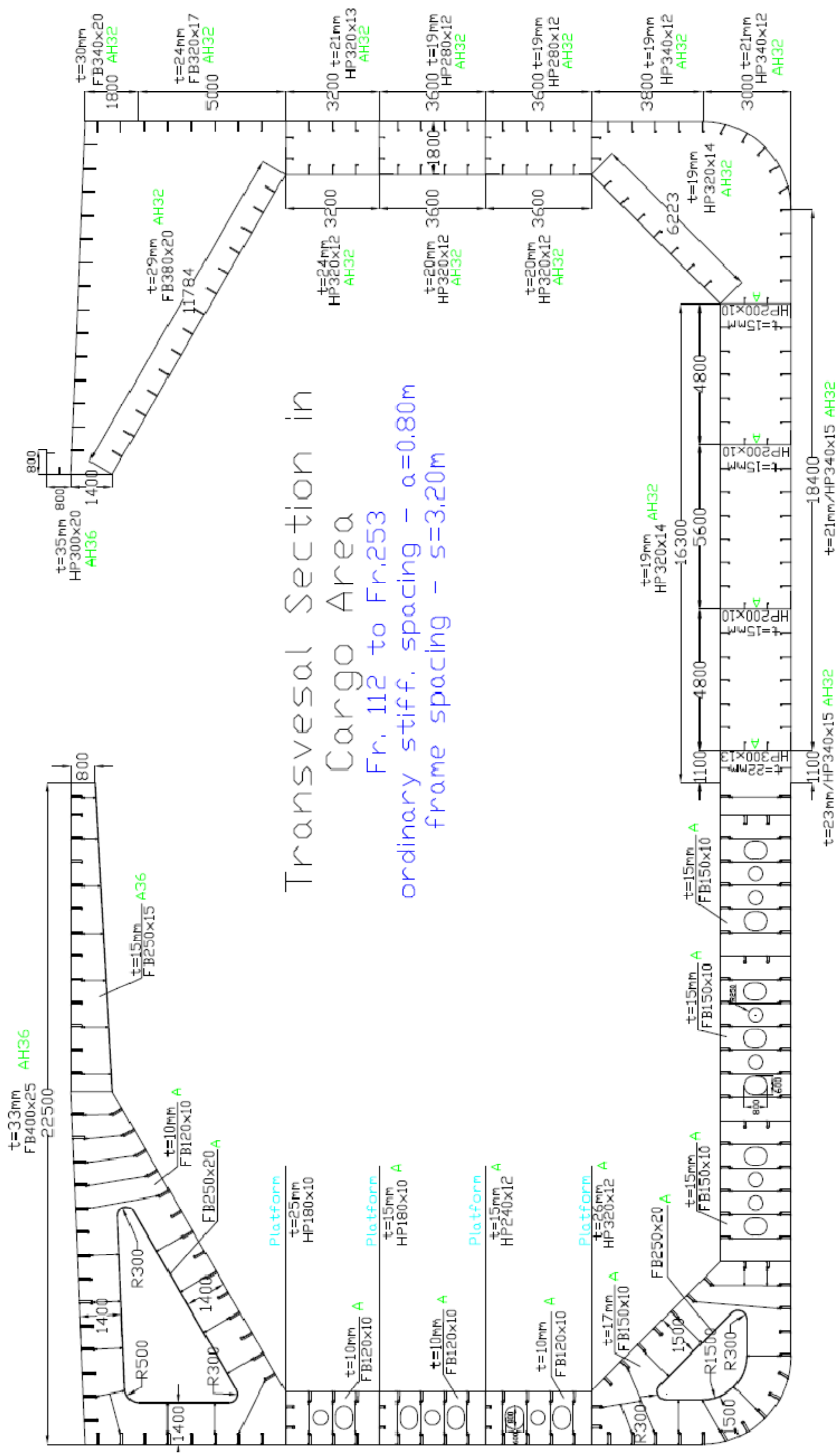

Figure 17 - Transversal section in cargo area, specific section for Fr.112 to Fr.253

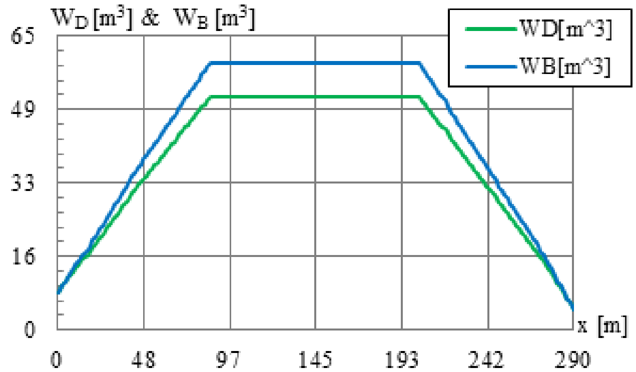

Figure 18. The diagram of the bending resistance modules of the extreme fibre for bottom and for deck (W_B and W_D [m^3])

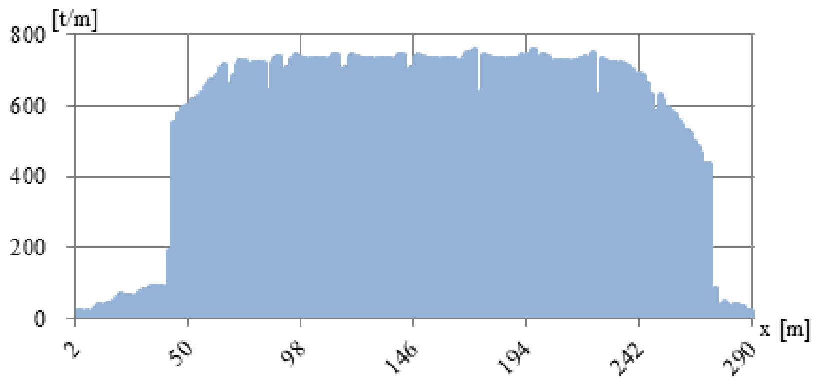

Figure 19. The diagram of mass distribution of the bulk carrier in full loading condition

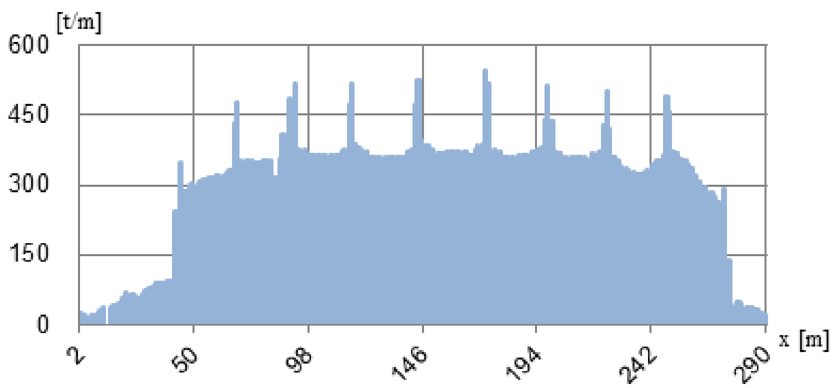

Figure 20.The diagram of mass distribution of the bulk carrier in ballast loading condition

Table 8 - Natural modes frequencies for the two loading conditions

Bulk Carrier			Oscillations f [Hz]		Vibrations f [Hz]		
Mode:			0	1	2	3	4
Nr.	Case						
1	Full Loading Condition (Figure 23)	dry hull	-	-	0.744	1.408	2.065
		hyd.mass	0.0940	0.1027	0.546	1.029	1.505
2	Ballast Loading Condition (Figure 24)	dry hull	-	-	0.963	1.837	2.681
		hyd.mass	0.1101	0.1151	0.663	1.248	1.822

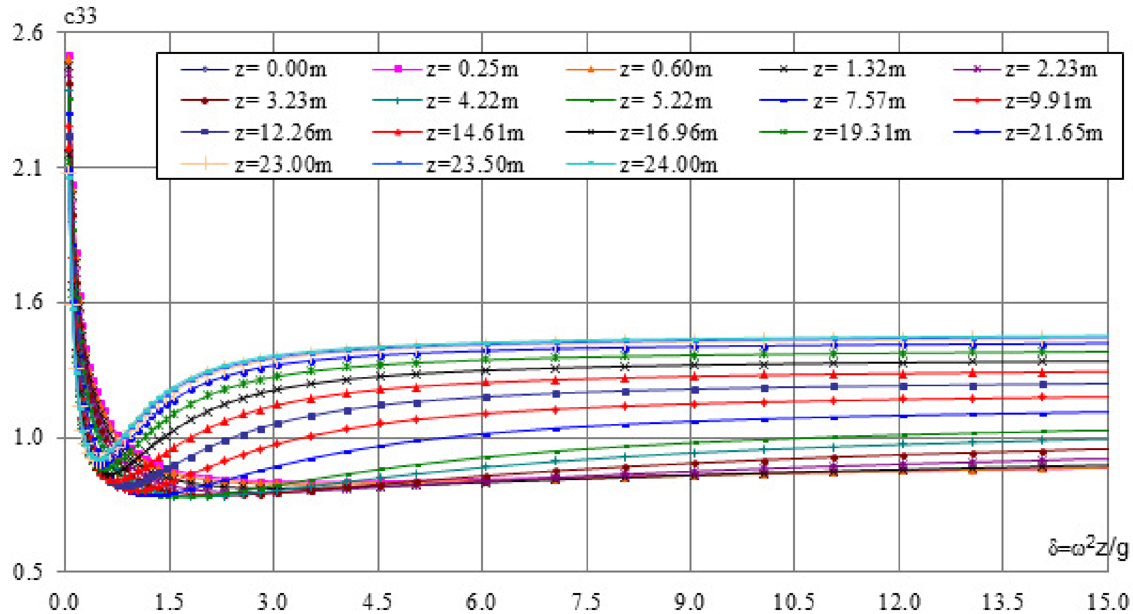

Figure 21. Vertical hydrodynamic mass coefficient $C_{33}$for amidships section x/L = 0.50 (heave oscillation and vertical vibration)

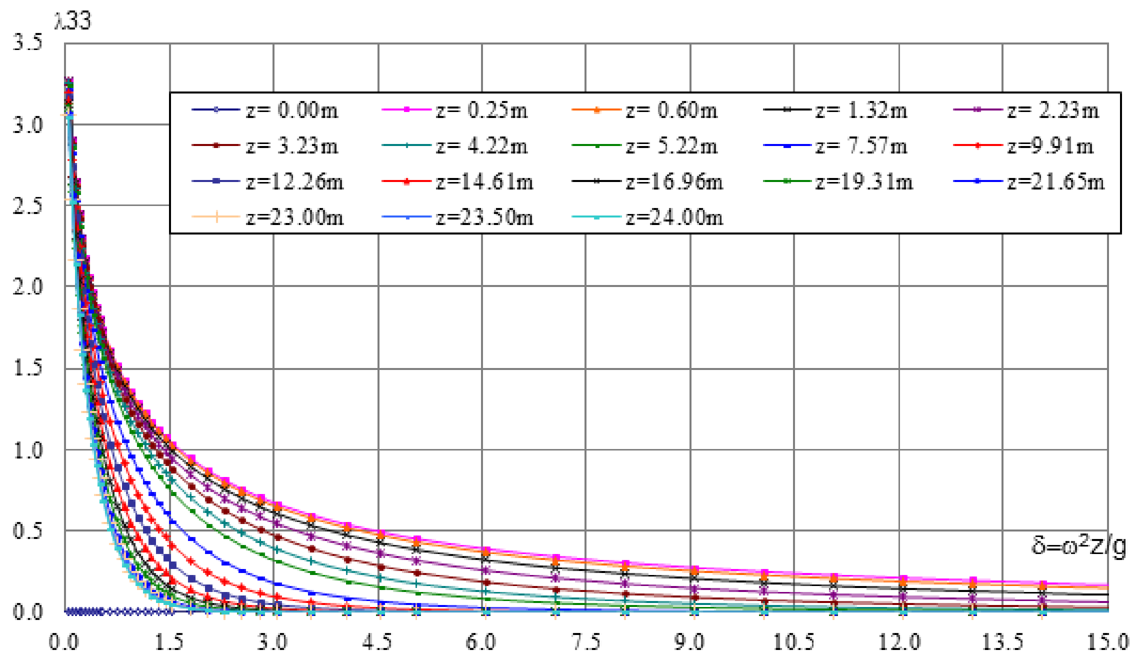

Figure 22. Vertical hydrodynamic damping coefficient λ_{33} fore amidships section (heave oscillation and vertical vibration)

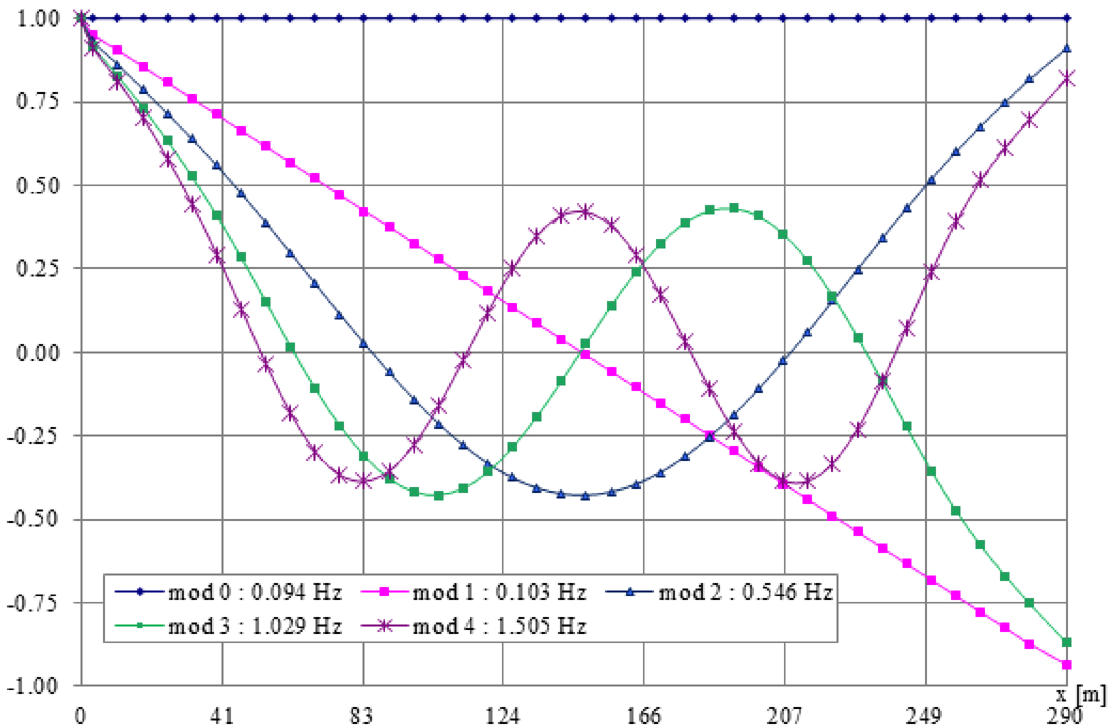

Figure 23.Natural modes in full loading condition

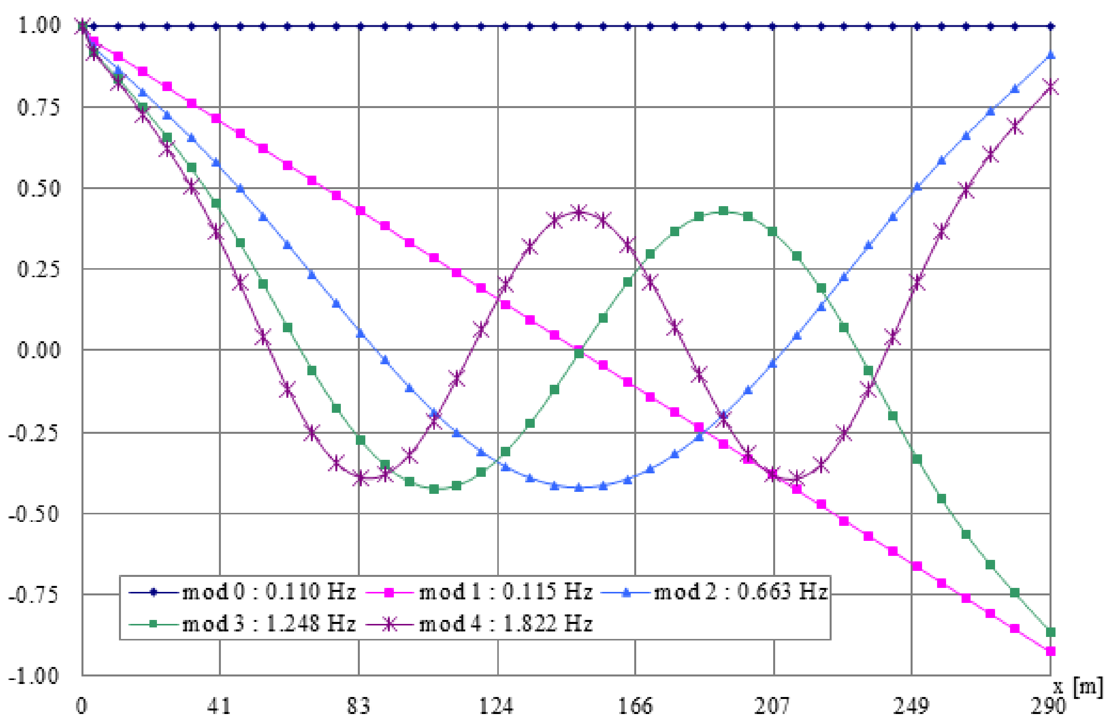

Figure 24.Natural modes in ballast loading condition

3.3. The Bulk Carrier Ship 3D-CAD/FEM Model – Model Presentation

3.3.1. Tools Used For Calculation

The ship shell surface was made in MaxSurf ver.13.0 (MaxSurf, 2012) and the ship hull main geometry (main deck, inner side, double bottom, transversal bulkheads etc.) was developed directly in Geometry module from FEMAP ver. 10.2 (Femap, 2010).

The 3D-FEM model developed over the full ship length was modelled with FEMAP ver. 10.2 (Femap, 2010). The global strength analysis (constraints, loads, stresses) was performed by NASTRAN NX for Windows using FEMAP ver. 10.2 (Femap, 2010) as interactive graphic software program pre and post-processor designed for calculation codes using finite element method.

3.3.2. Limits of the Model, Coordinate System, Units

The 3D-FEM full-extended model represents the entire ship structure including the deckhouse, as shown in Figure 30, the limits of the model are:

- on longitudinal direction: over the full ship length;
- on transversal direction: only one side (PS);
- on vertical direction: from the BL to the main deck of the ship.

The global coordinate system is positioned in AP of the studied bulk carrier, defined in the next figure (Figure 25):

- X-axis: Longitudinal, positive forward;
- Y-axis: Transverse, positive toward portside;
- Z-axis: Vertical, positive upward.

The following units are used in the global-local strength analysis using 3D-FEM model:

- length: millimetres (mm);
- force: Newton (N);
- mass: kilogram (kg).
- stress is in N/mm^2.

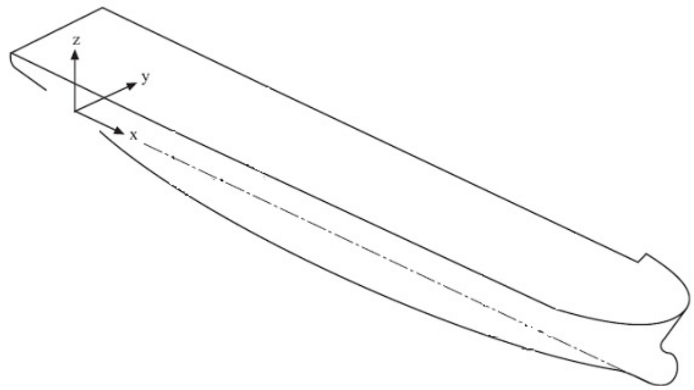

Figure 25. The global coordinate system (GL2011)

3.3.3. Geometry, Mesh and Thickness

The 3D-CAD model presented in Figure 26 was developed to improve the progress of mapped mesh of the 3D-FEM model. In Table 9 are presented the number of the geometrical and mesh objects. The types of elements used to model the structure for the 3D-FEM full-extended model are:

- plate elements used for shell plating, bottom, longitudinal, tank top, cargo tank plates and transverse web plates, primary stiffener webs;

- beam elements used for the rest of structure (secondary stiffeners, the transverse and girder web face plates).

The mesh size is with values between 600.00 - 800.00mm according to the stiffeners spacing for the ship hull structure.

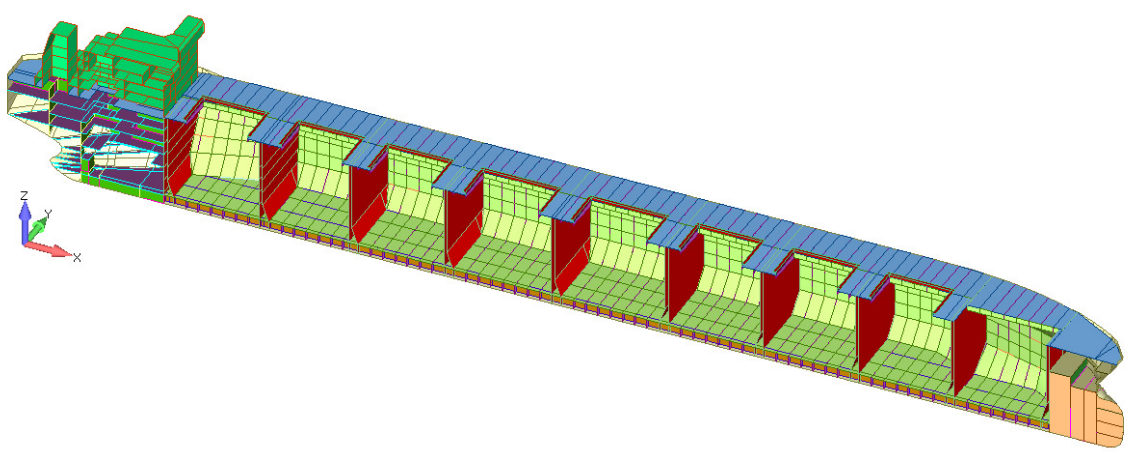

Figure 26. The 3D-CAD model of the bulk carrier ship structure

Table 9. The number of the geometric and mesh objects of the 3D-FEM model

Geometry components	Points	24385
	Curves	26425
	Surfaces	5022
	Solids	2967
Mesh components	Nodes	109810
	Elements	226405
Groups (in Appendix 2 are presented some of the most important structural elements)		26

3.3.4. 3D-FEM Model Description

The 3D-FEM model was modelled in accordance to the scantling calculation presented in Section 2.2. In Figure 27 and Figure 28 are presented typical transverse web frames. A transversal bulkhead from cargo area is presented in Figure 29. The 3D-FEM ship model extended over the full length is presented in Figure 30, and the cargo area is presented in Figure 32. The hull extremities and the machinery space of the ship are represented in the figures: Figure 34 and Figure 35. In Figure 36 is presented the deckhouse of the bulk carrier.

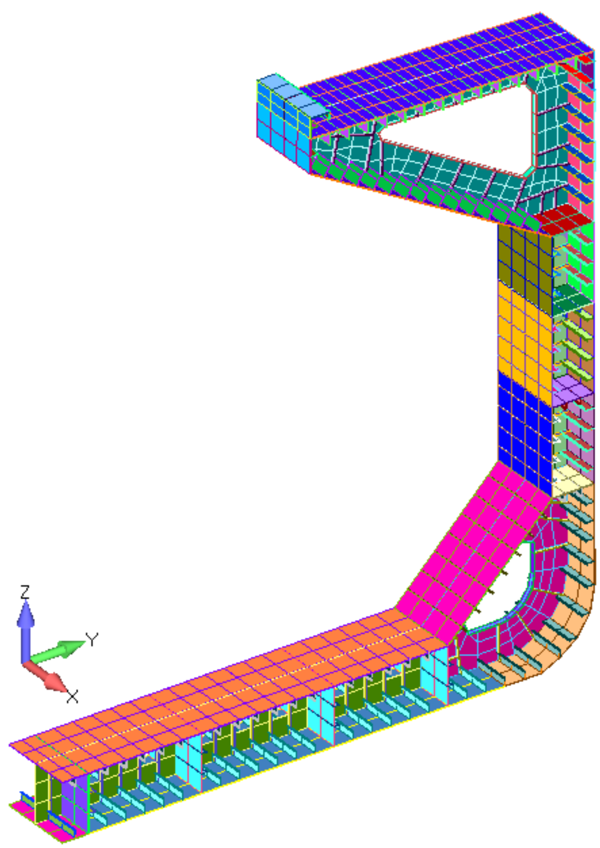

Figure 27. Typical Transverse Web Frame (cargo hold area), 3D-FEM model

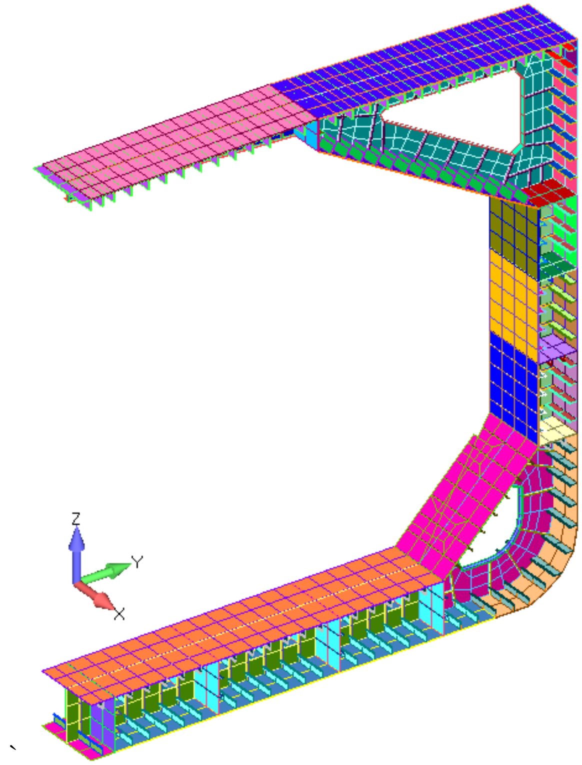

Figure 28.Typical Transverse Web Frame, 3D-FEM model

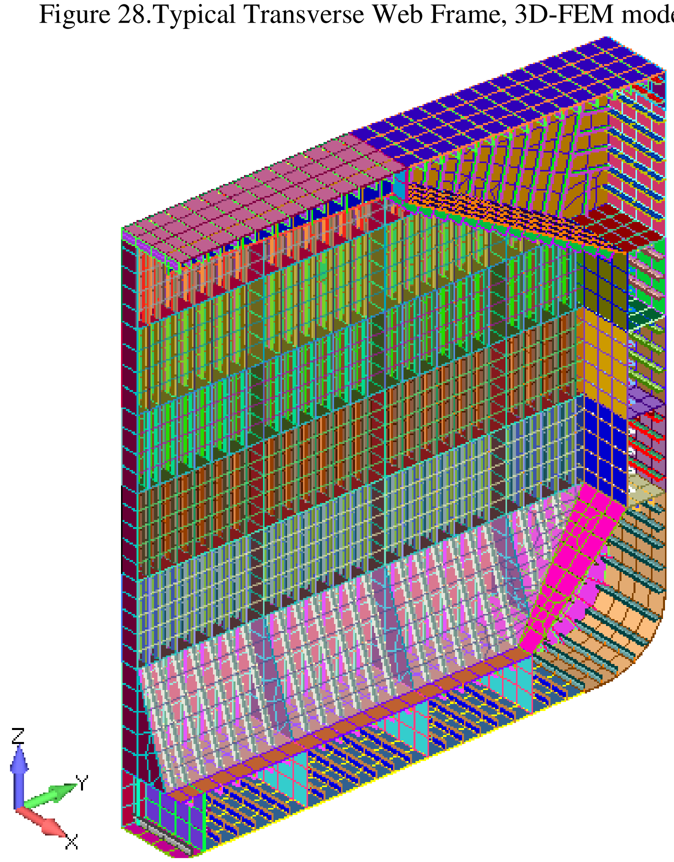

Figure 29.Transversal bulkhead from cargo area (TBH), 3D-FEM model

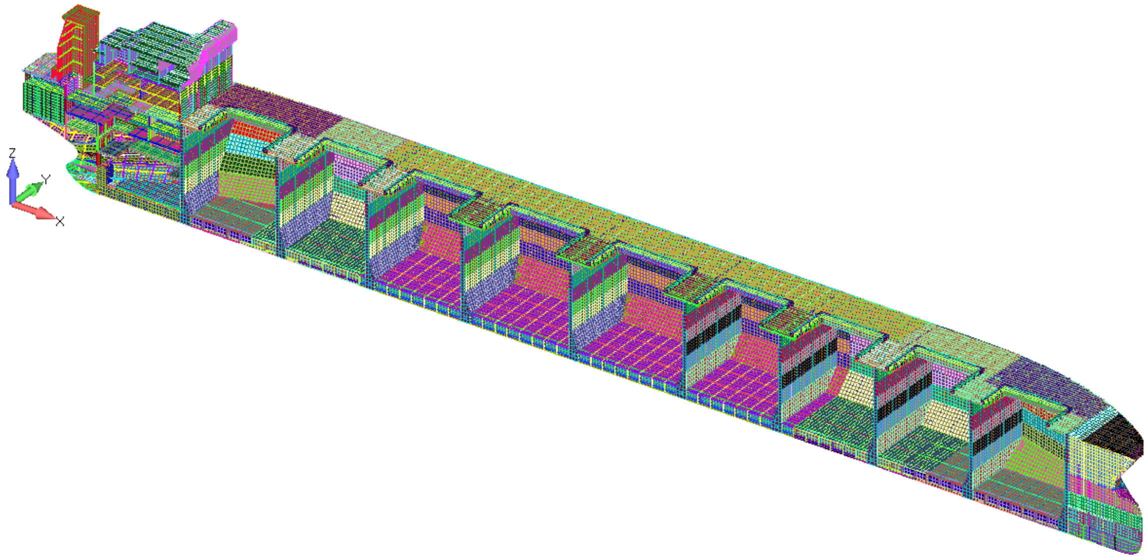

Figure 30. The 3D-FEM model over the full length of the ship, 3D-FEM model

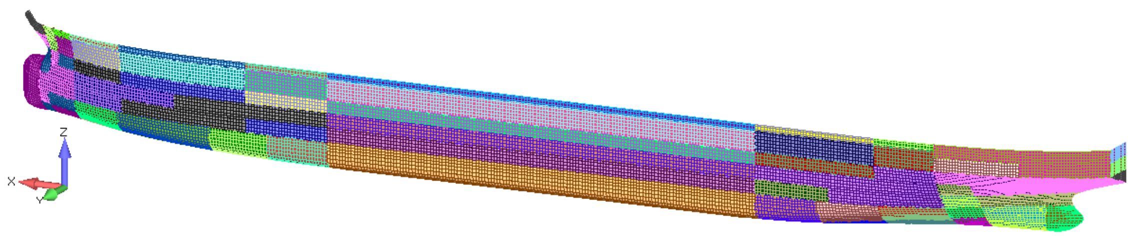

Figure 31 - The side shell of the studied bulk carrier - PS view; 3D-FEM model

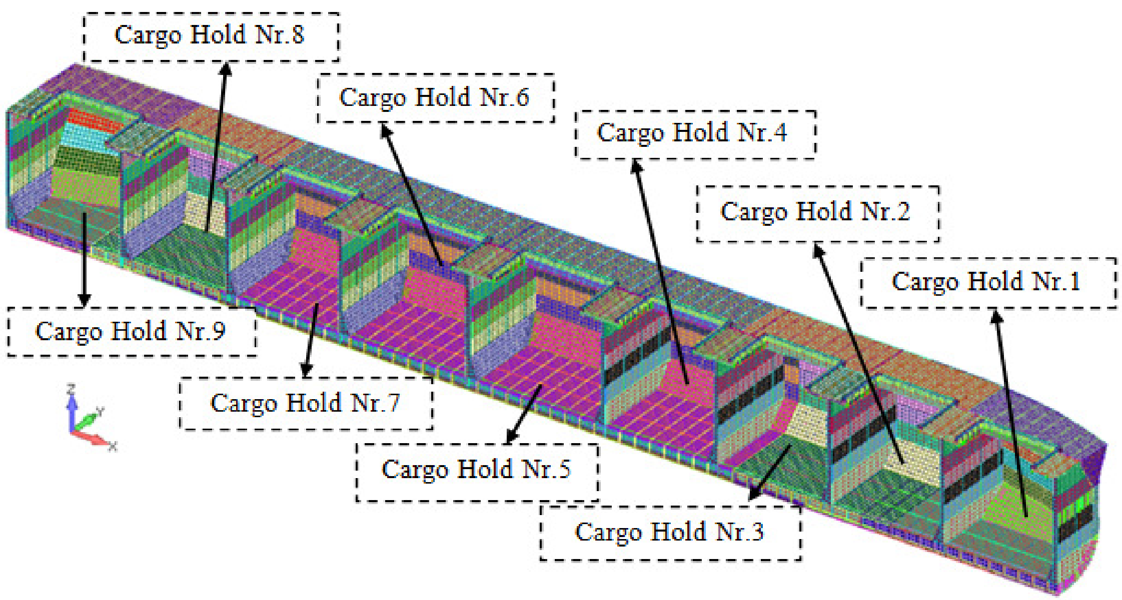

Figure 32.Cargo Area – Hold 1 to Hold 9, 3D-FEM model

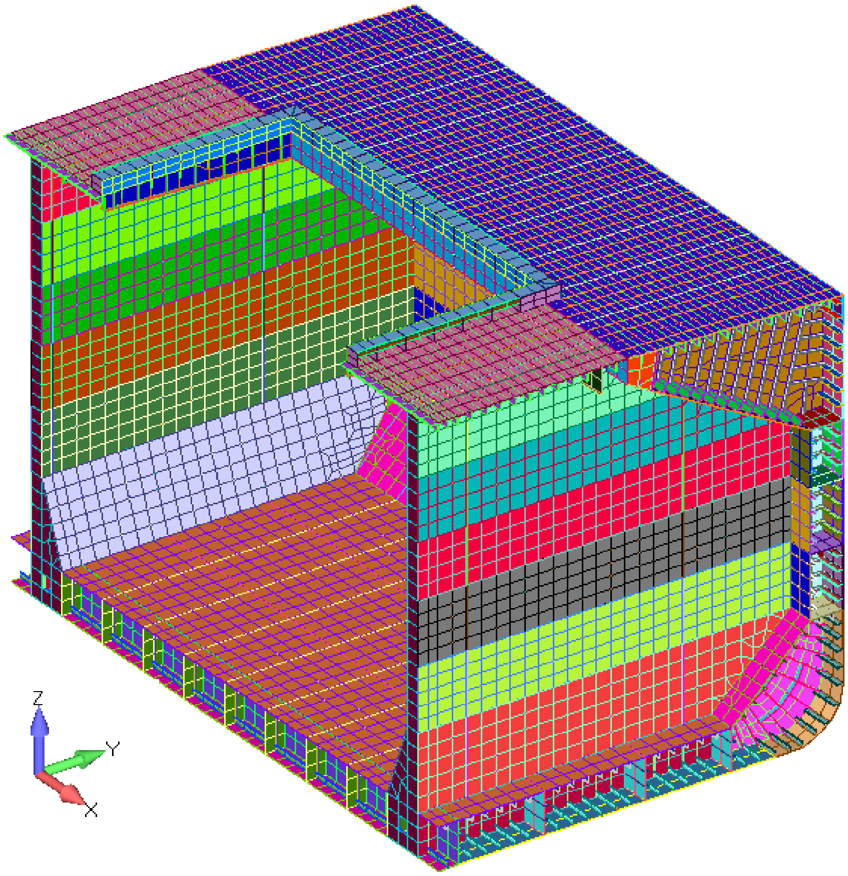

Figure 33. Cargo Hold 5, 3D-FEM model

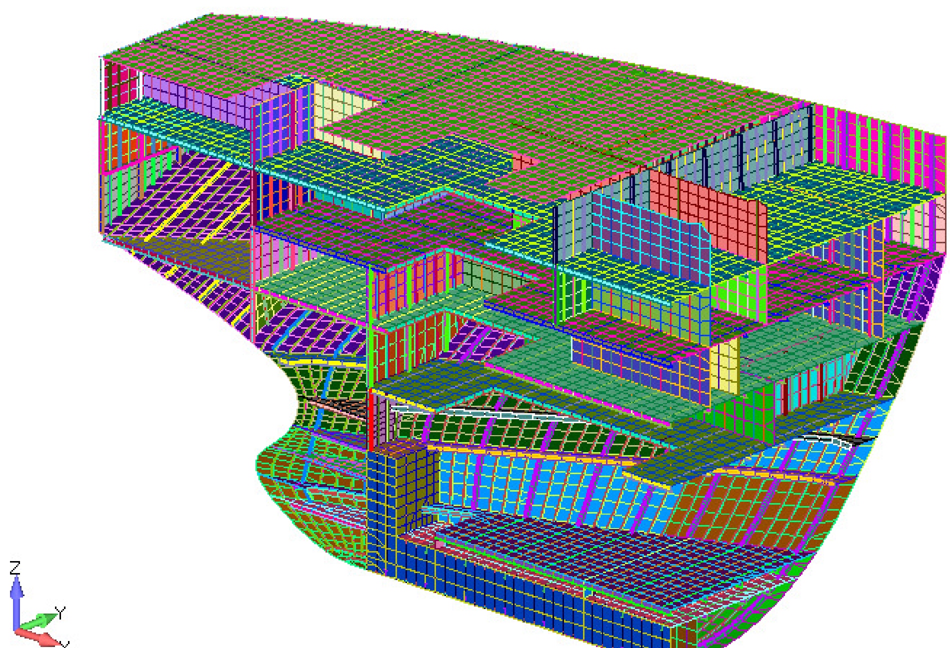

Figure 34.Aft part and machinery space, 3D-FEM model

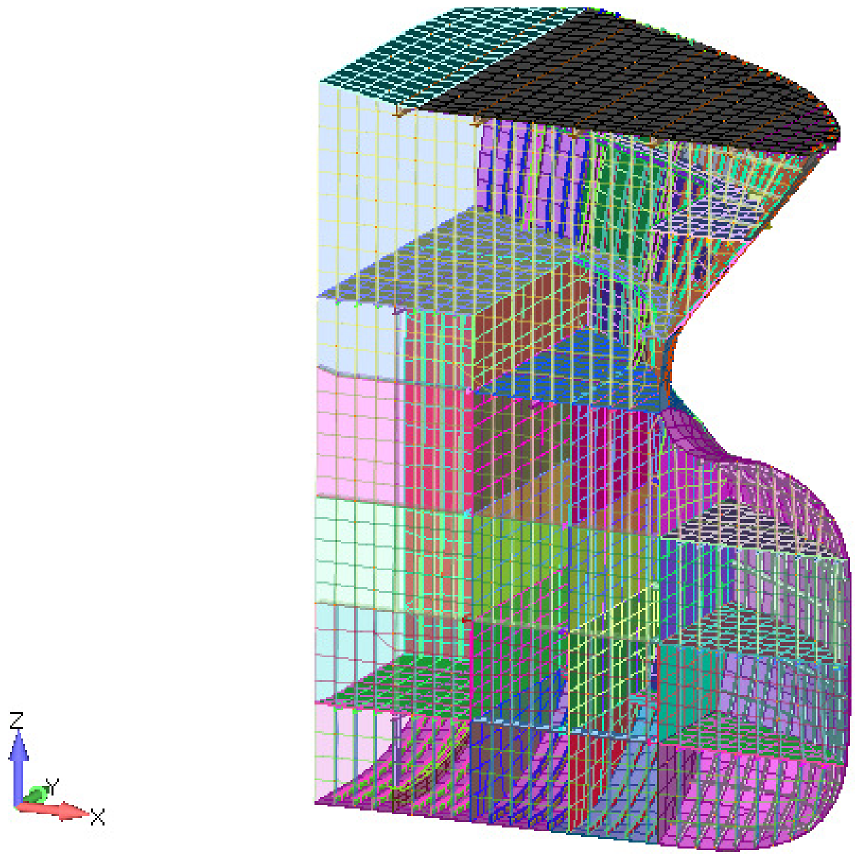

Figure 35.For Part, 3D-FEM Model. 3D-FEM model

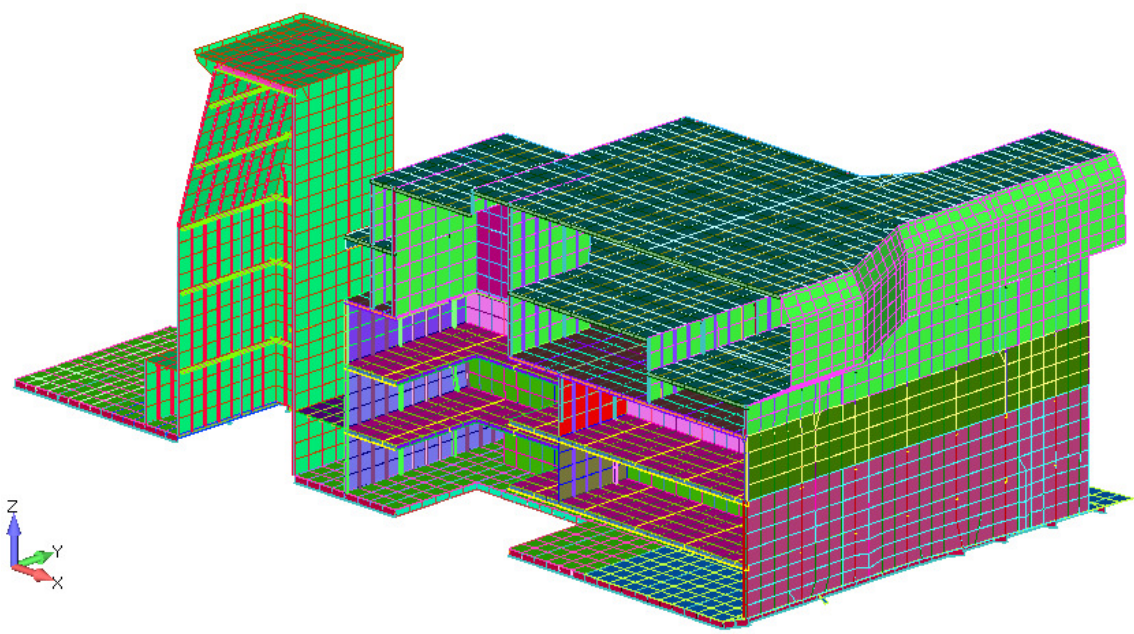

Figure 36**.** Deckhouse of the bulk carrier, 3D-FEM Model, 3D-FEM model

3.3.5. Boundary Conditions

The boundary conditions used for the 3D-FEM full extended model are:

- the first set of boundary conditions were modelled in order to consider the symmetry of the model, for this constraints were modelled in every nod of the CL of the ship (see Table 10 and Figure 37);

- the second set of boundary conditions were the vertical support conditions. For this were modelled two nodes on the extremities of the ship in the centre line plane, noted ND_{pv} at aft peak and ND_{pp} at fore peak (see Table 10 and Figure 37).

Table 10 – Boundary Conditions for 3D-FEM full extended model

Location of the independent point	Translational			Rotational		
	Ux	Uy	Uz	Rx	Ry	Rz
ND_{pv} at aft peak	Fix	Fix	Fix	Fix	-	Fix
ND_{pp} at fore peak	-	Fix	Fix	Fix	-	Fix
Symmetry Condition in CL	-	Fix	-	Fix	-	-

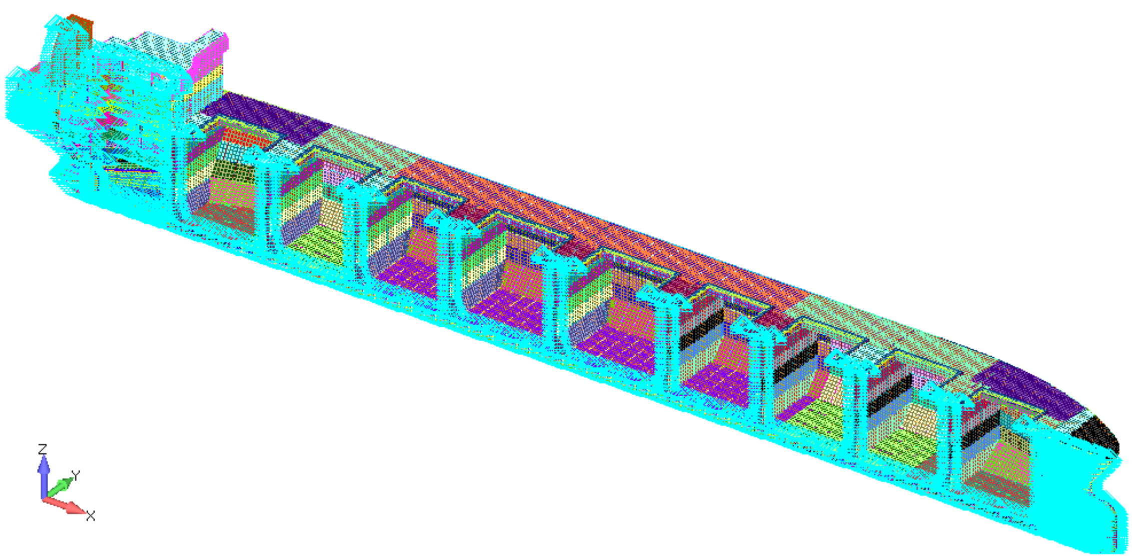

Figure 37 - Boundary Conditions for 3D-FEM full extended model

3.3.6. Loading Conditions

There were modelled two loading cases: full cargo load case (LC_F) and Ballast load case (LC_B). These loading conditions were modelled according to CSR for Bulk Carrier – Ch. 4 – Design Loads – App. 2 – Standard Loading Condition for Direct Strength Analysis and GL – I Ship Technology – Part 1 – Ch. 1 – Hull Structures – Sec. 4 – Design Loads and Sec. 5 – Longitudinal Strength.

The analysis was performed using the still water conditions (h_w = 0) and the equivalent quasi-static head waves with the wave height h_w = 1.0 to 12.0 m for sagging and hogging conditions and for the specific wave height h_w = 10.65m (GL2011) also in sagging and hogging conditions.

In Table 11 to Table 14 the next notations represent: the medium this case the medium draft (d_m), aft draft (d_{pp}), forward draft (d_{pv}) and trim parameters that define the position of the median plane of the equivalent quasi-static wave.

The full cargo loading conditions (LC_F) in still water and h_w = 1.0 to 12.0m in hogging and sagging are presented in Table 11 and
Table 12, in this case all cargo hold are loaded to their maximum capacity and the ballast tanks are empty. In Table 13 and Table 14 are presented the ballast loading conditions (LC_B) in still water and h_w = 1.0 to 12.0m in hogging and sagging, in this case all the ballast tanks are loaded to their maximum capacity.

Table 11. Full cargo loading conditions (LC_F) in still water (h_w=0.0) and hogging for h_w = 1.0 to 12.0m

	Load Case	h_w[m]	d_m [m]	d_{aft} [m]	d_{fore} [m]	trim [rad]
Still Water Cond.	LC_F 1	0	14.796	15.359	15.073	0.00194
Hogging Cond. Tank Load: the 9 cargo holds are loaded to the maximum capacity.	LC_F 2	-1	14.739	15.273	15.003	0.00184
	LC_F 3	-2	14.667	15.198	14.929	0.00183
	LC_F 4	-3	14.579	15.130	14.851	0.0019
	LC_F 5	-4	14.472	15.076	14.770	0.00208
	LC_F 6	-5	14.348	15.032	14.686	0.00236
	LC_F 7	-6	14.204	15.001	14.599	0.00275
	LC_F 8	-7	14.048	14.977	14.508	0.00321
	LC_F 9	-8	13.875	14.966	14.414	0.00376
	LC_F 10	-9	13.691	14.959	14.318	0.00437
	LC_F 11	-10	13.496	14.958	14.219	0.00504
	LC_F 12	-10.65	13.364	14.962	14.154	0.00551
	LC_F 13	-11	13.291	14.964	14.118	0.00577
	LC_F 14	-12	13.077	14.974	14.015	0.00654

Table 12.Full cargo loading conditions (LC_F) in sagging for h_w = 1.0 to 12.0m

	Load Case	h_w [m]	d_m [m]	d_{aft} [m]	d_{fore} [m]	rim [rad]
Sagging Cond. Tank Load: the 9 cargo holds are loaded to the maximum capacity.	LC_F 15	1	14.839	15.451	15.140	0.00211
	LC_F 16	2	14.871	15.549	15.204	0.00234
	LC_F 17	3	14.890	15.653	15.265	0.00263
	LC_F 18	4	14.898	15.762	15.321	0.00298
	LC_F 19	5	14.902	15.871	15.377	0.00334
	LC_F 20	6	14.902	15.981	15.429	0.00372
	LC_F 21	7	14.903	16.086	15.481	0.00408
	LC_F 22	8	14.904	16.189	15.531	0.00443
	LC_F 23	9	14.907	16.288	15.581	0.00476
	LC_F 24	10	14.911	16.3846	15.629	0.00508
	LC_F 25	10.65	14.916	16.442	15.659	0.00526
	LC_F 26	11	14.919	16.473	15.676	0.00536
	LC_F 27	12	14.929	16.557	15.722	0.00561

Table 13. Ballast loading conditions (LC_B) in still water (hw=0.0m) and hogging h_w = 1.0 to 12.0m

	Load Case	h_w[m]	d_m[m]	d_{aft} [m]	d_{fore} [m]	trim [rad]
Still Water Cond.	LC_B 1	0	8.922	8.142	8.511	-0.00269
Hogging Cond. Tank Load: all ballast tanks are loaded to their maximum capacity.	LC_B 2	-1	9.134	8.134	8.607	-0.00345
	LC_B 3	-2	8.472	8.170	8.313	-0.00104
	LC_B 4	-3	8.237	8.188	8.211	-0.00017
	LC_B 5	-4	7.999	8.205	8.108	0.00071
	LC_B 6	-5	7.754	8.227	8.003	0.00163
	LC_B 7	-6	7.502	8.250	7.896	0.00258
	LC_B 8	-7	7.247	8.273	7.788	0.00354
	LC_B 9	-8	6.988	8.296	7.677	0.00451
	LC_B 10	-9	6.723	8.321	7.564	0.00551
	LC_B 11	-10	6.450	8.347	7.449	0.00654
	LC_B 12	-10.65	6.269	8.363	7.372	0.00722
	LC_B 13	-11	6.169	8.373	7.330	0.0076
	LC_B 14	-12	5.874	8.406	7.207	0.00873

Table 14. Ballast loading conditions (LC_B) in sagging for h_w = 1.0 to 12.0m

	Load Case	h_w[m]	d_m[m]	d_{aft} [m]	d_{fore} [m]	trim [rad]
Sagging Cond. Tank Load: all ballast tanks are loaded to their maximum capacity.	LC_B 15	1	9.134	8.134	8.607	-0.00345
	LC_B 16	2	9.333	8.132	8.700	-0.00414
	LC_B 17	3	9.519	8.138	8.791	-0.00476
	LC_B 18	4	9.691	8.151	8.880	-0.00531
	LC_B 19	5	9.847	8.174	8.965	-0.00577
	LC_B 20	6	9.982	8.207	9.047	-0.00612
	LC_B 21	7	10.099	8.252	9.126	-0.00637
	LC_B 22	8	10.196	8.308	9.202	-0.00651
	LC_B 23	9	10.274	8.377	9.275	-0.00654
	LC_B 24	10	10.332	8.459	9.346	-0.00646
	LC_B 25	10.65	10.366	8.516	9.392	-0.00638
	LC_B 26	11	10.379	8.549	9.417	-0.00631
	LC_B 27	12	10.406	8.652	9.483	-0.00605

3.4. The Numerical Analysis of the Ship Hull Global-local Strength based on Equivalent 1D-girder and 3D-FEM Full Extended Models

The numerical results presented in this part of the study are the maximum deck, bottom and side shell stresses, based on 3D-FEM and 1D girder models. These results are used to complete the stress 3D/1D correlation factors calculation, as input data for the next parts of this study.

3.4.1. Full Loading Case

In the next figures are presented the numerical results of the ship hull global-local strength analysis for the full load case:

- in Table 15 is presented in the maximum ship girder deformation in vertical direction in sagging and hogging conditions;

- the bottom stress distribution are presented in Figure 38 and Figure 41 based on the 1D-girder analysis (σ_{xB} in [N/mm^2]) and in Figure 45 and Figure 49 based on the 3D-FEM analysis (σ_{vonB} in [N/mm^2]), for head waves h_w =0.0 to 12.0m in sagging and hogging conditions;

- the deck stress distribution are presented in Figure 39 and Figure 42 based on the 1D-girder analysis (σ_{xD} in [N/mm^2]) and in Figure 46 and Figure 50 based on the 3D-FEM analysis (σ_{vonD} in [N/mm^2]) , for head waves h_w =0.0 to 12.0m in sagging and hogging conditions;

- the shear stress distribution in the neutral axis (τ_{xz} in [N/mm^2]) are presented in Figure 40 and Figure 43 based on the 1D-girder analysis and in Figure 47 and Figure 51 based on the 3D-FEM analysis, for head waves h_w =0.0 to 12.0m in sagging and hogging conditions;

- in Figure 44 and Figure 48 is present the wave pressure distribution at h_w=10.65m in sagging and hogging conditions.

Table 15. The maximum ship girder deflection in vertical direction, 3D-FEM model, LC_F

h_w [m]	$\lvert w_z \rvert sag$ [m]	$\lvert w_z \rvert hog$ [m]	$\lvert w_z \rvert adm = L/500$ [m]	$\lvert w_z \rvert max / \lvert w_z \rvert adm$
10.65	0.412	0.310	0.580	0.710

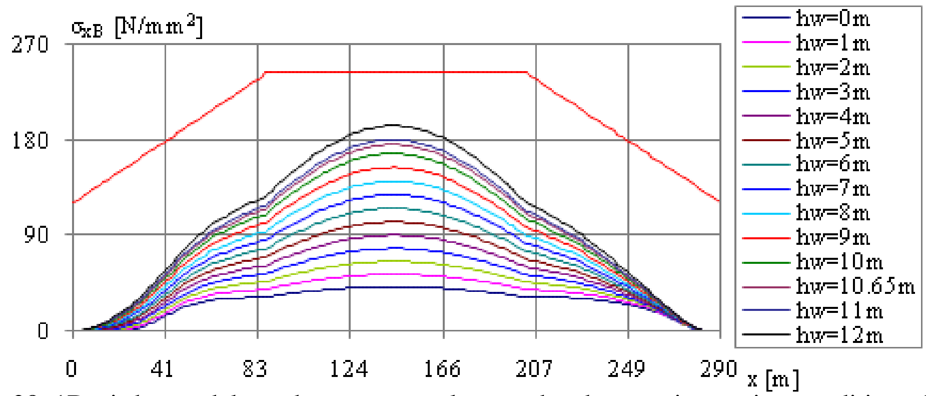

Figure 38. 1D-girder model, σ_{xB} bottom normal stress, head waves in sagging conditions, LC_F

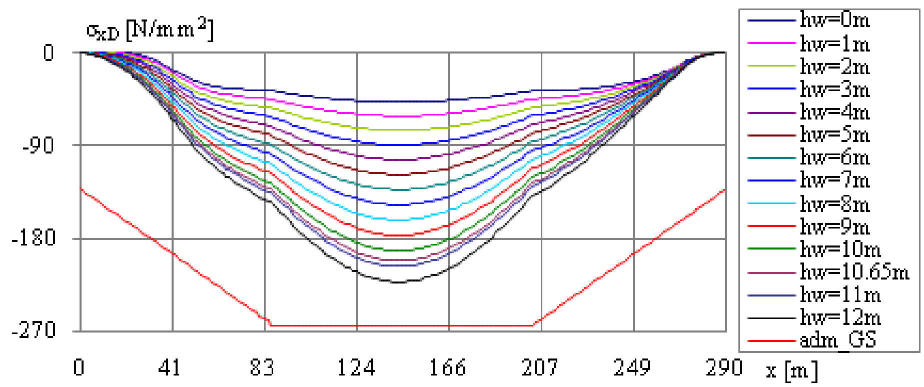

Figure 39.1D-girder model, σ_{xD} deck normal stress, head waves in sagging conditions, LC_F

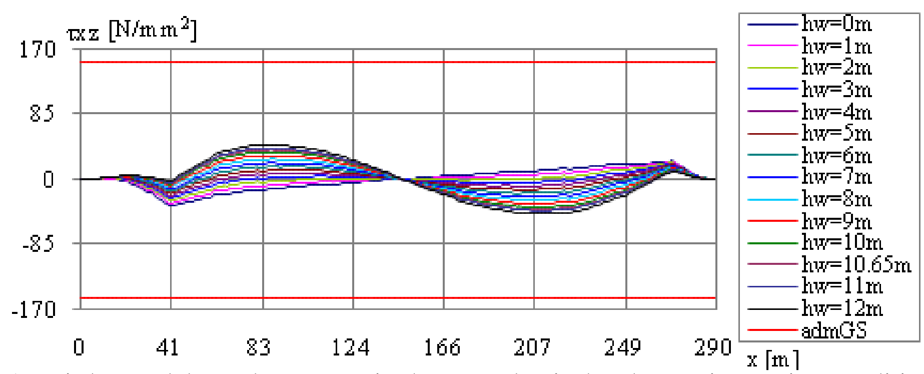

Figure 40.1D-girder model, τ_{xz} shear stress in the neutral axis, head wave in sagging conditions. LC_F

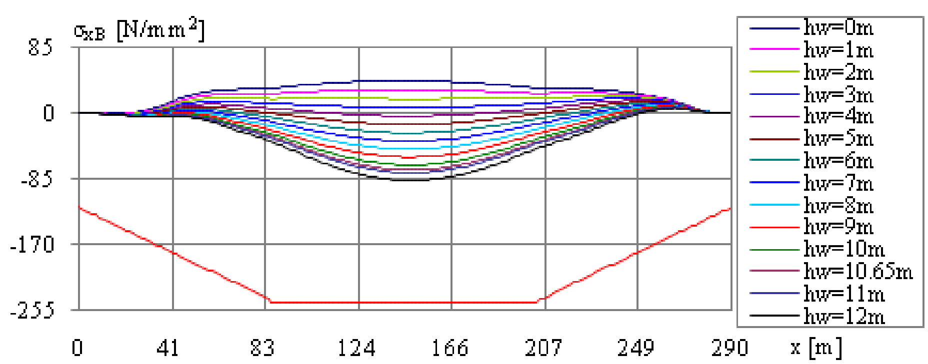

Figure 41. 1D-girder model, σ_{xB} bottom normal stress, head waves in hogging conditions, LC_F

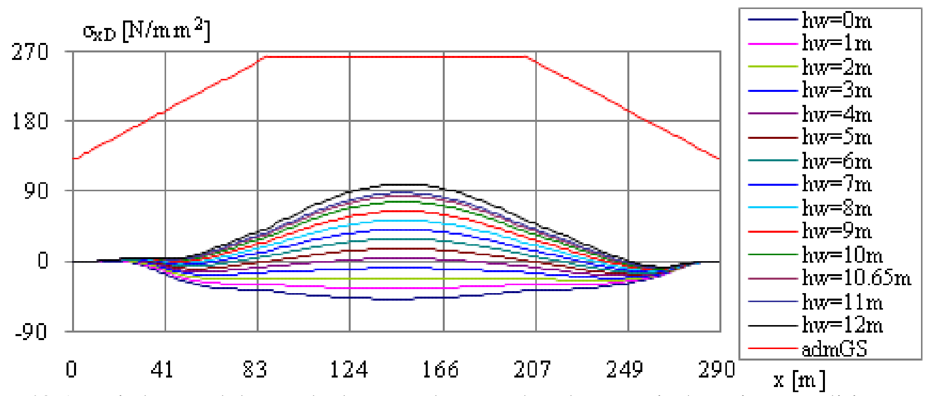

Figure 42.1D-girder model, σ_{xD} deck normal stress, head waves in hogging conditions, LC_F

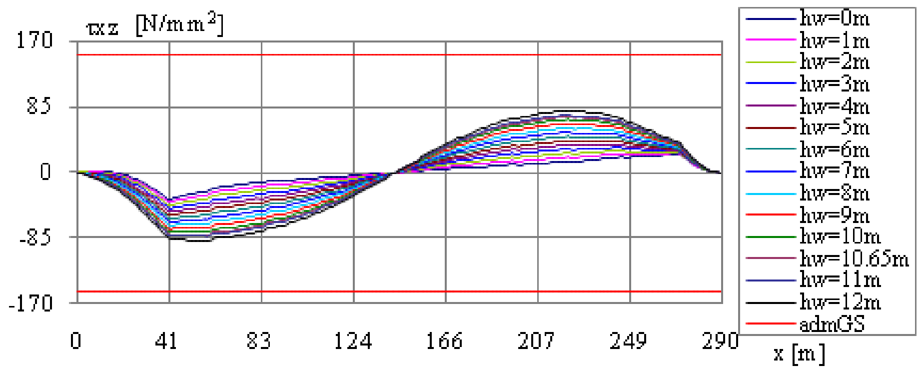

Figure 43.1D-girder model, τ_{xz} shear stress in the neutral axis, head wave in hogging conditions, LC_F

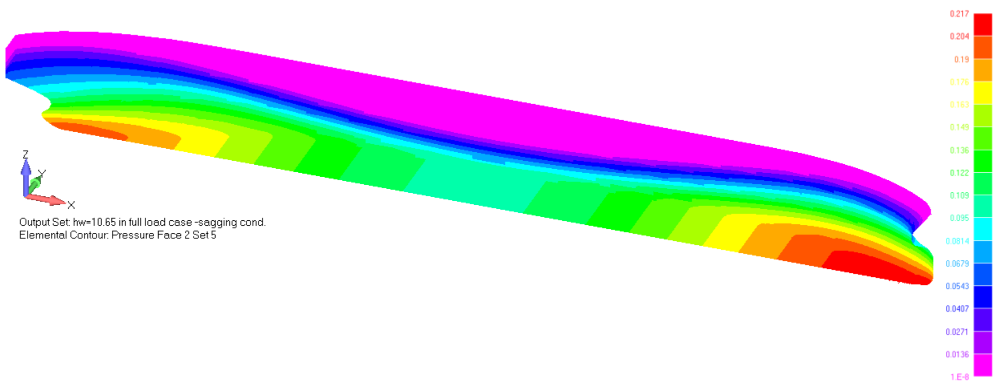

Figure 44. Wave pressure distribution at h_w=10.65m at full load case - sagging conditions

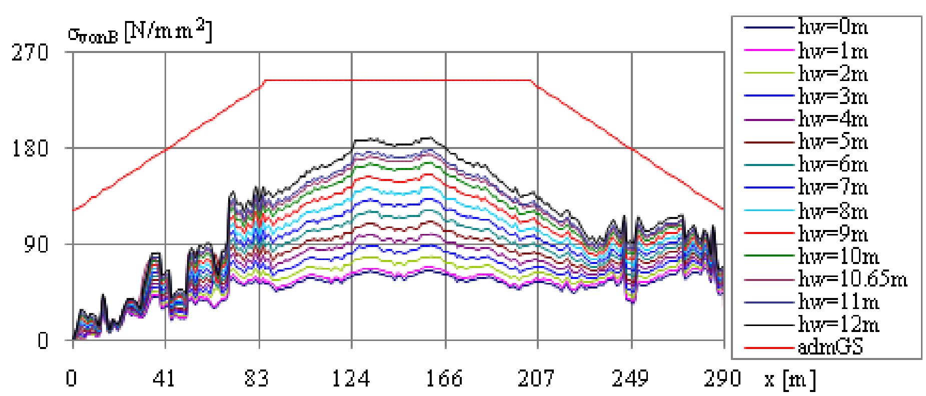

Figure 45. 3D-FEM model, σ_{vonB} bottom von Mises stress, head waves in sagging conditions, LC_F

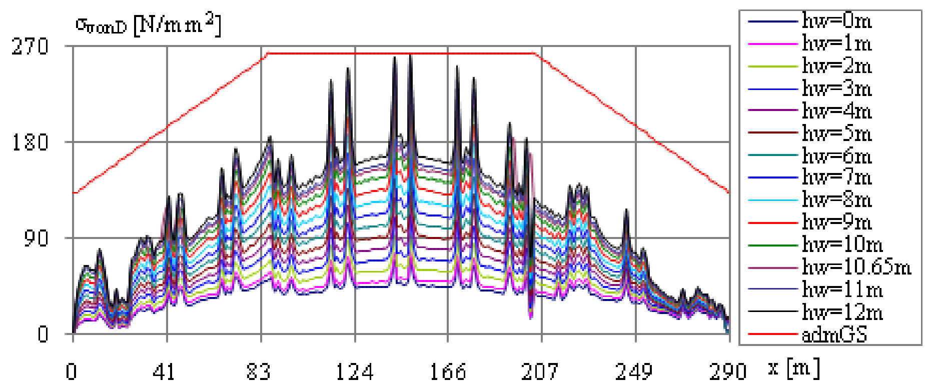

Figure 46. 3D-FEM model, σ_{vonD} deck von Mises stress, head waves in sagging conditions, LC_F

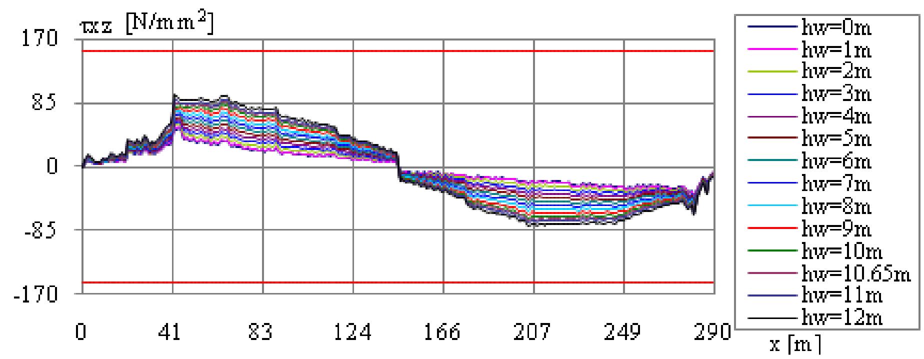

Figure 47. 3D_FEM model, τ_{xz} shear stress in the neutral axis, head wave in hogging cond., LC_F

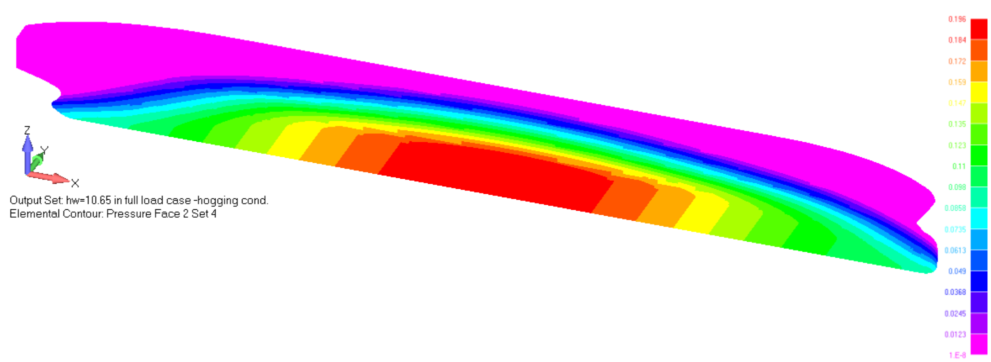

Figure 48. Wave pressure at h_w=10.65m at full load case - hogging conditions

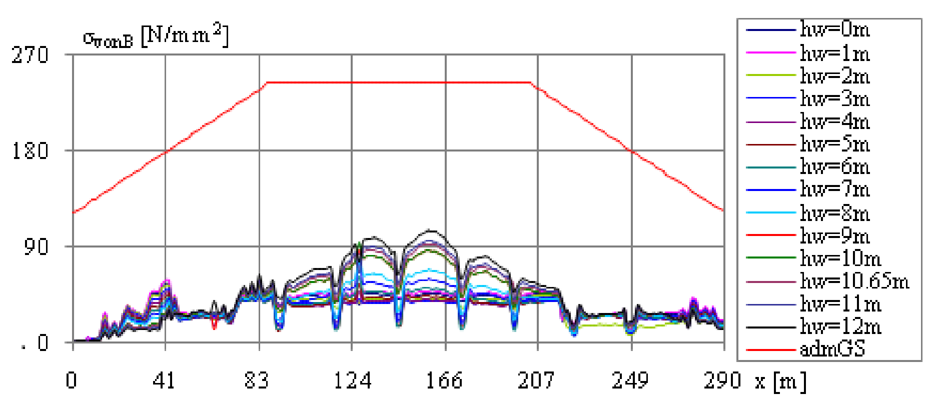

Figure 49. 3D-FEM model, σ_{vonB} bottom von Mises stress, head waves in hogging conditions, LC_F

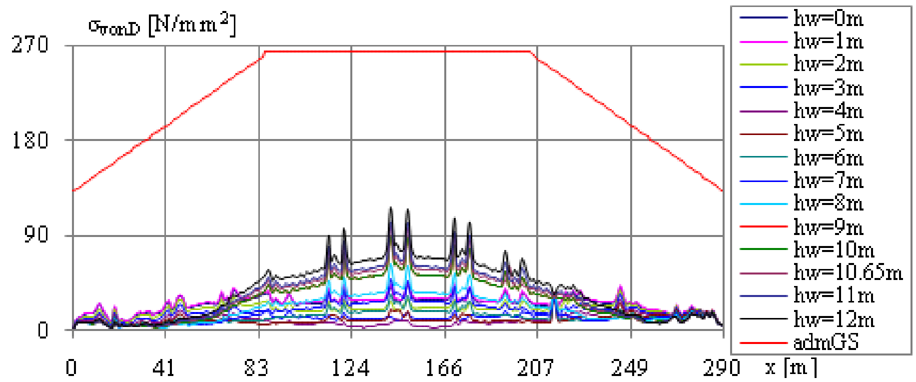

Figure 50. 3D-FEM model, σ_{vonD} deck von Mises stress, head waves in hogging conditions, LC_F

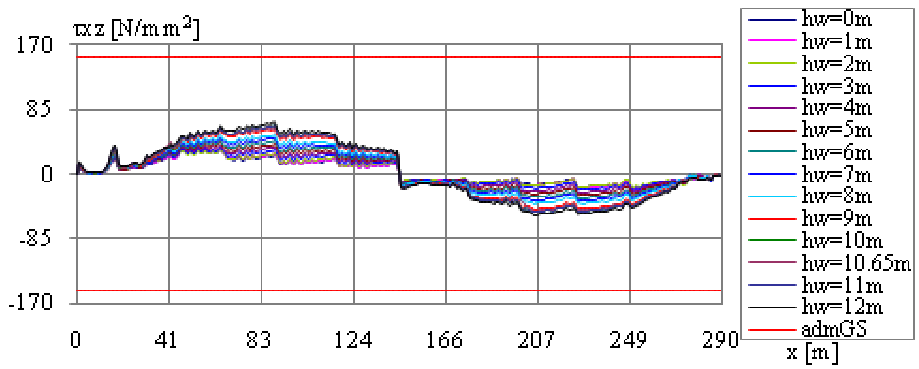

Figure 51. 3D-FEM model, τ_{xz} shear stress in the neutral axis, head wave in hogging cond., LC_F

3.4.2. Ballast Loading Case

For the ballast load case the numerical results of the ship hull global-local strength analysis are presented in the following figure:

- in Table 16 is presented in the maximum ship girder deformation in vertical direction in sagging and hogging conditions;

- the bottom stress distribution are presented in Figure 52 and Figure 55 based on the 1D-girder analysis (σ_{xB} in [N/mm^2]) and in Figure 59 and Figure 63 based on the 3D-FEM analysis (σ_{vonB} in [N/mm^2]), for head waves h_w =0.0 to 12.0m in sagging and hogging conditions;

- the deck stress distribution are presented in Figure 53 and Figure 56 based on the 1D-girder analysis (σ_{xD} in [N/mm^2]) and in Figure 60 and Figure 64 based on the 3D-FEM analysis (σ_{vonD} in [N/mm^2]), for head waves h_w =0.0 to 12.0m in sagging and hogging conditions;

- the shear stress distribution in the neutral axis (τ_{xz} in [N/mm^2]) are presented in Figure 54 and Figure 57 based on the 1D-girder analysis and in Figure 61 and Figure 65 based on the 3D-FEM analysis, for head waves h_w =0.0 to 12.0m in sagging and hogging conditions;

- in Figure 58 and Figure 62 is present the wave pressure distribution at h_w=10.65m in sagging and hogging conditions.

Table 16. The maximum ship girder deflection in vertical direction, 3D-FEM model, LC_B

h_w [m]	$\lvert w_z \rvert sag$ [m]	$\lvert w_z \rvert hog$ [m]	$\lvert w_z \rvert adm = L/500$ [m]	$\lvert w_z \rvert max / \lvert w_z \rvert adm$
10.65	0.305	0.271	0.580	0.525

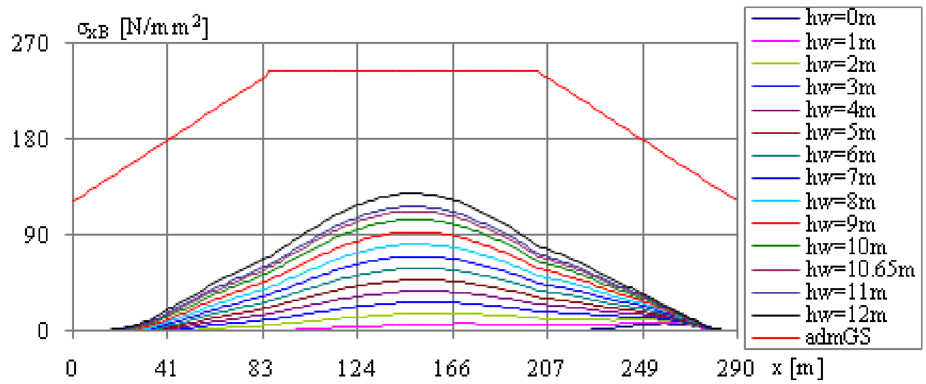

Figure 52. 1D-girder model, σ_{xB} bottom normal stress, head waves in sagging conditions, LC_B

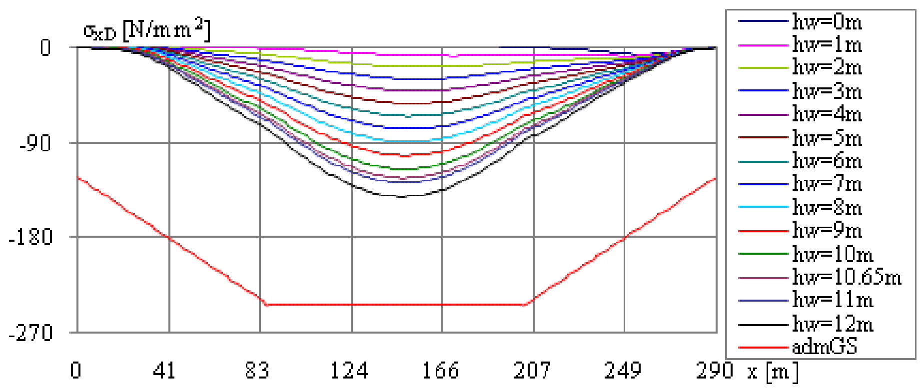

Figure 53.1D-girder model, σ_{xD} deck normal stress, head waves in sagging conditions, LC_B

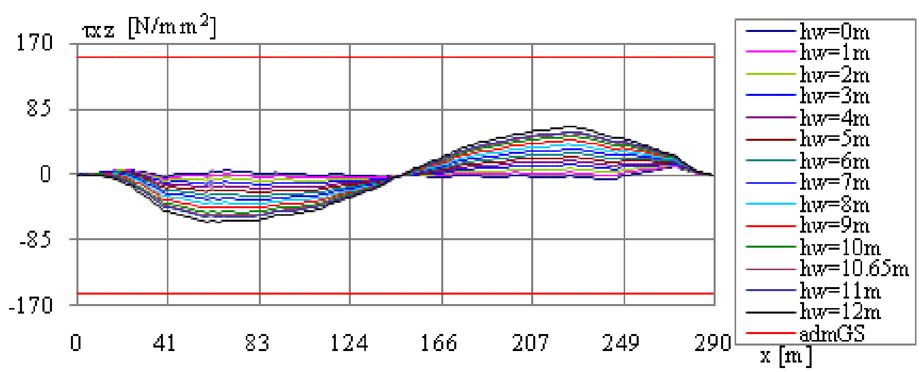

Figure 54.1D-girder model, τ_{xz} shear stress in the neutral axis, head wave in sagging conditions. LC_B

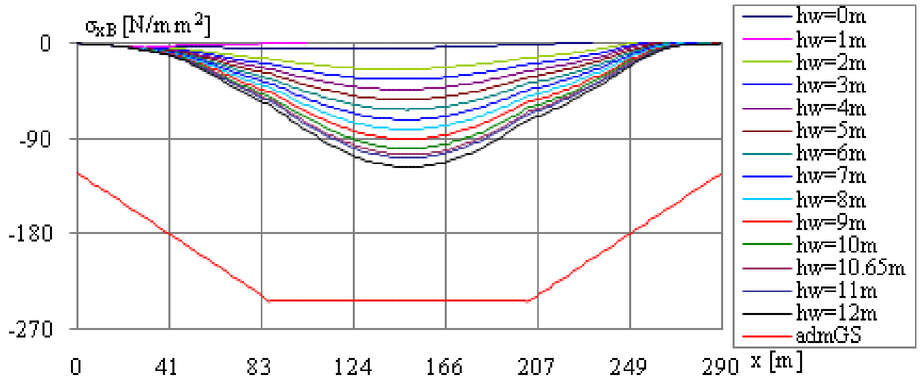

Figure 55. 1D-girder model, σ_{xB} bottom normal stress, head waves in hogging conditions, LC_B

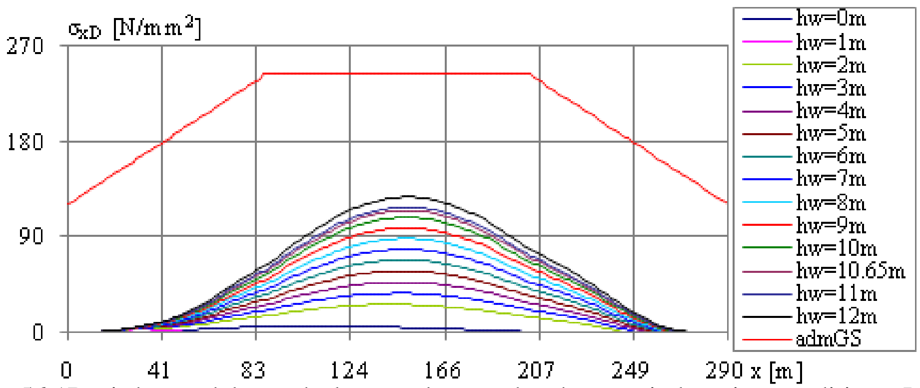

Figure 56.1D-girder model, σ_{xD} deck normal stress, head waves in hogging conditions, LC_B

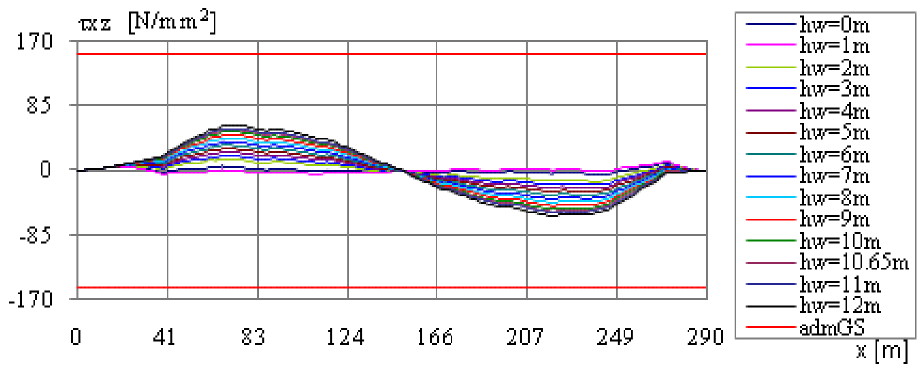

Figure 57.1D-girder model, τ_{xz} shear stress in the neutral axis, head wave in hogging conditions ,LC_B

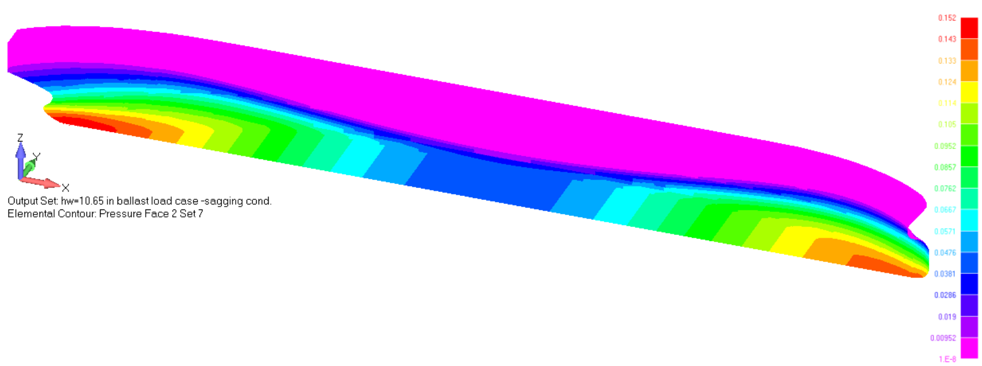

Figure 58. Wave pressure at h_w=10.65m at ballast load case - sagging conditions

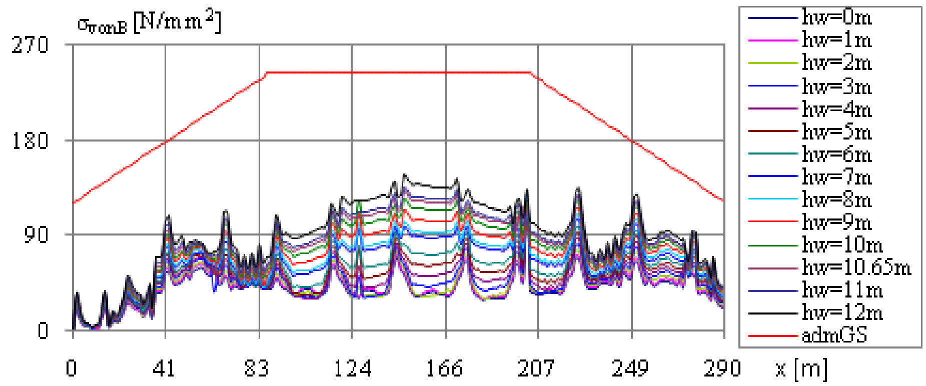

Figure 59. 3D-FEM model, σ_{vonB} bottom von Mises stress, head waves in sagging conditions, LC_B

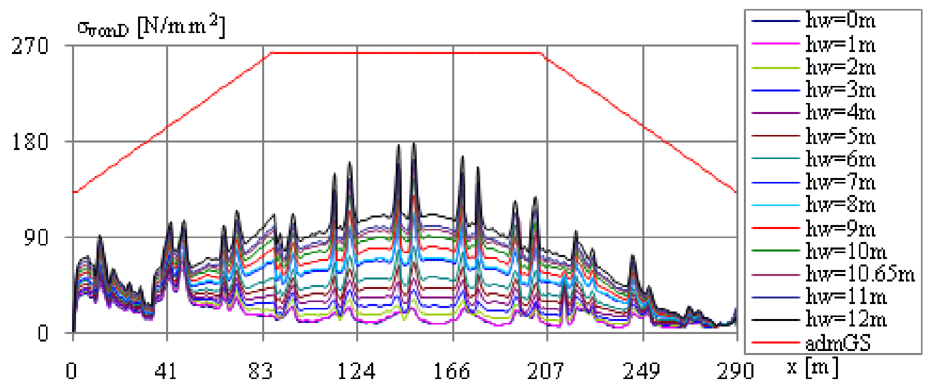

Figure 60. 3D-FEM model, σ_{vonD} deck von Mises stress, head waves in sagging conditions, LC_F

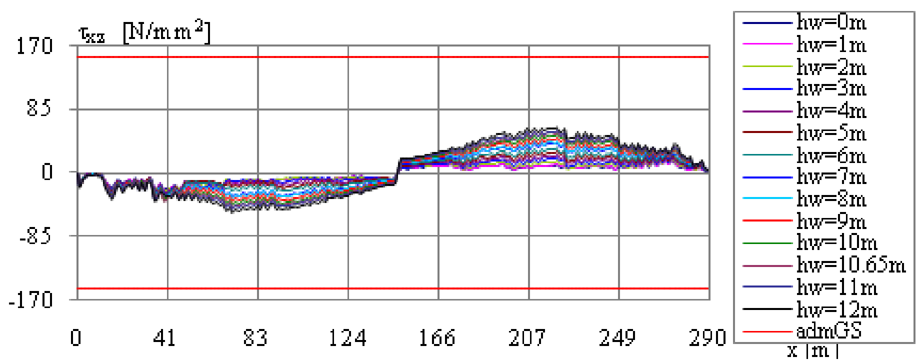

Figure 61. 3D-FEM model, τ_{xz} shear stress in the neutral axis, head wave in sagging cond. ,LC_B

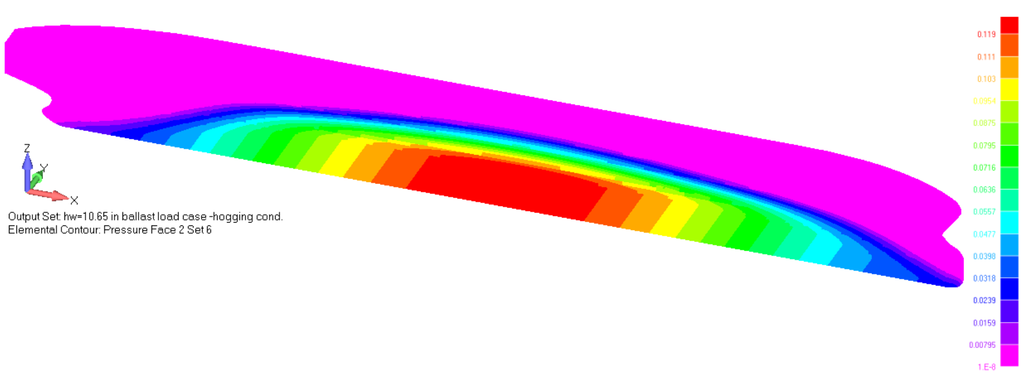

Figure 62. Wave pressure at h_w=10.65m at ballast load case - hogging conditions

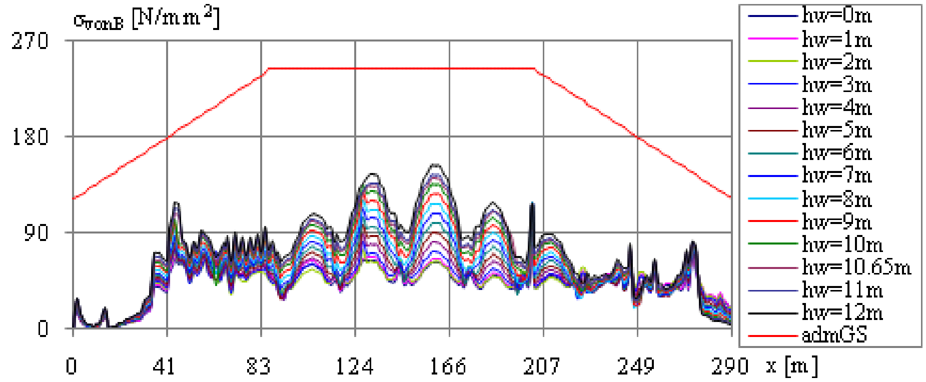

Figure 63. 3D-FEM model, σ_{vonB} bottom von Mises stress, head waves in hogging conditions, LC_B

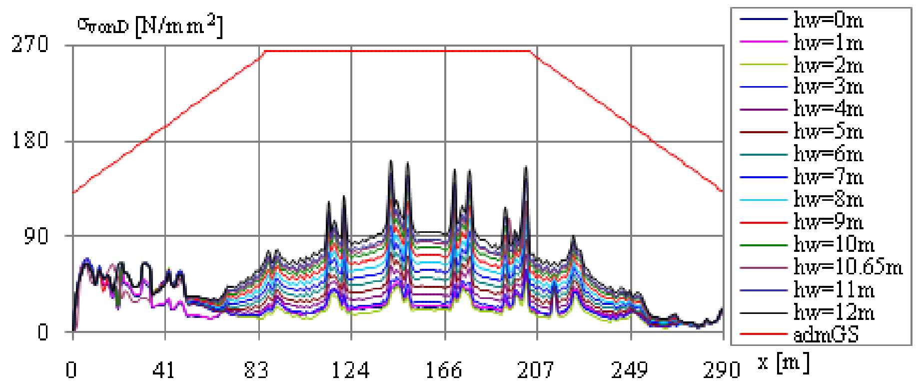

Figure 64. 3D-FEM model, σ_{vonD} deck von Mises stress, head waves in hogging conditions, LC_B

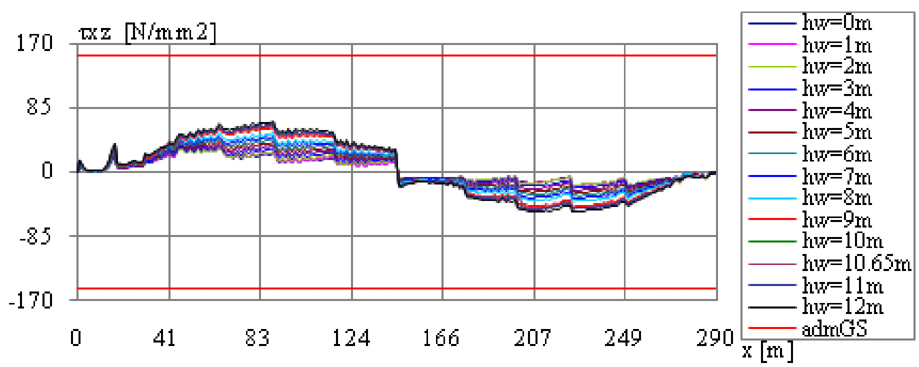

Figure 65. 3D-FEM model, τ_{xz} shear stress in the neutral axis, head wave in hogging cond. ,LC_B

4. NUMERICAL HYDROELASTIC LINEAR AND NON-LINEAR DYNAMIC RESPONSE

In this section of the study the numerical analysis is focused on the ship girder dynamic response. Based on the hydroelasticity theory, the analysis was carried out on the two selected loading conditions (full and ballast loads) for the studied bulk carrier.

4.1. The Theoretical Model for the Analysis of Linear and Non-linear Ship Dynamic Response based on Hydroelasticity Theory

4.1.1. The Hydroelastic Linear Dynamic Response at Coupled Oscillations and Vibrations in the Vertical Plane

The dynamic analysis at coupled oscillations and vibrations in vertical plane is allowing to determinate the hydroelastic linear dynamic response with the next components: linear vertical oscillations coupled in vertical plane and the global vibration in vertical plane at the resonance between the modal modes of the ship girder and the linear head wave model Airy (Bishop & Price 1979, Bertram 2000).

In the next paragraphs is presented the theory of the hydroelastic linear dynamic response (Bishop & Price 1979, Domnisoru 1998), under the linear wave model Airy, considering the ship as an equivalent 1D-girder elastic, model type Timoshenko, and hydrodynamic forces model using strip theory, in generalized formulation of Gerritsma and Beukelman, taking into account the ship vertical deformations. The dynamic response of the ship hull is decomposed using the modal analysis method, taking in considerations the first two oscillations modes (r = 0,1 - vertical and pitch), and the first natural vibrations mode in vertical plane of the ship hull (r = 2,n). In this case of the analysis are neglected all the geometric and hydrodynamic nonlinearities.

Based on the dynamic equilibrium equations of the elastic ship hull in vertical plane, the generalized motion equation have the following expression:

$$\begin{gathered} m(x)\ddot{w}(x,t) - \left[GA_{fz}(x)(\gamma(x,t) + \alpha(x)\dot{\gamma}(x,t))\right]' = F_h(x,t); \\ j_y(x)\ddot{\theta}(x,t) - \left[EI_y(x)\left(\theta'(x,t) + \beta\dot{\theta}'(x,t)\right)\right]' - GA_{fz}(x)[\gamma(x,t) + \alpha(x)\dot{\gamma}(x,t)] = 0 \\ w'(x,t) = \theta(x,t) + \gamma(x,t) \end{gathered} \tag{10}$$

where: $w(x,t)$, $\theta(x,t)$ and $\gamma(x,t)$ represent the total motion in vertical plane, the rotation angle at bending and shearing, position x $\in$ [0,L] on the ship length, at a given time moment t, E,G the material characteristics: Young's modulus and shear modulus; $I_y(x)$, $A_{fz}(x)$ the strength characteristics of the ship girder; $m(x)$, $jy(x)$ the inertial characteristics of the hull per unit length; $\alpha(x)$, $\beta(x)$ the damping coefficients at shear and bending; $F_h(x,t)$ the hydrodynamic force per unit length.

The natural vibration modes used to decompose the hydroelastic dynamic response have to satisfy the next orthogonality conditions:

$$\int_0^L m(x)w_r(x)w_s(x)\,dx + \int_0^L j_y(x)\theta_r(x)\theta_s(x)dx = \begin{vmatrix} a_{ss} & r = s \\ 0 & r = s \end{vmatrix}$$
$$\int_0^L EI_y(x)\theta_{r'}(x)\theta_{s'}(x)\,dx + \int_0^L GA_{fz}(x)\gamma_r(x)\gamma_s(x)dx = \begin{vmatrix} c_{ss} & r = s \\ 0 & r = s \end{vmatrix} \quad (11)$$

Using the modal analysis method, the dynamic response of the ship girder is discomposed on the n first natural oscillations and vibrations modes of the ship hull, as following:

$$w(x,t) = \sum_{r=0}^{n} w_r(x)p_r(t);\quad \theta(x,t) = \sum_{r=0}^{n} \theta_r(x)p_r(t);\quad \gamma(x,t) = \sum_{r=0}^{n} \gamma_r(x)p_r(t) \quad (12)$$

where: - $p_r(t)$, $r= 0,n$ represent the principal modal coordinates.

Based on equations (10) and (12), the motion equation system expressed in principal modal coordinates, can be written using the following expressions:

$$[a]\{\ddot{p}(t)\} + [b]\{\dot{p}(t)\} + [c]\{p(t)\} = \{F_h(t)\}$$
$$a_{ss} = \int_0^L \left[m(x)w_s^2(x) + j_y(x)\theta_s^2(x)\right]dx;\quad r,s = 0,n$$
$$b_{rs} = \int_0^L \alpha_r(x)GA_{fz}(x)\gamma_r(x)\gamma_s(x)dx + \int_0^L \beta_r(x)EI_y(x)\theta_{r'}(x)\theta_{s'}(x)dx \quad (13)$$
$$c_{ss} = \int_0^L \left[EI_y(x)\left(\theta_{s'}(x)\right)^2 + GA_{fz}(x)\gamma_s^2(x)\right]dx;\quad F_{hs}(t) = \int_0^L F_h(x,t)w_s(x)dx$$

where: [a], [b], [c] are the inertia, damping and rigidity matrix; {$p(t)$} is the vector of the principal modal coordinates; {$F_h(t)$} is the vector of the generalized hydrodynamic forces.

For the ship with linear wave model Airy, with elongation $\bar{\zeta}_v^*(x,t)$, the relative ship-wave position has the following expression:

$$z_r(x,t) = w(x,t) - \bar{\zeta}_v^*(x,t);\quad \bar{\zeta}_v^*(x,t) = a_w f_s(x)\varepsilon(x)e^{i(kx\cos\mu - \omega_e t)} \quad (14)$$

where: a_w is the wave amplitude; $f_s(x)$, $\varepsilon(x)$ are the correction coefficients of the wave (Smith, averaging on ship breath) ; $k=\omega^2/g$ wave number; ω_e ship-wave encountering circular frequency; μ ship heading angle (180°).

Using the generalized strip theory of Gerritsma and Beukelman, taking into account the total displacement and deformation of the ship hull in vertical plane, the hydroelastic hydrodynamic force per unit length in vertical plan has the following expression:

$$F_h(x,t) = -\left\{\frac{D}{D_t}\left[m_{33}(x)\frac{D_{Zr}(x,t)}{Dt}\right] + N_{33}(x)\frac{D_{Zr}(x,t)}{Dt} + \rho g b_0(x) z_r(x,t)\right\}; \quad (15)$$

$$D/Dt = \partial/\partial t - u_s \cdot \partial/\partial t$$

where: u_s is the ship speed; $m_{33}(x)$, $N_{33}(x)$ are the vertical motion hydrodynamic coefficients per unit length; ρ water density; g gravity acceleration; $b_0(x)$ is the still water line breath function.

From the relations (13) to (15) it can be obtained the vector of the hydrodynamic generalized excitation force:

$$\{F_h(t)\} = -\{[A_h]\{\ddot{p}(t)\} + [B_h]\{\dot{p}(t)\} + [C_h]\{p(t)\} + [\{F_1\} + \{F_2\}]a_w e^{-i\omega_e t}\} \quad (16)$$

$$A_{hsr} = \int_0^L m_{33}(x) w_r(x) w_s(x) dx; \quad r,s = 0,n$$

$$B_{hsr} = \int_0^L [N_{33}(x) - u_s m'_{33}(x)] w_s(x) w_r(x) dx - 2u_s \int_0^L m_{33}(x) w_s(x) w'_r(x) dx$$

$$C_{hsr} = \int_0^L \rho g b_0(x) w_s(x) w_r(x) dx - u_s \int_0^L [N_{33}(x) - u_s m'_{33}(x)] w_s(x) w_{r'}(x) + u_s^2 \int_0^L m_{33}(x) w_s(x) w''_r(x) dx$$

$$F_{1s} = \int_0^L f_1(x) w_s(x) dx; \; F_{2s} = \int_0^L f_2(x) w_s(x) dx; \; s = 0,n$$

$$\alpha_1 = \varepsilon(x) f_s(x)[-\omega^2 m_{33}(x) + \rho g b_0(x)]; \; \alpha_2 = \varepsilon(x) f_s(x) \omega [N_{33}(x) - u_s m'_{33}(x)]$$

$$f_1(x) = \alpha_1 cos(kxcos\mu) + \alpha_2 sin(kxxos\mu); \; f_2(x) = \alpha_1 sin(kxcos\mu) + \alpha_2 cos(kxxos\mu)$$

where: $[A_h]$, $[B_h]$, $[C_h]$ are the inertia, damping and restoring hydrodynamic matrix of the radiation terms; $\{F_1\}$, $\{F_2\}$ are the diffraction terms for the linear wave model Airy.

Using the relations (13) to (16) it can be determinate the final motion equation system:

$$[A]\{\ddot{p}(t)\} + [B]\{\dot{p}(t)\} + [C]\{p(t)\} = [\{F_1\} + i\{F_2\}]a_w e^{-iw_e t} \quad (17)$$

$$[A] = [a] + [A_h]; \quad [B] = [B] + [B_h]; \quad [C] = [c] + [C_h]$$

The steady state dynamic response in the principal modal coordinates formulation, at the excitations with linear wave Airy, has the next expression:

$$\{p(t)\} = [\{p_1\} + i\{p_2\}]e^{-i\omega_e t} \tag{18}$$

From the equations (17) and (18) the differential equations system in complex formulation is transformed in a linear algebraic system formulation that can be solved using numerical procedures (Gauss): (19)

$$[D(\omega_e)]\{p^*\} = \{F^*\}; \quad \{p^*\} = \{\{p_1\},\{p_2\}\}^T; \quad \{F^*\} = \{\{F_1\},\{F_2\}\}^T$$
$$[D(\omega_e)] = \begin{bmatrix} [C(\omega_e)] - \omega_e^2[a(\omega_e)] & \omega_e[B(\omega_e)] \\ -\omega_e[B(\omega_e)] & [C(\omega_e)] - \omega_e^2[A(\omega_e)] \end{bmatrix}$$

The transfer functions for the steady state hydroelastic dynamic response, displacement and deformations, shear forces and bending moments, have the next expressions:

$$H_w(x,\omega_e) = \sqrt{[w^1(x,\omega_e)/a_w]^2 + [w^2(x,\omega_e)/a_w]^2}$$
$$w^1(x,\omega_e) = \sum_{r=0}^{4} w_r(x)p_{1r}\,; \quad w^2(x,\omega_e) = \sum_{r=0}^{4} w_r(x)p_{2r} \tag{20}$$

$$H_T(x,\omega_e) = \sqrt{[T^1(x,\omega_e)/a_w]^2 + [T^2(x,\omega_e)/a_w]^2}$$
$$T^1(x,\omega_e) = GA_{fz}(x)\sum_{r=2}^{4}\gamma_r(x)[p_{1r} + \alpha_r(x)\omega_e p_{1r}]; \tag{21}$$
$$T^2(x,\omega_e) = GA_{fz}(x)\sum_{r=2}^{4}\gamma_r(x)[p_{2r} + \alpha_r(x)\omega_e p_{1r}]$$

$$H_M(x,w_e) = \sqrt{[M^1(x,\omega_e)/a_w]^2 + [M^2(x,\omega_e)/a_w]^2}$$
$$M^1(x,\omega_e) = -EI_y(x)\sum_{r=2}^{4}\theta_r'(x)[p_{1r} + \beta_r(x)\omega_e p_{2r}] \tag{22}$$
$$M^2(x,\omega_e) = -EI_y(x)\sum_{r=2}^{4}\theta_r'(x)[p_{2r-}\beta_r(x)\omega_e p_{1r}]$$

The theoretical model presented in this section was implemented in HEL module of the DYN program (Domnisoru et. al 2009, 2011) used to perform the numerical hydroelastic dynamic response of the studied bulk carrier in head waves (model Airy). If we consider only the linear oscillation response component, the results are marked as ADV.

4.1.2. Short-term statistical parameters

In the general matrix formulation of the linear analysis and the excitation from wave model Airy, the system of differential motion equations can be expressed as following:

$$[A(\omega_e)]\{\ddot{Y(t)}\} + [B(\omega_e)]\{\dot{Y}(t)\} + [C(\omega_e)]\{Y(t)\} = \{\bar{F}\}e^{-i\omega_e t} \tag{23}$$

From this equation result the solution of the steady state dynamic response:

$$\{Y(t)\} = \{\bar{Y}\}e^{-i\omega_e t}; \quad \{\bar{Y}(\omega_e)\} = [H(\omega_e)]\{\bar{F}(\omega_e)\} \tag{24}$$

$$[H(\omega_e)] = [D(\omega_e)]^{-1}; \quad [D(\omega_e)] = -\omega_e^2[A(\omega_e)] - i\omega_e[B(\omega_e)] + [C(\omega_e)]$$

where: $[H(\omega_e)]$ represent the transfer functions matrix of the ship hull-wave dynamic system.

For the dynamic response on a degree of freedom $Y(t)$, at linear wave Airy model with wave amplitude a_w, using the relation (24) the transfer function has the next expression:

$$H_y(\omega_e) = \frac{Y(\omega_e)}{a_w} = Y(\omega_e)\big|_{a_w=1} \tag{25}$$

Based on the statistical models for short term, the wave energy $\zeta_v(t)$ is characterized by the power spectral density function $\Phi_{\zeta v \zeta v}(\omega)$ (Price and Bishop 1974). In the case of the mobile system related to the ship, becomes function of ω_e using the expression:

$$\Phi_{\zeta v \zeta v}(\omega_e) = \frac{\Phi_{\zeta v \zeta v}(\omega)}{\left|1 - 2u_s \frac{\omega}{g} cos\mu\right|} \tag{26}$$

where: μ is the ship-wave angle.

To characterize the dynamic response Y(t) in energetic terms, similar with equation (26) can be defined the function of the power spectral density function $\Phi_{yy}(\omega_e)$:

$$\Phi_{yy}(\omega_e) = \left|H_y\right|^2 \Phi_{\zeta v \zeta v}(\omega_e) \tag{27}$$

For the wave spectrum is defined the moment of the power spectral density function using the following equation:

$$m_n = \int_0^\infty \omega^n \Phi(\omega) d\omega; \quad \forall n \tag{28}$$

In the case of this study was used ITTC wave power density spectrum (Bertram 2000, Domnisoru 2001, Price & Bishop 1974), with the next expression:

$$\Phi_{\zeta v \zeta v}(\omega)\Big|_{ITTC} = \frac{A}{\omega^5} e^{-\frac{B}{\omega^5}}; \quad A = 0.7795; \quad B = \frac{3.11}{h_{1/3}^2}; \quad T_1 = 3.55\sqrt{h_{1/3}} \tag{29}$$

In the case of ship-wave system it can be considered that the wave $\zeta_v(t)$ and the dynamic response Y(t) are random processes with Rayleigh short term probability function, having $\sigma^2 = m_0$ (dispersion) and $\mu = 0$:

$$f_y(y) = \frac{y}{2\sigma^2} e^{-\frac{y^2}{2\sigma^2}}; \quad y \in \{\zeta_v, Y\}; \quad \int_0^\infty f_y(y)dy = 1 \tag{30}$$

For the wave excitations and the random dynamic responses , with the Rayleigh probability density function (30), are define the next parameters for the short term analysis:

- the most probable statistic value (root mean square): $RMS_y = y_{mp} = \sqrt{m_0^{(y)}}$;
- the medium statistic value: $y_1 = y_{med} = 1.25\sqrt{m_0^{(y)}}$;
- the significant statistic value: $y_{1/3} = y_s 2\sqrt{m_0^{(y)}}$; (31)
- the medium period statistic value: $T_1^{(y)} = T_{med}^{(y)} = 2\pi\sqrt{\frac{m_0^{(y)}}{m_2^{(y)}}}$.

4.1.3. The Hydroelastic Non-Linear Dynamic Response at Coupled Oscillations and Vibrations in the Vertical Plane

In the case of the hydroelastic non-linear dynamic response, the theoretical method presented in section 4.1.1. need to be updated using the geometrical and hydrodynamic nonlinearities, taking into account the instantaneous ship-wave position. Also for the non-linear analysis is necessary to replace the linear wave model Airy with the second order wave Longuet - Higgins model (with wave interference components), solving the motion equations system by direct integration in time domain (Jensen & Pedersen, 1981, Domnisoru et. al,1998).

The elongation of the wave model Lomguet-Higgins, with interface components, with first order ITTC wave power density spectrum (29), has the next expression:

$$\zeta_v^*(x,t) = \zeta_{v1}^*(x,t) + \zeta_{v2}^{*+}(x,t) + \zeta_{v3}^{*-}(x,t) \tag{32}$$

$$\zeta_{v1}^*(x,t) = \sum_{i=1}^{m}[a_{1i}(x)cos\omega_{ei}t - b_{1i}(x)sin\omega_{ei}t]; \;\; a_{i,j} = \sqrt{2S_{\zeta v}(w_{i,j})\Delta\omega} \;\; i,j = 1,m$$

$$\zeta_{v2}^{*+}(x,t) = \sum_{i=1}^{m}[a_{2i}(x)cos2\omega_{ei}t - b_{2i}(x)sin2\omega_{ei}t] + \sum_{i=1}^{m-1}\sum_{j=i+1}^{m}\left[a_{2ij}^{+}(x)\cos(\omega_{ei}+\omega_{ej})\,t - b_{2ij}^{+}(x)\sin\,(\omega_{ei}+\omega_{ej})t\right]$$

$$\zeta_{v2}^{*-}(x,t) = \sum_{i=1}^{m-1}\sum_{j=i+1}^{m}\left[a_{2ij}^{-}(x)\cos(\omega_{ei}+\omega_{ej})\,t - b_{2ij}^{-}(x)\sin\,(\omega_{ei}+\omega_{ej})t\right]$$

$$a_{1i}(x) = a_i f_{Si}(x)\cos(k_i x - \varepsilon_i)\,; \quad b_{1i}(x) = a_i f_{Si}(x)\sin(k_i x - \varepsilon_i)\,; \quad i = 1, m$$
$$a_{2i}(x) = \frac{1}{2} a_i^2 f_{S_{2i}^*}(x) k_i \cos 2(k_i x - \varepsilon_i)\,; \quad b_{2i}(x) = \frac{1}{2} a_i^2 f_{S_{2i}^*}(x) k_i \cos 2(k_i x - \varepsilon_i)$$
$$a_{2ij}^{\pm}(x) = \pm\frac{1}{2} a_i a_i f_{S_{2i\pm j}^*}(x)\left|k_i \pm k_j\right| \cos\left[(\mathrm{k_i} \pm \mathrm{k_j})\mathrm{x} - (\varepsilon_\mathrm{i} \pm \varepsilon_\mathrm{j})\right]; \quad \mathrm{i} = 1, \mathrm{m} - 1$$
$$b_{2ij}^{\pm}(x) = \pm\frac{1}{2} a_i a_i f_{S_{2i\pm j}^*}(x)\left|k_i \pm k_j\right| \sin\left[(\mathrm{k_i} \pm \mathrm{k_j})\mathrm{x} - (\varepsilon_\mathrm{i} \pm \varepsilon_\mathrm{j})\right]; \quad \mathrm{j} = \mathrm{i} + 1, \mathrm{m}$$

where: a_i, a_j, $i,j = 1,m$ represent the wave component amplitudes with the circular frequency ω_i, ω_j for first order ITTC wave power density spectrum; ε_i, ε_j are wave components random phases; m the number of the first order components based on ITTC wave power density spectrum.

By generalizing the equation (15), using the geometric and hydrodynamic nonlinearities and the slamming - impact component, the hydrodynamic force per length unit has the expression:

$$F_h(x,t) = -\frac{D}{Dt}\left[m_{33}(x,t)\frac{D_{Zr}(x,t)}{Dt}\right] - N_{33}(x,t)\frac{D_{Zr}(x,t)}{Dt} - \rho g b_0(x) + \rho g A_{nl}|_{Zr}(x,t) + K_{slam}(x,t)\left[\frac{D_{Zr}(x,t)}{Dt}\right]^2 \qquad (33)$$

where: A_{nl} is the correction of the immersed area at the x abscise corresponding to the relative ship-wave position $z_r\,(x,t)$; $K_{slam}\,(x,t)$ is the bottom impact slamming coefficient.

Considering the absolute displacement decomposed into the linear component $w_o(x,t)$ and the non-linear component $w_{nl}(x,t)$, the relative ship-wave position is:

$$z_r(x,t) = z_{ro}(x,t) + w_{nl}(x,t); \quad z_{ro}(x,t) = w_o(x,t) - \zeta_v^*(x,t) \qquad (34)$$
$$w(x,t) = w_o(x,t) + w_{nl}(x,t)$$

The hydrodynamic coefficients at the instantaneous ship-wave position can be also decomposed into linear and non-linear components, as follows:

$$m_{33}(x,t) = m_{33o}(x) + m_{33onl}|_{Z_r}(x,t); \quad N_{33}(x,t) = N_{33o}(x) + N_{33nl}|_{Z_r(x,t)} \qquad (35)$$

The system of the differential motion equations (13) has the same mathematical expression, the difference being in the expression of the generalized hydrodynamic force and the excitation wave Lomguet-Higgins elongation :

$$[a] = \{\ddot{p}(t)\} + [b]\{\dot{p}(t)\} + [c]\{p(t)\} = \{F_h(t)\} \qquad (36)$$
$$F_{hs}(t) = \int_0^L F_h(x,t)\, w_s(x) dx; \quad s = 0, n; \quad w(x,t) = \sum_{s=0}^{n} w_s(x)\, p_s(t)$$

where: the vector of the principal modal coordinates can be decomposed into the linear and non-linear components: $\{p(t)\} = \{p_o(t)\} + \{p_{nl}(t)\}$.

Based on the relations (32) to (36) the motion equations system is decomposed in two parts (linear and non-linear components):

$$[a]\{\ddot{p}_0(t)\} + [b]\{\dot{p}_0(t)\} + [c]\{p_o(t)\} = \{F_{h0}(t)\} \tag{37}$$

$$[a]\{\ddot{p}_{nl}(t)\} + [b]\{\dot{p}_{nl}(t)\} + [c]\{p_{nl}(t)\} = \{F_{h01}(t)\} + \{F_{h1}(t)\} \tag{38}$$

where the components of the hydrodynamic forces (33) have the next expressions:

$$\begin{aligned}
F_{h0}(x,t) &= -\left\{\frac{D}{Dt}\left[m_{33o}(x)\frac{D_{Z_{ro}}}{Dt}\right] + N_{33o}(x)\frac{D_{Z_{ro}}}{Dt} + \rho g b_0(x) z_{ro}\right\} \\
F_{h01}(x,t) &= -\left\{\frac{D}{Dt}\left[m_{33o}(x)\frac{D_{w_{nl}}}{Dt}\right] + N_{33o}(x)\frac{D_{w_{nl}}}{Dt} + \rho g b_0(x) w_{nl}\right\} \\
F_{h1}(x,t) &= -\left\{\frac{D}{Dt}\left[m_{33nl}|_{Z_r}\frac{D_{(Z_{ro}+W_{nl})}}{Dt}\right] + N_{33nl}|_{Z_r}\frac{D_{(Z_{ro}+W_{nl})}}{Dt} + \rho g A_{nl}|_{Z_r}\right\} \\
&\quad + K_{imp}\Big|_{Z_r}\left[\frac{D_{(Z_{ro}+W_{nl})}}{Dt}\right]^2
\end{aligned} \tag{39}$$

The linear dynamic response from equation (37), in the case of the wave excitation model Longuet - Higgins (32), is obtained in frequency domain, using a similar technique presented in equation (19). The motion equation system in frequency domain, in principal coordinates can be solved using a numerical procedure for the linear algebraic systems and has the next compact expression for ω_e wave excitation component:

$$\begin{aligned}
&[D_{1i}(\omega_{ei})]\{X_{1i}\} = \{F_{1i}(\omega_{ei})\}|_{i=1,m} \rightarrow \quad \{P_{1i}\},\{Q_{1i}\}\ i = 1,m \\
&[D_{2i}(2\omega_{ei})]\{X_{2i}\} = \{F_{2i}(2\omega_{ei})\}|_{i=1,m} \rightarrow \quad \{P_{2i}\},\{Q_{2i}\}\ i = 1,m \\
&\left[D_{2ij}^{\pm}\left(\omega_{ei} \pm \omega_{ej}\right)\right]\left\{X_{2ij}^{\pm}\right\} = \left\{F_{2ij}^{\pm}\left(\omega_{ei} \pm \omega_{ej}\right)\right\}\Big|_{j=i+1,m}^{i=1,m-1} \rightarrow \quad \left\{P_{2ij}^{\pm}\right\},\left\{Q_{2ij}^{\pm}\right\} \\
&p_{os}(t) = \sum_{i=1}^{m}\left[p_{s\,i}^{2} cos\omega_{ei}t - Q_{s\,i}^{2} sin\omega_{ei}t\right];\ p_{s\,o}^{2-} \\
&\qquad = \sum_{i=1}^{m-1}\sum_{j=i+1}^{m}\left[p_{s\,ij}^{2-}\cos\left(\omega_{ei} - \omega_{ej}\right)t - Q_{s\,ij}^{2-} sin\left(\omega_{ei} - \omega_{ej}\right)t\right] \\
&p_{s\,o}^{2+} = \sum_{i=1}^{m}\left[p_{s\,i}^{2} cos2\omega_{ei}t - Q_{s\,i}^{2} sin\omega_{ei}t\right] \\
&\qquad + \sum_{i=1}^{m-1}\sum_{j=i+1}^{m}\left[p_{s\,ij}^{2+}\cos\left(\omega_{ei} + \omega_{ej}\right)t - Q_{s\,ij}^{2+} sin\left(\omega_{ei} + \omega_{ej}\right)t\right]
\end{aligned} \tag{40}$$

From the relations (38) and (39) the motion equation system for the non-linear component has the next formulation:

$$\begin{aligned}
&[A]\{\ddot{p}_{nl}(t)\} + [B]\{\dot{p}_{nl}(t)\} + [C]\{p_{nl}(t)\} = \{F_{h1}(t,\{p_{nl}\},\{\dot{p}_{nl}\},\{\ddot{p}_{nl}\})\} \\
&[A] = [a] + [A_h]|_{\omega_2}^{\omega_{osc}};\ \ [B] = [b] + [B_h]|_{\omega_2}^{\omega_{osc}};\ \ [C] = [c] + [C_h]|_{\omega_2}^{\omega_{osc}}
\end{aligned} \tag{41}$$

In order to solve the equation system for non-linear component (41), it is used an iterative procedure coupled with a differential motion equations numerical direct integration in time domain method $t \in [0, T_s]$, Ts=80s, with time step $\delta t = 0.01$ [s], as following:

$$iter.0:\ \{p_{nl}(t)\}^{(o)} = 0 \rightarrow \{F_{h1}(t)\}^{(1)} = \{F_{h10}(t)\}^{(0)} + F_{h12}(t)^{(0)}; \tag{42}$$

$$iter.1:\ [A]\{\ddot{p}_{nl}(t)\}^{(1)} + [B]\{\dot{p}_{nl}(t)\}^{(1)} + [C]\{p_{nl}(t)\}^{(1)} = \{F_{h1}(t)\}^{(1)}$$

$$iter.k: \{p_{nl}(t)\}^{(k)}$$

$$iter.k+1: [A]\{\ddot{p}_{nl}(t)\}^{(k+1)} + [B]\{\dot{p}_{nl}(t)\}^{(k+1)} + [C]\{p_{nl}(t)\}^{(k+1)} = \{F_{h1}(t)\}^{(k+1)}$$

$$\{F_{h1}(t)\}^{(k+1)} = \left\{F_{h1}\left(t, \{p_{nl}(t)\}^{(k)}, \{\dot{p}_{nl}(t)\}^{(k)}, \{\ddot{p}_{nl}(t)\}^{(k)}\right)\right\}$$

- the iteration keeps on until it is satisfied the convergence criterion:

$$\frac{max_{r,t}\left|p_{nl\,r}^{(k+1)}(t) - p_{nl\,r}^{(k)}(t)\right|}{max_{r,t}\left|p_{nl\,r}^{(k)}(t)\right|} \le \varepsilon = 0.001$$

The total linear and non-linear hydroelastic dynamic responses in time domain induced by head wave model Longuet - Higgins, for first order ITTC spectrum, in displacements, deformations, shear forces and bending moments, according to the modal analysis technique, have the following formulations:

$$w(x,t) = \sum_{r=0}^{n} w_r(x)\,[p_{o\,r}(t) + p_{nl\,r}(t)];\quad p_r(t) = p_{o\,r}(t) + p_{nl\,r}(t);\ \ r = 0, n$$

$$M(x,t) = -EI_y(x)\sum_{r=0}^{n} \theta_r'(x)[p_r(t) + \beta_r(x)\dot{p}_r(t)]; \tag{43}$$

$$T(x,t) = GA_{fz}(x)\sum_{r=0}^{n} \gamma_r(x)[p_r(x) + \alpha_r(x)\dot{p}_r(t)]$$

the notations used in the above equation are explained in Section 4.1.1.

In order to obtain at a given x section the total hydroelastic dynamic response in frequency domain (amplitude spectrum), and also the significant short term statistical parameters, the dynamic response in time domain (43) is processed using the Fast Fourier Transformation procedure (FFT).

The theoretical model presented in this section was implemented in DYN-LIN (linear response, with Longuet-Higgins waves) and DYN-NLN (linear and non-linear response, with Longuet-Higgins waves) modules of the DYN program (Domnisoru et al., 2009, 2011) for the analysis of the numerical hydroelastic dynamic response of the ship hull in irregular head waves.

4.2. The Numerical Analysis of Linear and Non-linear Ship Bulk Carrier Dynamic Response based on Hydroelasticity Theory

The analysis in this section was carried out according to the theoretical model presented in Section 4.1, and the pre-processing, the numerical analysis and the post-processing of the bulk carrier hull dynamic response were carried on with the programs package DYN (Domnisoru et al. 2009, 2011).

The input data for the studied bulk carrier necessary to complete this task of the study are:

- the main dimensions of the studied bulk carrier presented in Table 1 (Section 2.1);
- the offset line - for this analysis the equivalent ship girder is divided over the total length L = 289.87m in 40 equal elements, based on the original ship offset lines presented in Figure 3 from section 2.1. The selected 40 transversal sections are disposed at the middle of each element; and each transversal station was described by 20 points;
- in order to obtain the rigidity transversal sections characteristics for the studied bulk carrier were used the data presented in Table 7 from Section 3.2., the inertial bending moment I_{yy} [m^4] (see Figure 13), and the equivalent shear area (with the averaged tangential stress hypothesis) A_{fz} [m^2] (see Figure 14);
- the load cases analysed, in this study were completed for full and ballast load conditions, with their mass diagrams presented in Figure 19 and Figure 20 (see Section 3.2);
- natural ship modes frequencies at oscillations / vibrations are presented in Table 8 from Section 3.2. In order to obtain the ship hull vibration modes, there was taken into account the hydrodynamic added masses (Figure 21 from Section 3.2) and for the natural frequencies at heave and pitch oscillations, there were used standard relations form the seakeeping theory.

4.3.1. Full Loading Case

In the following paragraphs are presented the numerical analyses of the linear and non-linear dynamic response of the studied bulk carrier for the full loading condition. For the full loading case (Longuet-Higgins wave excitation) in the following figures are presented:

- in Figure 66 and Figure 67 are presented the time record and the amplitude spectrum FFT for wave model Longuet-Higgins, with the first order power density spectrum function ITTC, for significant wave height $h_{1/3}$=10.65m, at section x/L = 0.50;

- in Figure 68 to Figure 71 are presented the time record and the amplitude spectrum FFT for the dynamic displacement at oscillations and vibrations (hydroelasticity), at linear and non-linear analyses, for $h_{1/3}$=10.65m, at section x/L = 0.50;

- in Figure 72 to Figure 83 are presented the time record and the amplitude spectrum FFT for the dynamic bending moments at oscillations and vibrations (hydroelasticity), at linear and non-linear analyses, for $h_{1/3}$=10.65m, at sections x/L = 0.25, 0.50 and 0.75;

- in Figure 85 to Figure 95 are presented the time record and the amplitude spectrum FFT for the dynamic shear forces at oscillations and vibrations (hydroelasticity), at linear and non-linear analyses, for $h_{1/3}$=10.65m, at sections x/L = 0.25, 0.50 and 0.75.

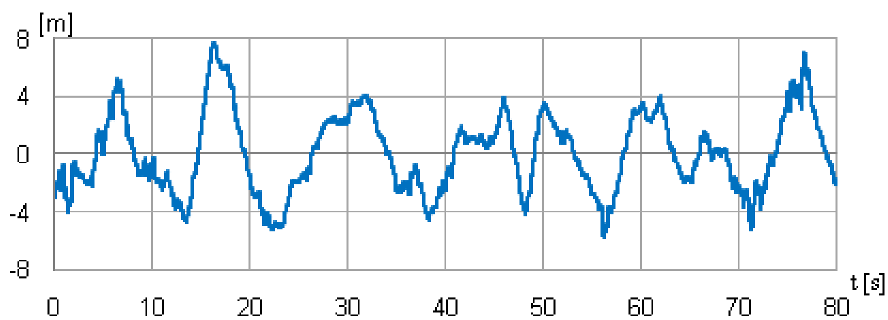

Figure 66. Time record for wave model Longuet-Higgins, with the first order power density spectrum function ITTC, for significant wave height $h_{1/3}$=10.65m at x/L=0.50 – LC_F

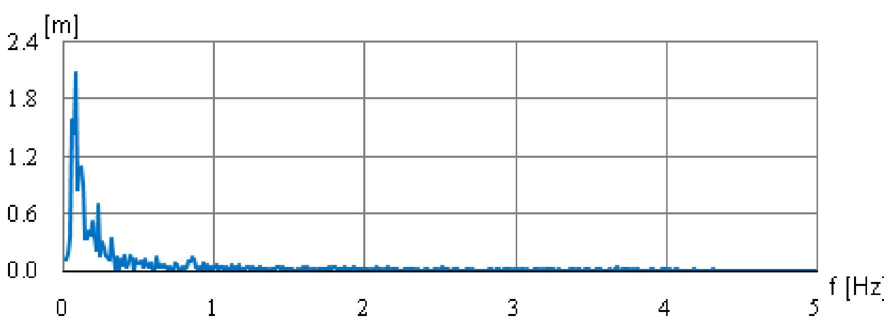

Figure 67. Amplitude spectrum FFT wave model Longuet-Higgins, with the first order power density spectrum function ITTC, for significant wave height $h_{1/3}$=10.65m at x/L=0.50 – LC_F

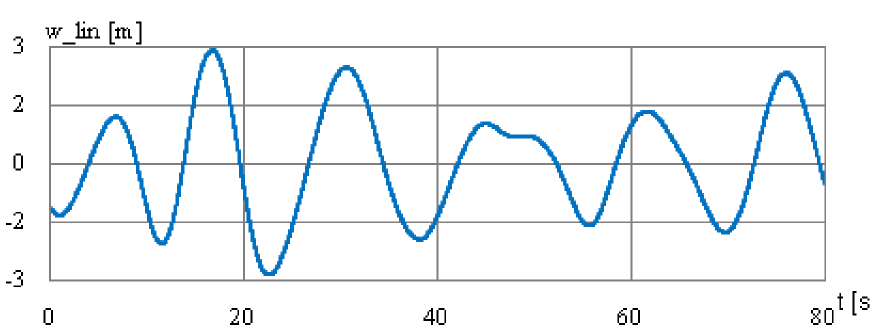

Figure 68.Time record for the dynamic displacement at oscillations and vibrations at linear analysis, significant wave height $h_{1/3}$=10.65m at x/L=0.50 – LC_F

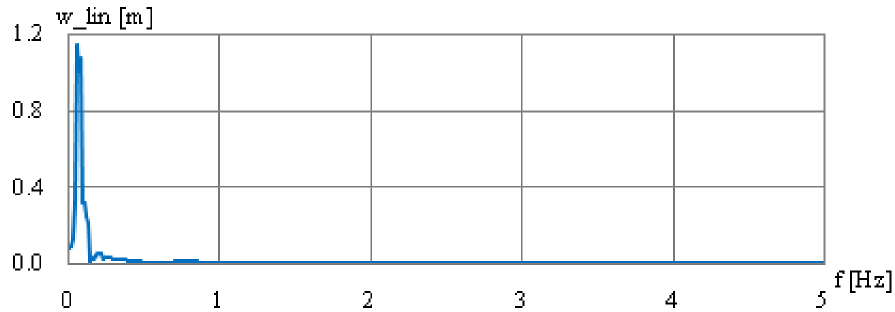

Figure 69. Amplitude spectrum FFT for the dynamic displacement at oscillations and vibrations at linear analysis, significant wave height $h_{1/3}$=10.65m at x/L=0.50 – LC_F

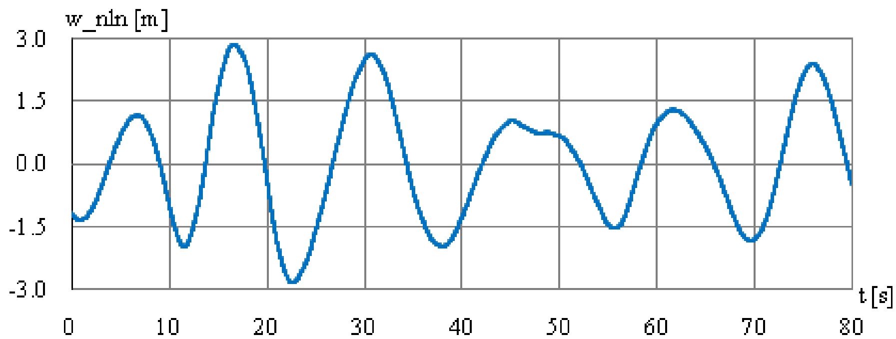

Figure 70. Time record for the dynamic displacement at oscillations and vibrations at non-linear analysis, significant wave height $h_{1/3}$=10.65m at x/L=0.50 – LC_F

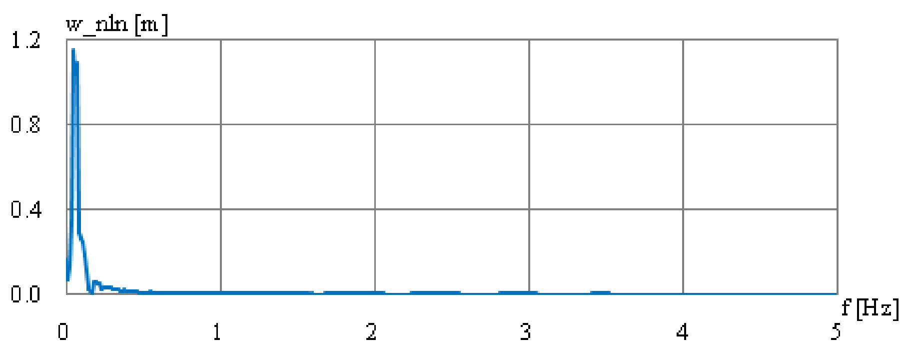

Figure 71. Amplitude spectrum FFT for the dynamic displacement at oscillations and vibrations at non-linear analysis, significant wave height $h_{1/3}$=10.65m at x/L=0.50 – LC_F

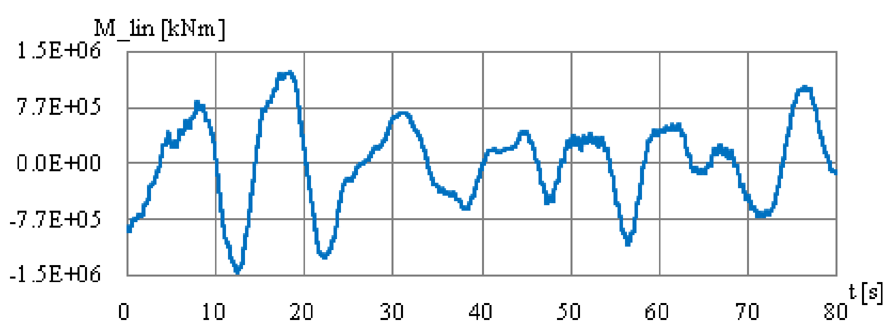

Figure 72. Time record for the dynamic bending moments at oscillations and vibrations at linear analysis, significant wave height $h_{1/3}$=10.65m at x/L=0.25 – LC_F

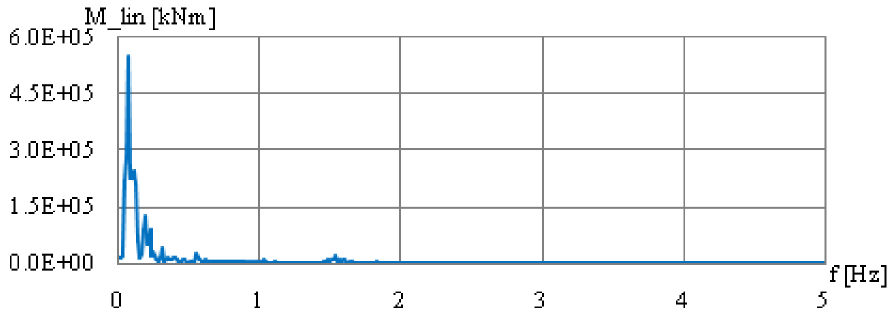

Figure 73. Amplitude spectrum FFT for the dynamic bending moment at oscillations and vibrations at linear analysis, significant wave height $h_{1/3}$=10.65m at x/L=0.25 – LC_F

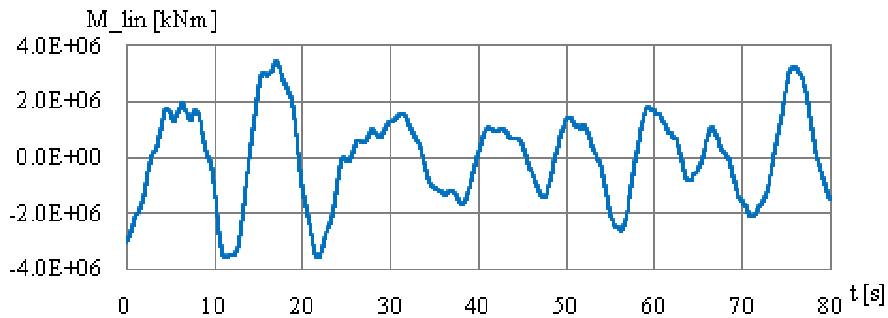

Figure 74. Time record for the dynamic bending moments at oscillations and vibrations at linear analysis, significant wave height $h_{1/3}$=10.65m at x/L=0.50 – LC_F

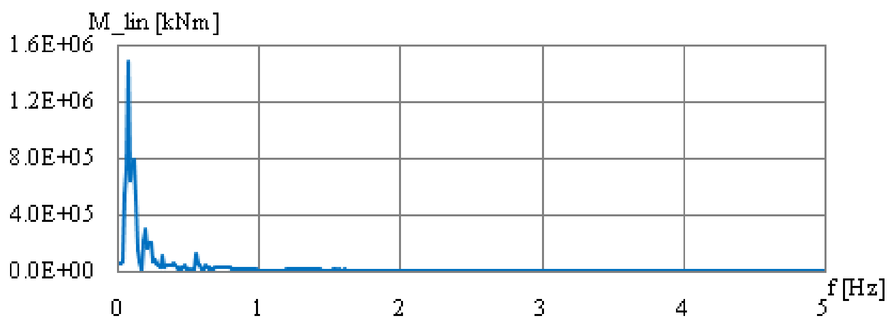

Figure 75. Amplitude spectrum FFT for the dynamic bending moment at oscillations and vibrations at linear analysis, significant wave height $h_{1/3}$=10.65m at x/L=0.5 – LC_F

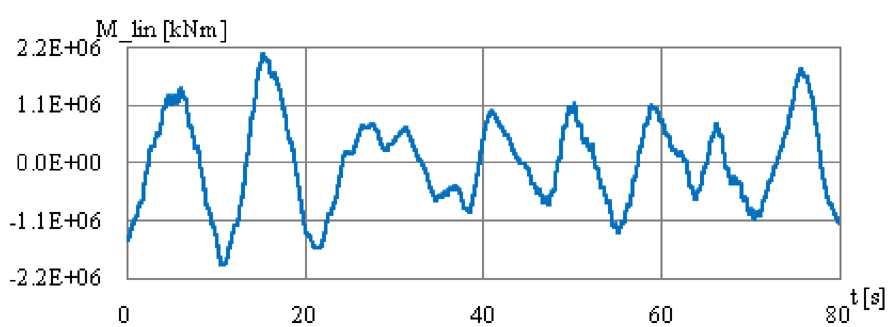

Figure 76.Time record for the dynamic bending moments at oscillations and vibrations at linear analysis, significant wave height $h_{1/3}$=10.65m at x/L=0.75 – LC_F

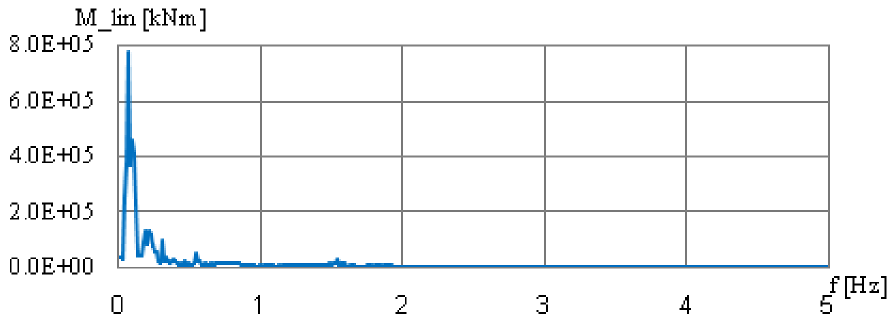

Figure 77. Amplitude spectrum FFT for the dynamic bending moment at oscillations and vibrations at linear analysis, significant wave height $h_{1/3}$=10.65m at x/L=0.75 – LC_F

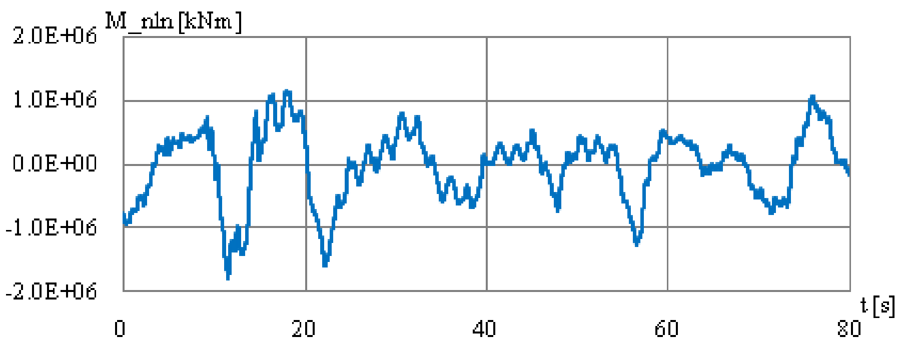

Figure 78.Time record for the dynamic bending moments at oscillations and vibrations at non-linear analysis, significant wave height $h_{1/3}$=10.65m at x/L=0.25 – LC_F

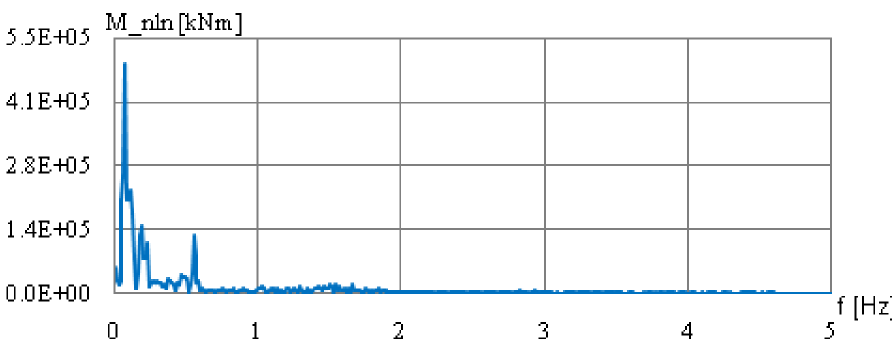

Figure 79. Amplitude spectrum FFT for the dynamic bending moment at oscillations and vibrations at non-linear analysis, significant wave height $h_{1/3}$=10.65m at x/L=0.25 – LC_F

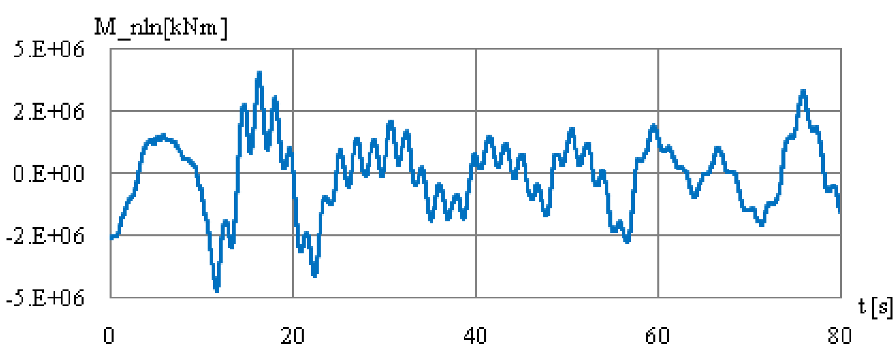

Figure 80. Time record for the dynamic bending moments at oscillations and vibrations at non-linear analysis, significant wave height $h_{1/3}$=10.65m at x/L=0.50 – LC_F

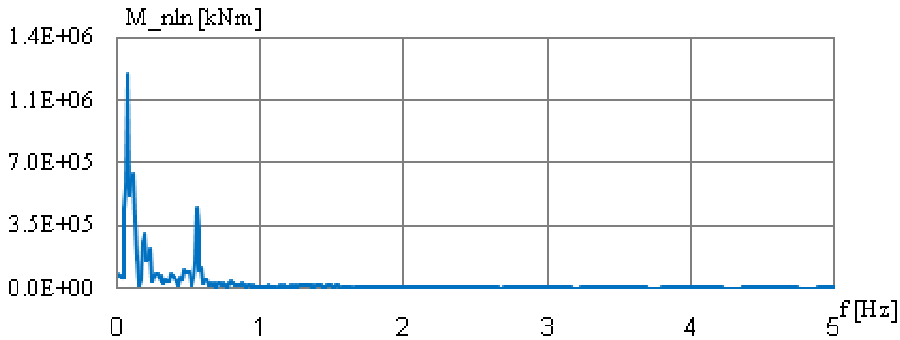

Figure 81. Amplitude spectrum FFT for the dynamic bending moment at oscillations and vibrations at non-linear analysis, significant wave height $h_{1/3}$=10.65m at x/L=0.50 – LC_F

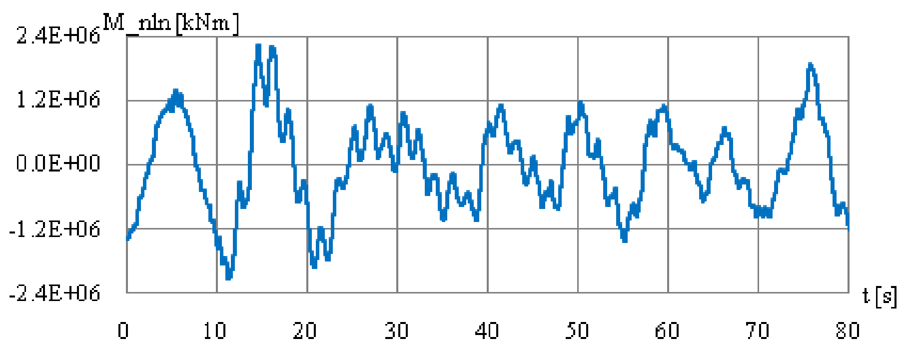

Figure 82. Time record for the dynamic bending moments at oscillations and vibrations at non-linear analysis, significant wave height $h_{1/3}$=10.65m at x/L=0.75 – LC_F

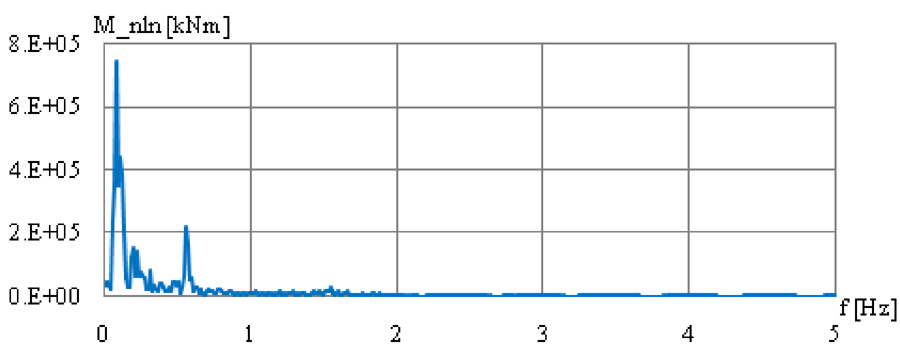

Figure 83. Amplitude spectrum FFT for the dynamic bending moment at oscillations and vibrations at non-linear analysis, significant wave height $h_{1/3}$=10.65m at x/L=0.75 – LC_F

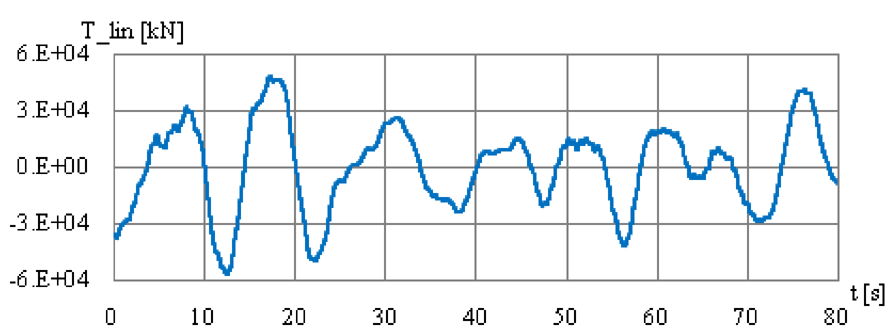

Figure 84.Time record for the dynamic shear forces at oscillations and vibrations at linear analysis, significant wave height $h_{1/3}$=10.65m at x/L=0.25 – LC_F

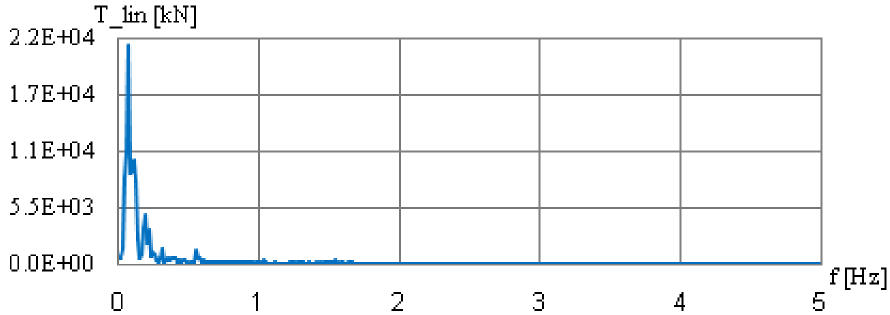

Figure 85. Amplitude spectrum FFT for the dynamic shear forces at oscillations and vibrations at linear analysis, significant wave height $h_{1/3}$=10.65m at x/L=0.25 - LC_F

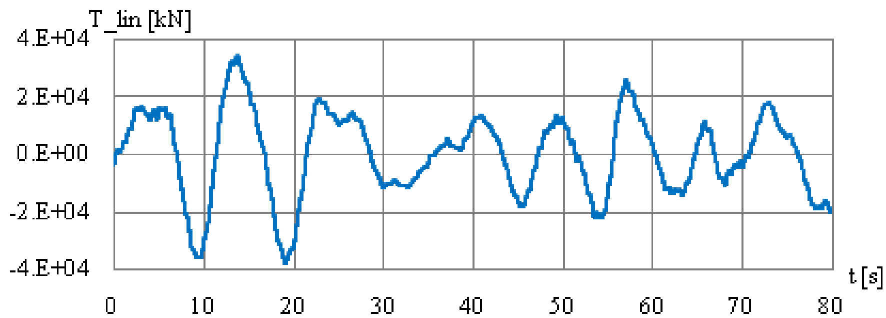

Figure 86. Time record for the dynamic shear forces at oscillations and vibrations at linear analysis, significant wave height $h_{1/3}$=10.65m at x/L=0.50 – LC_F

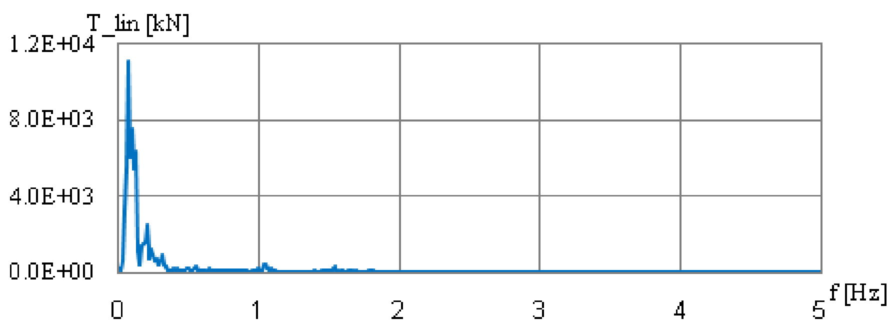

Figure 87. Amplitude spectrum FFT for the dynamic shear forces at oscillations and vibrations at linear analysis; significant wave height $h_{1/3}$=10.65m at x/L=0.50 - LC_F

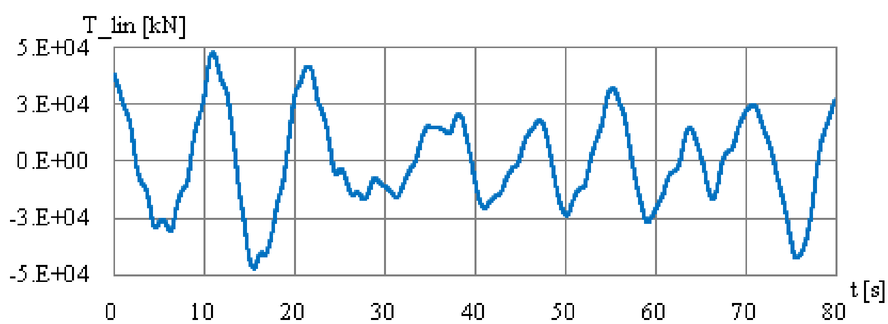

Figure 88. Time record for the dynamic shear forces at oscillations and vibrations at linear analysis, significant wave height $h_{1/3}$=10.65m at x/L=0.75 – LC_F

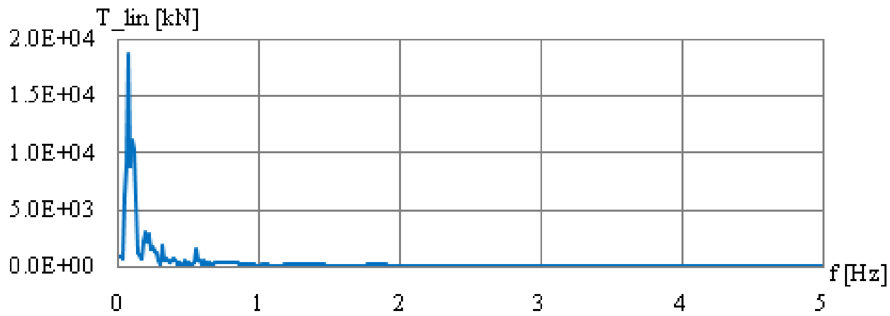

Figure 89 - Amplitude spectrum FFT for the dynamic shear forces at oscillations and vibrations at linear analysis; significant wave height $h_{1/3}$=10.65m at x/L=0.75 - LC_F

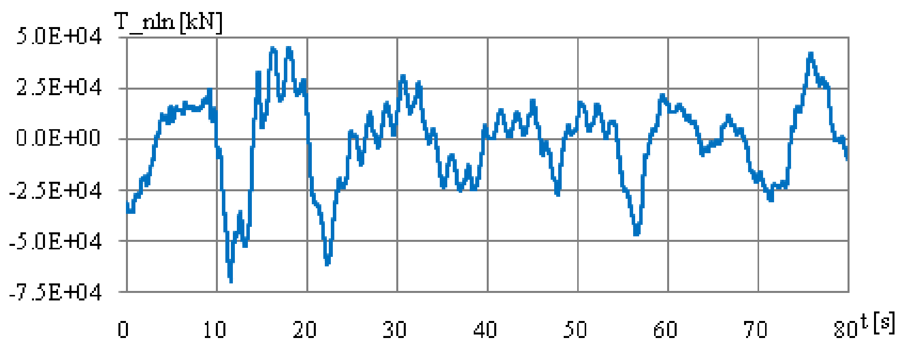

Figure 90. Time record for the dynamic shear forces at oscillations and vibrations at non-linear analysis, significant wave height $h_{1/3}$=10.65m at x/L=0.25 – LC_F

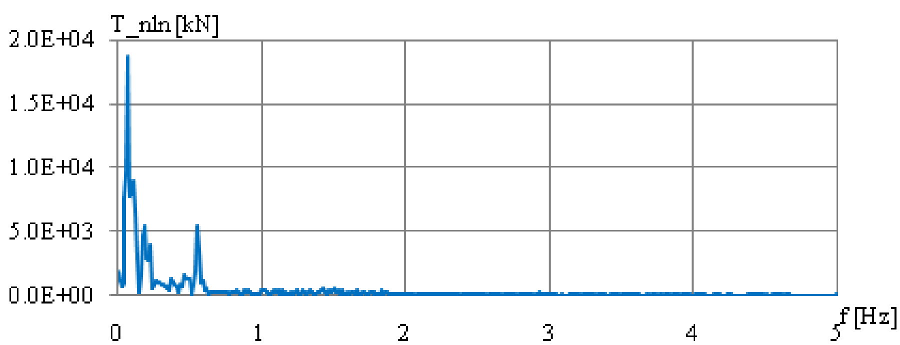

Figure 91. Amplitude spectrum FFT for the dynamic shear forces at oscillations and vibrations at non-linear analysis, significant wave height $h_{1/3}$=10.65m at x/L=0.25– LC_F

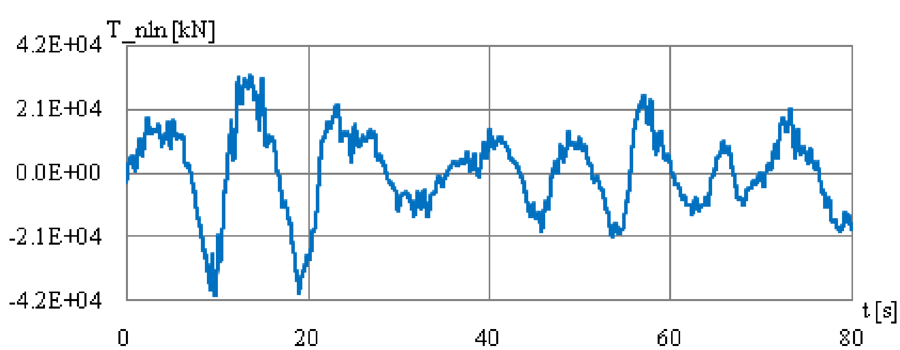

Figure 92. Time record for the dynamic shear forces at oscillations and vibrations at non-linear analysis, significant wave height $h_{1/3}$=10.65m at x/L=0.50 – LC_F

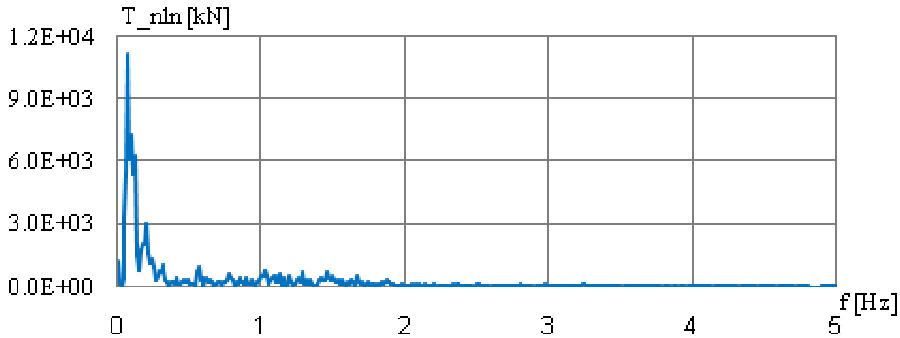

Figure 93. Amplitude spectrum FFT for the dynamic shear forces at oscillations and vibrations at non-linear analysis, significant wave height $h_{1/3}$=10.65m at x/L=0.50– LC_F

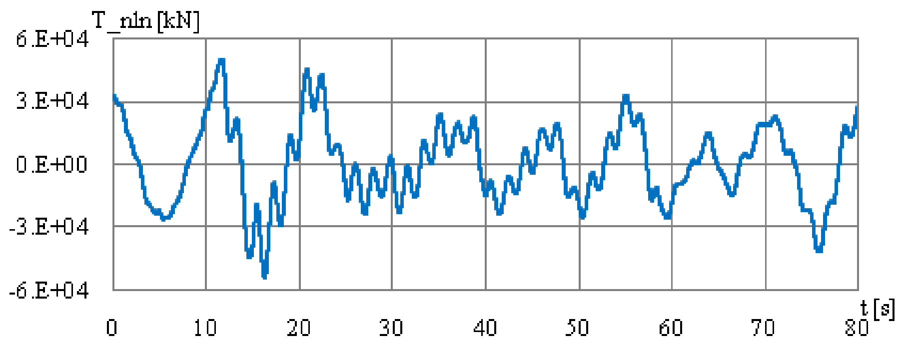

Figure 94. Time record for the dynamic shear forces at oscillations and vibrations at non-linear analysis, significant wave height $h_{1/3}$=10.65m at x/L=0.75 – LC_F

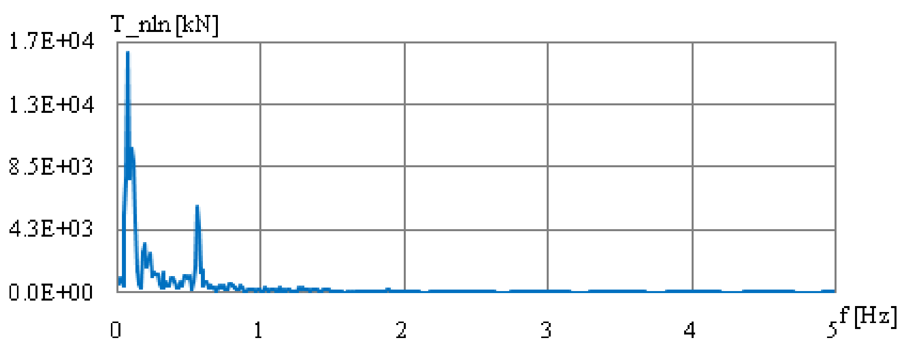

Figure 95. Amplitude spectrum FFT for the dynamic shear forces at oscillations and vibrations at non-linear analysis, significant wave height $h_{1/3}$=10.65m at x/L=0.75 – LC_F

The numerical results presented in the following tables and figures are for full load condition:

- in Table 17 is presented the ratio between the significant deformation at fundamental natural vibration mode and the significant displacement at the ship rigid hull oscillations, at linear and non-linear dynamic analyses, based on hydroelasticity theory;

- in Table 18 is presented the ratio between the significant bending moment at fundamental natural vibration mode and the significant bending moment at the ship rigid hull oscillations, at linear and non-linear dynamic analyses. based on hydroelasticity theory;

- in Table 19 is presented the ratio between the significant shear force at fundamental natural vibration mode and the significant shear force at the ship rigid hull oscillations, at linear and non-linear dynamic analyses, based on hydroelasticity theory;

- in Table 20 are presented the maximum values of the bending moments and the shear forces for the following components: still water, oscillations, vibrations on fundamental mode, at linear and non-linear numerical analysis;

- in Figure 96 and Figure 97 are presented the still water bending moments and shear forces diagrams for full load conditions;

- in Figure 98 to Figure 101 are presented the distribution of the significant bending moments at oscillations over the ship length, at dynamic linear and non-linear analysis, for $h_{1/3}$ = 0.0-12.0m;

- in Figure 102 to Figure 105 are presented the distribution of the significant bending moments at vibration on fundamental mode over the ship length, at dynamic linear and non-linear analysis, for $h_{1/3}$ = 0.0-12.0m;

- in Figure 106 to Figure 109 the distribution of the bending moments at oscillations and vibrations over the ship length, at dynamic linear and non-linear analysis added to still water values, for $h_{1/3}$ = 0.0-12.0m;

- in Figure 110 to Figure 113 the distribution of the significant shear forces at oscillation over the ship length, at dynamic linear and non-linear analysis, for $h_{1/3}$ = 0.0-12.0m

- in Figure 114 to Figure 117 the distribution of the significant shear forces at vibration on fundamental mode over the ship length, at dynamic linear and non-linear analysis, for $h_{1/3}$ = 0.0-12.0m;

- in Figure 118 to Figure 121 the distribution of the shear forces at oscillations and vibrations over the ship length, at dynamic linear and non-linear analysis added to still water values, for $h_{1/3}$ = 0.0-12.0m.

Table 17. Ratio between the significant vibration deformation $w_{1/3\_vib}$ and the significant oscillation displacement $w_{1/3\_osc}$ (for full loading condition)

Full Load Cond.		$w_{1/3}$_vib / $w_{1/3}$_osc ref. $h_{1/3}$=10.65m				$h_{1/3}$ [m] limit		
Nr	Section	x[m]	x/L	%vib/osc linear	%vib/osc nonlinear	bottom slamming	side slamming	green sea
1	aft	14.5	0.05	6.00	6.09	> 5.75	Yes	> 11.5
2	L/4	72.5	0.25	5.22	5.28			
3	L/2	145.0	0.50	4.80	4.98			
4	3L/4	217.50	0.75	6.05	6.11			
5	fore	275.50	0.95	6.34	6.44	> 12	Yes	> 10.65
		average value:		**5.68**	**5.78**			

Table 18. Ratio between the significant vibration bending moment $M_{1/3\_vib}$ and the significant oscillation bending moment $M_{1/3\_osc}$ (for full loading condition)

Full Load Cond.		$M\_vib_{1/3}$ / $M\_osc_{1/3}$ ref. $h_{1/3}$=10.65m				DYN LIN & NLN	
Nr	Section	x[m]	x/L	%vib/osc linear	%vib/osc nonlinear	springing	whipping
1	aft	14.50	0.05	12.83	27.11	*linear:* very reduced *nonlinear:* small	high
2	L/4	72.50	0.25	13.74	30.71		
3	L/2	145.00	0.50	17.54	44.68		
4	3L/4	217.50	0.75	16.08	34.72		
5	fore	275.50	0.95	15.16	28.57		
		average value:		**15.07**	**33.16**		

Table 19. Ratio between the significant vibration shear force $T_{1/3\_vib}$ and the significant oscillation shear force $T_{1/3\_osc}$ (for full loading condition)

Full Load Cond.		$T\_vib_{1/3}$ / $T\_osc_{1/3}$ ref. $h_{1/3}$=10.27m				DYN LIN & NLN	
Nr	Section	x[m]	x/L	%vib/osc linear	%vib/osc nonlinear	springing	whipping
1	aft	14.50	0.05	12.59	24.93	*linear:* very reduced *nonlinear:* small	high
2	L/4	72.50	0.25	14.40	31.62		
3	L/2	145.00	0.50	10.41	14.90		
4	3L/4	217.50	0.75	16.99	38.53		
5	fore	275.50	0.95	14.92	26.90		
		average value:		**13.86**	**27.37**		

Table 20. Maximum bending moments and shear forces in full loading conditions

Full Loading Cond.		$h_{1/3}$=10.65m	
Bending moment maximal [kNm]		Shear force maximal [kN]	
|Msw| still water	2.45E+06	|Tac| still water	4.83E+04
$M\_osc_{1/3}\_ADV$-lin	3.38E+06	$T_{1/3}\_osc\_ADV$-lin	5.22E+04
$M\_osc_{1/3}\_HEL$-lin	3.38E+06	$T_{1/3}\_osc\_HEL$-lin	5.22E+04
$M\_vib_{1/3}\_HEL$-lin	4.28E+05	$T_{1/3}\_vib\_HEL$-lin	5.57E+03
$M\_osc_{1/3}\_DYN$-lin	3.34E+06	$T_{1/3}\_osc\_DYN$-lin	5.14E+04
$M\_vib_{1/3}\_DYN$-lin	6.03E+05	$T_{1/3}\_vib\_DYN$-lin	8.17E+03
$M\_os_{1/3}c\_DYN$-nln	3.39E+06	$T_{1/3}\_osc\_DYN$-nln	5.35E+04
$M\_vib_{1/3}\_DYN$-nln	1.55E+06	$T_{1/3}\_vib\_DYN$-nln	1.88E+04

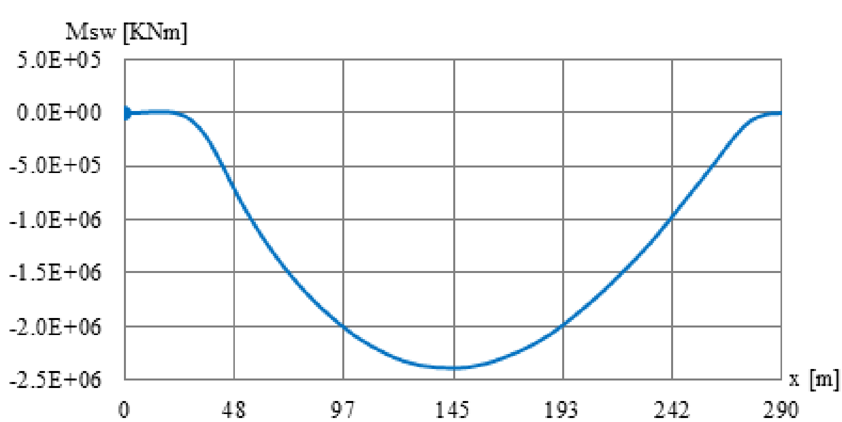

Figure 96. Still water bending moment diagram in full loading condition

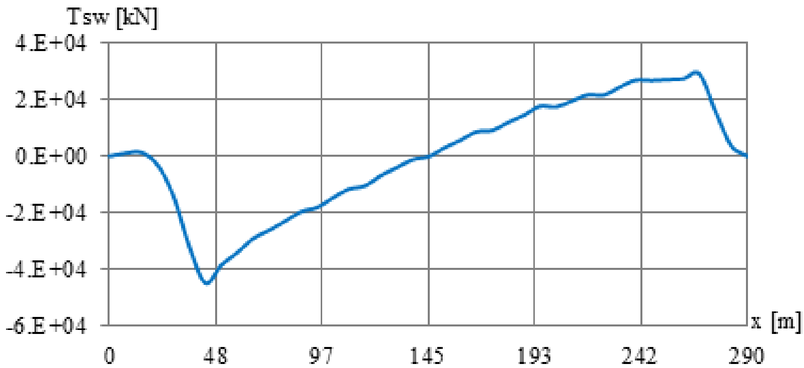

Figure 97. Still water shear forces diagram in full loading condition

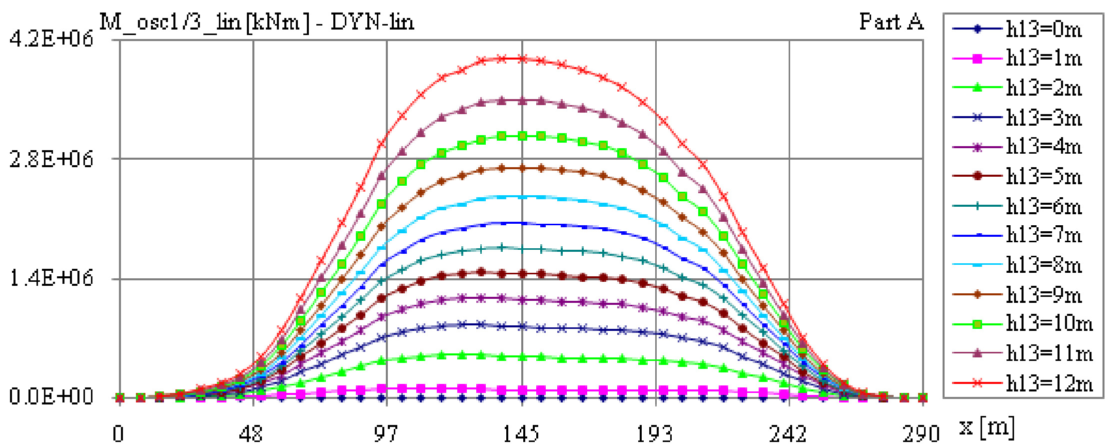

Figure 98. The distribution of the significant bending moments at oscillations over the ship length, at dynamic linear analysis for $h_{1/3}$ = 0.0 to 12.0m (step 1.0m, part A) – LC_F

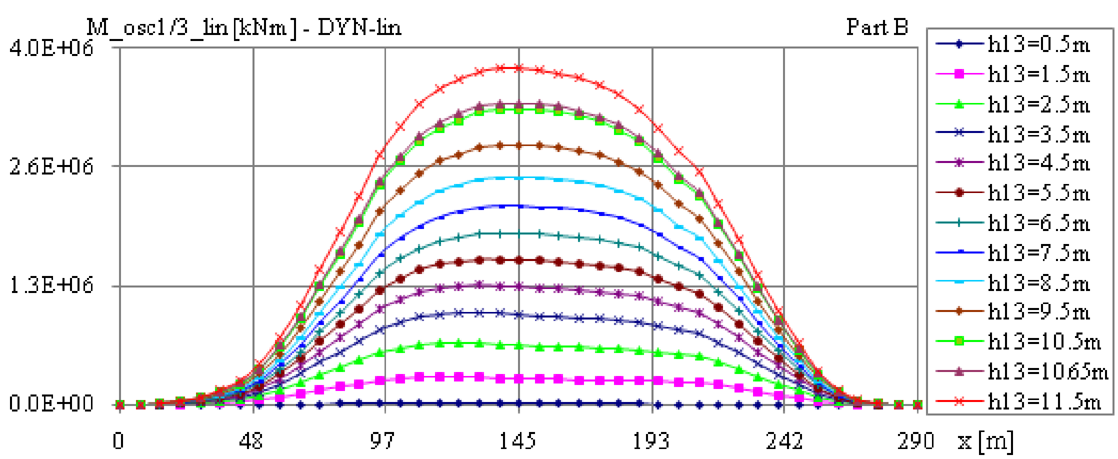

Figure 99. The distribution of the significant bending moments at oscillations over the ship length, at dynamic linear analysis for $h_{1/3}$ = 0.5 to 11.5m (step 1.0m, part B) – LC_F

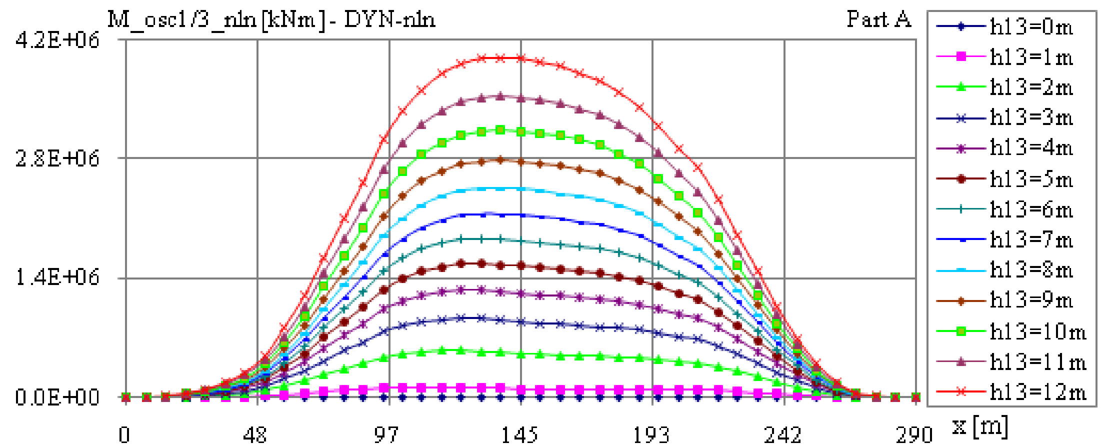

Figure 100. The distribution of the significant bending moments at oscillations over the ship length, at dynamic non-linear analysis for $h_{1/3}$ = 0.0 to 12.0m (step 1.0m, part A) – LC_F

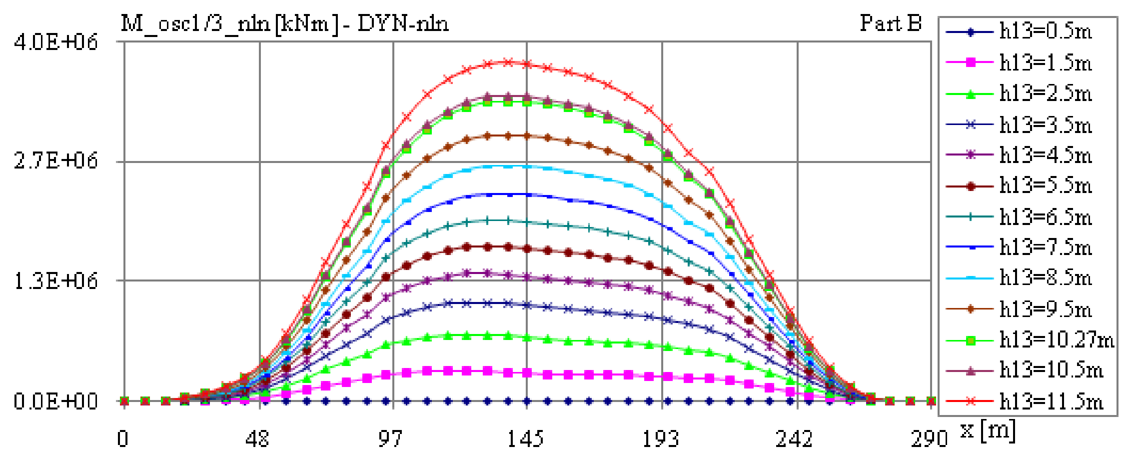

Figure 101. The distribution of the significant bending moments at oscillations over the ship length, at dynamic non-linear analysis for $h_{1/3}$ = 0.5 to 11.5m (step 1.0m, part B) – LC_F

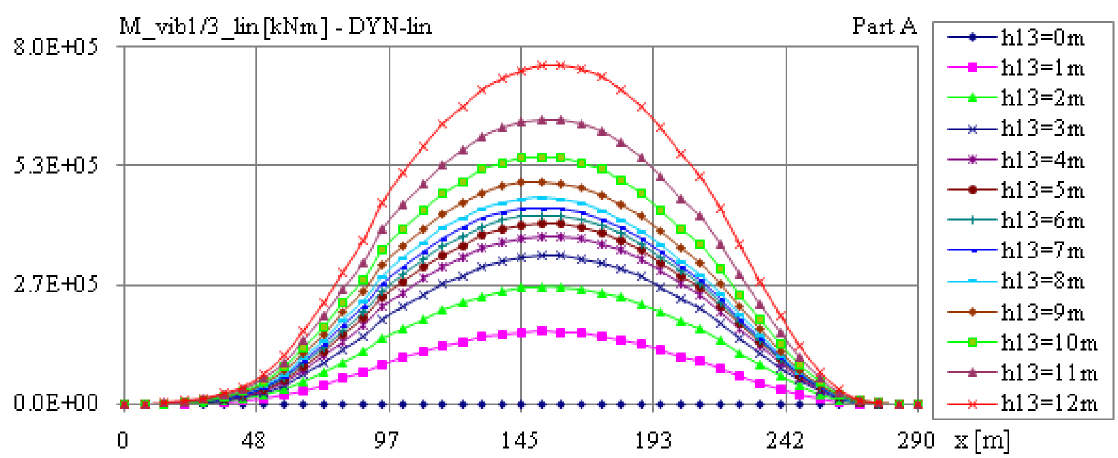

Figure 102. The distribution of the significant bending moments at vibrations over the ship length, at dynamic linear analysis for $h_{1/3}$ = 0.0 to 12.0m (step 1.0m, part A) – LC_F

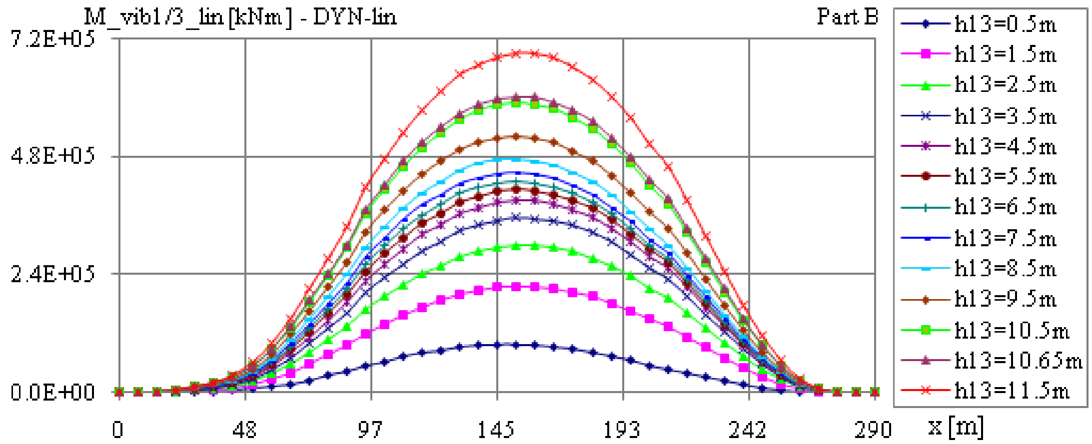

Figure 103 - The distribution of the significant bending moments at vibrations over the ship length, at dynamic linear analysis for $h_{1/3} = 0.5$ to 11.5m (step 1.0m, part B) – LC_F

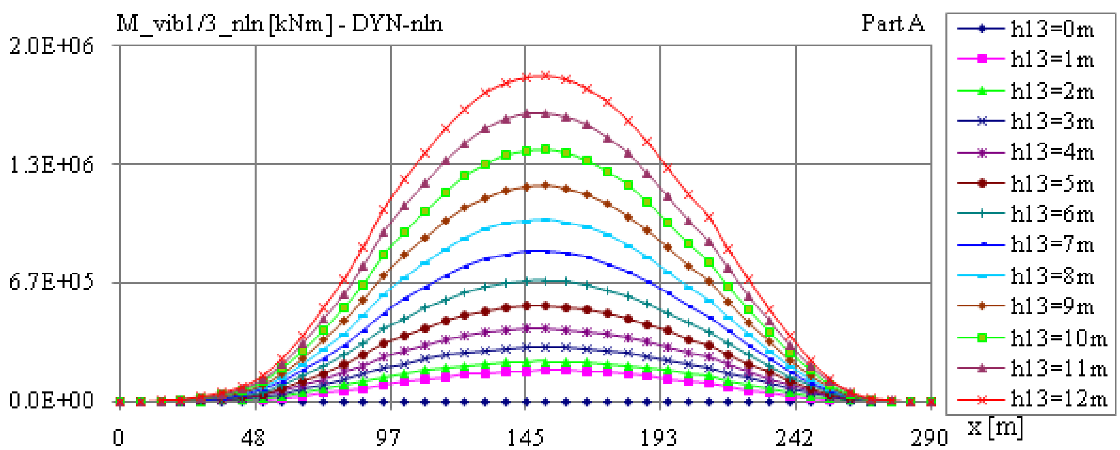

Figure 104.The distribution of the significant bending moments at vibrations over the ship length, at dynamic non-linear analysis for $h_{1/3} = 0.0$ to 12.0m (step 1.0m, part A) – LC_F

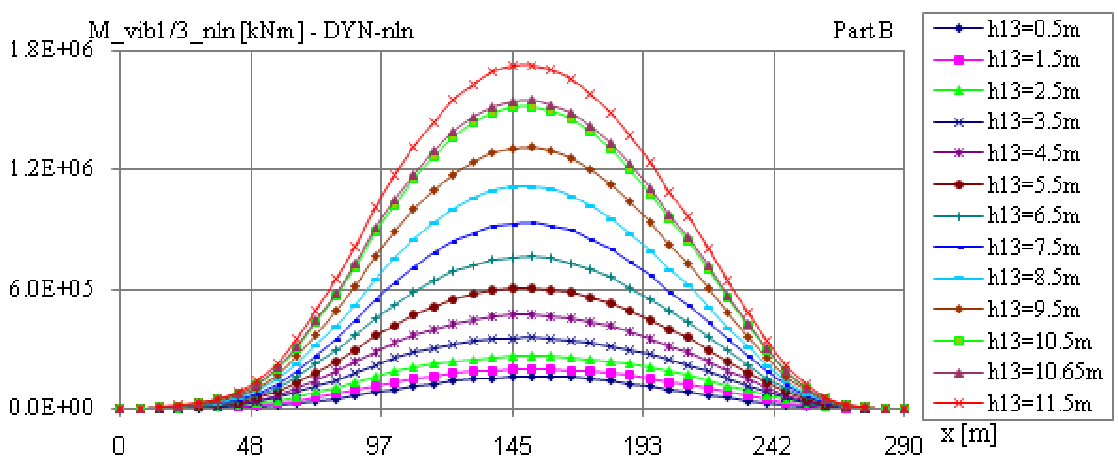

Figure 105. The distribution of the significant bending moments at vibrations over the ship length, at dynamic non-linear analysis for $h_{1/3} = 0.5$ to 11.5m (step 1.0m, part B) – LC_F

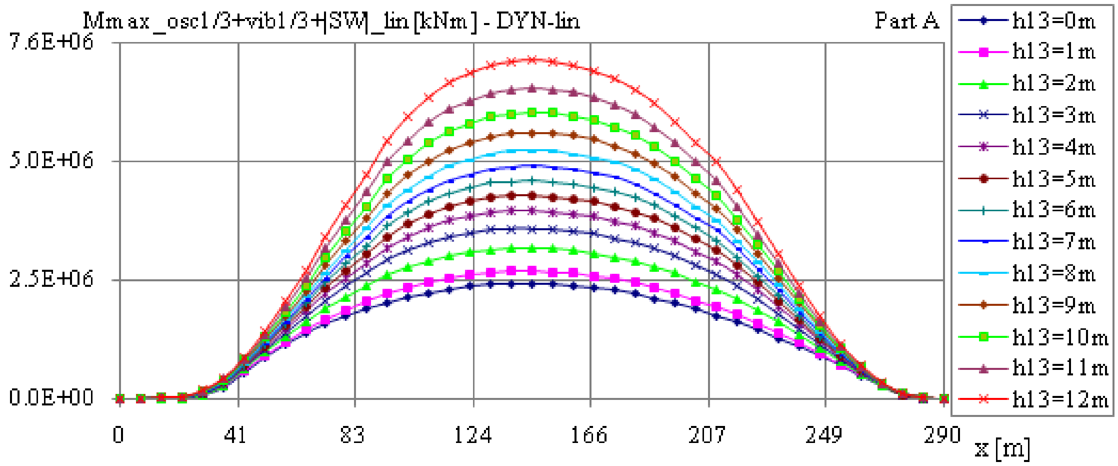

Figure 106. The distribution of the significant bending moments at still water + oscillation + vibrations over the ship length, at dynamic linear analysis for $h_{1/3}$ = 0.0 to 12.0m (step 1.0m, part A) – LC_F

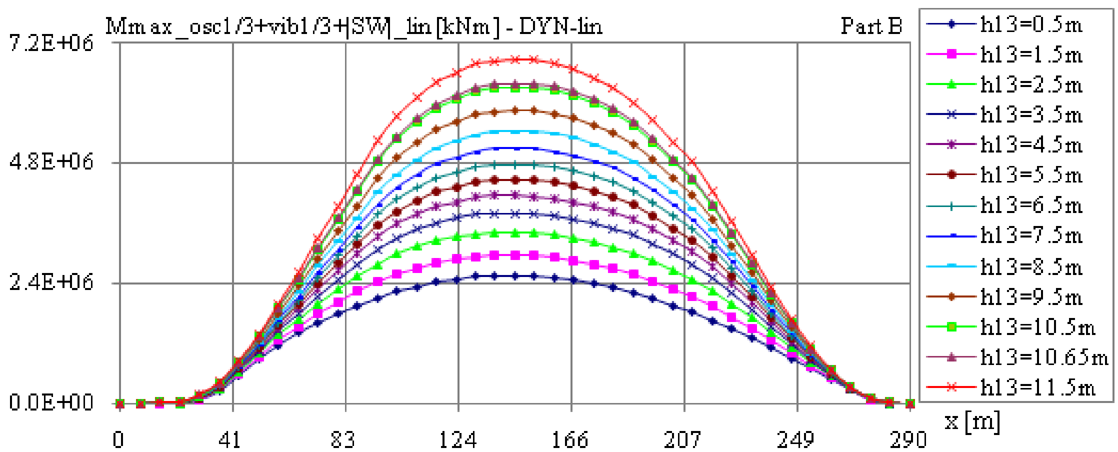

Figure 107. The distribution of the significant bending moments at still water + oscillation + vibrations over the ship length, at dynamic linear analysis for $h_{1/3}$ = 0.5 to 11.5m (step 1.0m, part B) – LC_F

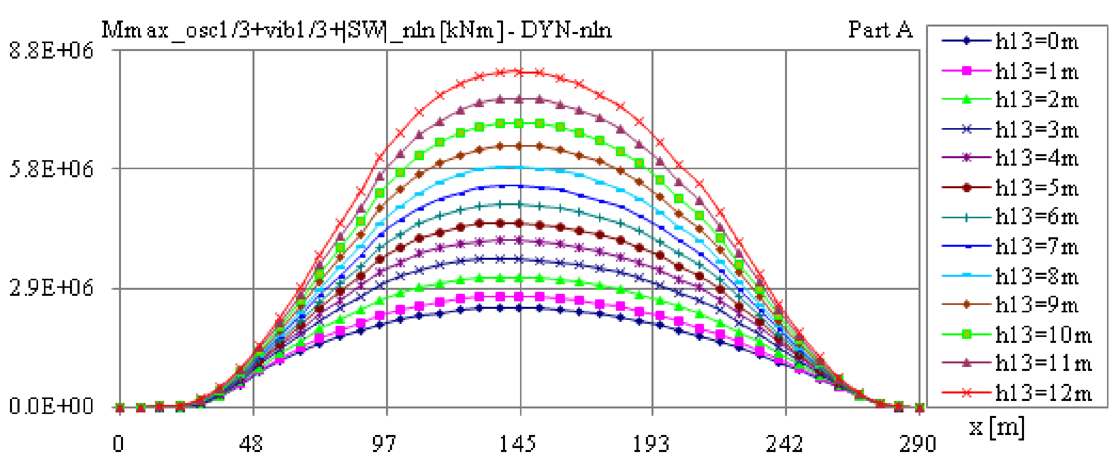

Figure 108. The distribution of the significant bending moments at still water + oscillation + vibrations over the ship length, at dynamic non-linear analysis for $h_{1/3}$ = 0.0 to 12.0m (step 1.0m, part A) – LC_F

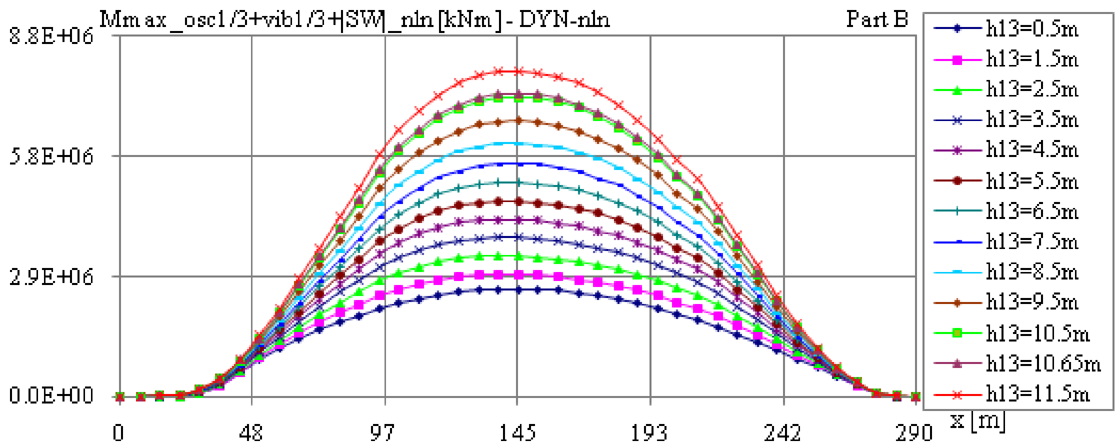

Figure 109. The distribution of the significant bending moments at still water + oscillation + vibrations over the ship length, at dynamic non-linear analysis for $h_{1/3}$ = 0.5 to 11.5m (step 1.0m, part B) – LC_F

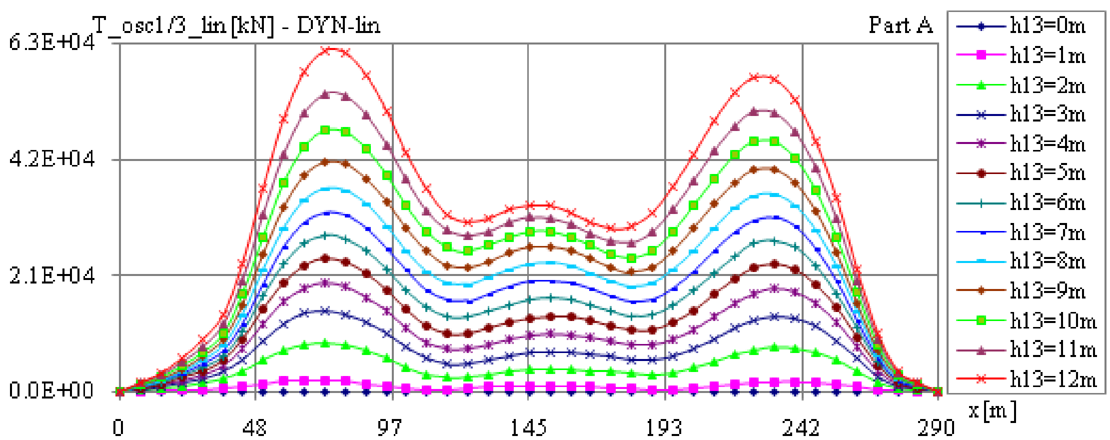

Figure 110. The distribution of the significant shear forces at oscillations over the ship length, at dynamic linear analysis for $h_{1/3}$ = 0.0 to 12.0m (step 1.0m, part A) – LC_F

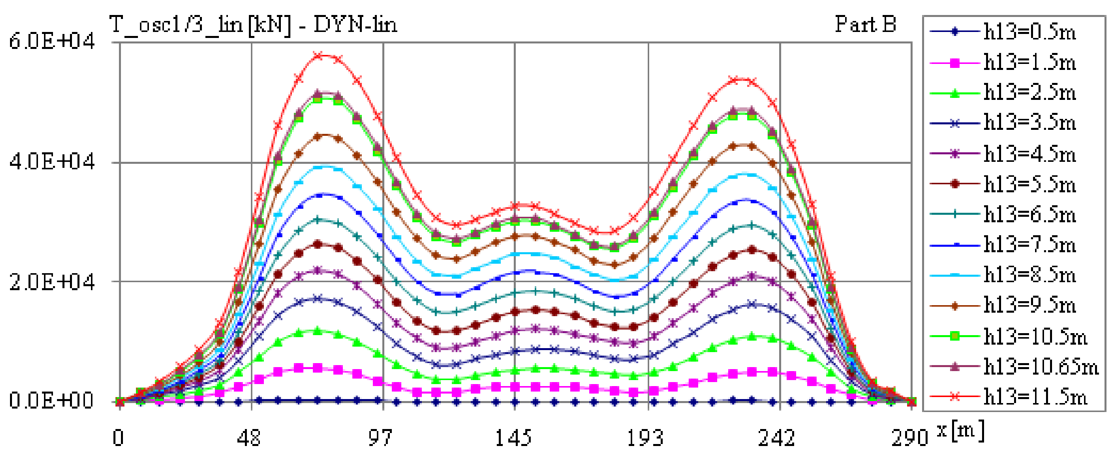

Figure 111. The distribution of the significant shear forces at oscillations over the ship length, at dynamic linear analysis for $h_{1/3}$ = 0.5 to 11.5m (step 1.0m, part B) – LC_F

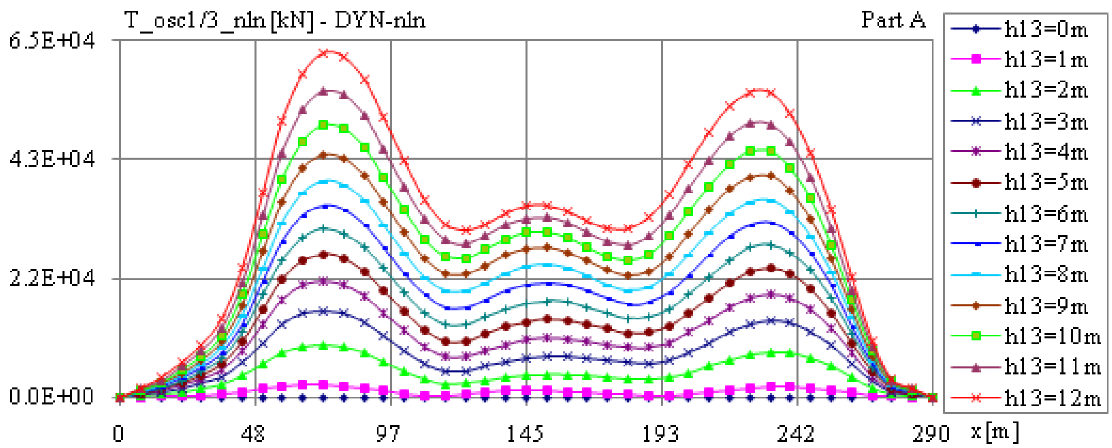

Figure 112. The distribution of the significant shear forces at oscillations over the ship length, at dynamic non-linear analysis for $h_{1/3}$ = 0.0 to 12.0m (step 1.0m, part A) – LC_F

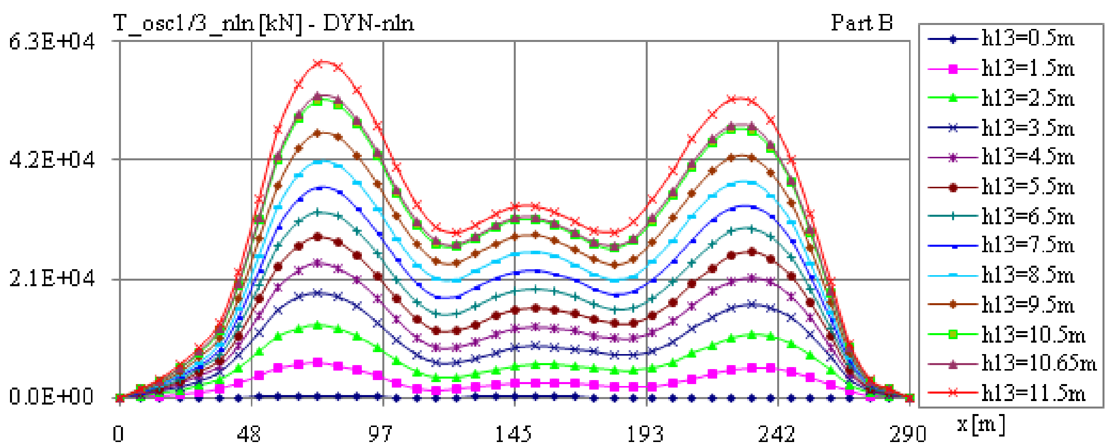

Figure 113. The distribution of the significant shear forces at oscillations over the ship length, at dynamic non-linear analysis for $h_{1/3}$ = 0.5 to 11.5m (step 1.0m, part B) – LC_F

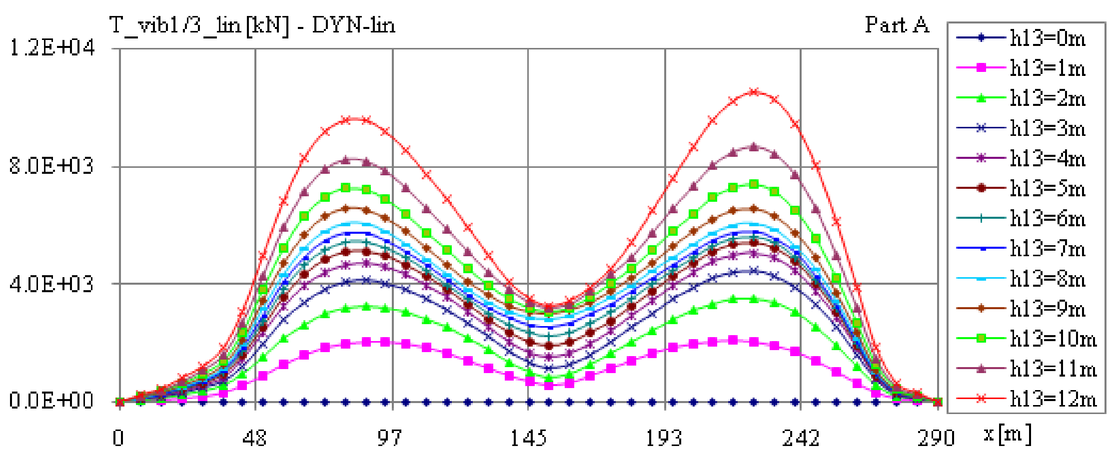

Figure 114. The distribution of the significant shear forces at vibrations over the ship length, at dynamic linear analysis for $h_{1/3}$ = 0.0 to 12.0m (step 1.0m, part A) – LC_F

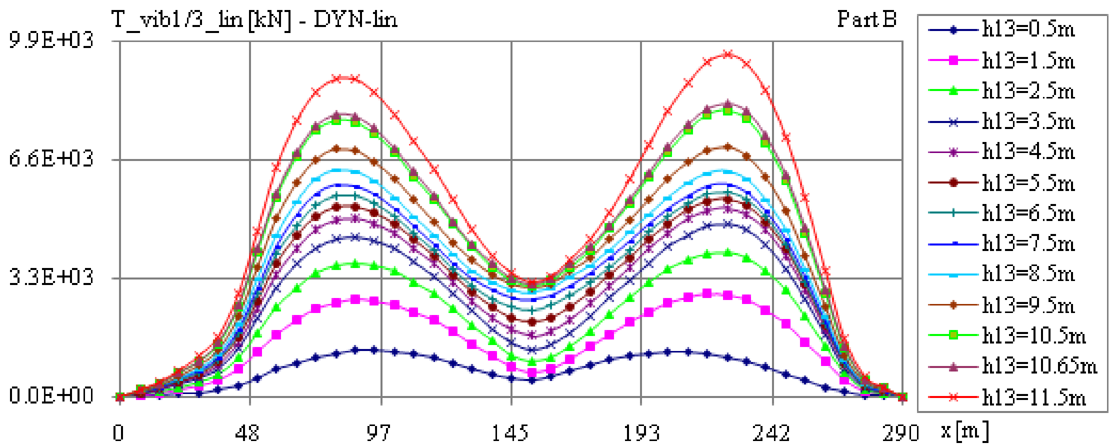

Figure 115. The distribution of the significant shear forces at vibrations over the ship length, at dynamic linear analysis for $h_{1/3}$ = 0.5 to 11.5m (step 1.0m, part B) – LC_F

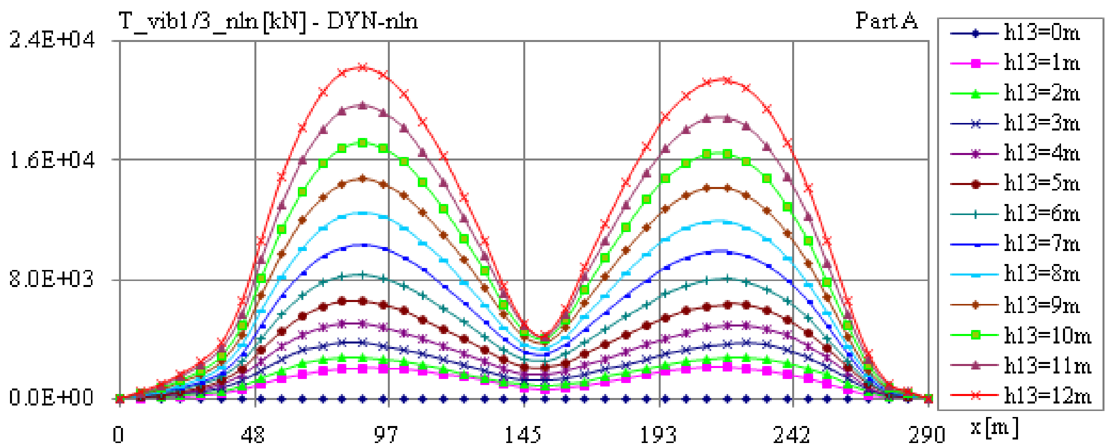

Figure 116. The distribution of the significant shear forces at vibrations over the ship length, at dynamic non-linear analysis for $h_{1/3}$ = 0.0 to 12.0m (step 1.0m, part A) – LC_F

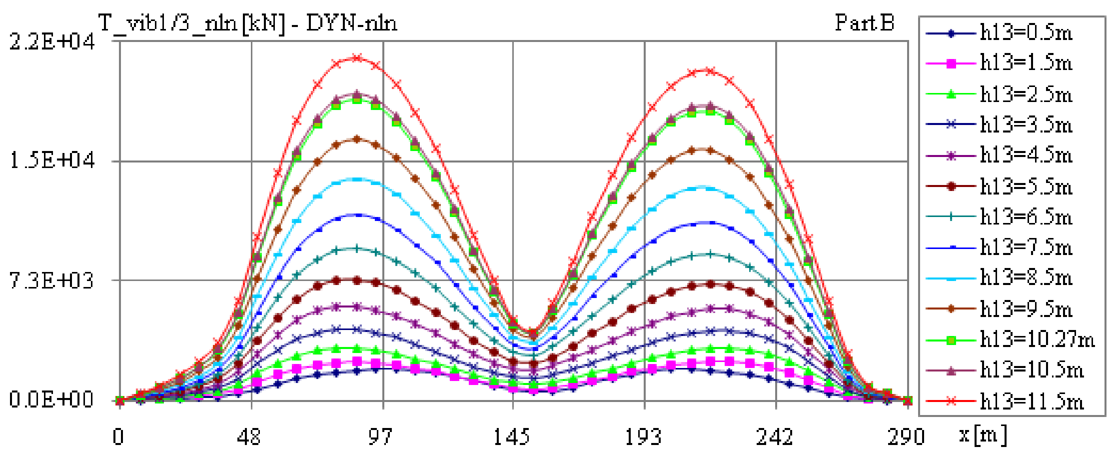

Figure 117. The distribution of the significant shear forces at vibrations over the ship length, at dynamic non-linear analysis for $h_{1/3}$ = 0.5 to 11.5m (step 1.0m, part B) – LC_F

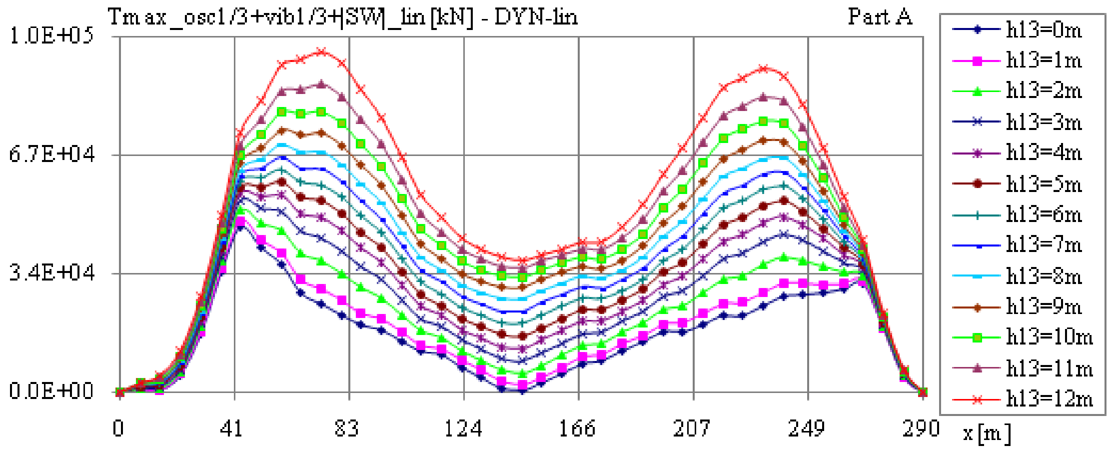

Figure 118. The distribution of the significant shear forces at still water + oscillations + vibrations over the ship length, at dynamic linear analysis for $h_{1/3}$ = 0.0 to 12.0m (step 1.0m, part A) – LC_F

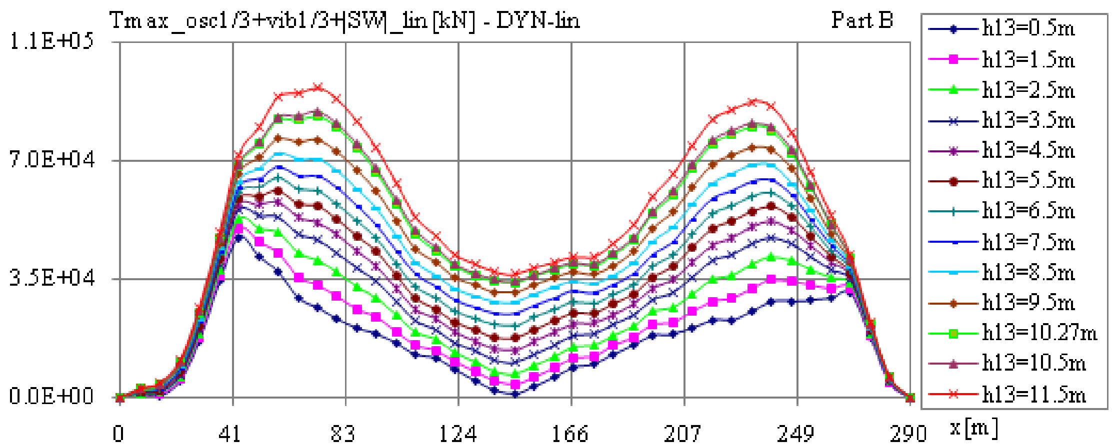

Figure 119. The distribution of the significant shear forces at still water + oscillations + vibrations over the ship length, at dynamic linear analysis for $h_{1/3}$ = 0.5 to 11.5m (step 1.0m, part B) – LC_F

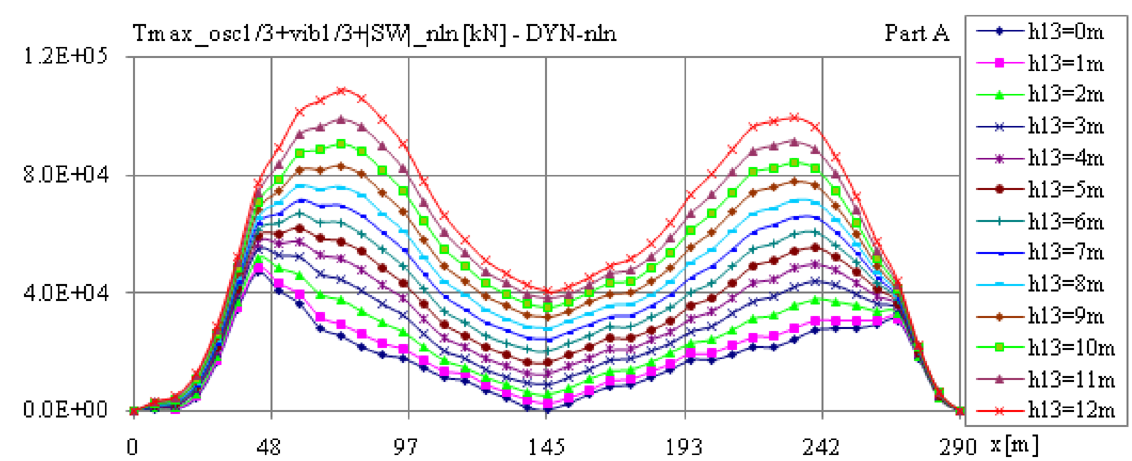

Figure 120.The distribution of the significant shear forces at still water + oscillations + vibrations over the ship length, at dynamic non-linear analysis for $h_{1/3}$ = 0.0 to 12.0m (step 1.0m, part A) – LC_F

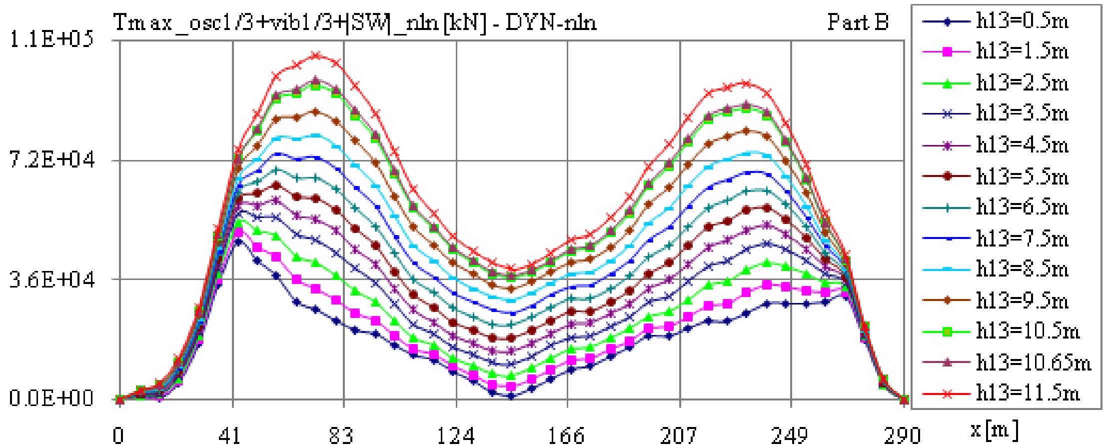

Figure 121.The distribution of the significant shear forces at still water + oscillations + vibrations over the ship length, at dynamic non-linear analysis for $h_{1/3}$ = 0.5 to 11.5m (step 1.0m, part B) – LC_F

4.3.2. Ballast Loading Case

In the following section are presented the numerical analyses of the linear and non-linear dynamic response of the studied bulk carrier for the ballast loading condition.

For the ballast loading case in the following figures are presented:

- in Figure 122 and Figure 123 are presented the time record and the amplitude spectrum FFT for wave model Longuet-Higgins, with the first order power density spectrum function ITTC, for significant wave height $h_{1/3}$=10.65m, at section x/L = 0.50;

- in Figure 124 to Figure 127 are presented the time record and the amplitude spectrum FFT for the dynamic displacement at oscillations and vibrations, at linear and non-linear analyses, for $h_{1/3}$=10.65m, at section x/L = 0.50;

- in Figure 128 to Figure 139 are presented the time record and the amplitude spectrum FFT for the dynamic bending moments at oscillations and vibrations (hydroelasticity), at linear and non-linear analyses, for $h_{1/3}$=10.65m, for sections x/L = 0.25, 0.50 and 0.75;

- in Figure 140 to Figure 151 are presented the time record and the amplitude spectrum FFT for the dynamic shear forces at oscillations and vibrations (hydroelasticity), at linear and non-linear analyses, for $h_{1/3}$=10.65m, for sections x/L = 0.25, 0.50 and 0.75.

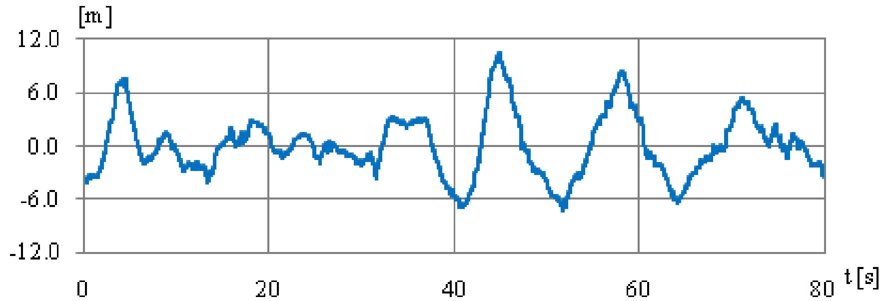

Figure 122. Time record for wave model Longuet-Higgins, with the first order power density spectrum function ITTC, at significant wave height $h_{1/3}$=10.65m at x/L=0.50 – LC_B

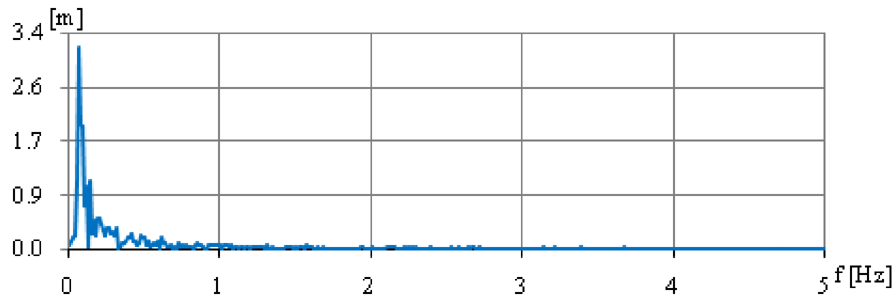

Figure 123. Amplitude spectrum FFT wave model Longuet-Higgins, with the first order power density spectrum function ITTC, at significant wave height $h_{1/3}$=10.65m at x/L=0.50 – LC_B

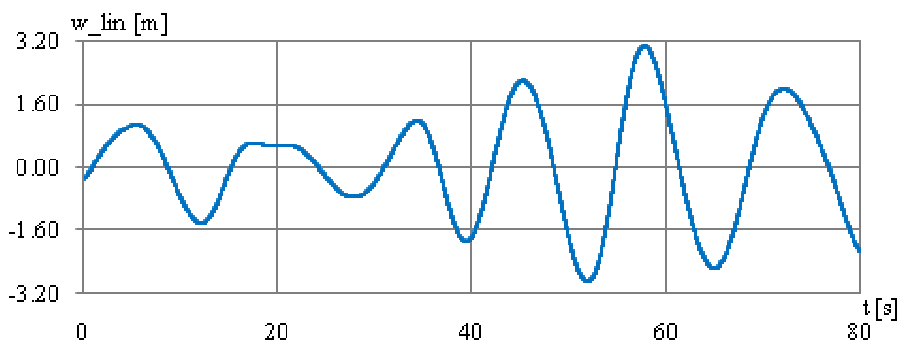

Figure 124. Time record for the dynamic displacement at oscillations and vibrations at linear analysis, significant wave height $h_{1/3}$=10.65m at x/L=0.50 – LC_B

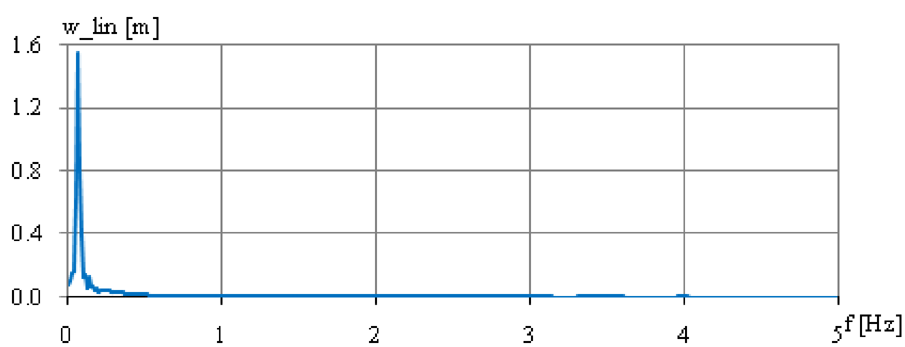

Figure 125. Amplitude spectrum FFT for the dynamic displacement at oscillations and vibrations at linear analysis, significant wave height $h_{1/3}$=10.65m at x/L=0.50 – LC_B

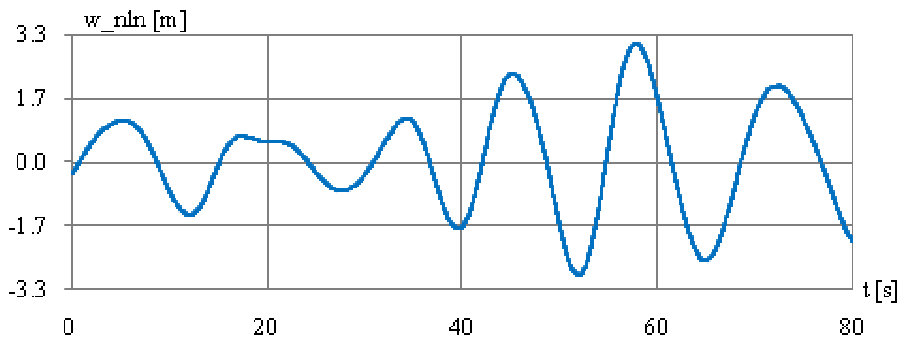

Figure 126. Time record for the dynamic displacement at oscillations and vibrations at non-linear analysis, significant wave height $h_{1/3}$=10.65m at x/L=0.50 – LC_B

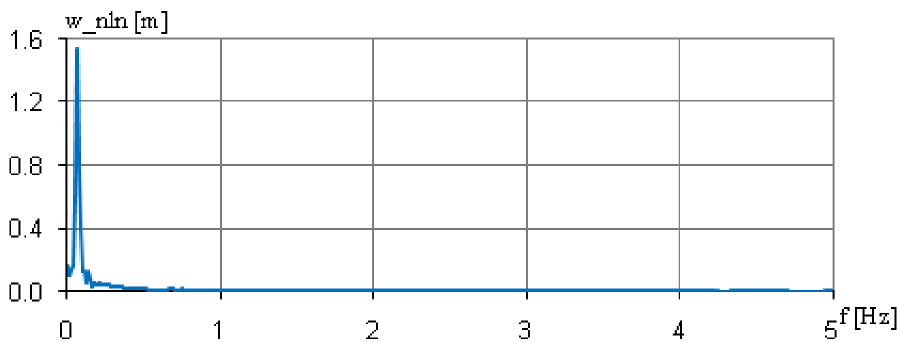

Figure 127. Amplitude spectrum FFT for the dynamic displacement at oscillations and vibrations at non-linear analysis, significant wave height $h_{1/3}$=10.65m at x/L=0.50 – LC_B

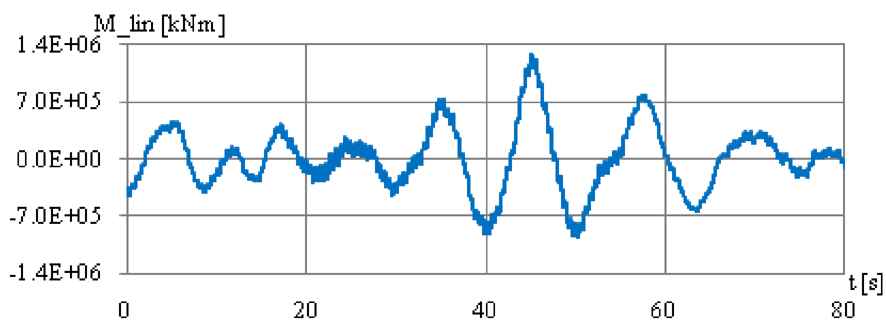

Figure 128. Time record for the dynamic bending moments at oscillations and vibrations at linear analysis, significant wave height $h_{1/3}$=10.65m at x/L=0.25 – LC_B

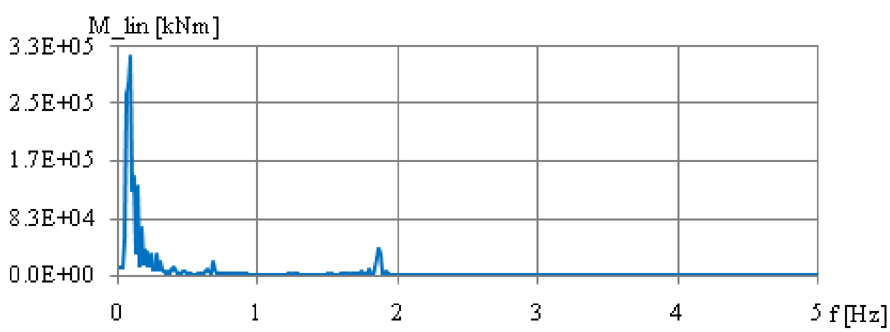

Figure 129. Amplitude spectrum FFT for the dynamic bending moment at oscillations and vibrations at linear analysis, significant wave height $h_{1/3}$=10.65m at x/L=0.25 – LC_B

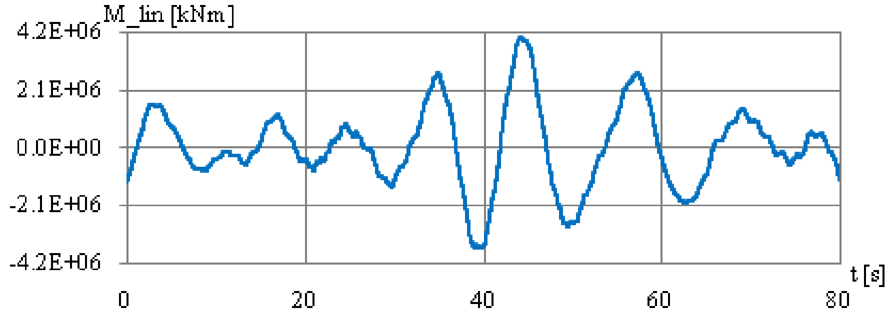

Figure 130. Time record for the dynamic bending moments at oscillations and vibrations at linear analysis, significant wave height $h_{1/3}$=10.65m at x/L=0.50 – LC_B

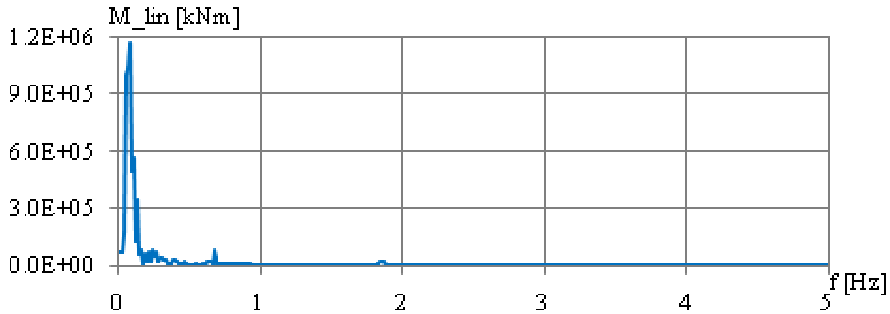

Figure 131. Amplitude spectrum FFT for the dynamic bending moment at oscillations and vibrations at linear analysis, significant wave height $h_{1/3}$=10.65m at x/L=0.50 – LC_B

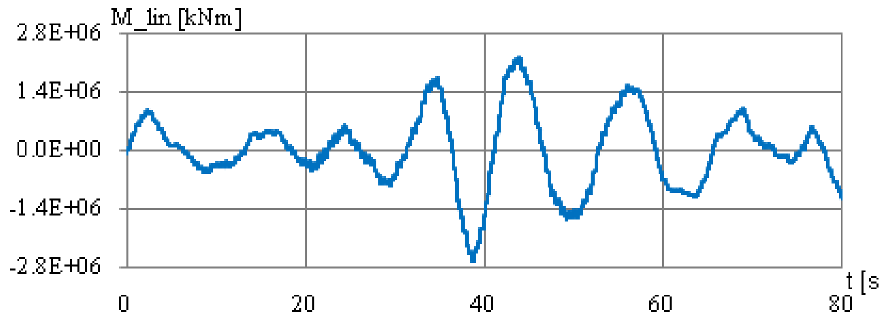

Figure 132. Time record for the dynamic bending moments at oscillations and vibrations at linear analysis, significant wave height $h_{1/3}$=10.65m at x/L=0.75 – LC_B

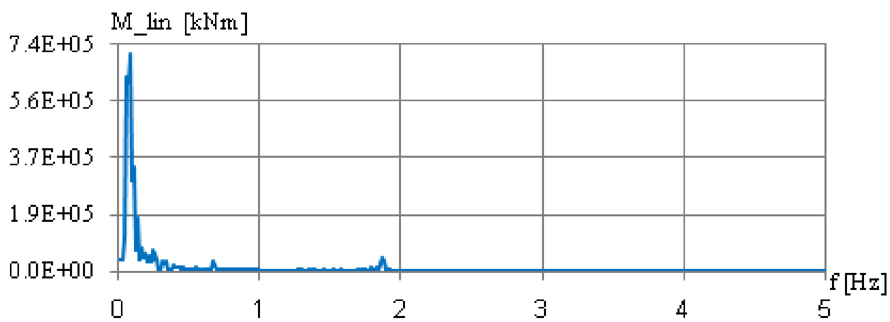

Figure 133. Amplitude spectrum FFT for the dynamic bending moment at oscillations and vibrations at linear analysis, significant wave height $h_{1/3}$=10.65m at x/L=0.75 – LC_B

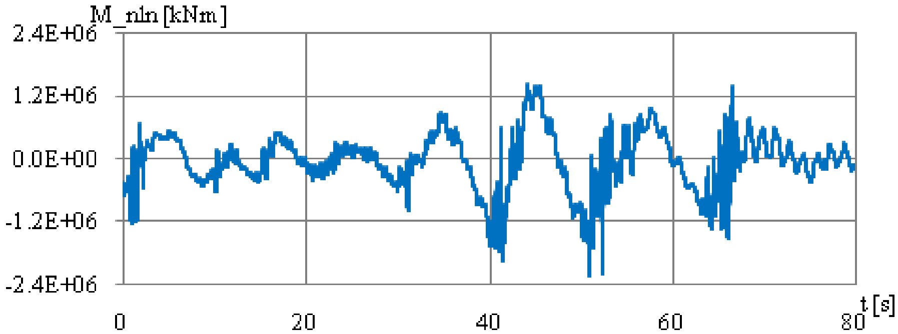

Figure 134. Time record for the dynamic bending moments at oscillations and vibrations at non-linear analysis, significant wave height $h_{1/3}$=10.65m at x/L=0.25 – LC_B

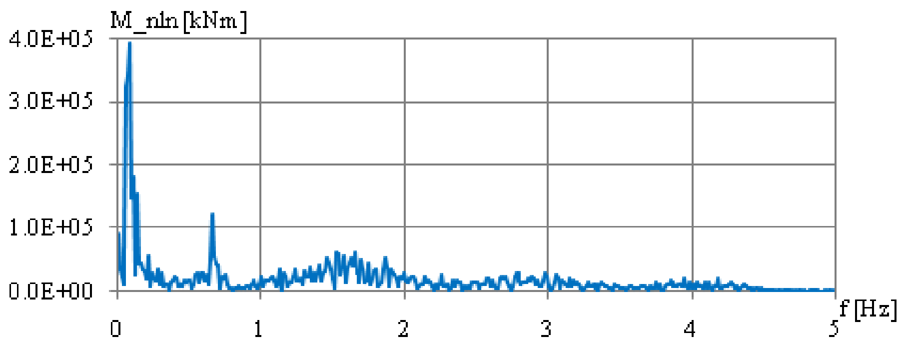

Figure 135. Amplitude spectrum FFT for the dynamic bending moment at oscillations and vibrations at non-linear analysis, significant wave height $h_{1/3}$=10.65m at x/L=0.25 – LC_B

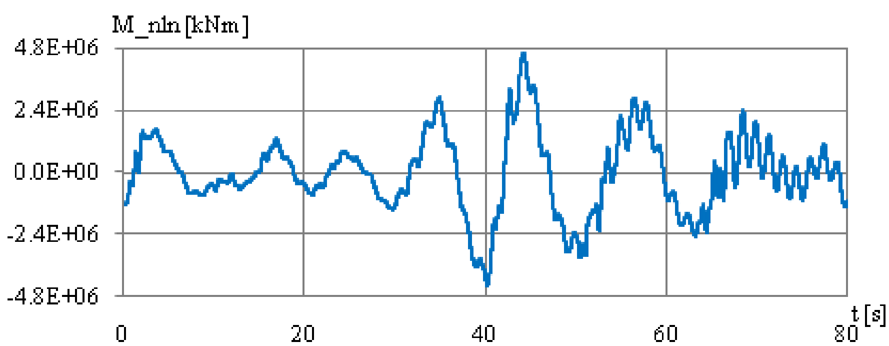

Figure 136. Time record for the dynamic bending moments at oscillations and vibrations at non-linear analysis, significant wave height $h_{1/3}$=10.65m at x/L=0.50 – LC_B

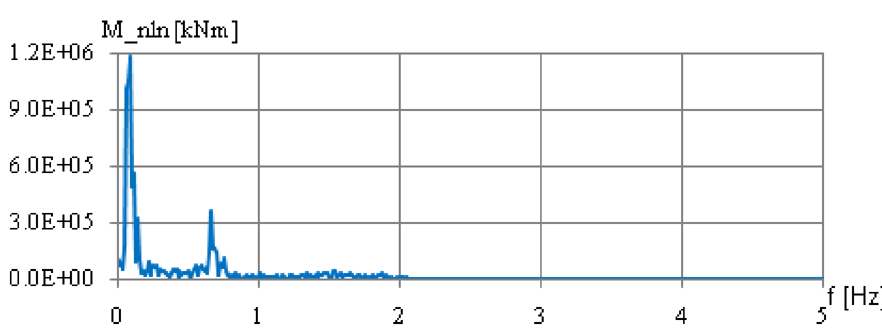

Figure 137. Amplitude spectrum FFT for the dynamic bending moment at oscillations and vibrations at non-linear analysis, significant wave height $h_{1/3}$=10.65m at x/L=0.50 – LC_B

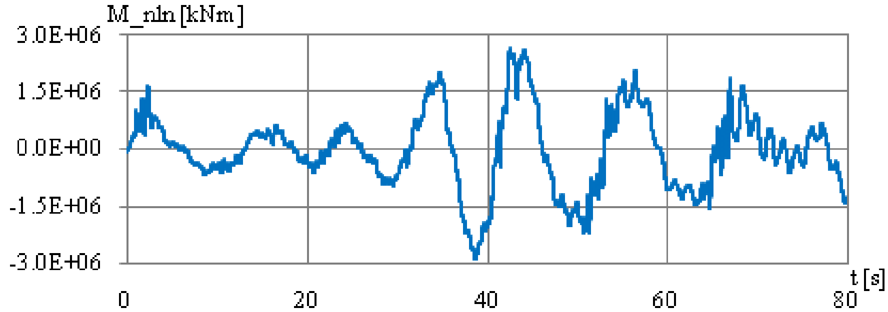

Figure 138. Time record for the dynamic bending moments at oscillations and vibrations at non-linear analysis, significant wave height $h_{1/3}$=10.65m at x/L=0.75 – LC_B

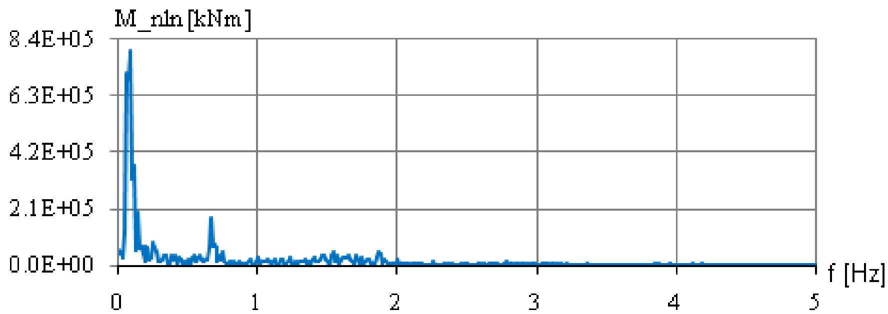

Figure 139. Amplitude spectrum FFT for the dynamic bending moment at oscillations and vibrations at non-linear analysis, significant wave height $h_{1/3}$=10.65m at x/L=0.75 – LC_B

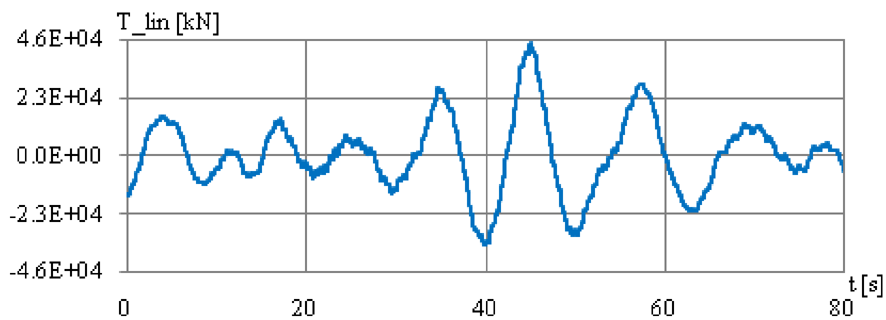

Figure 140. Time record for the dynamic shear forces at oscillations and vibrations at linear analysis, significant wave height $h_{1/3}$=10.65m at x/L=0.25 – LC_B

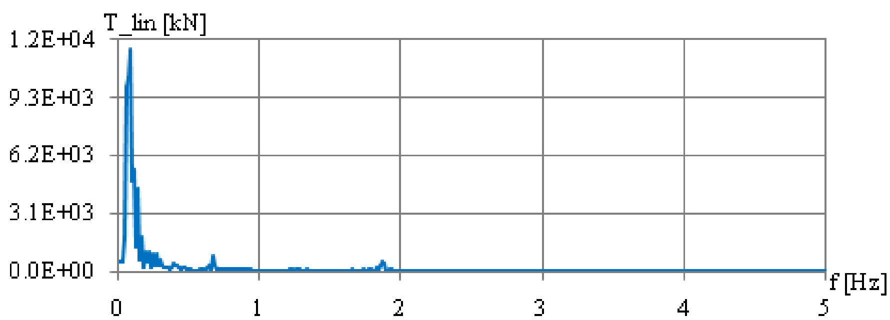

Figure 141. Amplitude spectrum FFT for the dynamic shear forces at oscillations and vibrations at linear analysis, significant wave height $h_{1/3}$=10.65m at x/L=0.25 – LC_B

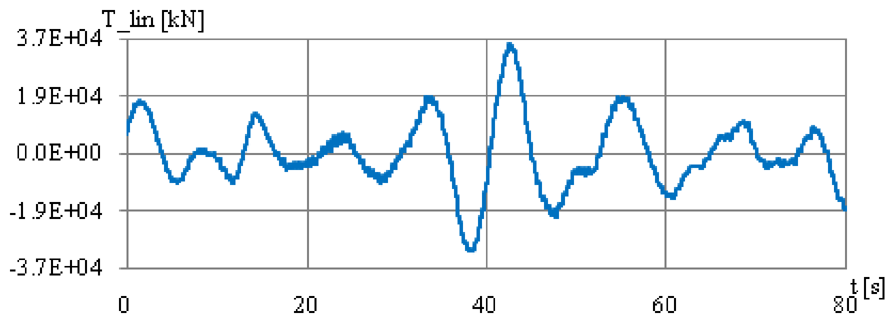

Figure 142. Time record for the dynamic shear forces at oscillations and vibrations at linear analysis, significant wave height $h_{1/3}$=10.65m at x/L=0.50 – LC_B

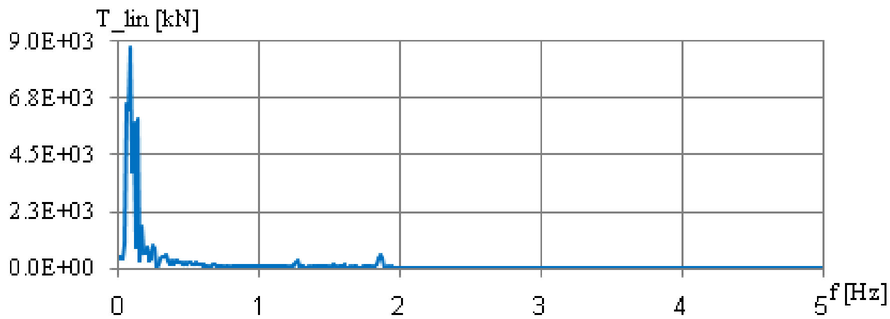

Figure 143. Amplitude spectrum FFT for the dynamic shear forces at oscillations and vibrations at linear analysis, significant wave height $h_{1/3}$=10.65m at x/L=0.50 – LC_B

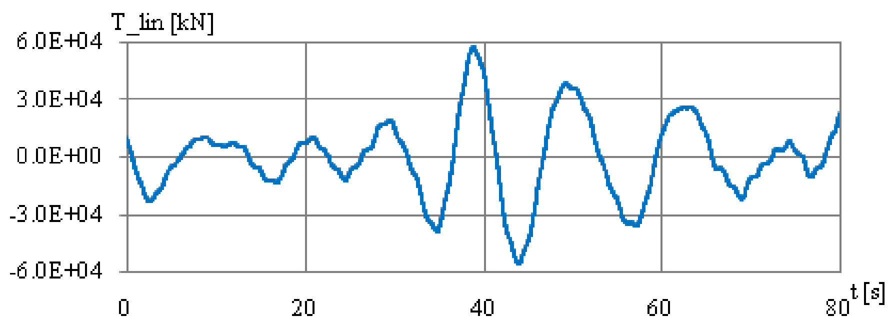

Figure 144. Time record for the dynamic shear forces at oscillations and vibrations at linear analysis, significant wave height $h_{1/3}$=10.65m at x/L=0.75 – LC_B

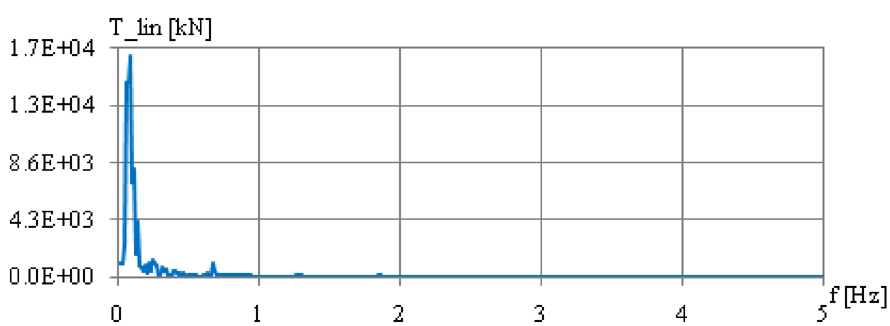

Figure 145. Amplitude spectrum FFT for the dynamic shear forces at oscillations and vibrations at linear analysis, significant wave height $h_{1/3}$=10.65m at x/L=0.75 – LC_B

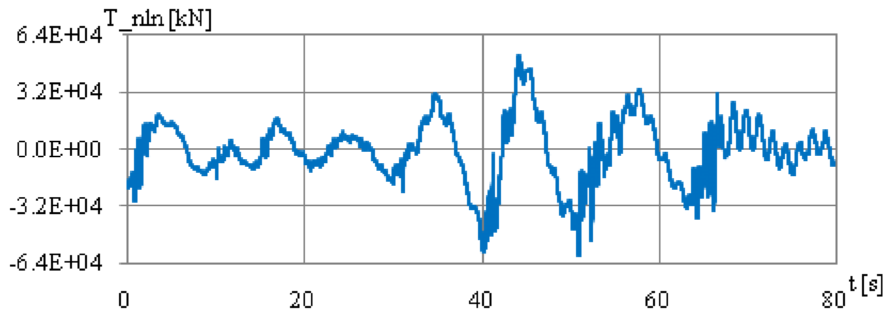

Figure 146. Time record for the dynamic shear forces at oscillations and vibrations at non-linear analysis, significant wave height $h_{1/3}$=10.65m at x/L=0.25 – LC_B

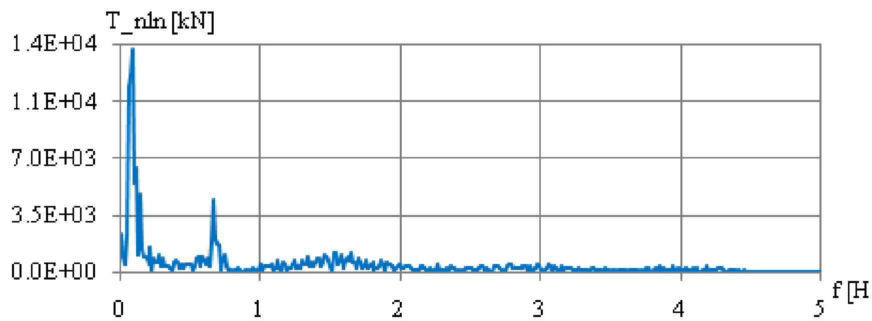

Figure 147. Amplitude spectrum FFT for the dynamic shear forces at oscillations and vibrations at non-linear analysis, significant wave height $h_{1/3}$=10.65m at x/L=0.25– LC_B

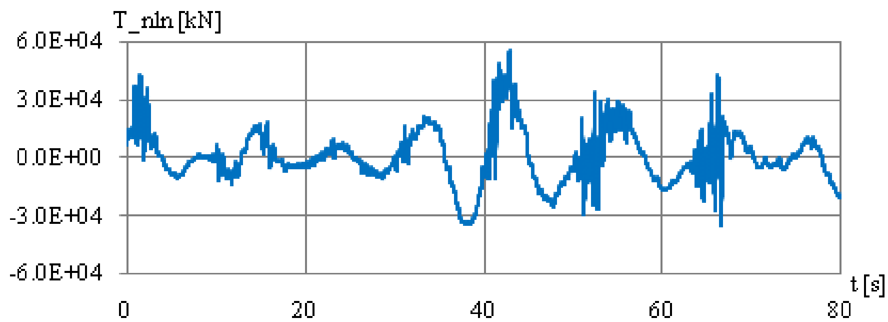

Figure 148. Time record for the dynamic shear forces at oscillations and vibrations at non-linear analysis, significant wave height $h_{1/3}$=10.65m at x/L=0.50 – LC_B

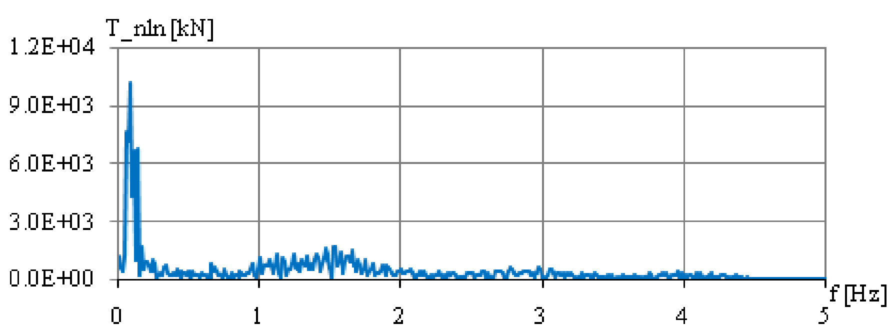

Figure 149. Amplitude spectrum FFT for the dynamic shear forces at oscillations and vibrations at non-linear analysis, significant wave height $h_{1/3}$=10.65m at x/L=0.50– LC_B

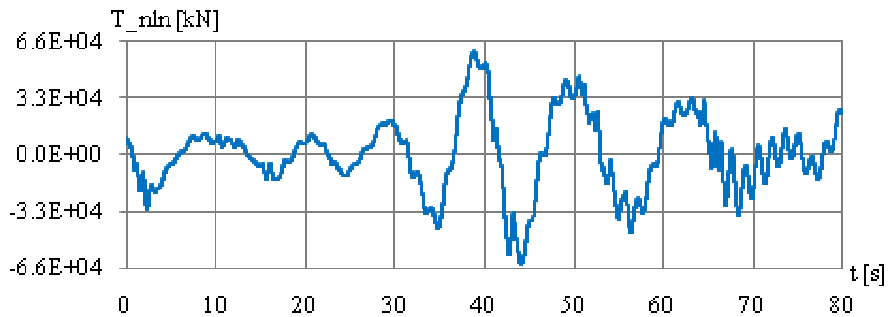

Figure 150. Time record for the dynamic shear forces at oscillations and vibrations at non-linear analysis, significant wave height $h_{1/3}$=10.65m at x/L=0.75 – LC_B

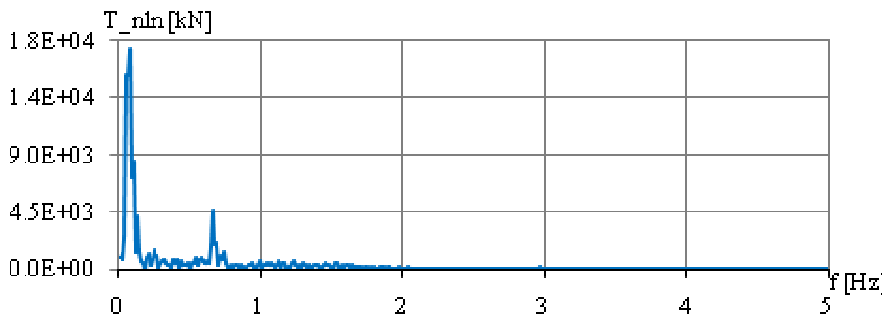

Figure 151. Amplitude spectrum FFT for the dynamic shear forces at oscillations and vibrations at non-linear analysis, significant wave height $h_{1/3}$=10.65m at x/L=0.75 – LC_B

The numerical result presented in the following tables and figures are for ballast load condition:

- in Table 21 is presented the ratio between the significant deformation at fundamental natural vibration mode and the significant displacement at the ship rigid hull oscillations, at linear and non-linear dynamic analyses, based on hydroelasticity theory;

- in Table 22
Table 22 is presented the ratio between the significant bending moment at fundamental natural vibration mode and the significant bending moment at the ship rigid hull oscillations, at linear and non-linear dynamic analyses, based on hydroelasticity theory;

- in Table 23 is presented the ratio between the significant shear force at fundamental natural vibration mode and the significant shear force at the ship rigid hull oscillations, at linear and non-linear dynamic analyses, based on hydroelasticity theory;

- in Table 24 are presented the maximum values of the bending moments and the shear forces for the following components: still water, oscillations, vibrations on fundamental mode, at linear and non-linear numerical analysis;

- in Figure 152 and Figure 153 are presented the still water bending moments and shear forces diagrams;

- in Figure 154 to Figure 157 are presented the distribution of the significant bending moments at oscillations over the ship length, at dynamic linear and non-linear analysis, for $h_{1/3} = 0.0\text{-}12.0$m;

- in Figure 158 to Figure 161 are presented the distribution of the significant bending moments at vibration on fundamental mode over the ship length, at dynamic linear and non-linear analysis, for $h_{1/3} = 0.0\text{-}12.0$m;

- in Figure 162 to Figure 165 the distribution of the bending moments at oscillations and vibrations over the ship length, at dynamic linear and non-linear analysis added to still water values, for $h_{1/3} = 0.0\text{-}12.0$m;

- in Figure 166 to Figure 169 the distribution of the significant shear forces at oscillation over the ship length, at dynamic linear and non-linear analysis, for $h_{1/3} = 0.0\text{-}12.0$m;

- in Figure 170 to Figure 173 the distribution of the significant shear forces at vibration on fundamental mode over the ship length, at dynamic linear and non-linear analysis, for $h_{1/3} = 0.0\text{-}12.0$m;

- in Figure 174 to Figure 177 the distribution of the shear forces at oscillations and vibrations over the ship length, at dynamic linear and non-linear analysis added to still water values, for $h_{1/3} = 0.0\text{-}12.0$m.

Table 21. Ratio between the significant vibration deformation $w_{1/3\_vib}$ and the significant oscillation displacement $w_{1/3\_osc}$ (for ballast loading condition)

Ballast Load Cond		$w_{1/3}$_vib / $w_{1/3}$_osc ref. $h_{1/3}$=10.65m				$h_{1/3}$ [m] limit		
Nr	Section	x[m]	x/L	%vib/osc linear	%vib/osc nonlinear	bottom slamming	side slamming	green sea
1	aft	14.5	0.05	3.16	3.27	> 0	Yes	No
2	L/4	72.5	0.25	3.23	3.29			
3	L/2	145.0	0.50	3.34	3.37			
4	3L/4	217.50	0.75	3.52	3.54			
5	fore	275.50	0.95	3.48	3.55	> 8.5	Yes	No
		average value:		**3.35**	**3.40**			

Table 22. Ratio between the significant vibration bending moment $M_{1/3\_vib}$ and the significant oscillation bending moment $M_{1/3\_osc}$ (for ballast loading condition)

Ballast Load Cond		M_vib$_{1/3}$ / M_osc$_{1/3}$ ref. $h_{1/3}$=10.65m				DYN LIN & NLN	
Nr	Section	x[m]	x/L	%vib/osc linear	%vib/osc nonlinear	springing	whipping
1	aft	14.50	0.05	10.63	32.71	*linear:* very reduced *nonlinear:* small	high
2	L/4	72.50	0.25	10.95	34.26		
3	L/2	145.00	0.50	10.94	35.67		
4	3L/4	217.50	0.75	9.59	26.10		
5	fore	275.50	0.95	9.12	20.74		
		average value:		**10.25**	**29.90**		

Table 23. Ratio between the significant vibration shear force $T_{1/3\_vib}$ and the significant oscillation shear force $T_{1/3\_osc}$ (for ballast loading condition)

Ballast Load Cond		$T\_vib_{1/3}$ / $T\_osc_{1/3}$ ref. $h_{1/3}$=10.27m				DYN LIN & NLN	
Nr	Section	x[m]	x/L	%vib/osc linear	%vib/osc nonlinear	springing	whipping
1	aft	14.50	0.05	10.41	29.96	*linear:* very reduced *nonlinear:* small	high
2	L/4	72.50	0.25	10.92	32.68		
3	L/2	145.00	0.50	9.73	17.92		
4	3L/4	217.50	0.75	10.02	28.78		
5	fore	275.50	0.95	8.98	19.78		
		average value:		**10.01**	**25.82**		

Table 24. Maximum bending moments and shear forces in ballast loading case

Ballast Loading Cond.		$h_{1/3}$=10.65m	
Bending moment maximal [kNm]		Shear force maximal [kN]	
|Msw| still water	3.15E+05	|Tac| still water	1.09E+04
$M\_osc_{1/3}\_ADV$-lin	3.31E+06	$T_{1/3}\_osc\_ADV$-lin	4.66E+04
$M\_osc_{1/3}\_HEL$-lin	3.31E+06	$T_{1/3}\_osc\_HEL$-lin	4.66E+04
$M\_vib_{1/3}\_HEL$-lin	1.39E+05	$T_{1/3}\_vib\_HEL$-lin	1.87E+03
$M\_osc_{1/3}\_DYN$-lin	3.56E+06	$T_{1/3}\_osc\_DYN$-lin	5.01E+04
$M\_vib_{1/3}\_DYN$-lin	3.87E+05	$T_{1/3}\_vib\_DYN$-lin	4.95E+03
$M\_osc_{1/3}\_DYN$-nln	3.57E+06	$T_{1/3}\_osc\_DYN$-nln	4.99E+04
$M\_vib_{1/3}\_DYN$-nln	1.28E+06	$T_{1/3}\_vib\_DYN$-nln	1.46E+04

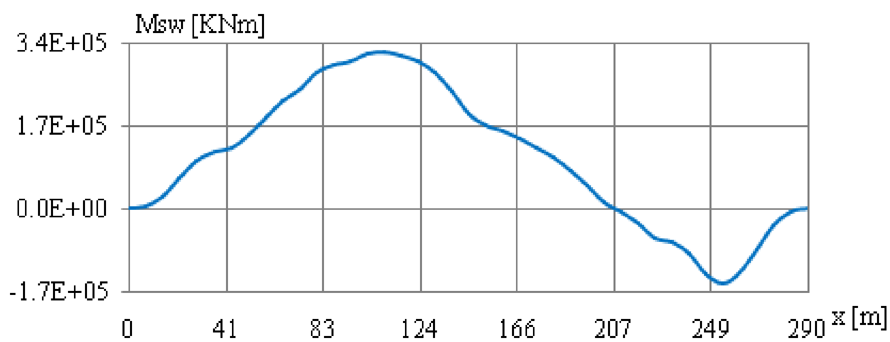

Figure 152. Still water bending moment diagram in ballast loading condition

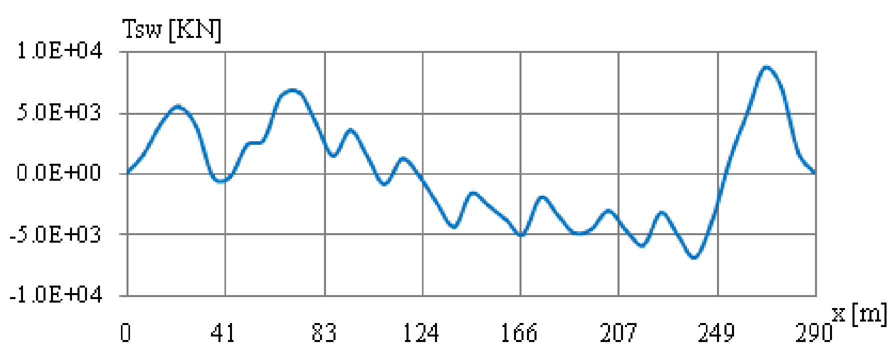

Figure 153. Still water shear forces diagram in ballast loading condition

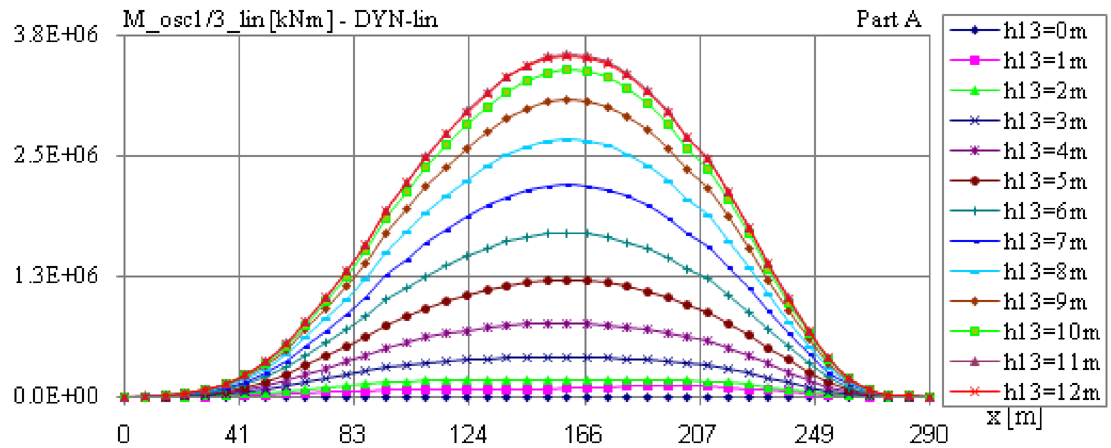

Figure 154. The distribution of the significant bending moments at oscillations over the ship length, at dynamic linear analysis for $h_{1/3}$ = 0.0 to 12.0m (step 1.0m, part A) – LC_B

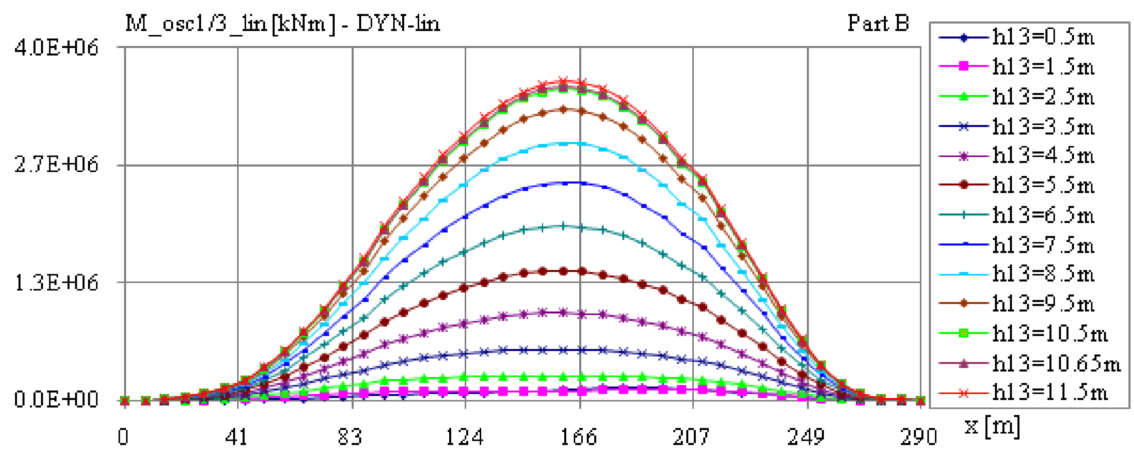

Figure 155. The distribution of the significant bending moments at oscillations over the ship length, at dynamic linear analysis for $h_{1/3}$ = 0.5 to 11.5m (step 1.0m, part B) – LC_B

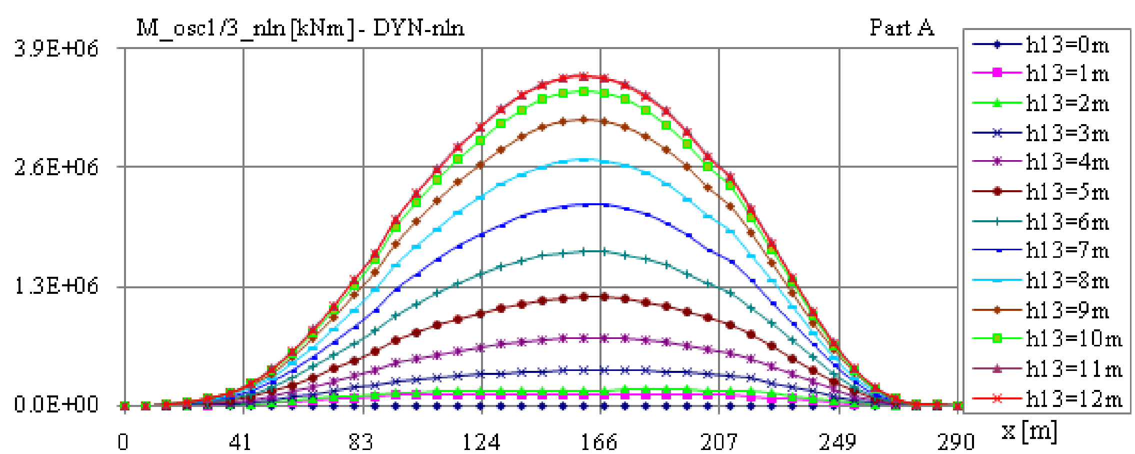

Figure 156. The distribution of the significant bending moments at oscillations over the ship length, at dynamic non-linear analysis for $h_{1/3}$ = 0.0 to 12.0m (step 1.0m, part A) – LC_B

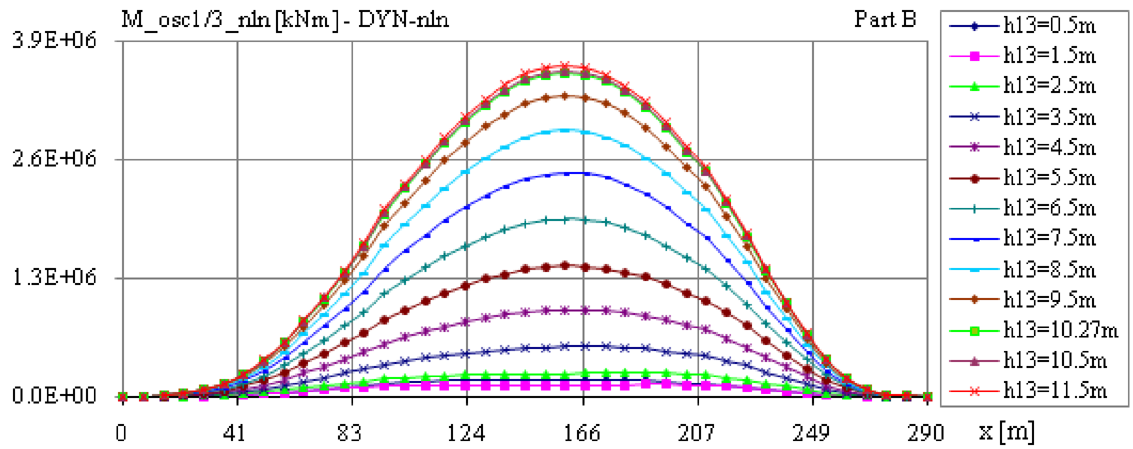

Figure 157. the distribution of the significant bending moments at oscillations over the ship length, at dynamic non-linear analysis for $h_{1/3}$=0.5 to 11.5m (step 1.0m, part B) - LC_B

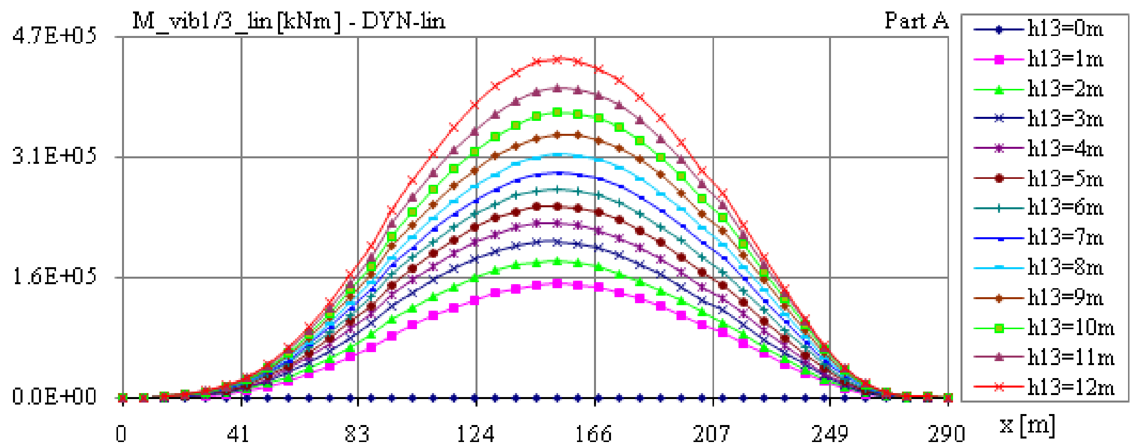

Figure 158. The distribution of the significant bending moments at vibrations over the ship length, at dynamic linear analysis for $h_{1/3}$ = 0 to 12m (step 1.0m, part A) – LC_B

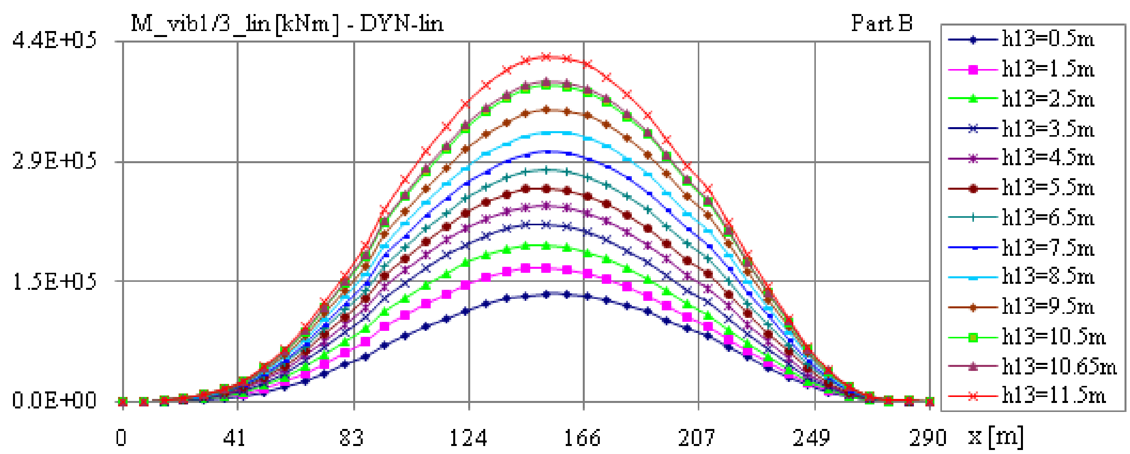

Figure 159 - The distribution of the significant bending moments at vibrations over the ship length, at dynamic linear analysis for $h_{1/3}$ = 0.5 to 11.5m (step 1.0m, part B) – LC_F

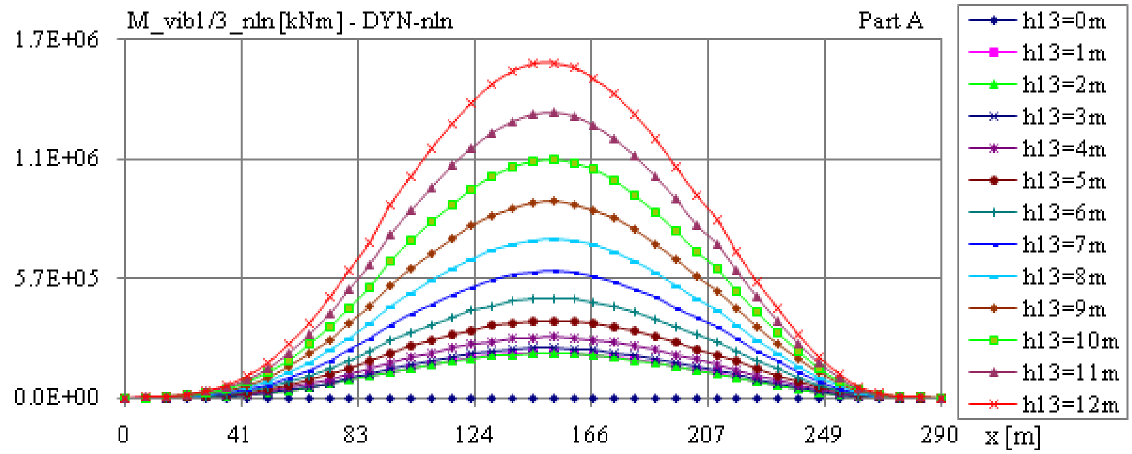

Figure 160. The distribution of the significant bending moments at vibrations over the ship length, at dynamic non-linear analysis for $h_{1/3} = 0.0$ to 12.0m (step 1.0m, part A) – LC_B

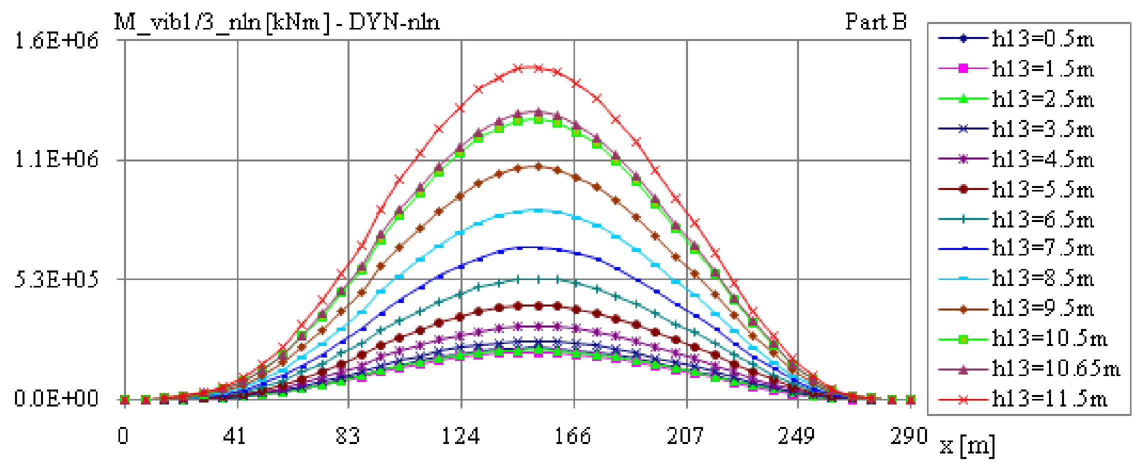

Figure 161. The distribution of the significant bending moments at vibrations over the ship length, at dynamic non-linear analysis for $h_{1/3} = 0.5$ to 11.5m (step 1.0m, part B) – LC_B

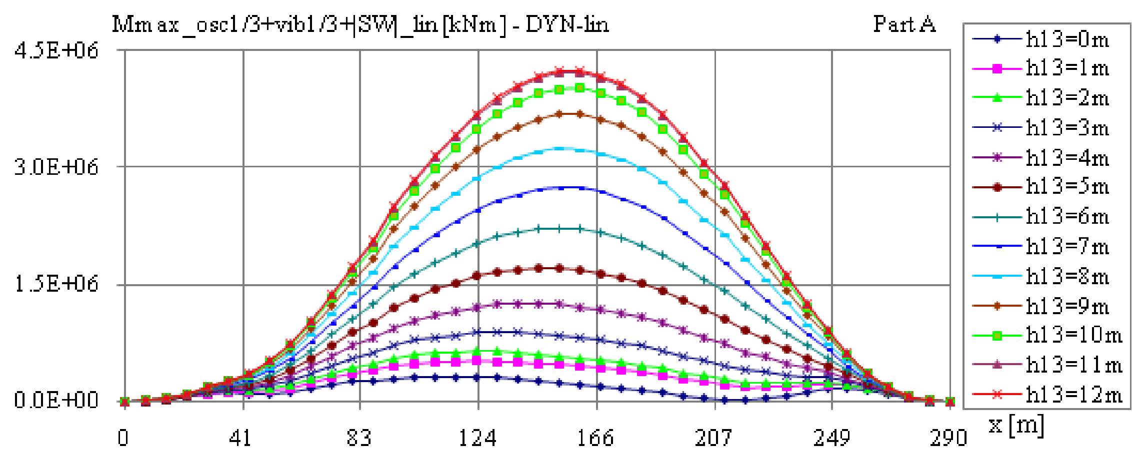

Figure 162. The distribution of the significant bending moments at still water + oscillation + vibrations over the ship length, at dynamic linear analysis for $h_{1/3} = 0.0$ to 12.0m (step 1m, part A) – LC_B

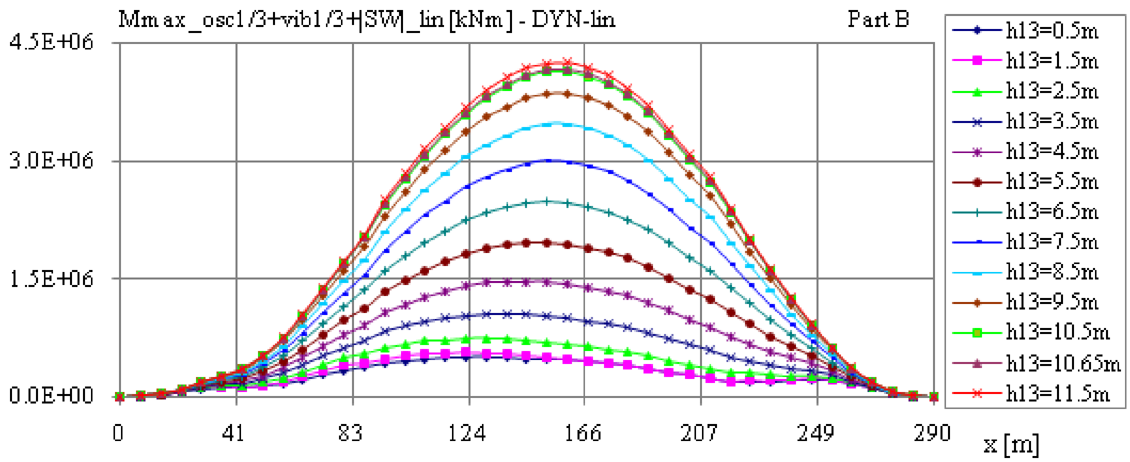

Figure 163. The distribution of the significant bending moments at still water + oscillation + vibrations over the ship length, at dynamic linear analysis for $h_{1/3}$ = 0.5 to 11.5m (step 1m, part B) – LC_B

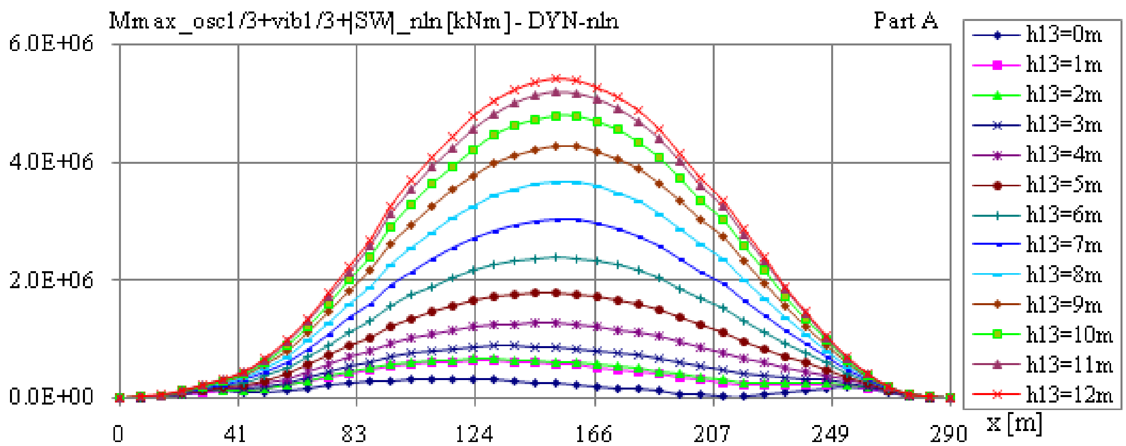

Figure 164. The distribution of the significant bending moments at still water + oscillation + vibrations over the ship length, at dynamic non-linear analysis for $h_{1/3}$ = 0.0 to 12.0m (step 1m, part A) – LC_B

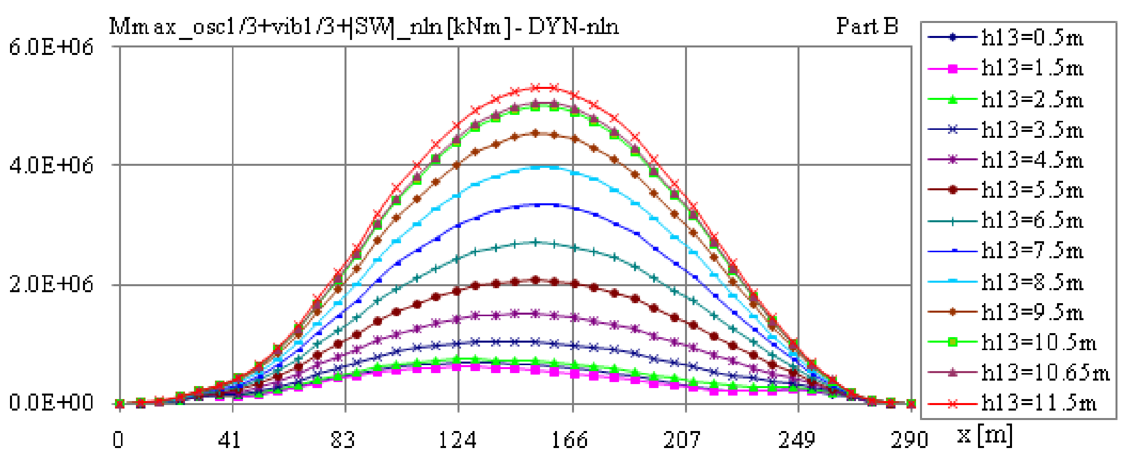

Figure 165. The distribution of the significant bending moments at still water + oscillation + vibrations over the ship length, at dynamic non-linear analysis for $h_{1/3}$ = 0.5 to 11.5m (step 1m, part B) – LC_B

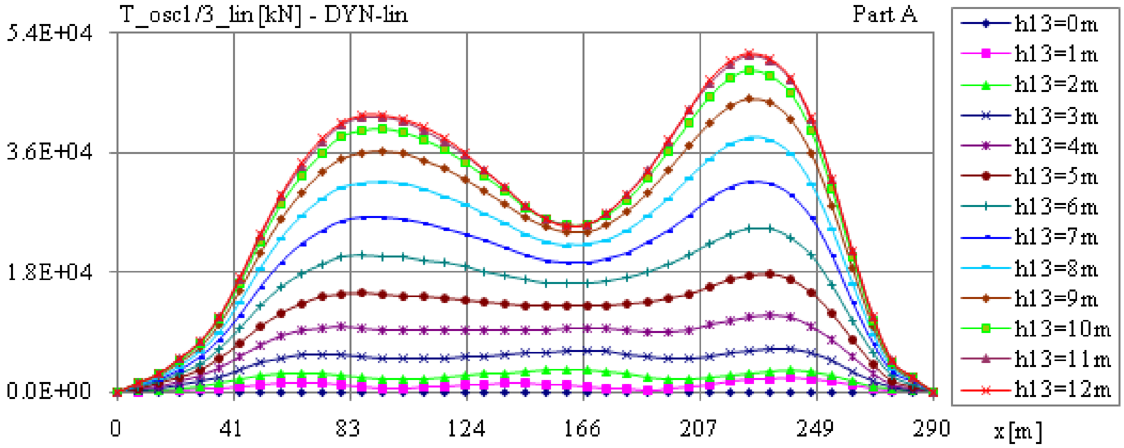

Figure 166. The distribution of the significant shear forces at oscillations over the ship length, at dynamic linear analysis for $h_{1/3} = 0.0$ to 12.0m (step 1.0m, part A) – LC_B

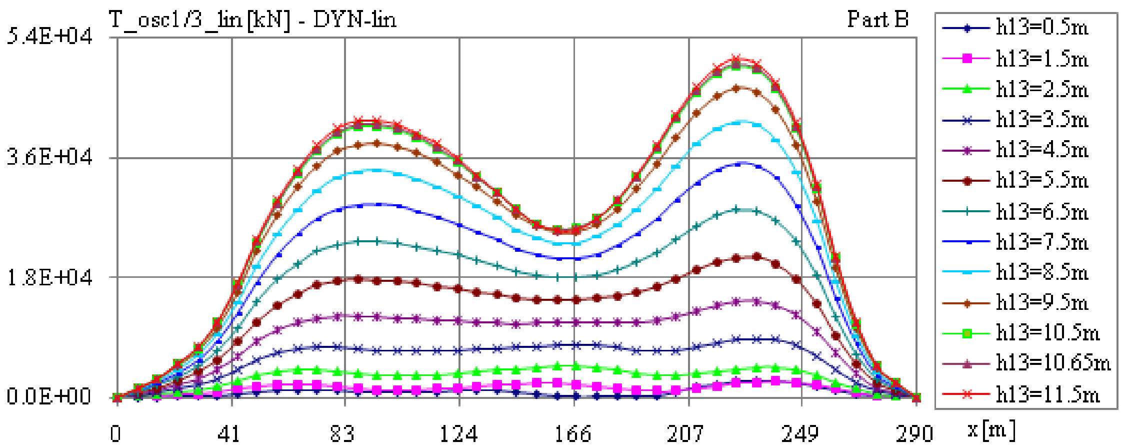

Figure 167. The distribution of the significant shear forces at oscillations over the ship length, at dynamic linear analysis for $h_{1/3} = 0.5$ to 11.5m (step 1.0m, part B) – LC_B

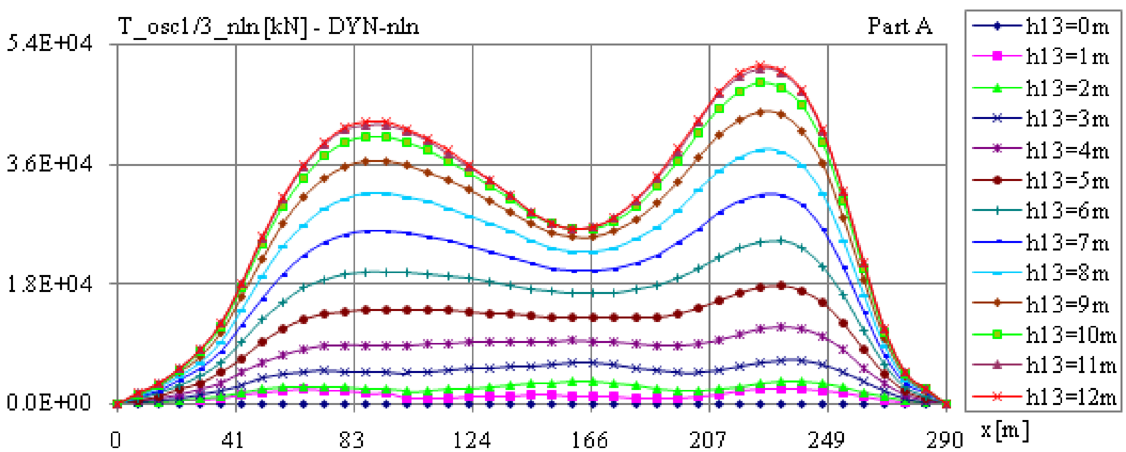

Figure 168. The distribution of the significant shear forces at oscillations over the ship length, at dynamic non-linear analysis for $h_{1/3} = 0.0$ to 12.0m (step 1.0m, part A) – LC_B

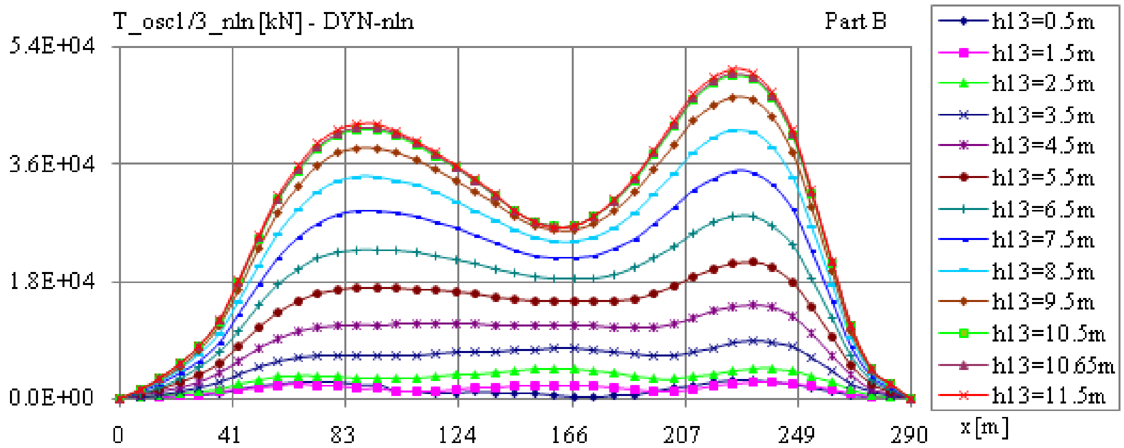

Figure 169. The distribution of the significant shear forces at oscillations over the ship length, at dynamic non-linear analysis for $h_{1/3}$ = 0.5 to 11.5m (step 1.0m, part B) – LC_B

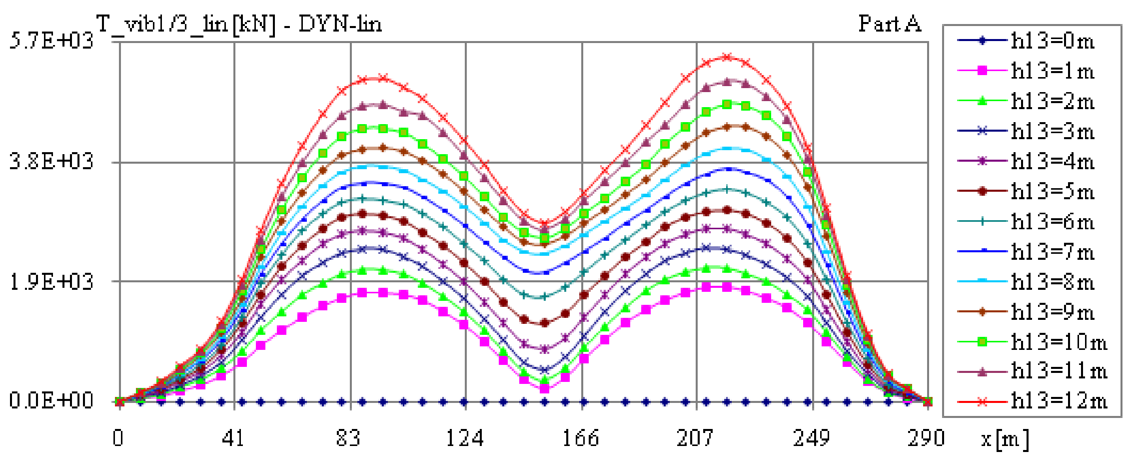

Figure 170. The distribution of the significant shear forces at vibrations over the ship length, at dynamic linear analysis for $h_{1/3}$ = 0.0 to 12.0m (step 1.0m, part A) – LC_B

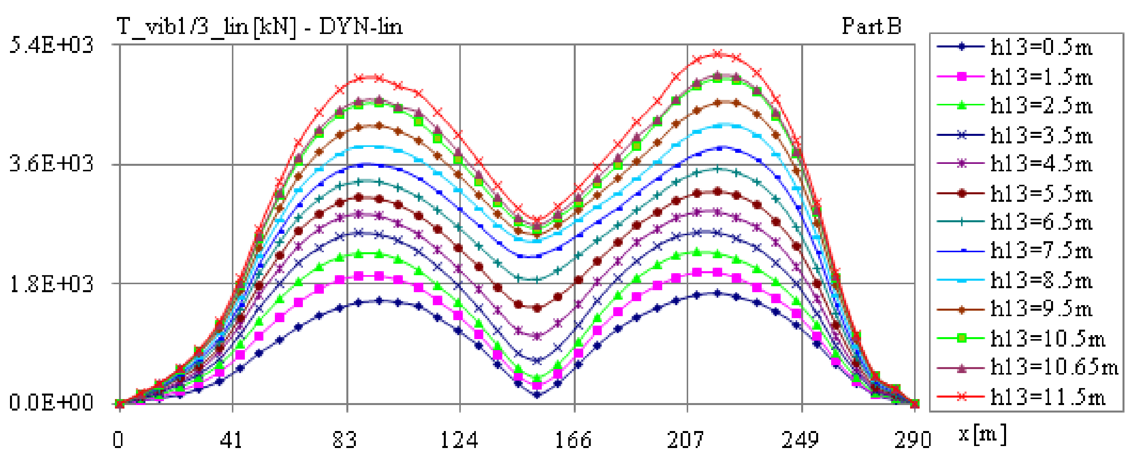

Figure 171. The distribution of the significant shear forces at vibrations over the ship length, at dynamic linear analysis for $h_{1/3}$ = 0.5 to 11.5m (step 1.0m, part B) – LC_B

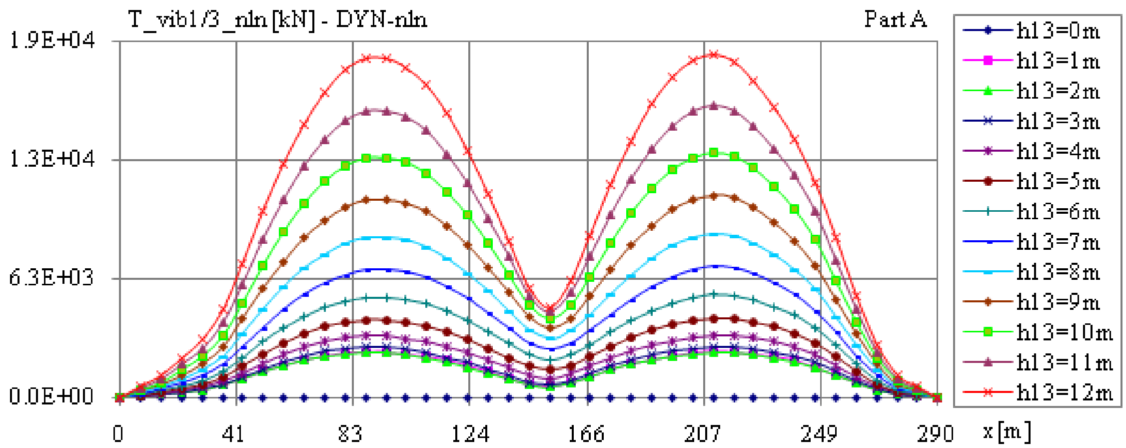

Figure 172. The distribution of the significant shear forces at vibrations over the ship length, at dynamic non-linear analysis for $h_{1/3}$ = 0.0 to 12.0m (step 1.0m, part A) – LC_B

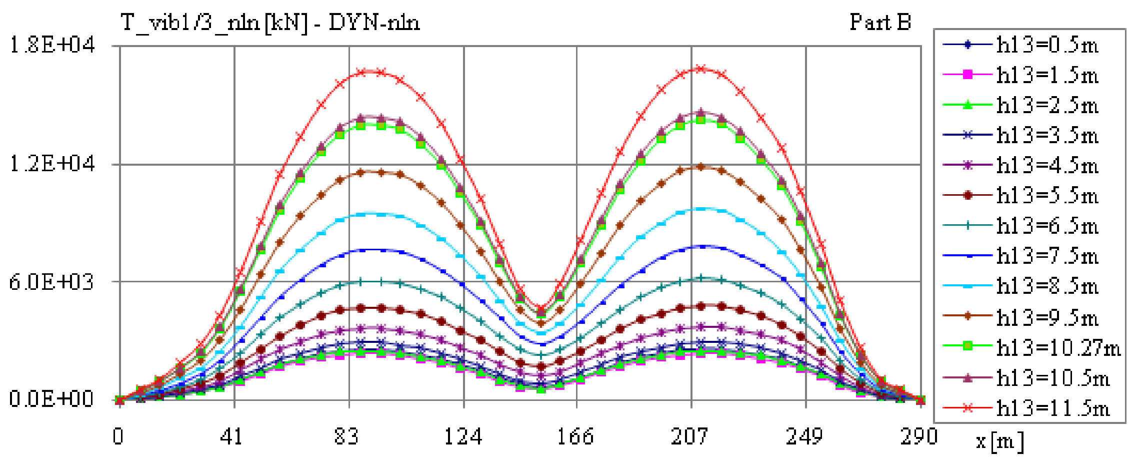

Figure 173. The distribution of the significant shear forces at vibrations over the ship length, at dynamic non-linear analysis for $h_{1/3}$ = 0.5 to 11.5m (step 1.0m, part B) – LC_B

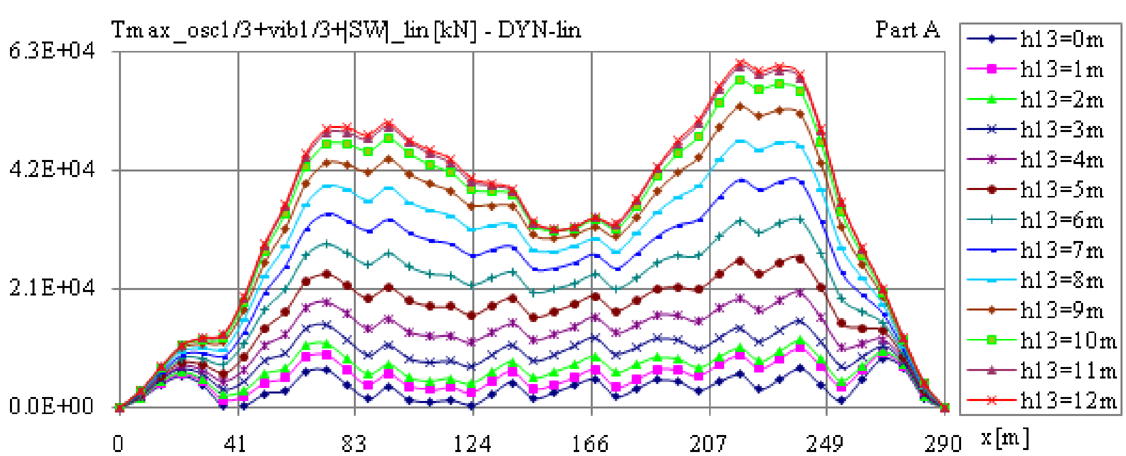

Figure 174. The distribution of the significant shear forces at still water + oscillations + vibrations over the ship length, at dynamic linear analysis for $h_{1/3}$ = 0.0 to 12.0m (step 1.0m, part A) – LC_B

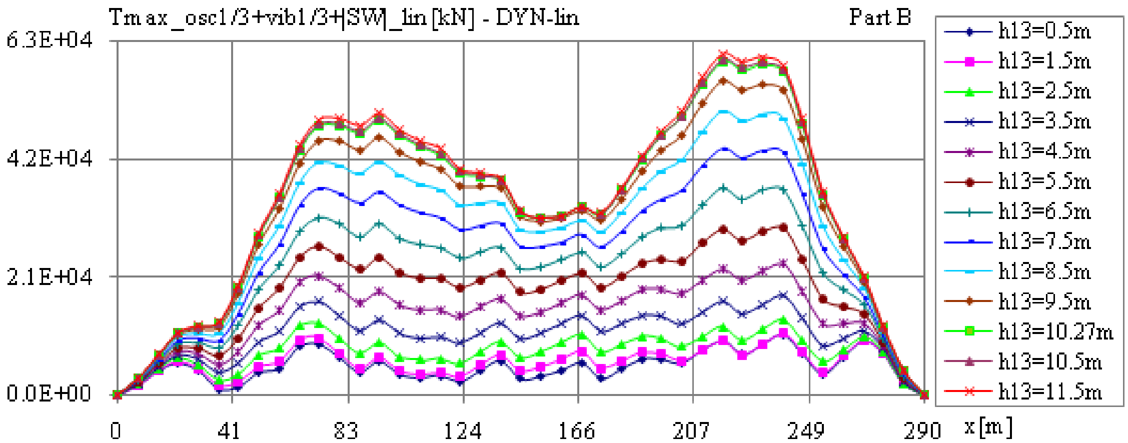

Figure 175. The distribution of the significant shear forces at still water + oscillations + vibrations over the ship length, at dynamic linear analysis for $h_{1/3} = 0.5$ to 11.5m (step 1.0m, part B) – LC_B

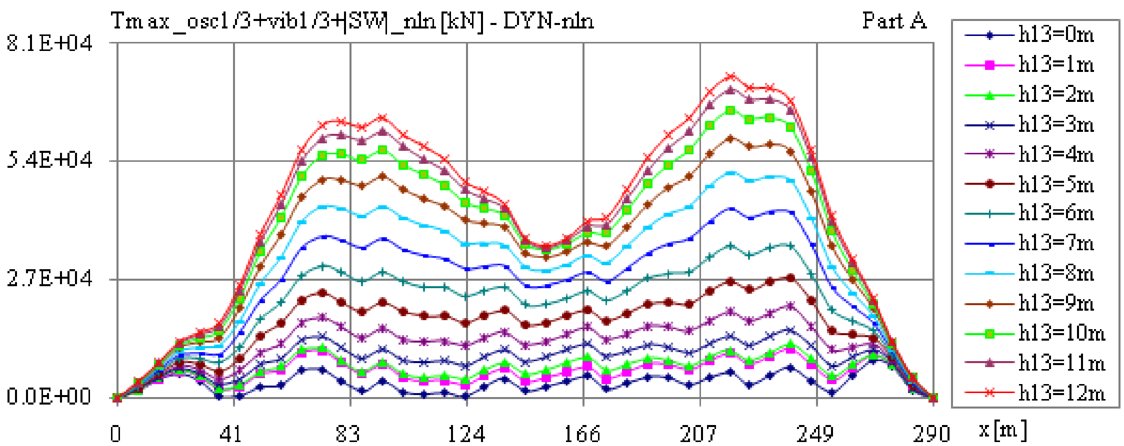

Figure 176. The distribution of the significant shear forces at still water + oscillations + vibrations over the ship length, at dynamic non-linear analysis for $h_{1/3} = 0.0$ to 12.0m (step 1m, part A) – LC_B

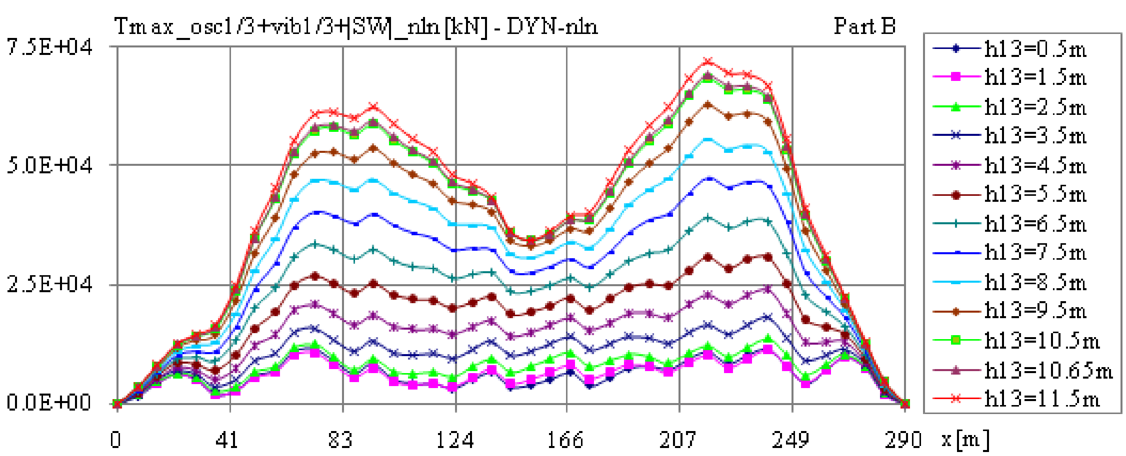

Figure 177. The distribution of the significant shear forces at still water + oscillations + vibrations over the ship length, at dynamic non-linear analysis for $h_{1/3} = 0.5$ to 11.5m (step 1m, part B) – LC_B

5. FATIGUE ANALYSIS AND PRELIMINARY SHIP SERVICE LIFE PREDICTION

This section is based on the methodology from the Classification Society Rules: Germanischer Lloyd (GL2011). The fatigue analysis is focused on the reduction of the cracks in structure induced by the waves dynamic loads, just from the design stage. Because of the random wave loads on the ship hull, coupled with the fabrication and material defects, the occurrence of the cracks cannot be fully eliminated at the design stage, so that the Classification Society requires periodic inspections of the ship hull structure. The fatigue analysis is made for the structural elements of the ship hull, which have the highest stress values, those having the main influence over the estimated expected ship exploitation life in safety structural conditions.

The steps that need to be followed in fatigue strengths analysis are:

- to identify the structural domains where significant dynamic loads occur;
- the fatigue analysis;
- the evaluation of the alternative constructive solutions with a lower risk from the point of view of the fatigues criterion.

5.1. The Theoretical Method for Fatigue Analysis and Preliminary Ship Service Life Prediction

In order to evaluate the ship fatigue strength criterion, with the Germanischer Lloyd Methodology (GL 2010), the cumulative damage ratio *D* method, based on Palmgren-Miner method and steel standard design S-N curves, are applied. From the short-term prediction analysis of the ship dynamic response, the significant stresses $\sigma_{1/3}$ of oscillation and vibration components, for the head wave significant height $h_{1/3}$, are obtained. In the present study the reference time is R = 20 years, and the cumulative damage ratio D has the expression:

$$
\begin{gathered}
D = D_{osc} + D_{vib} \ \leq 1; \\
D_{osc} = \sum_{i=1}^{m} \frac{n_{i\_osc}}{N_{i\_osc}}; \quad n_{i\_osc} = p_i \cdot n_{\max\_osc}; \quad N_{i\_osc} = f_{SN}\left(\Delta\sigma_{ci\_osc}\right) \\
D_{vib} = \sum_{i=1}^{m} \frac{n_{i\_vib}}{N_{i\_vib}}; \quad n_{i\_vib} = p_i \cdot n_{\max\_vib}; \quad N_{i\_vib} = f_{SN}\left(\Delta\sigma_{ci\_vib}\right) \\
n_{\max\_osc,vib} = 3.1526170^{7} R\, f_{osc,vib}; \quad \Delta\sigma_{ci_{osc},vib} = 2\sigma_{1/3_{osc},vib} \cdot f_c
\end{gathered}
\tag{44}
$$

where: $D_{osc,vib}$ are the damage ratio for oscillation or vibration modes; $f_{osc,vib}$ are the natural frequencies for oscillation or vibration modes; - $p_i(h_{1/3i})$, i=1,m are the probabilities from the North Atlantic (NA) or World Wide Trade (WWT) wave significant height $h_{1/3}$ histograms (Price & Bishop 1974); - $n_{max\_osc,vib}$ is the maximum number of cycles for oscillation or vibration modes; $n_{i\_osc,vib}$ is the number of stress cycles for sea state $h_{1/3i}$ at oscillation or vibration; $\Delta\sigma_{ci\_osc,vib}$ is the range of the significant stress obtained for the ship structure from the short term prediction analysis; $N_{i\ osc,vib}$ is the number of endured stress cycles for oscillation or vibration based on the steel standard design S-N curves for a stress range $\Delta\sigma_{ci\_osc,vib}$.

In order to characterize on long-term period the sea state in the selected navigation area, using the significant wave height $h_{1/3}$ and the wave medium period T_1, based on the oceanographic measurements data, can be obtained the scattering diagram presented in Table 25.

Table 25. The scattering diagram ($h_{1/3}$ /T_1), for the reference period T_b=1 year

$h_{1/3}$ /T_1	0 ÷ 1	1 ÷ 2	...	(j-1) ÷ j	...	20 ÷ 21	>21s	$\sum_j n_{ij}$
0 ÷ 1	$n_{1,1}$	$n_{1,2}$	...	$n_{1,j}$	...	$n_{1,21}$	$n_{1,22}$	n_1
1 ÷ 2	$n_{2,1}$	$n_{2,2}$	...	$n_{2,j}$	...	$n_{2,21}$	$n_{2,22}$	n_2
...	...	...	...	...	...	...	...	...
(i-1)+i	$n_{i,1}$	$n_{i,2}$	...	$n_{i,j}$	...	$n_{i,21}$	$n_{i,22}$	n_i
...	...	...	...	...	...	...	...	...
10 ÷ 11	$n_{11,1}$	$n_{11,2}$	...	$n_{11,j}$	...	$n_{11,21}$	$n_{11,22}$	n_{11}
10 ÷ 12	$n_{12,1}$	$n_{12,2}$	...	$n_{12,j}$	...	$n_{12,21}$	$n_{12,22}$	n_{12}
>12m	$n_{13,1}$	$n_{13,2}$	...	$n_{13,j}$	...	$n_{13,21}$	$n_{13,22}$	n_{13}
$\sum_i ij$	n_1	n_2	...	n_j	...	n_{21}	n_{22}	n_{ta}

For the cumulative damage ratio D method, based on short term first order ITTC wave power density spectrum, it is necessary to be extracted the significant wave height $h_{1/3}$ histogram based on the last column Table 25 scattering diagram ($h_{1/3}$ /T_1). In Table 26, Figure 178 and Figure 179 are presented the histograms of the significant wave height $h_{1/3}$ for North Atlantic (NA) and Word Wide Trade (WWT) at the reference period T_b=1 year.

Table 26. The histograms of the significant wave height $h_{1/3}$ on long-term period for North Atlantic and Word Wide Trade (for reference period T_b=1 year)

North Atlantic (see Figure 178) $P_{LTP20} = 0.9 \cdot 10^{-8}$		
$h_{1/3i}$ [m]	records	p_i
1	14690	0.14690
2	26167	0.26167
3	22196	0.22196
4	15590	0.15590
5	9775	0.09775
6	5639	0.05639
7	3042	0.03042
8	1547	0.01547
9	750	0.00750
10	348	0.00348
11	153	0.00153
12	65	0.00065
13	27	0.00027
14	11	0.00011
∑=	100000	1

Word Wide Trade (see Figure 179) $P_{LTP20} = 0.8 \cdot 10^{-8}$		
$h_{1/3i}$ [m]	records	p_i
1	26287	0.26287
2	34001	0.34001
3	20092	0.20092
4	10482	0.10482
5	5073	0.05073
6	2323	0.02323
7	1018	0.01018
8	432	0.00432
9	178	0.00178
10	70	0.00070
11	28	0.00028
12	11	0.00011
13	4	0.00004
14	1	0.00001
∑=	100000	1

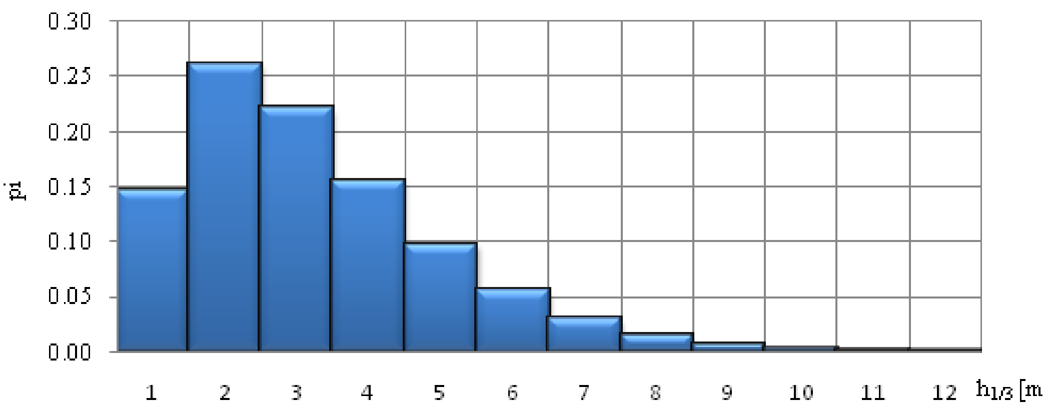

Figure 178. North Atlantic histogram $h_{1/3}$ [m]

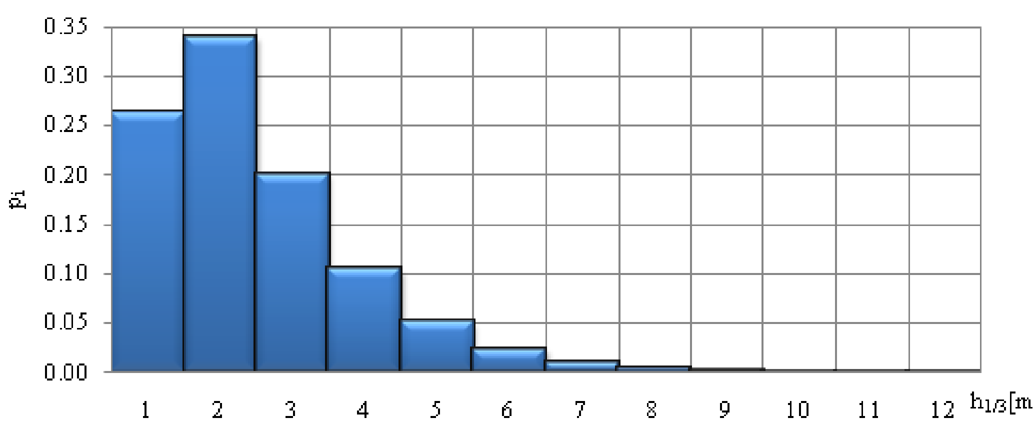

Figure 179. Word Wide Trade histogram $h_{1/3}$ [m]

The bulk carrier stress values in equation (44) are obtained based on the short term significant stress (are detailed in section 5.3), corresponding to the significant wave height $h_{1/3}$, using the next expressions:

$$\Delta\sigma_{ci} = \Delta\sigma_i \cdot f_c; \quad \Delta\sigma_i = 2\sigma_{1/3i}; \; f_c = \frac{1}{1 - \frac{\sigma_{SW}}{R_m}} \tag{45}$$

where: $\sigma_{1/3i}$ is the significant stress value of the analysed zone from the dynamic response of the bulk carrier for the significant wave height $h_{1/3}$, the normal stress from the 1D-gider analysis or the equivalent von Mises stress for the 3D/1D combined model, f_c the correction factor of the asymmetric cycle ($\sigma_{max} \neq |\sigma_{min}|$) at the equivalent symmetric cycle ($\sigma_{max} = |\sigma_{min}|$) , using the Morrow method; σ_{sw} is the still water normal or the equivalent von Mises stress of the analysed zone, R_m represent the tensile stress limit of the material.

For the N_{i_osc} and N_{i_vib} numbers of fatigue stress cycles for oscillation or vibrations resulted for the stress range $\Delta\sigma_{ci\_osc,vib}$, corresponding to the significant wave height $h_{1/3}$, can be used the steel standard design S-N curve. The S-N design diagram (presented in Figure 180) is the lower limit of a 95% from the material tests, corresponding to the survival probability of 97.5%, considering further occurrence of the significant fatigue damages in the complex structures.

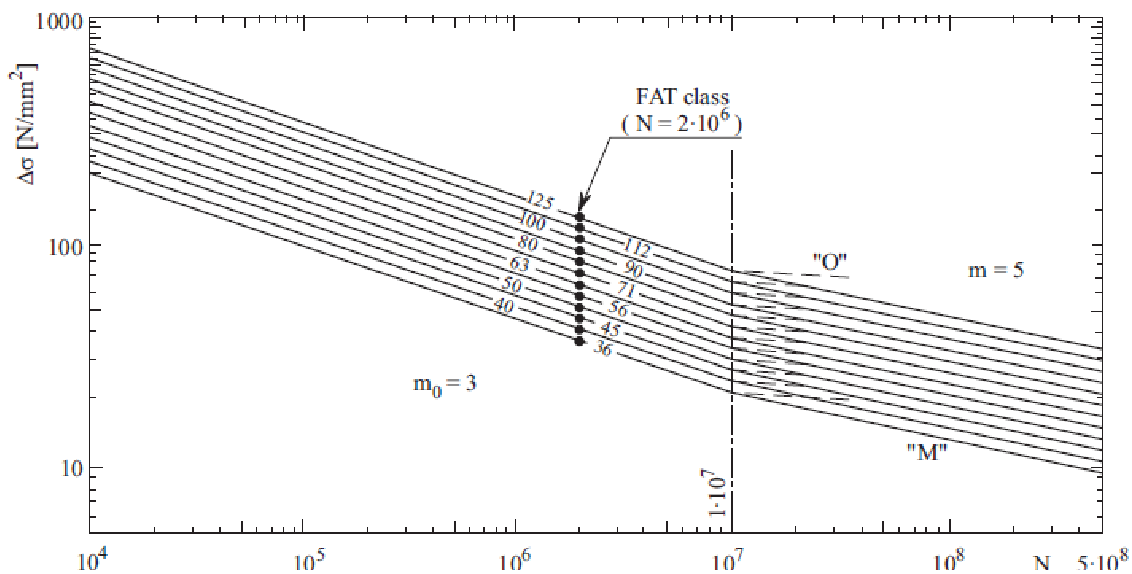

Figure 180. Stress-cycles S-N curves for welded joints, made of steel (GL2011)

According to GL2011, the S-N curve is idealized with a linear relation between $\log(\Delta\sigma)$ and $\log(N)$ (see Figure 180), having the next equations:

$$\log(N) = 7.0 + m \cdot Q; \quad Q = log(\Delta\sigma_{Rc}/\Delta\sigma_c) - 0.39794/m_0$$
$$\Delta\sigma_{Rc} = \Delta\sigma_R \cdot f_m \cdot f_R \cdot f_w \cdot f_s \cdot f_i$$
$$f_R = 1\, for\ \ \sigma_{SW} > \frac{\Delta\sigma_c}{2};\ \ f_R = 1 \div 0.15\left(1 - \frac{2\sigma_{SW}}{\Delta\sigma_c}\right) for\ -\frac{\Delta\sigma_c}{2} \leq \sigma_{SW} \leq \frac{\Delta\sigma_c}{2}; \tag{46}$$
$$f_R = 1.3\, for\ \ \sigma_{SW} < -\frac{\Delta\sigma_c}{2}$$

where: N is the number of endured stress cycles according to S-N curve; *m* slop exponent of S-N curve, $m = m_0$ for $N \leq 10^7$ and $Q \leq 0$ or $m = 2m_0 - 1$ for $N > 10^7$ and $Q > 0$; m_0 inverse slope in the rage $N \leq 10^7$, $m_0 = 3$ for $N \leq 5 \cdot 10^6$; $\Delta\sigma_R$ fatigue strength reference value of S-N curve at $2 \cdot 10^6$ cycles of stress range; $\Delta\sigma_{Rc}$ corrected fatigue strength reference value of S-N curve at $2 \cdot 10^6$ stress cycles; - $f_m = 1$ correction factor for material effect for welded joints; f_R correction factor for mean stress effect; $f_w = 1.0 \div 1.25$ correction factor for importance of structural element; f_s additional correction factor for structural stress analysis; f_i influence of importance of structural element.

The equations (44) is used only for a loading case of the ship. For more realistic fatigue analysis are considering more loading cases (j = 1,M, M is the number of the loading cases). In this case the cumulative damage ration D will be obtained using the next equation:

$$D = \sum_{ij=1}^{M} P_j \cdot D_j \leq 1; \quad L_{(years)} = \frac{R}{D}\ [years] \tag{47}$$

where: - P_j contribution of the load case; $L_{(years)}$ the estimated ship service life from the fatigue criteria; $R = 20$ years the imposed reference ship life.

In the case of bulk carrier ships the full and ballast loading cases are considered with the same occurrence probability (simplified scenario), and for this the cumulative damage ratio D can be obtain using the following expression:

$$D = 0.5 \cdot D_{full} + 0.5 \cdot D_{ballast} \leq 1; \quad for\ L_{[years]} = R/D \tag{48}$$

If the L < R (D > 1) it is necessary to apply structural design enhancement for the structure elements that do not satisfy the fatigue criterion, besides the programmed periodical technical inspection.

5.2. The Stress 3D/1D Models Correlation Factors

Analyzing the von Mises stress resulted from the global-local strength analysis based on the 3D-FEM model, see the Figure 45 to Figure 50 for full loading case and Figure 59 to Figure 64 for ballast loading case, it can be observed that the highest stress values are recorded around the cargo hold frame (deck structure) in sagging conditions for the both loading cases.

In Figure 181 and Figure 182 are presented the main deck selected three zones that will be analyzed at fatigue analysis and preliminary ship service life prediction, having the maximum stress values (hot-spots).

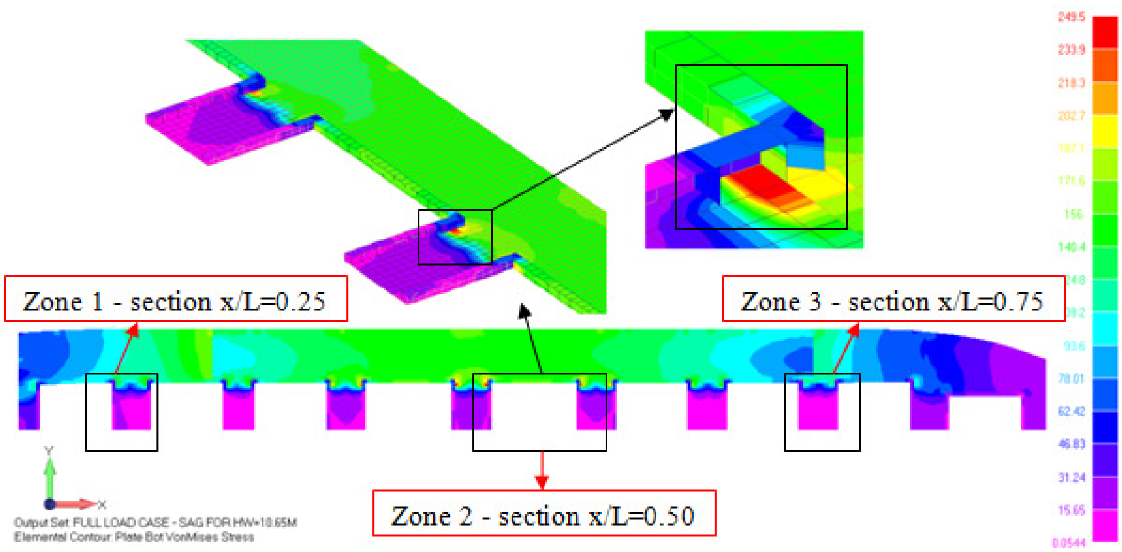

Figure 181. Hot-spot from full loading case (sagging), presentation of the three zones analyzed

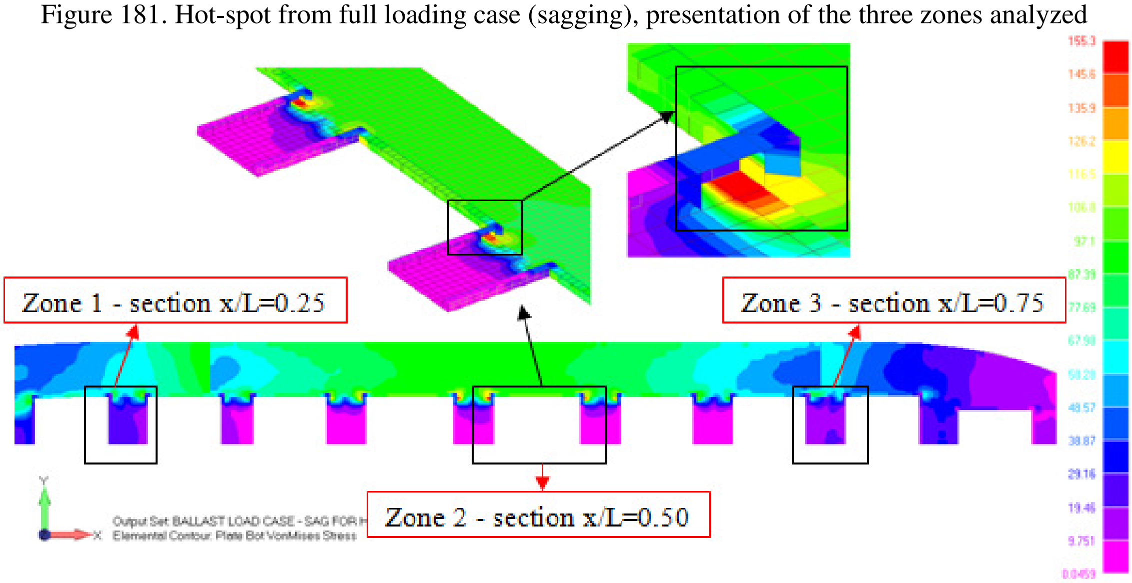

Figure 182. Hot-spot from ballast loading case (hogging), presentation of the three zones analyzed

In order to perform the fatigue analysis for the 3D-FEM model, it is used the stress 3D/1D correlation coefficient $k_{3D/1D}$. The values of the correlation coefficient $k_{3D/1D}$ are presented in Table 27 and it is calculated with the next expressions:

$$k_{3D/1D} = max\left\{\frac{\sigma_{VMD\_3D\_sag}}{\sigma_{xD\_1D\_sag}}, \frac{\sigma_{VMD\_3D\_hog}}{\sigma_{xD\_1D\_hog}}\right\} \quad for\ deck \tag{49}$$

where: $\sigma_{VMD\_3D\_sag}$ and $\sigma_{VMD\_3D\_hog}$ are the deck von Mises stress in the sagging and hogging conditions from 3D-FEM model; $\sigma_{xD\_1D\_sag}$ and $\sigma_{xD\_1\_hog}$ are the deck normal stress in the sagging and hogging conditions from the equivalent 1D-girder model (based on structural analyses with equivalent quasi-static head waves).

Table 27. The stress 3D/1D correlation coefficients $k_{3D/1D}$

Full Loading Case			
Zone	max($\sigma_{VMD\_3D\_sag}$, $\sigma_{VMD\_3D\_hog}$) [N/mm^2]	max($\sigma_{xD\_1D\_sag}$, $\sigma_{xD\_1D\_hog}$) [N/mm^2]	$k_{3D/1D}$
Section 1 - x/L=0.25	160.80	116.43	1.381
Section 2 - x/L=0.50	251.24	200.65	1.252
Section 3 - x/L=0.75	131.09	101.37	1.293
Ballast Loading Case			
Section 1 - x/L=0.25	75.32	54.41	1.384
Section 2 - x/L=0.50	156.18	122.89	1.271
Section 3 - x/L=0.75	86.44	61.39	1.408

5.3. Stress Values from Short Term Dynamic Analysis

To complete the fatigue analysis was used the stress values obtained from the short term prediction presented in Chapter 4 of this study. Analyzing the numerical results of the ship hull global dynamic analysis (see Chapter 3) and the hot spots domains presented in section 5.2, the stress from the short term prediction will be presented only for the main deck of the ship, because in those structural elements were obtained the highest normal and von Mises stresses from the entire studied bulk carrier hull structure.

5.3.1. Deck Normal Stress Distribution - Full Loading Case

The next figures represent the deck normal stress values from the short term linear and non-linear hydroelastic analysis for full loading case, as following:

in Figure 183 to Figure 186 are presented the distribution of the significant deck normal stress (σ_{xD}_osc$_{1/3}$ in [N/mm^2]) at oscillations over the ship length. at dynamic linear and non-linear analysis, for $h_{1/3}$ = 0.0-12.0m;

in Figure 187 to Figure 190 are presented the distribution of the significant deck normal stress (σ_{xD}_osc$_{1/3}$ in [N/mm^2]) at vibrations over the ship length. at dynamic linear and non-linear analysis, for $h_{1/3}$ = 0.0-12.0m.

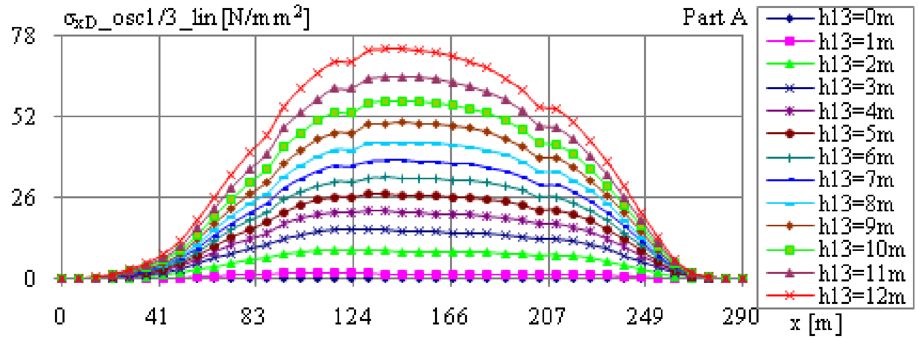

Figure 183. Distribution of the deck normal stress (σ_{xD}) at oscillations over the ship length, at dynamic linear analysis for $h_{1/3}$ = 0.0 to 12.0m (step 1m, part A) – LC_F

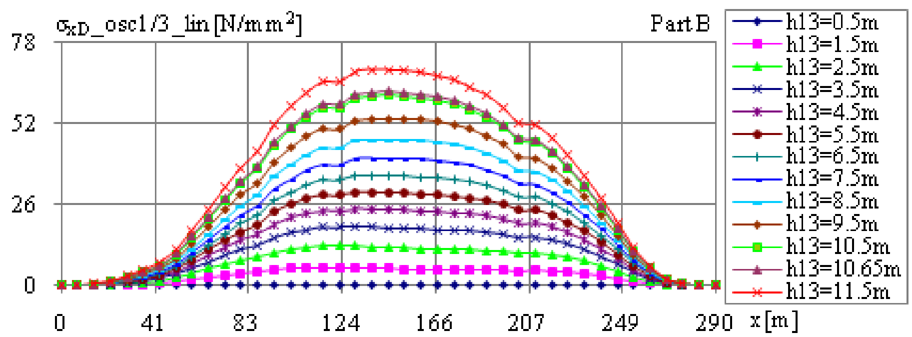

Figure 184. Distribution of the deck normal stress (σ_{xD}) at oscillations over the ship length, at dynamic linear analysis for $h_{1/3}$ = 0.5 to 11.5m (step 1m, part B) – LC_F

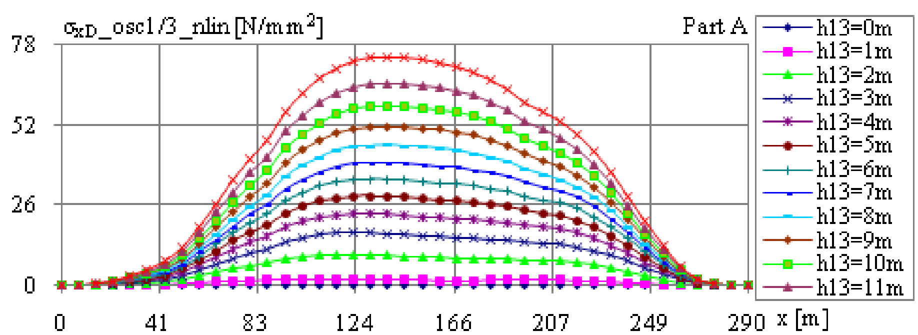

Figure 185. Distribution of the deck normal stress (σ_{xD}) at oscillations over the ship length, at dynamic non-linear analysis for $h_{1/3}$ = 0.0 to 12.0m (step 1m, part A) – LC_F

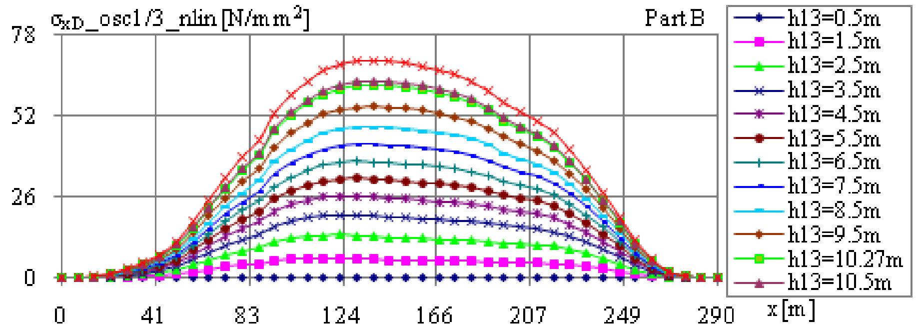

Figure 186. Distribution of the deck normal stress (σ_{xD}) at oscillations over the ship length, at dynamic non-linear analysis for $h_{1/3} = 0.5$ to 11.5m (step 1m, part B) – LC_F

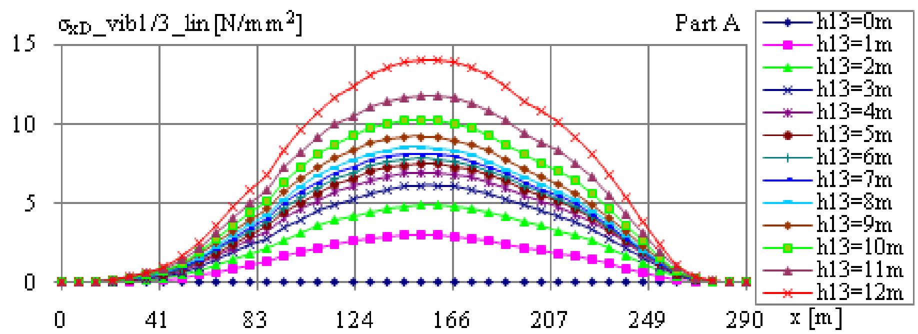

Figure 187. Distribution of the deck normal stress (σ_{xD}) at vibration over the ship length, at dynamic linear analysis for $h_{1/3} = 0.0$ to 12.0m (step 1m, part A) – LC_F

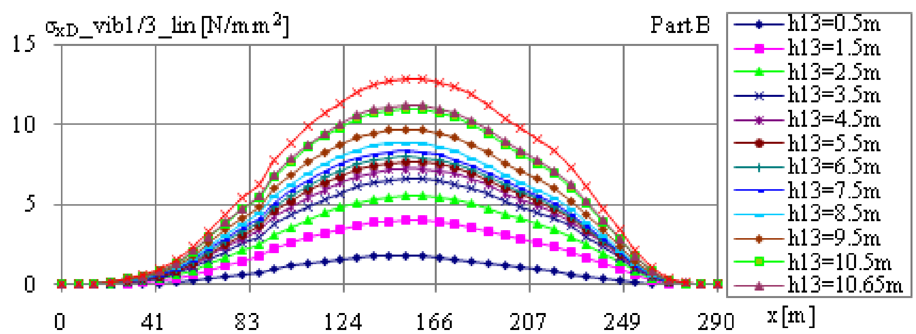

Figure 188. Distribution of the deck normal stress (σ_{xD}) at vibration over the ship length, at dynamic linear analysis for $h_{1/3} = 0.5$ to 11.5m (step 1m, part B) – LC_F

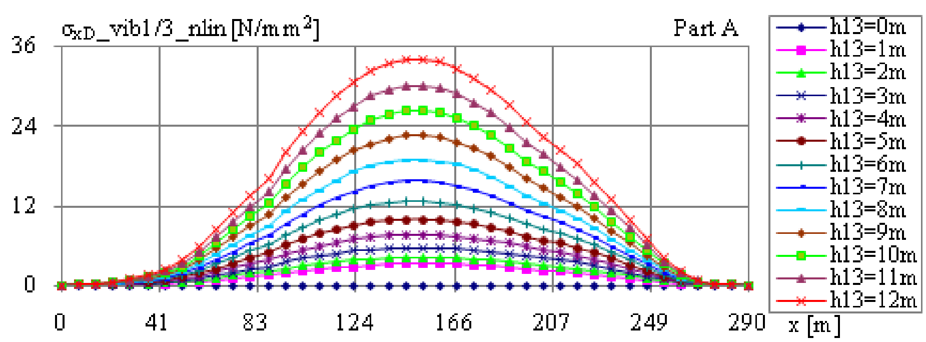

Figure 189. Distribution of the deck normal stress (σ_{xD}) at vibration over the ship length, at dynamic non-linear analysis for $h_{1/3} = 0.0$ to 12.0m (step 1m, part A) – LC_F

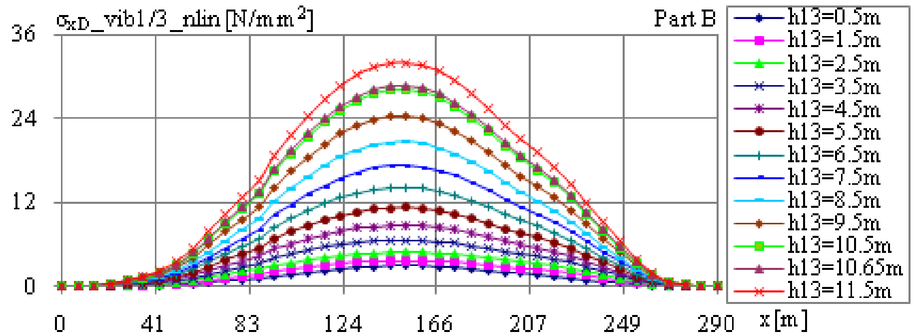

Figure 190. Distribution of the deck normal stress (σ_{xD}) at vibration over the ship length, at dynamic non-linear analysis for $h_{1/3} = 0.5$ to 11.5m (step 1m, part B) – LC_F

5.3.2. Deck Normal Stress Distribution - Ballast Loading Case

The next figures represent the deck normal stress values from the short term linear and non-linear hydroelastic analysis for ballast loading case, as following:

in Figure 191 to Figure 194 are presented the distribution of the significant deck normal stress (σ_{xD}_osc$_{1/3}$ in [N/mm^2]) at oscillations over the ship length. at dynamic linear and non-linear analysis, for $h_{1/3} = 0.0$-12.0m;

in Figure 195 to Figure 198 are presented the distribution of the significant deck normal stress (σ_{xD}_osc$_{1/3}$ in [N/mm^2]) at vibrations over the ship length. at dynamic linear and non-linear analysis, for $h_{1/3} = 0.0$-12.0m.

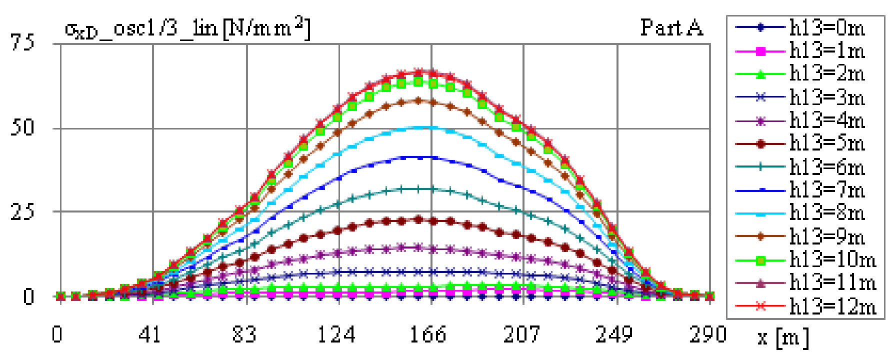

Figure 191. Distribution of the deck normal stress (σ_{xD}) at oscillations over the ship length, at dynamic linear analysis for $h_{1/3} = 0.0$ to 12.0m (step 1m, part A) – LC_B

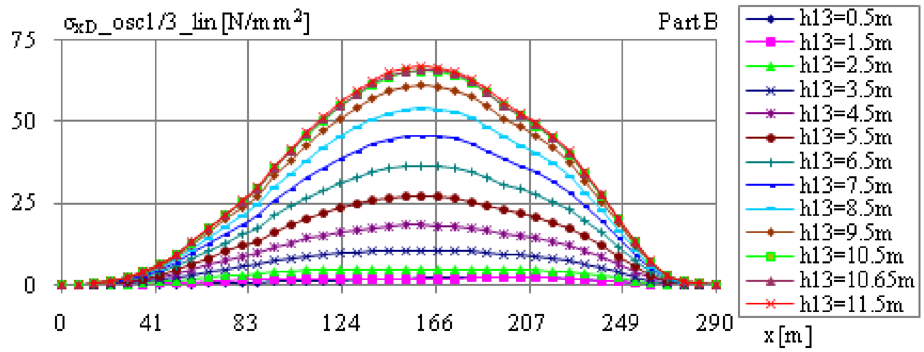

Figure 192. Distribution of the deck normal stress (σ_{xD}) at oscillations over the ship length, at dynamic linear analysis for $h_{1/3} = 0.5$ to 11.5m (step 1m, part B) – LC_B

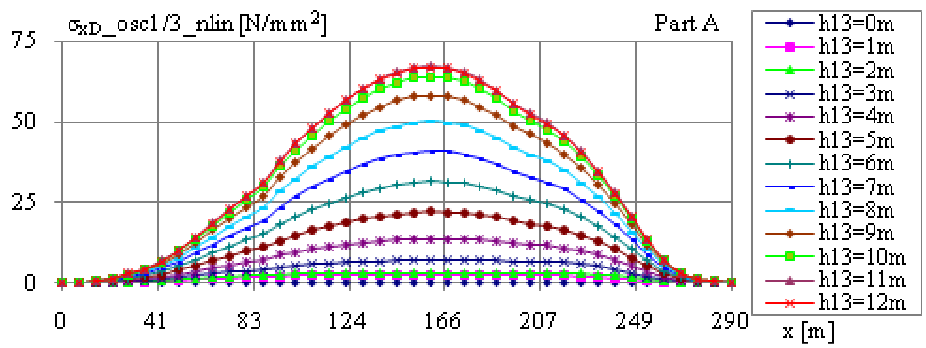

Figure 193. Distribution of the deck normal stress (σ_{xD}) at oscillations over the ship length, at dynamic non-linear analysis for $h_{1/3} = 0.0$ to 12.0m (step 1m, part A) – LC_B

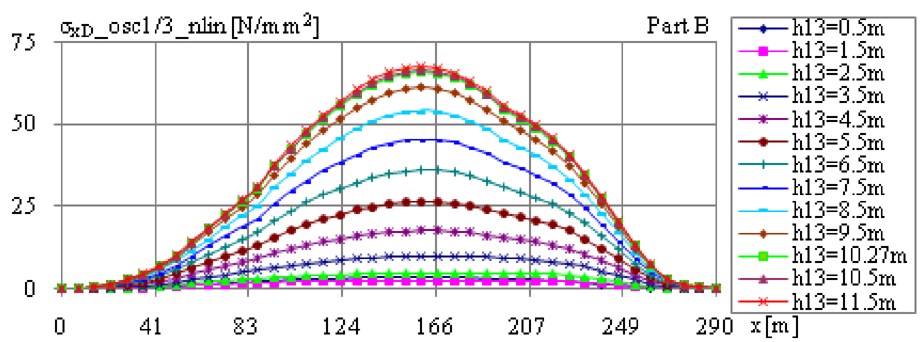

Figure 194. Distribution of the deck normal stress (σ_{xD}) at oscillations over the ship length, at dynamic non-linear analysis for $h_{1/3} = 0.5$ to 11.5m (step 1m, part B) – LC_B

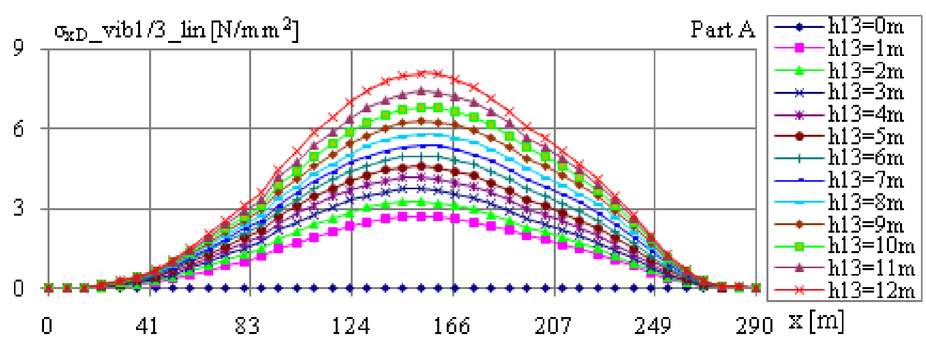

Figure 195. Distribution of the deck normal stress (σ_{xD}) at vibration over the ship length, at dynamic linear analysis for $h_{1/3} = 0.0$ to 12.0m (step 1m, part A) – LC_B

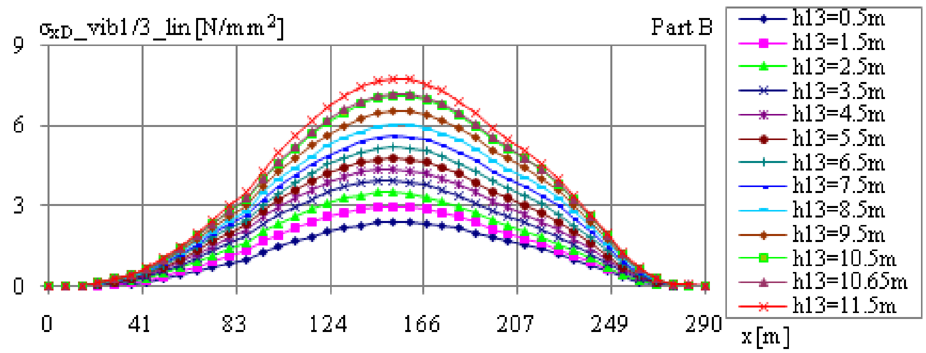

Figure 196. Distribution of the deck normal stress (σ_{xD}) at vibration over the ship length, at dynamic linear analysis for $h_{1/3} = 0.5$ to 11.5m (step 1m, part B) – LC_B

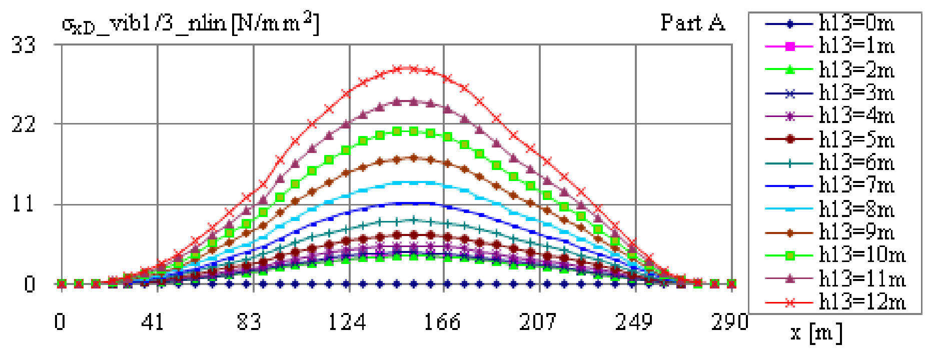

Figure 197. Distribution of the deck normal stress (σ_{xD}) at vibration over the ship length, at dynamic non-linear analysis for $h_{1/3} = 0.0$ to 12.0m (step 1m, part A) – LC_B

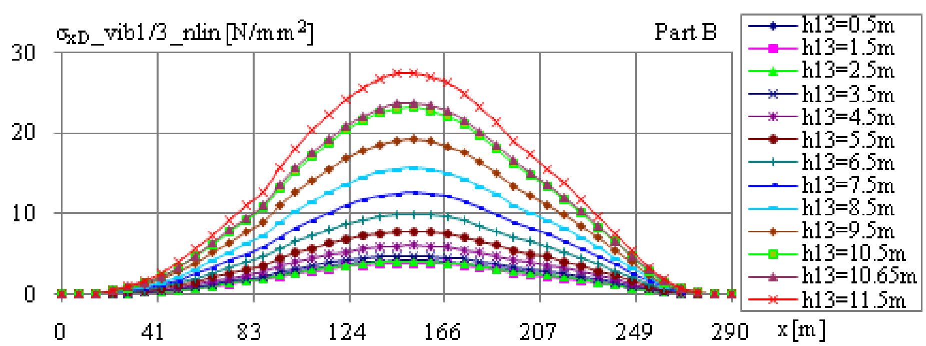

Figure 198. Distribution of the deck normal stress (σ_{xD}) at vibration over the ship length, at dynamic non-linear analysis for $h_{1/3} = 0.5$ to 11.5m (step 1m, part B) – LC_B

5.4. Fatigue Analysis and Preliminary Ship Service Life Prediction

In the following section are presented the numerical results of fatigue analysis and preliminary ship service life prediction. As it can be observed from section 5.2, the hot-spot are concentrated on the main deck of the studied bulk carrier, around the cargo hold frame. In this case the fatigue criteria check was completed only for the main deck in 3 different sections (x/L = 0.25, 0.50, 0.75) for two structural models: 1D-girder model and 3D/1D combined model. In Table 28 are presented the input data used for the fatigue check criteria, the values for $f_{\_osc,}$ and $f_{\_vib,}$ were selected from Table 8.

Table 28. Input data for fatigue analysis and initial ship service life prediction

Load Case	Full loading cond. LC_F	Ballast loading cond. LC_B
f_osc=	0.102 [Hz]	0.115 [Hz]
T_osc=	9.804 [s]	8.688 [s]
n_osc=	6.433E+07 [cycles]	9.074E+07 [cycles]
f_vib=	0.546 [Hz]	0.663 [Hz]
T_vib=	1.832 [s]	1.508 [s]
n_vib=	3.444E+08 [cycles]	5.227E+08 [cycles]
R_{eH}=	355 [N/mm^2]	
R_m=	490 [N/mm^2]	
f_R=	1.121 [N/mm^2]	
$\Delta\sigma_R$=	125.0 [N/mm^2] (see Figure 199)	
f_m=	1.0 - welded joint	
f_w=	1.4 - full penetration weld	
F_i=	1.0 - primary structural element	
m_0=	3.0 - for welded joint	
c=	0.15 - welded joint subjected to variable stress cycles	

To check the fatigue criteria of cargo hold frame was selected the joint configuration type B2 form GL2011 - I Part 1 Ch.1 Sec.20, is a continuous automatic longitudinal fully penetrated K-butt without stop/start positions (based on stress range in flange adjacent to weld).

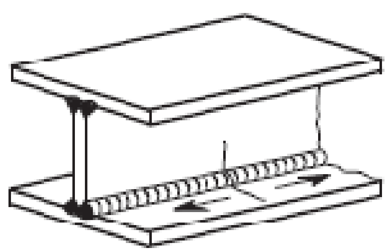

Figure 199. Joint configuration B2 from GL2011

The numerical results of the fatigue analysis and the preliminary ship service life evaluation, based on the Palmgen-Miner cumulative damage ratio D and design S-N curves, for full loading case, ballast loading case and the combination between them, are presented in the next tables:

- in Table 29 and Table 30 are presented the fatigue criteria check for North Atlantic and Word Wide Trade histogram based on 1D-girder analysis;

- in Table 31 and Table 32 are presented the fatigue criteria check for North Atlantic and Word Wide Trade histograms based on 3D/1D combined analysis.

Table 29. Fatigue criterion, based on D ratio and design S-N curves, for North Atlantic (NA) histogram, 1D-girder model

Section x/L = 0.25								
	Full Load		Ballast Load		0.5 full load + 0.5 ballast load			
Analysis	D_{SN_osc}	D_{SN_vib}	D_{SN_osc}	D_{SN_vib}	D_{SN_osc}	D_{SN_vib}	$D_{SN\_osc+vib}$	$L_{\_osc\_vib}$
ADV	0.0004	-	0.000	-	0.0004	-	0.0004	> 35
HEL	0.0004	1.3E-06	0.000	1.3E-06	0.0004	1.3E-06	0.0004	> 35
DYN-LN	0.0005	2.9E-07	0.001	2.9E-07	0.0005	2.9E-07	0.0005	> 35
DYN-NLN	0.0008	4.9E-06	0.001	4.9E-06	0.0008	4.9E-06	0.0008	> 35
Section x/L = 0.5								
	Full Load		Ballast Load		0.5 full load + 0.5 ballast load			
Analysis	D_{SN_osc}	D_{SN_vib}	D_{SN_osc}	D_{SN_vib}	D_{SN_osc}	D_{SN_vib}	$D_{SN\_osc+vib}$	$L_{\_osc\_vib}$
ADV	0.8739	-	0.291	-	0.5827	-	0.5827	34.3
HEL	0.8739	0.0060	0.291	1.1E-05	0.583	3.0E-03	0.586	34.1
DYN-LN	0.8868	0.0032	0.344	1.6E-04	0.616	1.7E-03	0.617	32.4
DYN-NLN	1.1133	0.0683	0.366	9.9E-03	0.740	3.9E-02	0.779	25.7
Section x/L = 0.75								
	Full Load		Ballast Load		0.5 full load + 0.5 ballast load			
Analysis	D_{SN_osc}	D_{SN_vib}	D_{SN_osc}	D_{SN_vib}	D_{SN_osc}	D_{SN_vib}	$D_{SN\_osc+vib}$	$L_{\_osc\_vib}$
ADV	0.0968	-	0.145	-	0.1207	-	0.1207	> 35
HEL	0.0968	0.0005	0.145	3.1E-06	0.121	2.7E-04	0.121	> 35
DYN-LN	0.1410	0.0003	0.174	3.0E-05	0.158	1.8E-04	0.158	> 35
DYN-NLN	0.1502	0.0039	0.177	1.3E-03	0.164	2.6E-03	0.166	> 35

Table 30. Fatigue criterion, based on D ratio and design S-N curves, for Word Wide Trade (WWT) histogram, 1D-girder model

Section x/L = 0.25								
	Full Load		Ballast Load		0.5 full load + 0.5 ballast load			
Analysis	D_{SN_osc}	D_{SN_vib}	D_{SN_osc}	D_{SN_vib}	D_{SN_osc}	D_{SN_vib}	$D_{SN\_osc+vib}$	$L_{\_osc\_vib}$
ADV	0.0001	-	0.0001	-	0.0001	-	0.0001	> 35
HEL	0.0001	1.2E-06	0.0001	1.2E-06	0.000	1.2E-06	0.0001	> 35
DYN-LN	0.0002	1.5E-07	0.000	1.5E-07	0.000	1.5E-07	0.0001	> 35
DYN-NLN	0.0003	1.4E-06	0.000	1.4E-06	0.000	1.4E-06	0.0001	> 35
Section x/L = 0.5								
	Full Load		Ballast Load		0.5 full load + 0.5 ballast load			
Analysis	D_{SN_osc}	D_{SN_vib}	D_{SN_osc}	D_{SN_vib}	D_{SN_osc}	D_{SN_vib}	$D_{SN\_osc+vib}$	$L_{\_osc\_vib}$
ADV	0.2651	-	0.087	-	0.1759	-	0.1759	> 35
HEL	0.2651	0.0051	0.087	9.8E-06	0.176	2.5E-03	0.178	> 35
DYN-LN	0.3095	0.0018	0.096	9.5E-05	0.203	9.4E-04	0.204	> 35
DYN-NLN	0.4037	0.0183	0.104	2.4E-03	0.254	1.0E-02	0.264	> 35
Section x/L = 0.75								
	Full Load		Ballast Load		0.5 full load + 0.5 ballast load			
Analysis	D_{SN_osc}	D_{SN_vib}	D_{SN_osc}	D_{SN_vib}	D_{SN_osc}	D_{SN_vib}	$D_{SN\_osc+vib}$	$L_{\_osc\_vib}$
ADV	0.0274	-	0.043	-	0.0351	-	0.0351	> 35
HEL	0.0274	0.0005	0.043	2.7E-06	0.035	2.3E-04	0.035	> 35
DYN-LN	0.0480	0.0002	0.049	1.6E-05	0.048	1.0E-04	0.049	> 35
DYN-NLN	0.0518	0.0011	0.050	3.1E-04	0.051	6.9E-04	0.052	> 35

Table 31. Fatigue criterion, based on D ratio and design S-N curves, for North Atlantic (NA) histogram, .3D/1D combined model

Section x/L = 0.25								
	Full Load		Ballast Load		0.5 full load + 0.5 ballast load			
Analysis	D_{SN_osc}	D_{SN_vib}	D_{SN_osc}	D_{SN_vib}	D_{SN_osc}	D_{SN_vib}	$D_{SN\_osc+vib}$	$L_{\_osc\_vib}$
ADV	0.0037	-	0.003	-	0.0032	-	0.0032	> 35
HEL	0.0037	1.1E-05	0.003	8.7E-07	0.0032	6.1E-06	0.0032	> 35
DYN-LN	0.0045	2.5E-06	0.005	1.5E-06	0.0046	2.0E-06	0.0046	> 35
DYN-NLN	0.0065	4.2E-05	0.006	7.7E-05	0.0060	5.9E-05	0.0061	> 35
Section x/L = 0.5								
	Full Load		Ballast Load		0.5 full load + 0.5 ballast load			
Analysis	D_{SN_osc}	D_{SN_vib}	D_{SN_osc}	D_{SN_vib}	D_{SN_osc}	D_{SN_vib}	$D_{SN\_osc+vib}$	$L_{\_osc\_vib}$
ADV	0.8739	-	0.992	-	0.9330	-	0.9330	21.4
HEL	0.8739	0.0060	0.992	0.0000	0.933	3.0E-03	0.936	21.4
DYN-LN	0.8868	0.0032	1.092	0.001	0.990	1.9E-03	0.992	20.2
DYN-NLN	1.1133	0.0683	1.157	0.037	1.135	5.3E-02	1.188	**16.8**
Section x/L = 0.75								
	Full Load		Ballast Load		0.5 full load + 0.5 ballast load			
Analysis	D_{SN_osc}	D_{SN_vib}	D_{SN_osc}	D_{SN_vib}	D_{SN_osc}	D_{SN_vib}	$D_{SN\_osc+vib}$	$L_{\_osc\_vib}$
ADV	0.4934	-	0.825	-	0.6591	-	0.6591	30.3
HEL	0.4934	0.0030	0.825	0.00002	0.659	1.5E-03	0.661	30.3
DYN-LN	0.7179	0.0019	0.939	0.0002	0.829	1.0E-03	0.830	24.1
DYN-NLN	0.7625	0.0213	0.953	0.008	0.858	1.4E-02	0.872	22.9

Table 32. Fatigue criterion, based on D ratio and design S-N curves, for Word Wide Trade (WWT) histogram, 3D/1D combined model

Section x/L = 0.25								
	Full Load		Ballast Load		0.5 full load + 0.5 ballast load			
Analysis	D_{SN_osc}	D_{SN_vib}	D_{SN_osc}	D_{SN_vib}	D_{SN_osc}	D_{SN_vib}	$D_{SN\_osc+vib}$	$L_{\_osc\_vib}$
ADV	0.0037	-	0.0008	-	0.0023	-	0.0023	> 35
HEL	0.0037	1.1E-05	0.0008	8.1E-07	0.002	6.1E-06	0.002	> 35
DYN-LN	0.0045	2.5E-06	0.0014	8.1E-07	0.003	1.7E-06	0.003	> 35
DYN-NLN	0.0065	4.2E-05	0.0016	1.9E-05	0.004	3.0E-05	0.004	> 35
Section x/L = 0.5								
	Full Load		Ballast Load		0.5 full load + 0.5 ballast load			
Analysis	D_{SN_osc}	D_{SN_vib}	D_{SN_osc}	D_{SN_vib}	D_{SN_osc}	D_{SN_vib}	$D_{SN\_osc+vib}$	$L_{\_osc\_vib}$
ADV	0.2651	-	0.305	-	0.2849	-	0.2849	> 35
HEL	0.2651	0.0051	0.305	3.7E-05	0.285	2.5E-03	0.287	> 35
DYN-LN	0.3095	0.0018	0.319	3.5E-04	0.314	1.1E-03	0.315	> 35
DYN-NLN	0.4037	0.0183	0.344	9.0E-03	0.374	1.4E-02	0.387	> 35
Section x/L = 0.75								
	Full Load		Ballast Load		0.5 full load + 0.5 ballast load			
Analysis	D_{SN_osc}	D_{SN_vib}	D_{SN_osc}	D_{SN_vib}	D_{SN_osc}	D_{SN_vib}	$D_{SN\_osc+vib}$	$L_{\_osc\_vib}$
ADV	0.1429	-	0.250	-	0.1964	-	0.1964	> 35
HEL	0.1429	0.0025	0.250	0.0	0.196	1.3E-03	0.198	> 35
DYN-LN	0.2528	0.0011	0.274	0.0	0.263	5.8E-04	0.264	> 35
DYN-NLN	0.2725	0.0059	0.278	0.0	0.275	3.9E-03	0.279	> 35

6. REMARKS AND CONCLUSIONS

The main objectiv of this study was to evaluate the ship hull structure integrity during the exploitation life (with reference 20 years for a bulk carrier), using an integrated methodology, based on a combination between the correlation 3D/1D factors from global-local strength analysis models and the short term hydroelastic dynamic response into a long term fatigue analysis. The influence of linear and non-linear, oscillations and vibration dynamic response (hydroelastic), are consider for the analysis of preliminary ship service life prediction.

In this section will be highlighted the main conclusions that are resulting from the numerical results obtained in this study.

Based on the numerical results presented in Section 3.4, from the global-local strength analysis, under equivalent quasi-static head waves, are resulting the following conclusions:

- the maximum vertical deflections are smaller as the admissible value in both loading conditions (see Table 15 and Table 16, full cargo and ballast);
- the maximum stress values from the 3D-FEM model for the both loading cases (see Figure 44 to Figure 50 and Figure 58 to Figure 64) are smaller as the admissible values, with 5% for full load case and 30.5% for ballast case;
- from the last conclusion and the stress distribution in the 3D-FEM model (section 3), for both loading case, it can be observed that the hot spots values are in the deck cargo part, around the cargo hold frames;
- the distribution of the maximum stresses in the ship hull structure (see Section 3.4), justifies the selection of the material with stress values R_{eH} = 355 N/mm^2 (AH36) for deck and 315 N/mm^2 (AH32) for bottom.

Based on the numerical results presented in Section 4.2, from the hydroelastic linear and non-linear dynamic response analysis (irregular head waves), are resulting the following conclusions:

- the average ratio between the significant deformation on first order vibration mode and the significant displacement at ship oscillation modes are: 5.68% at linear analysis and 5.78% at non-linear analysis for full load (see Table 17), and 3.35% at linear analysis and 3.40% at non-linear analysis for ballast load (see Table 21);
- the average ratio between the significant bending moment on first order vibration mode and the significant bending moment at ship oscillation modes are: 15.07% at linear

analysis and 33.16% at non-linear analysis for full load (see Table 18), and 10.25% at linear analysis and 29.90% at non-linear analysis for ballast load (see Table 22);

- the average ratio between the significant shear force on first order vibration mode and the significant shear force at ship oscillation modes are: 13.86% at linear analysis and 27.37% at non-linear analysis for full load (see Table 18 and Table 19), and 10.01% at linear analysis and 25.82% at non-linear analysis for ballast load (see Table 23);

- based on the significant total displacements (diagrams not included in the report), from the Table 17 results that bottom slamming occurs only at aft peak (aft $h_{1/3}$>5.75m & fore $h_{1/3}$>12m) in the case of full cargo loading case and form Table 21 results that bottom slamming occurs at both ship extremities (aft $h_{1/3}$>0 m & fore $h_{1/3}$>8.5m) in the case of ballast loading case. The side slamming phenomenon occurs on both loading cases due to flare ship extremities shape. The green sea water on the main deck might occur only for the full loading case, in extreme wave conditions ($h_{1/3}$>10.65m);

- from Table 18, Table 19, Table 22 and Table 23 it results that the linear springing phenomenon occurs with very reduce intensity and the non-linear springing phenomena with small intensity, for both loading cases. The whipping phenomenon is high being induced by bottom and side slamming;

- based on the 1D equivalent beam characteristics (Figure 18, section 3.2, $W_D<W_B$), the maximum stresses from the hydroelastic dynamic analysis are also (as in section 3.4) recorded in the deck shell (section 5.3).

Based on the numerical results presented in Section 5.5, from fatigue analysis for preliminary ship service life prediction, are resulting the following conclusions:

- the fatigue criterion based in the cumulative damage ration method for North Atlantic - NA wave significant height histogram (see Table 26 and Figure 178), based on the significant normal deck stresses presented in Section 5.3 (linear and non-linear hydroelastic analysis), is satisfied for maximum $D_{SN(1D)}$ = 0.779 < 1 (see Table 29) in the case of the 1D-girder model. Analogue, based on the significant von Mises deck stresses, for the 3D/1D combined model (using the correlation coefficient $k_{3D/1D}$, see Table 27, applied on deck 1D stress values from section 5.3), it results for non-linear hydroelastic analysis maximum $\mathbf{D_{SN(3D)} = 1.188 > 1}$ and $\mathbf{L = 16.8 < 20}$ years (see Table 31) and for linear hydroelastic analysis analysis maximum is $D_{SN(3D)}$ = 0.992 < 1. In the non-linear hydroelastic case 3D/1D model the fatigue criteria is not satisfied.

- the fatigue criterion based on the cumulative damage ratio method for World Wide Trade - WWT wave significant height histogram (see Table 26 and Figure 179), based on the significant normal deck stresses presented in Section 5.3 (linear and non-linear hydroelastic analysis), is satisfied for maximum $D_{SN(1D)} = 0.264 < 1$ (see Table 30) for the 1D-girder model. Analogue, based on the significant von Mises deck stresses, for the 3D/1D combined model (using the correlation coefficient $k_{3D/1D}$, see Table 27, applied on deck 1D stress values from section 5.3), it results for non-linear hydroelastic analysis maximum $D_{SN(3|D)} = 0.387 < 1$ (see Table 32) and for linear hydroelastic analysis maximum $D_{SN(3|D)} = 0.315 < 1$, satisfying the fatigue criteria (L > 20 years).

- based on Tables 29 to 32, in the case of linear oscillations analysis (ADV) the cumulative damage ratio (for both wave significant height histograms) has maximum values $D_{SN(1D)} = 0.1759 - 0.5827 < 1$ and $D_{SN(3D)} = 0.2849 - 0.9330 < 1$, satisfying the fatigue criteria (L > 20 years);

- compared the results from Tables 29 to 32, it is to observe that the North Atlantic navigation conditions are harder than the World Wide Trade navigation conditions;

- compared the above conclusions, it results that for large elastic ships the fatigue analysis has to be carried out using data from non-linear hydroelastic short term analysis for the significant hot spot structural details.

- even using the high steel quality, from fatigue analysis point of view the results would not be improved, this is why the only solution that can be considering is re-designing the structural area with significant hot-spot and higher cumulative damage factor (D > 1).

Based on all conclusions present above and taken into consideration that a big amount of the results are close to the shipbuilding rules requirements, it is recommended that the study should continue with a finer mesh 3D-FEM model analysis in the areas where were identified the hot-spots (in the main deck structure cargo holds part).

In conclusion, in this study was presented a complex analysis used to determine the structural limit states of a commercial ship (bulk carrier). The numerical results are pointing out that for large ships having high wave induced global vibration response (whipping and springing), it is necessary to carry out an non-linear hydroelastic analysis (short term), under irregular waves (with interference components), in order to have a more realistic long term fatigue analysis and better ship's exploitation life prediction. Those results should be considered for the improvement of the existing long term structural criteria assessment.

7. ACKNOWLEDGEMENTS

The master thesis "Non-linear hydroelastic response analysis in irregular head waves, for a large bulk carrier structure, and fatigue based preliminary ship service life prediction" was developed in the frame of the Emship Master Course in "Integrated Advances Ship Design Ref. 159652-1-2009-1-BE-ERA MUNDUS-EMMC.

First of all I would like to express my sincere gratitude to Professor Leonard Domnisoru for the guidance and useful suggestion during the master thesis development.

I would like to ICEPRONAV S.A from Galati for the time spent there to develop my master thesis and for all the useful information provided for the bulk carrier analysed. I would like to thank to Mr. Petrus Dimitriu and to all the members of structural department that help me during the internship program.

And I would like to express my sincere gratitude to Professor Dario Boote as external reviewer for his revision and all remarks and comments regarding my mater thesis.

Finally, I would like to express my gratitude to my family, friends, and colleagues for their support and patience.

8. REFERENCES

B

Baldwin, B., Lomax, H., 1978 *Thin Layer Approximation and Algebraic Model for Separated Turbulent Flows*, AIAA Paper No. 78-257;

Betram, V., 2000. *Practical Ship Hydrodynamics*. Oxford: Butterworth Heinemann;

Bhattacharyya, R., 1978. *Dynamics of marine vehicles*. New York: John Wiley & Sons Publication;

Bishop, R.E.D., & Price, W.G., 1979. *Hydroelasticity of ships*. Cambridge: University Press Cambridge;

C

Chen, H.-C., Huang, E., 1998. *Validation of a Chimera RANS Method for Transient Flows Induced by a Full-Scale Berthing Ship*. Proc. 22nd Symp.Naval Hydro., Washington, pp. 948–963;

Chorin, A. J., 1967. *A Numerical Solution for Solving Incompressible Viscous Flow Problems*, J. Comp. Physics, 2, pp. 12–26;

D

Domnisoru, L., 2006. *Structural Analysis and Hydroelasticity of Ship.* Galati: The University Foundation „Dunarea de Jos" Publishing House;

Domnisoru, L., 2001. *Finite Element Method in Shipbuilding* Bucharest: Technical Publishing;

Domnisoru, L., & Ioan, A., 2007. *Non-linear Hydroelastic Response Analysis in Head Waves, for a Large Bulk Carrier Ship Hull.* Advancements in Marine Structures – Carlos Guedes Soares & Purnendu K. Das (Editors) from Taylor & Francis Group, London, pp. 147-156;

Domnisoru, L., & Domanisoru, D., 1998 *The Unified Analysis of Spring and Whipping Phenomena*. The Royal Institution of Nava Architects Publication, London, pp.19-34;

G

Garbatov, Y., Guedes, C.S., 2005. *Fatigue Damage Assessment of a newly Built FPSO Hull.* IMAM International Conference from Lisbon;

Guedes, Soares, C., Fonseca, P., Pascal, R., 2004. *Long-term Prediction of Nonlinear Vertical Bending Moments on a Fast Mono-hull.* J. Applied Ocean Research, Vol. 26;

Guedes, Soares, C., Schellin, T.E., 1998. *Nonlinear Effects on Long-term Distributions of Wave-induces Loads for Tankers*. J. Offshore Mechanics and Arctic Engineering, Vol. 120;

Guidelines for Fatigue Strength Analyses of Ship Structures from Germanischer Lloyd. 2000. Hamburg: Germanischer Lloyd;

H

Hirdaris, S.E., & Chunhua, G., 2005. *Review and Introduction to Hydroelasticity of Ship*. London: Lloyd's Register - Report 8;

Hirdaris, S.E. , Price, W.G., Temarel, P., 2003. *Two and Three-dimensional Hydroelastic Modelling of a Bulk Carrier in Regular Waves*. Marine Structures;

Hirdaris, S.E., Chunhua, G., 2005. *Review and Introduction of Hydroelasticity of Ships*. London: Lloyd’s Register, Report 8;

I

IACS (*International Association of Classification Societies*), 2008. CSR for Bulk Carrier;

ITTC (*International Towing Tank Conference*), 2008. “The Seakeeping Committee—Final Report and Recommendations to 25th ITTC” Proceedings 25th ITTC, Fukuoka, Japan;

J

Jensen, J.J., & Pedersen, P.T., 1981. *Bending Moments and Shearing Forces in Ships Sailing in Irregular Waves*. Journal of Ship Research pp. 243-251;

L

Lehmann, E., 1998. *Guidelines for Strength Analyses of Ship Structures with the Finite Element Method.* Hamburg: Germanischer Lloyd;

O

Ozsoysal, R., A, 2004. *Review of Recent Ship Vibration Papers*. The Shock and Vibration Digest, Sage Journals Online;

Owen, F. Hughes, and Jeom, Kee, Paik, 2010. *Ship Structural Analysis and Design.* The Society of Naval Architects and Marine Engineers, New Jersey;

P

Paik, J.K., Thayamballi, A.K., 2007. *Ship-Shaped Offshore Installations, Design, Building and Operation*. Cambridge University Press;

Park, J.H., & Temarel, P., 2007. *The Influence of Nonlinearities on Wave-induced Motions and Loads Predicted by Two Dimensional Hydroelasticity Analysis.* ABS-PRADS 1–5 Oct. 2007, Houston (1): pp. 27–34;

Perunovic, J.V., Jensen, J.J., 2005. *Non-linear Springing Excitation Due to a Bidirectional Wave Field*, Marine Structures;

Porter, W., 1960. *Pressure Distribution, Added Mass and Damping Coefficients for Cylinders Oscillating in a Free Surface*. California: University of California Engineering Publishing Series 82-16;

Price, W.G., & Bishop, R.E.D., 1974. *Probabilistic Theory of Ship Dynamics*. London: Chapman and Hall;

R

Rozbicki, M., Das Purnendu, K., & Crow, A., 2001. *The Preliminary Finite Element Modelling of a Full Ship*. International Shipbuilding Progress, 49(1), pp.5-35;

Rules for Classification and Construction GL, 2011. *Hull Structures Rules*. Hamburg: Germanischer Lloyd;

S

Shipbuilding and Marine Engineering. 2004. JSEA Magazine;

Stoicescu, L., & Domanisoru, L., 2007. *Global-local Strength Analysis in Head Waves, for Tanker with Longitudinal Uniform Structure.* Taylor & Francis Group, London, pp.10-29;

T

Tao, Z., Incecik, A., 2000. *Nonlinear Ship Motion and Global Bending Moment Predictions in Regular Head Seas.* International Shipbuilding Progress;

X

Xing, J.T., Price, W.G., 2000. *The Theory of Non-linear Elastic Ship-water Interaction Dynamics.* Journal of Sound and Vibrations.

Analysis Tools

DYN program code package made by Domnisoru. 2011;

GL - Poseidon ND.11. 2011 - licence at Galati "Dunarea de Jos" University;

MaxSurf ver. 13.0. 2012 - academic licence;

Nastran NX for FEMAP ver. 10.2 Finite Element Modelling and Post processing. 2010 - licence provided by ICEPRONAV S.A. Galati.

Appendix 1. Hull Structural Scantling - Final Results

In the following Table 33 are presented the final dimensions of the longitudinal plates and ordinary stiffeners from the most difficult loading cases (LC1 to LC3), this dimensions were used to complete the 3D-FEM model.

Table 33.Longitudinal Plates and Ordinary Stiffeners of the Long. Structural Elements

Position	Area	Plate t [mm]	Ordinary Stiffeners		Material	
			Type	Dimensions [mm]	Mat. No.	Yield Stress [N/mm2]
Keel	Fr.31 to Fr.54	17	HP	220 x 12	1	235
	Fr.54 to Fr.73	20	HP	300 x 14	2	315
	Fr.73 to Fr.92	21	HP	320 x 12		
	Fr.92 to Fr.112	22	HP	340 x 13		
	Fr.112 to Fr.253	23	HP	340 x 15		
	Fr.253 to Fr.273	22	HP	340 x 13		
	Fr.273 to Fr.292	21	HP	320 x 12		
	Fr.292 to Fr.325	20	HP	300 x 14		
	Fr.325 to Fr.342	19	HP	300 x 14		
	Fr.342 to 358	15	T	250x12/100x15	1	235
Bottom	Fr.18 to Fr.54	17	HP	220 x 12	1	235
	Fr.54 to Fr.73	18	HP	300 x 14	2	315
	Fr.73 to Fr.92	19	HP	320 x 12		
	Fr.92 to Fr.112	20	HP	340 x 13		
	Fr.112 to Fr.253	21	HP	340 x 15		
	Fr.253 to Fr.273	20	HP	340 x 13		
	Fr.273 to Fr.292	19	HP	320 x 12		
	Fr.292 to Fr.325	18	HP	300 x 14		
	Fr.325 to Fr.342	17	HP	300 x 14		
	Fr.342 to 358	15	T	250x12/100x15	1	235
Bilge	Fr.18 to Fr.54	17	HP	220 x 12	1	235
	Fr.54 to Fr.73	18	HP	300 x 14	2	315
	Fr.73 to Fr.92	19	HP	320 x 12		
	Fr.92 to Fr.112	20	HP	340 x 13		
	Fr.112 to Fr.253	21	HP	340 x 12		
	Fr.253 to Fr.273	20	HP	340 x 13		
	Fr.273 to Fr.292	19	HP	320 x 12		
	Fr.292 to Fr.325	18	HP	300 x 14		
	Fr.325 to Fr.342	17	HP	300 x 14		
	Fr.342 to 358	15	T	250x12/100x15	1	235
Side Shell between 3000/BL and 6800/BL	Fr.18 to Fr.54	17	HP	220 x 12	1	235
	Fr.54 to Fr.73	16	HP	300 x 12	2	315
	Fr.73 to Fr.92	17	HP	300 x 13		
	Fr.92 to Fr.112	18	HP	320 x 12		
	Fr.112 to Fr.253	19	HP	340 x 12		
	Fr.253 to Fr.273	18	HP	320 x 12		
	Fr.273 to Fr.292	16	HP	320 x 12		
	Fr.292 to Fr.325	17	HP	300 x 13		
	Fr.325 to Fr.342	16	HP	300 x 12		

	Fr.342 to 358	15	T	220x12/100x10	1	235
Side Shell between 6800/BL and 10400/BL	Fr.18 to Fr.54	17	HP	220 x 12	1	235
	Fr.54 to Fr.73	16	HP	240 x 12	2	315
	Fr.73 to Fr.92	17	HP	260 x 12		
	Fr.92 to Fr.112	18	HP	280 x 10		
	Fr.112 to Fr.253	19	HP	280 x 12		
	Fr.253 to Fr.273	18	HP	280 x 10		
	Fr.273 to Fr.292	17	HP	260 x 12		
	Fr.292 to Fr.325	16	HP	240 x 12		
	Fr.325 to Fr.342	16	HP	240 x 12		
	Fr.342 to 358	15	T	220x12/100x10	1	235
Side Shell between 10400/BL and 14000/BL	Fr.18 to Fr.54	15	HP	200 x 12	1	235
	Fr.54 to Fr.73	16	HP	240 x 12	2	315
	Fr.73 to Fr.92	17	HP	260 x 12		
	Fr.92 to Fr.112	18	HP	280 x 10		
	Fr.112 to Fr.253	19	HP	280 x 12		
	Fr.253 to Fr.273	18	HP	280 x 10		
	Fr.273 to Fr.292	17	HP	260 x 12		
	Fr.292 to Fr.325	16	HP	240 x 12		
	Fr.325 to Fr.342	16	HP	240 x 12		
	Fr.342 to 358	14	T	220x12/100x10	1	235
Side Shell between 14000/BL and 17200/BL	Fr.18 to Fr.54	15	HP	200 x 12	1	235
	Fr.54 to Fr.73	18	HP	280 x 12	2	315
	Fr.73 to Fr.92	19	HP	300 x 13		
	Fr.92 to Fr.112	20	HP	320 x 11		
	Fr.112 to Fr.253	21	HP	320 x 13		
	Fr.253 to Fr.273	20	HP	320 x 11		
	Fr.273 to Fr.292	19	HP	300 x 13		
	Fr.292 to Fr.325	18	HP	280 x 12		
	Fr.325 to Fr.342	17	HP	260 x 10		
	Fr.342 to 358	14	T	220x12/100x10	1	235
Side Shell between 172000/BL and 20800/BL	Fr.18 to Fr.54	14	HP	200 x 10	1	235
	Fr.54 to Fr.73	18	FB	280 x 12	2	315
	Fr.73 to Fr.92	19	FB	300 x 12		
	Fr.92 to Fr.112	20	FB	320 x 13		
	Fr.112 to Fr.253	21	FB	320 x 14		
	Fr.253 to Fr.273	20	FB	320 x 13		
	Fr.273 to Fr.292	19	FB	300 x 12		
	Fr.292 to Fr.325	18	FB	280 x 12		
	Fr.325 to Fr.342	17	FB	280 x 10		
	Fr.342 to 358	14	T	220x12/100x10	1	235
Side Shell between 20800/BL and Main Deck	Fr.18 to Fr.54	14	HP	200 x 10	1	235
	Fr.54 to Fr.73	20	FB	320 x 14	2	315
	Fr.73 to Fr.92	26	FB	330 x 14		
	Fr.92 to Fr.112	28	FB	340 x 15		
	Fr.112 to Fr.253	30	FB	340 x 20		
	Fr.253 to Fr.273	28	FB	340 x 15		
	Fr.273 to Fr.292	26	FB	330 x 14		
	Fr.292 to Fr.325	20	FB	320 x 14		
	Fr.325 to Fr.342	18	FB	300 x 12		
	Fr.342 to 358	15	T	220x12/100x10	1	235

Main Deck	Fr.18 to Fr.54	16	T	300x10/150x10	2	315
	Fr.54 to Fr.73	26	FB	350 x 19	3	355
	Fr.73 to Fr.92	28	FB	360 x 20		
	Fr.92 to Fr.112	32	FB	380 x 22		
	Fr.112 to Fr.253	33	FB	400 x 25		
	Fr.253 to Fr.273	33	FB	380 x 22		
	Fr.273 to Fr.292	28	FB	360 x 20		
	Fr.292 to Fr.325	26	FB	350 x 19		
	Fr.325 to Fr.342	23	FB	350 x 17		
	Fr.342 to 358	18	T	350x12/150x15	1	235
Wing Tank	Fr.54 to Fr.73	20	FB	320 x 14	2	315
	Fr.73 to Fr.92	23	FB	340 x 16		
	Fr.92 to Fr.112	26	HP	360 x 18		
	Fr.112 to Fr.253	29	FB	380 x 20		
	Fr.253 to Fr.273	26	FB	360 x 18		
	Fr.273 to Fr.292	23	FB	340 x 16		
	Fr.292 to Fr.325	20	FB	320 x 14		
	Fr.325 to Fr.342	18	FB	300 x 14		
Inner Side between 6800/BL and 14000/BL	Fr.54 to Fr.73	17	HP	260 x 10	2	315
	Fr.73 to Fr.92	18	HP	280 x 12		
	Fr.92 to Fr.112	19	HP	300 x 12		
	Fr.112 to Fr.253	20	HP	320 x 12		
	Fr.253 to Fr.273	19	HP	300 x 12		
	Fr.273 to Fr.292	18	HP	280 x 12		
	Fr.292 to Fr.325	17	HP	260 x 12		
	Fr.325 to Fr.342	16	HP	260 x 12		
Inner Side between 14000/BL and 17200/BL	Fr.54 to Fr.73	20	HP	260 x 12	2	315
	Fr.73 to Fr.92	21	HP	280 x 12		
	Fr.92 to Fr.112	23	HP	300 x 13		
	Fr.112 to Fr.253	24	HP	320 x 12		
	Fr.253 to Fr.273	23	HP	300 x 13		
	Fr.273 to Fr.292	22	HP	280 x 12		
	Fr.292 to Fr.325	21	HP	260 x 12		
	Fr.325 to Fr.342	20	HP	260 x 10		
Hopper Tank .	Fr.54 to Fr.73	16	HP	300 x 14	2	315
	Fr.73 to Fr.92	17	HP	300 x 12		
	Fr.92 to Fr.112	18	HP	340 x 12		
	Fr.112 to Fr.253	19	HP	340 x 14		
	Fr.253 to Fr.273	18	HP	340 x 13		
	Fr.273 to Fr.292	16	HP	300 x 14		
	Fr.292 to Fr.325	17	HP	300 x 12		
	Fr.325 to Fr.342	17	HP	280 x 10		
Inner Bottom	Fr.54 to Fr.73	16	HP	300 x 14	2	315
	Fr.73 to Fr.92	17	HP	300 x 12		
	Fr.92 to Fr.112	18	HP	340 x 12		
	Fr.112 to Fr.253	19	HP	340 x 14		
	Fr.253 to Fr.273	18	HP	340 x 13		
	Fr.273 to Fr.292	16	HP	300 x 14		
	Fr.292 to Fr.325	17	HP	300 x 12		
	Fr.325 to Fr.342	17	HP	280 x 10		
	Fr.54 to Fr.73	18	FB	260 x 10		
	Fr.73 to Fr.92	19	HP	280 x 12		

Central Girder from Inner Bottom	Fr.92 to Fr.112	22	HP	300 x 13	1	235
	Fr.112 to Fr.253	22	HP	300 x 13		
	Fr.253 to Fr.273	22	HP	300 x 13		
	Fr.273 to Fr.292	19	HP	280 x 12		
	Fr.292 to Fr.325	18	HP	260 x 10		
	Fr.325 to Fr.342	17	HP	240 x 10		
Secondary Girder from DB at : 5900, 11500 and 16300 from CL	Fr.54 to Fr.73	13	HP	160 x 10	1	235
	Fr.73 to Fr.92	14	HP	180 x 10		
	Fr.92 to Fr.112	15	HP	180 x 10		
	Fr.112 to Fr.253	15	HP	200 x 10		
	Fr.253 to Fr.273	15	HP	180 x 10		
	Fr.273 to Fr.292	14	HP	180 x 10		
	Fr.292 to Fr.325	13	HP	160 x 10		
	Fr.325 to Fr.342	12	HP	160 x 10		
Platform in IS at: 6800 from BL	Fr.54 to Fr.73	18	HP	280 x 10	1	235
	Fr.73 to Fr.92	21	HP	300 x 10		
	Fr.92 to Fr.112	24	HP	300 x 12		
	Fr.112 to Fr.253	26	HP	320 x 12		
	Fr.253 to Fr.273	21	HP	300 x 12		
	Fr.273 to Fr.292	18	HP	300 x 10		
	Fr.292 to Fr.325	18	HP	280 x 10		
	Fr.325 to Fr.342	17	HP	260 x 10		
Platform in IS at: 10400 and 14000 from BL	Fr.54 to Fr.73	13	HP	160 x 10	1	235
	Fr.73 to Fr.92	14	HP	160 x 10		
	Fr.92 to Fr.112	15	HP	180 x 10		
	Fr.112 to Fr.253	15	HP	180 x 10		
	Fr.253 to Fr.273	15	HP	180 x 10		
	Fr.273 to Fr.292	14	HP	160 x 10		
	Fr.292 to Fr.325	13	HP	160 x 10		
	Fr.325 to Fr.342	13	HP	140 x 12		
Platform in IS at: 17200 from BL	Fr.54 to Fr.73	13	HP	160 x 10	1	235
	Fr.73 to Fr.92	14	HP	160 x 10		
	Fr.92 to Fr.112	15	HP	180 x 10		
	Fr.112 to Fr.253	15	HP	180 x 10		
	Fr.253 to Fr.273	15	HP	180 x 10		
	Fr.273 to Fr.292	14	HP	160 x 10		
	Fr.292 to Fr.325	13	HP	160 x 10		
	Fr.325 to Fr.342	13	HP	140 x 12		

The transversal elements of the structure were calculate also with Poseidon ND.11 (GL2011) and in the cases were the program don't give results was used direct calculation using IACS Common Structural Rules and Complementary Rules of Germanischer Lloyd for Bulk Carriers – Ch.6. – Sec.4 (2008). In Table 34 are presented the final dimensions of the transversal elements of the structure.

Table 34. Transversal Elements of the Hull Structure

Position	Area	Plate t [mm]	Ordinary Stiffeners		Material	
			Type	Dimensions [mm]	Mat. No.	Yield Stress [N/mm2]
Web Frames in Inner Bottom	Fr.54 to Fr.112	12	FB	120 x 12	1	235
	Fr.112 to Fr.253	15	FB	150 x 15		
	Fr. 253 to Fr.342	13	FB	130 x 12		
Web Frames in Hopper Tank	Fr.54 to Fr.112	12	FB	120 x 12	1	235
			FB	250 x 15		
	Fr.112 to Fr.253	17	FB	150 x 15		
			FB	280 x 17		
	Fr. 253 to Fr.342	13	FB	130 x 12		
			FB	250 x 15		
Web Frames in Inner Side	Fr.54 to Fr.112	10	FB	100 x 10	1	235
	Fr.112 to Fr.253	10	FB	120 x 10		
	Fr. 253 to Fr.342	11	FB	100 x 10		
Web Frames in Wing Tank	Fr.54 to Fr.112	8	FB	100 x 10	1	235
	Fr.112 to Fr.253	10	FB	120 x 10		
	Fr. 253 to Fr.342	9	FB	100 x 10		
Cargo Hold Frame	All 9 Cargo Frames	35	HP	300 x 20	3	315
Main Deck	All Trans. Frames	-	T	800x20/320x22		

Appendix 2. 3D-FEM Model - Groups Presentation

In Table 35 are presented some of the most important groups from the 3D-FEM model.

Table 35. Groups from the 3D-FEM Model

Group Name	Figure
Aft extremity without shell	Figure 200
Deck house without external bulk heads	Figure 201
Fore extremity without shell	Figure 202
Shell plate	Figure 203
Shell stiffeners	Figure 204
Main deck	Figure 205
Inner hull	Figure 206
Girders in inner bottom and platforms in inner side	Figure 207
Web frames from inner hull	Figure 208
Transversal bulk heads from cargo area	Figure 209

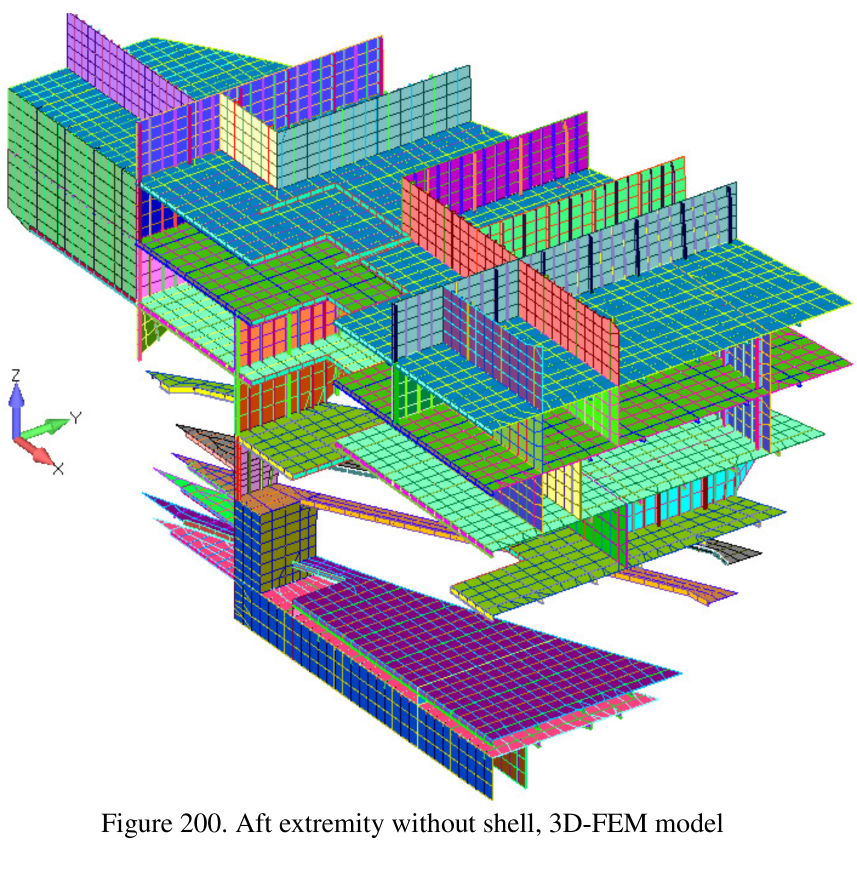

Figure 200. Aft extremity without shell, 3D-FEM model

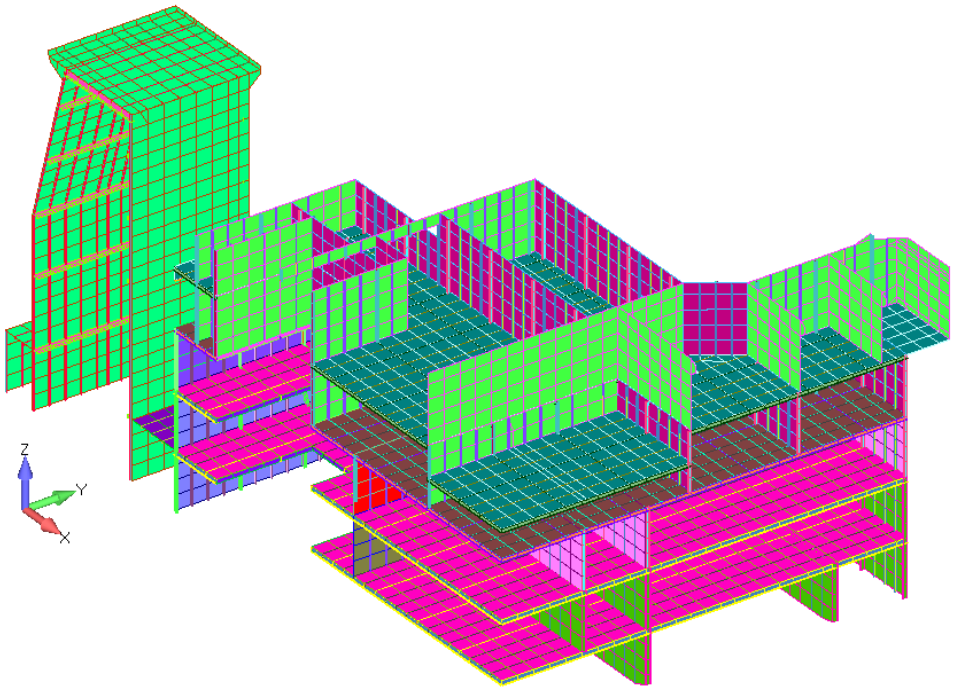

Figure 201. Deck house without external bulk heads. 3D-FEM model

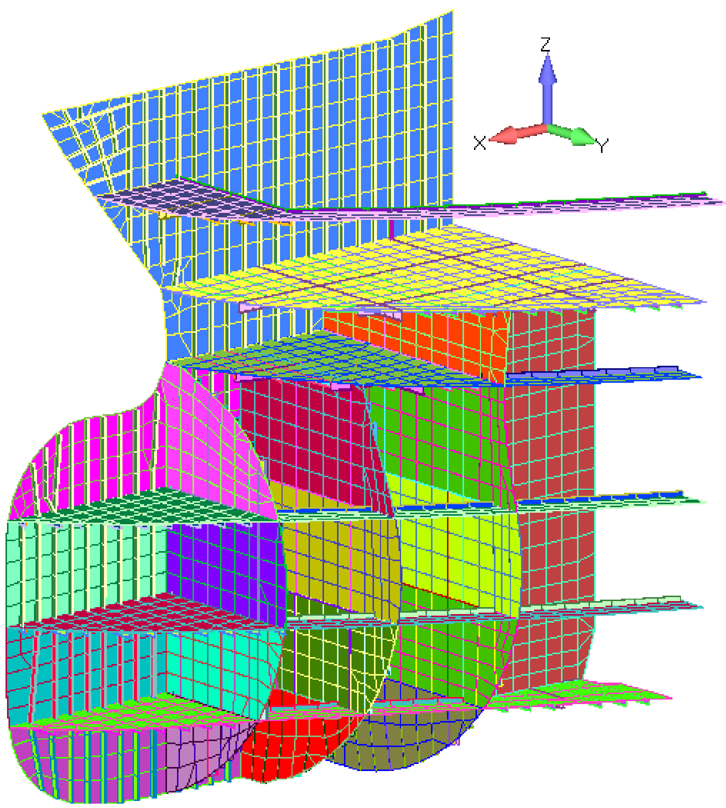

Figure 202. Fore extremity without shell, 3D-FEM model

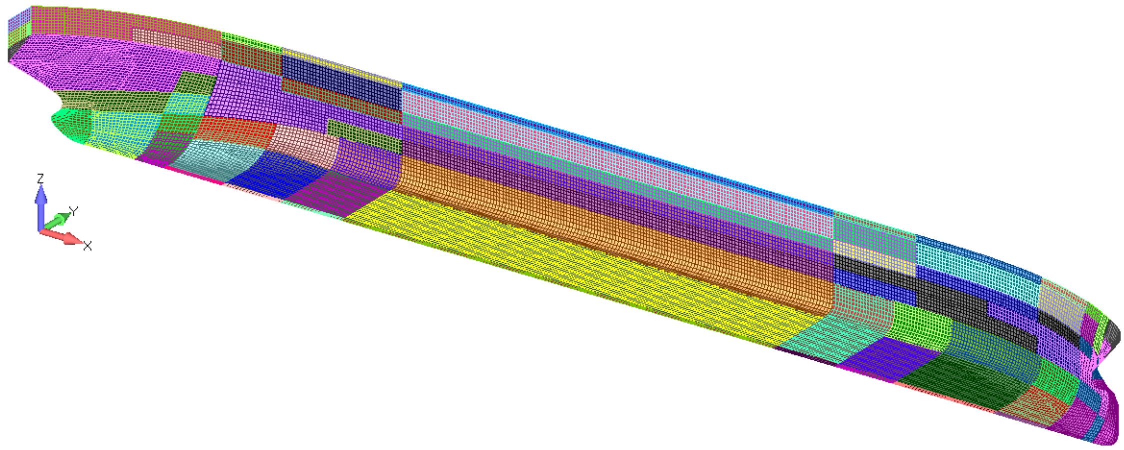

Figure 203. Shell plate, 3D-FEM model

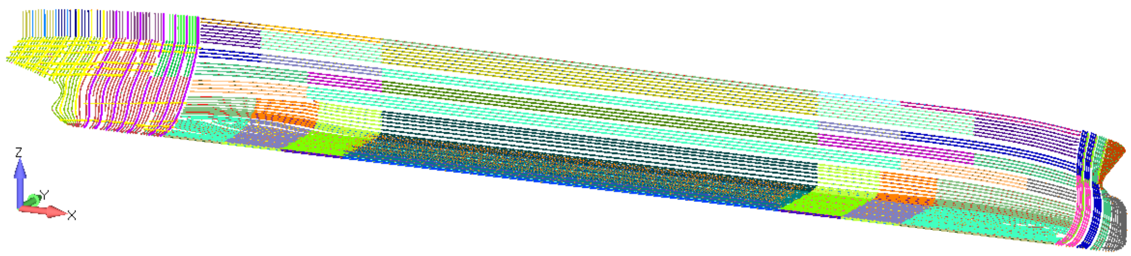

Figure 204. Shell ordinary stiffeners, 3D-FEM model

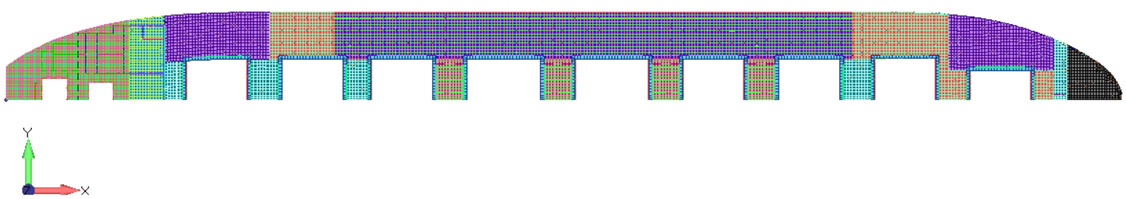

Figure 205. Main deck, 3D-FEM model

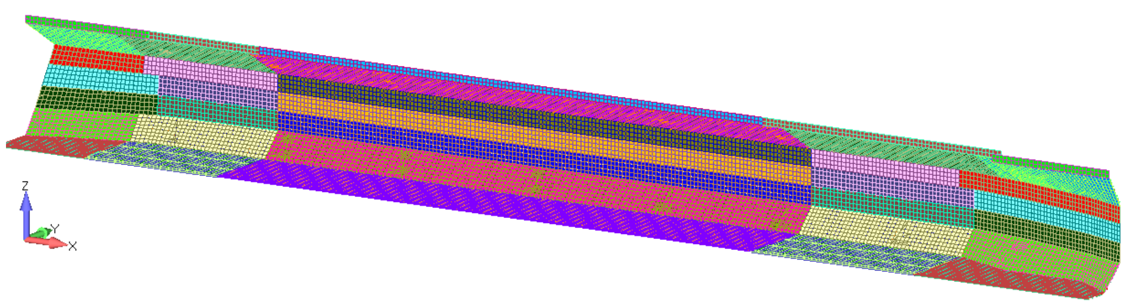

Figure 206. Inner hull, 3D-FEM model

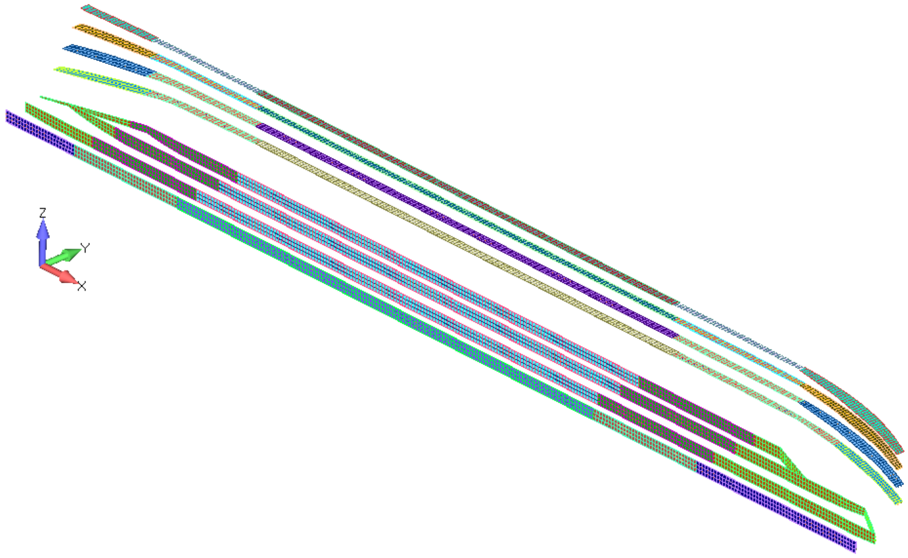

Figure 207. Girders in inner bottom and platforms in inner side, 3D-FEM model

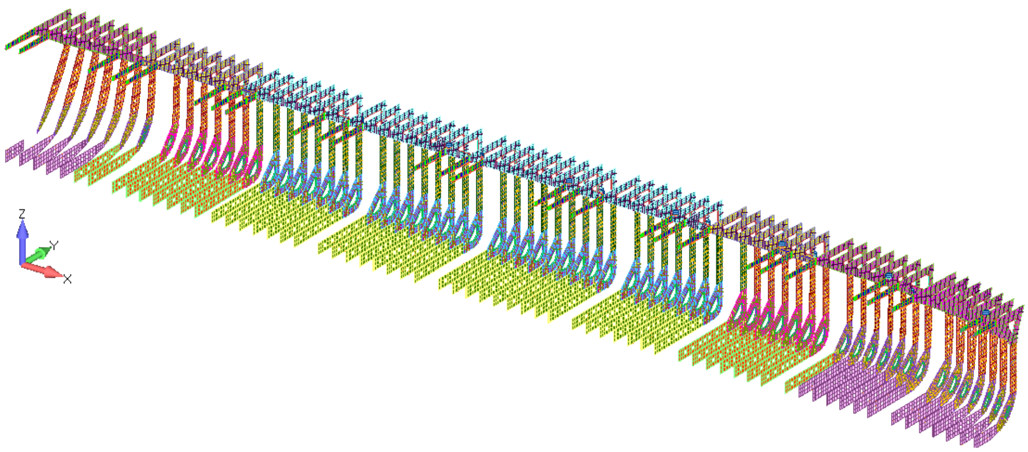

Figure 208. Web frames from inner hull, 3D-FEM model

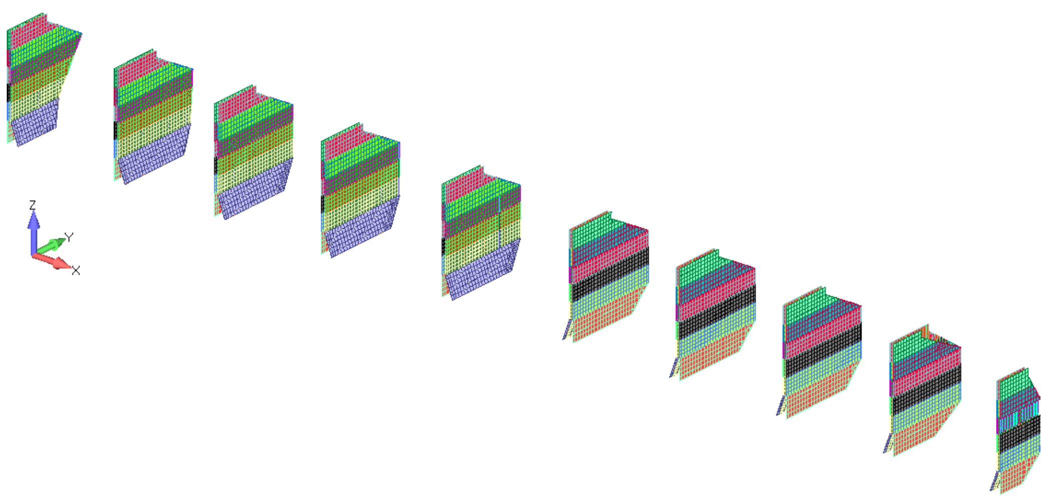

Figure 209. Transversal bulk heads from cargo area, 3D-FEM model